N° d'ordre: 41401

Thèse

pour l'obtention du grade de

Docteur de l'Université Lille 1
Mention Mécanique

présentée par

Davis Naidoo Ramasami

Laboratoire de Mécanique de Lille (UMR CNRS 8107)
Ecole doctorale Sciences Pour l'Ingénieur (SPI) n° 72
Université Lille 1

Titre de la thèse :

Influence of friction material & test sequence on disc brake squeal

Soutenue le 17 Juin 2014 devant la commission d'examen.

Composition du jury :

Alain Iost	Prof., Arts & Métiers Paristech, Centre de Lille (France)	*Président*
Caroline Richard	Prof., Université de Tours (France)	*Rapporteur*
Patrice Coorevits	Prof., Université de Picardie Jules Verne (France)	*Rapporteur*
Norbert Hoffmann	Prof., Imperial college of London (Angleterre)	*Examinateur*
Francesco Massi	Prof., Université de La Sapienza (Italie)	*Examinateur*
Philippe Dufrénoy	Prof., Université Lille 1 (France)	*Directeur de thèse*
Jean-François Brunel	M.d.C., Université Lille 1 (France)	*Encadrant*
Vincent Magnier	M.d.C., Université Lille 1 (France)	*Encadrant*
Thierry Chancelier	Ing., Chassis Brakes International (France)	*Invité*
Gabriel Rejdych	Ing., Chassis Brakes International (France)	*Invité*
Bart Van de Worp	Ing., Lapinus Fibres (Pays-Bas)	*Invité*

,

A Elodie

Acknowledgments

Je voudrais tout d'abord adresser mes plus sincères remerciements à Philippe DUFRENOY pour m'avoir fait confiance en dirigeant cette thèse. Après 7 années de travail ensemble, d'abord en tant que professeur lors de mon cycle d'ingénieur, puis tuteur de stage de fin d'étude, et enfin directeur de thèse, je suis fier d'avoir été dans son équipe. La justesse de ses commentaires, son souhait de toujours aller plus loin, les très nombreuses discussions, les points presque quotidiens, les échanges de mails à 2h du matin, ont fait de ce travail une passionnante expérience de vie. Ses qualités scientifiques et humaines m'ont permis de me surpasser à maintes reprises et pour cela, je l'en suis reconnaissant.

Je tiens à remercier Jean-François BRUNEL pour avoir accepté d'encadrer mon travail. Il a toujours su en quelques minutes de temps comprendre mes interrogations et m'orienter sur la bonne piste. Je garderais comme souvenir les *toto* et autres variables qui auront agrémenté les lignes de codes communes.

Je tiens ensuite à remercier Caroline RICHARD et Francesco MASSI d'avoir accepté d'être les rapporteurs de cette thèse et de l'intérêt qu'il porte à mon travail. Je souhaite également remercier Norbert HOFFMAN, Olivier THOMAS, Thierry PASQUET et Didier CHICOT d'avoir accepté de faire partie de mon jury. C'est un honneur d'avoir un jury de cette qualité scientifique.

Je souhaite aussi exprimer mes remerciements à Thierry CHANCELIER & Gabriel REJDYCH. Cela fait maintenant 4 ans que l'on travaille ensemble et ça a été pour moi une des expériences les plus enrichissantes de mon cursus. Les longues discussions sur le sujet comme les trajets entre Drancy et Roermond ont été de très bons souvenirs. Je tiens aussi à remercier l'ensemble du département ETF de CBI pour leur accueil toujours chaleureux et leurs conseils toujours avisés.

I would like to thanks Bart VAN DE WORP for its full support during my PhD work. It has been a real pleasure sharing our knowledges. We have launched great projects together and your advices were always thoughtful. This was an excellent experience, always in a good mood. I would like to also thank the entire staff at Lapinus Fibres for their kindness.

Je tiens à exprimer tout mes remerciements à Anne-Lise CRISTOL, Yannick DESPLANQUES et Alain IOST pour leur patience et leur expertise qui m'a permis de parfaire mes compétences et d'aborder la problématique différement. Mention spéciale à Vincent MAGNIER qui aura passé de nombreuses heures à m'aider sur mon modèle numérique (et à cliquer frénétiquement!).

Je remercie chaleureusement toute l'équipe ER5 du LML de m'avoir accueilli. J'ai une pensée spéciale pour l'équipe Polytech': Kévin, Martin, Mathilde, Florent, Amavi, Loïc, Alexandre, Pierre, Loïc, Sofiane, Jessie, Xavier, et Joachim. Les pauses cafés auront été le lieu de débats philosophiques de haut vol et cela va me manquer.

Je tiens à remercier ma famille qui m'a toujours soutenu lors de mes études et qui m'ont permis de mener à terme tout mes projets. Si j'en suis arrivé là c'est grâce à vous.

Je tiens également à remercier les amis de toujours, de Lille à Paris ou ailleurs. La liste est bien trop longue pour vous citer et c'est pour ça que je ne dirai qu'une seule chose: "seuls les vrais savent". Merci à vous tous.

Enfin, Je finis par celle qui m'a accompagné et porté tout le long de ce travail. Elodie, tu as été là chaque jour et tu m'as montré, par ton amour et ton soutien sans condition, que je pouvais y arriver. Si je te dédie cette thèse, c'est que quelque part elle t'appartient aussi.

Abstract

Keywords : braking, instability, squeal, friction, heterogeneity, materials

Abstract In the automotive industry, the noise is a major problem. Brake squeal is a medium-high frequency noise reinforced by the vibrations of the system and mode lock-in components. It is also assumed the contact properties the pad and the disc play an important role. The aim of this work is to link the squeal occurrence with transformations of the friction material and profile.

Three friction material formulations were tested. They were formulated with the same manufacturing process and a reduced number of components. These formulations are compared with a commercial brake pad. Mechanical and thermal properties of the materials were characterized and significant heterogeneity is observed.

Instrumented noise tests are performed on brake systems to compare formulations. By comparing the noise level and frequencies involved, a strong influence of formulation, temperature and braking history is observed on squeal occurrence.

Following these acoustic tests, additional tests were conducted and stopped at different states of friction: at virgin state, before and after a high thermal load, in silent or noisy conditions. Profile measurements and observations on pads surfaces are made to observe their evolutions.

The originality of this work is to consider the evolution of the friction material with braking sequence and especially its mechanical properties and their heterogeneities. These properties are separated in two levels: at the surface and onto the volume via indentation tests. Firstly, it is shown the evolution of the properties is linked to thresholds of material degradation with temperature reached during the test sequence. Secondly, the identified parameters are implemented in a finite element simplified braking system to analyse the dynamic stability through a complex eigenvalue resolution. The heterogeneity and distribution of the volume and contact properties of the material appears to have a significant role in the system stability.

Résumé

Mots-clés : freinage, instabilité, crissement, frottement, hétérogénéité, matériaux

Résumé

Dans l'industrie automobile, le bruit reste un problème majeur. Le crissement de frein est un bruit moyenne-haute fréquence renforcée par les vibrations du système et par un couplage de modes instable entre les composants. On suppose également que les propriétés du contact entre la plaquette et le disque jouent un rôle. Le but de ce travail est de lier l'apparition du crissement avec les transformations du matériau de friction et de son profil.

Trois formulations de matériaux sont testées. Elles ont été formulées avec le même procédé de fabrication et un nombre réduit de composants. Ces formulations sont comparées à une plaquette de frein commerciale. Les propriétés mécaniques et thermiques des matériaux ont été caractérisées et une forte hétérogénéité est constatée.

Des essais de bruit instrumentés sont exécutés sur des systèmes de freins pour comparer les formulations. En comparant le niveau de bruit et les fréquences, on note une forte influence de la formulation, de la température et de l'historique de freinage sur les occurrences de crissement.

A la suite de ces essais acoustiques, des essais sur banc additionnels ont été réalisés et interrompus à différents états de frottement: vierge, avant et après une charge thermique élevée, dans des états silencieux ou bruyants. Des mesures du profil et des observations des surfaces sont réalisées pour observer leurs évolutions.

L'originalité de ce travail est d'étudier l'évolution du matériau de friction avec la séquence de freinage et en particulier ses propriétés mécaniques et ses hétérogénéités. Ces propriétés sont considérées sur deux niveaux: à la surface et dans le volume via des tests d'indentation. D'abord, il est montré que l'évolution des propriétés est liée à des seuils de dégradation du matériau avec la température atteinte au cours de la séquence de test. Ensuite, les paramètres identifiés sont implémentés dans le modèle numérique d'un système de freinage simplifié pour analyser la stabilité dynamique à travers une résolution aux valeurs propres complexes. L'hétérogénéité et la distribution des propriétés de contact et de volume semblent avoir un rôle important dans la stabilité du système.

Contents

Introduction

From the very first brake lining in the early 20th century to the common brake pad known today, several breakthrough have been performed to improve performance such as general force, power dissipation and recovery, pedal feel, durability, weight, etc. However, one of the top issue automotive industry encounters is noise.

Indeed, the contact interface between the disc and the pad generate numerous kinds of high-pitched noises and, even if it doesn't significantly affect performances, the consequence is a high customer complaints warranty cost each year. Because it is annoying and appears to the customer as the presence of a problem, and in a matter of being competitive in the current marketplace, most of the industry has focus their efforts in controlling it. On most cars, disc brake systems are being used, and what is encountered the most is squeal noise. This is a high-pitched noise between 1 and 10 kHz up to 120 dB. In order to reduce this kind of noise problem by identifying the source and the mechanisms attached, it is necessary to take a look at the full process (fig.1) of supplying a classic disc brake system.

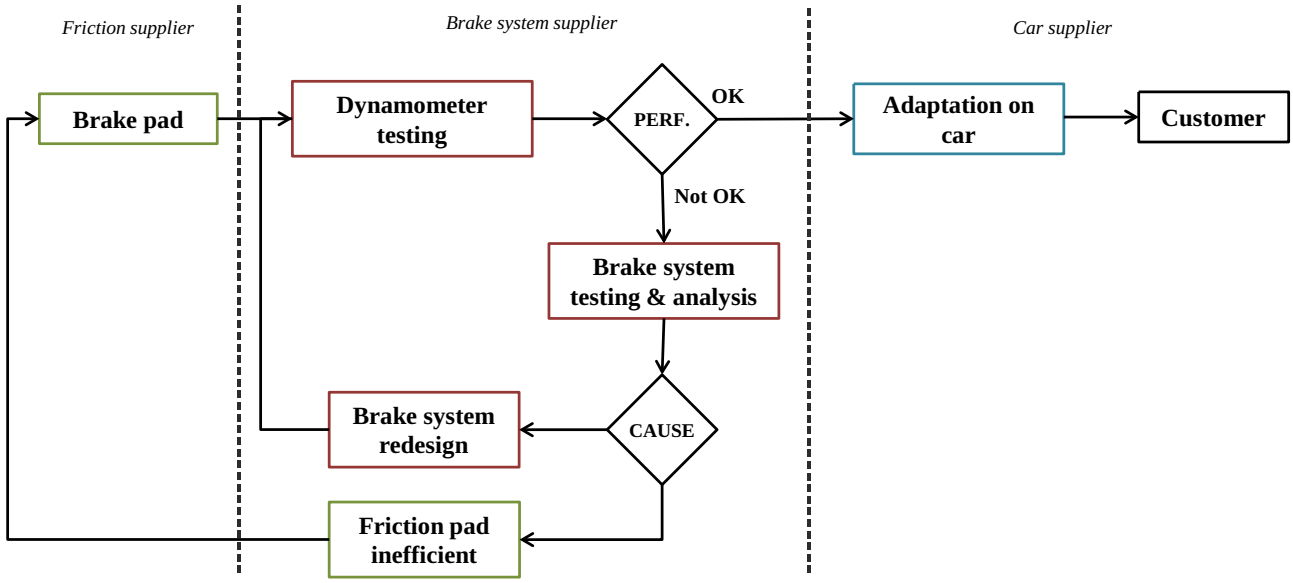

Figure 1: Industrial supply chain of an assembled brake system

When a brake system supplier sells a product to the car manufacturer, the brake pads are often provided by a friction material provider. Systematically, they are tested on a normalized performance test bench equipped with the associated brake. If the performances targeted are obtained, the brake systems with the associated pads are validated.

However, when the performance test results as a failure passing through the industry requirements, the question asked is the source of the issue. Considering the brake system has been tested and validated with several brake pad references, it can rest to the friction material used and/or the interactions with the system itself. Complementary

performance tests, laboratory and computed analysis are performed to conclude on the problem nature.

Two main conclusions can be done after this study:

- The complete assembly with the brake pad is inefficient and the problem can be solved by redesigning the brake system, putting additional part such as shims for example more damping, or moreover modifying the brake pad shape in order to change coupling with the disc.
- The brake pad doesn't fit with the normalized requirement regarding noise, modal behaviour, performances (friction coefficient, compressibility, wear, durability)

In the second case, the responsibility is charged to the friction material supplier. Since there are confidentiality restrictions on the manufacturing of brake pads, it is difficult for the brake system supplier to understand the physic behind friction materials and moreover the link with the appearance of noise.

Nowadays, the main understanding of brake squeal noise in the automotive industry is focus on the use of finite element simulation. This process is easy to set-up, cheaper than experimental testing and acceptable for cast iron components (caliper, knuckle, piston, etc.) due to their homogeneity and elastic behaviour. The modelling of brake pads is another topic. Friction materials are complex composites composed of many raw materials. Each has a function to fill and intrinsic properties. Due to the process of fabrication and the heterogeneities of these compounds, the final product has non-linear viscoelastic behaviour which implies complex characterisation regarding actual theories. Therefore, one can ask: how disc brake squeal simulation process can be improved? What is the current modelling of friction material?

In the literature, it has been shown the brake system is subject to particular vibrations implying mostly the pad and the disc coupling. These unstable vibrations, called mode lock-in, are generated by contact issues. Hence, many studies have focused on the interface between both components which is not flat and evolves during the tests. However, the surfaces are generally perfectly flat in numerical models. This evolution is due in one hand to the braking conditions, and in another hand by the brake pad raw components which are more or less degraded regarding these conditions.

In this work, it is shown there is a coupling instability issue leading to squeal and even more the pad formulation influence and the physic-chemical interactions which transform the pad surface during friction. It seems friction material lead to a multi-scale problem (fig.2).

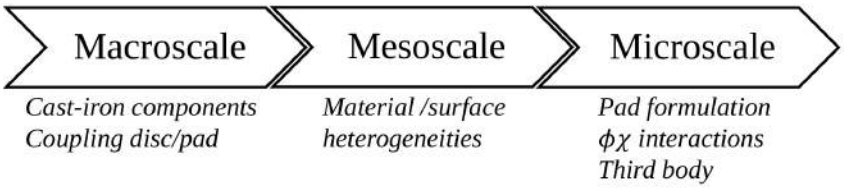

Figure 2: Disc brake squeal noise scales

The complexity of understanding the contribution of each scale on the squeal noise is tremendous. This is the main reason why for the next years, the brake squeal simulation process must include the complete characterisation of the brake pad and consider the interactions at pad/disc interface and moreover think of a strategy in how to implement this process in the pad production process. Hence, two main goals emerge:

1. **identify relevant parameters on disc brake squeal noise at different scales**
2. **link friction material formulation and process with the occurrence of disc brake squeal noise**

In this frame of work, the Laboratoire de Mécanique de Lille (LML) and Chassis Brakes International (CBI) have started a study in order to study the role of friction material and its formulation on the occurrence of disc brake

squeal noise. The first issue in this kind of project lives in the understanding of brake pads. Therefore, simplified formulations are developed and compared to an industrial one. The mechanical and thermal properties of these brake pads are studied in order to understand the physico-chemical transformation implied during braking and the pad overall response to loading. This identification is necessary before testing pads onto a real brake system. Then, specific brake sequences on an inertia dynamometer are done to track the noise evolution under different sets of parameters. A first link could be done between these properties and noise response. However, the direct physical output from squeal is the interface between pad and disc.

The output brake pads from these NVH tests are dedicated to mechanical and morphological multi-scale analysis. Knowing the pad surface evolves with friction, it appears to be interesting to extract datas from it, from a new to a used pad, in term of profile, mechanical properties and distribution. Several characterisations (microscopic observations, surface profile analysis, hardness acquisition) are performed at different steps of a braking procedure and at different states of friction. The goal is to obtain data of materials and surfaces through these tribologic measurements which will assess individual behaviour of components and their interactions during friction, the missing link between squeal and formulation.

Thus, the present dissertation will be divided in 5 chapters. First of all, chapter 1 positions the current work into the current literature. An effort is made to cover multi-scale and multi-physics phenomenon and breaktroughs surrounding the problematic. Chapter 2 presents the raw materials characteristics (dimensions, content, etc.). Then, simplified friction formulations are designed with few components and known process. The final pads intrisic properties are compared to raw materials and then with an industrial formulation. The elastic properties of the pads are studied regarding loading and excitation frequency. Participation of the natural macroscopic heterogeneity of the pad is shown. Following the industrial testing, the pads performances (noise, friction level) are studied through a benchmark done on a commercial brake and a noise testing procedure. The influence of friction history and temperature impact are compared from a formulation to another. The goal of this chapter is at last to understand the high impact of formulation choice and production process of brake pad on elastic properties and furthermore on noise response.

After using and completing the industrial procedure in the selection of brake pad, it is mandatory to focus on the friction material itself by using a more basic system concerning the whole system dynamic. In chapter 3, a simplifed fixed caliper is used because of his known frequency response and the easiness of unmounting and analyse surfaces. The simplified formulations are compared. Pad geometry impact is also shown through experimental testing and compared with a complete finite element eigenvalue analysis. Brake pad contact surface is tracked and observed at different steps of test procedure for each formulation. Heterogeneities are brought out by microscopic analysis which are the response of formulation/production process and sliding conditions (mostly temperature). This analysis highlights the need of measuring the mechanical properties locally.

Thus leads to chapter 4 where a second NVH measurement campaign is perform. One simplified formulation is compared to the industrial one at different friction stage of the procedure. Thereby, wear evolution is observed on its geometric aspect on three level (shape, waviness and roughness) and chemical composition is shown. Afterward, indentation is employed as a stochastic tool to show local elastic properties mapping for each pad, at each friction step. Requirement of linking profile, surface mechanical properties and chemical composition is shown.

In chapter 5, elastic properties estimated by indentation are considered load dependant and a proposition of post-processing measurements taking into account profile and volume stiffening is developped. Therefore, a complex eigenvalue analysis of a simplified pad/disc model is used to implement the contact & volumic elastic properties into the brake pad. For each friction situation developped in chapter 4, an associated mapping is used and impact on the mode lock-in properties is studied.

Finally, the general conclusions in the final chapter highlight the main results of this study and open on the outlooks.

Chapter 1

State of the art, a review of literature

Contents

Disc brake squeal is a multi-scale problem and multi-phenomena problem. Until now, there have been numerous studies related to these topics and, thus, it is not possible to cover every aspect of these areas of research.

The aim of this literature review is, therefore, to concentrate on the historical background and the most recent developments in disc brake squeal studies. Therefore, focus will be made on local parameters of the contact interface.
Further information on disc brake squeal research can also be found in the literature reviews conducted by [Papinniemi et al., 2002], [Kinkaid et al., 2003], and [Ouyang et al., 2005].

1.1 Disc brake assembly

1.1.1 Brake components

A disc brake system is a simple device in its main function: decelerating the car velocity. The brake pads squeeze the rotor by a hydraulically transmitted force. Friction between the pads and the disc slows the disc down.

A complete brake system can be sum-up into three sub-assembly (fig. 1.1):

- The brake pads
- The caliper, which contains a piston
- The rotor, which is mounted to the hub

The disc is attached to the wheel-hub and the caliper is linked to the car by a mounting bracket, which depend on the type of caliper (fig. 1.1).

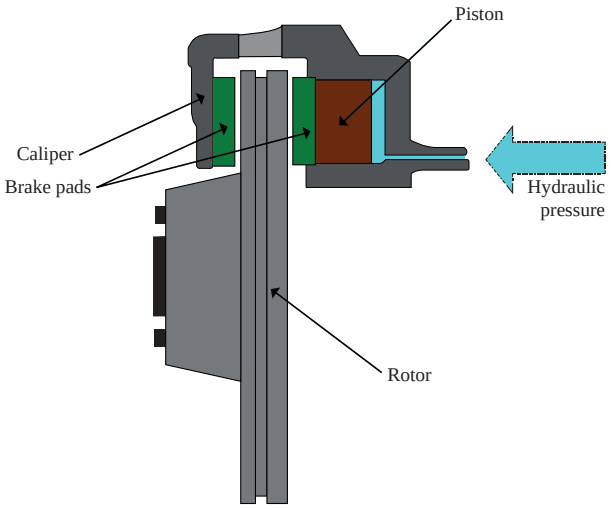

Figure 1.1: Floating-caliper disc brake

Indeed, a caliper can be of two-types: fixed or sliding/floating. A fixed caliper is solidly mounted and commonly uses a pair of pistons to apply pressure symmetrically. A floating-caliper is in most case made of one piston on the inner side of the disc. Since the disc doesn't translate on its axis, the force applied to the piston pulls the sliding caliper unto the other side of the disc, and then both pads are applied on it.

The advantages of the floating caliper is that it is cheaper and lighter than the fixed caliper as it uses less parts and is more compact. A fixed caliper provides better performance in term of pedal feel (pressure response on the disc versus force applied by the driver on the pedal) and force transmitted, which is required for heavy or

sport-dedicated vehicle. The fixed caliper can apply more power and apply that power more evenly during braking as force is directly applied to both sides. An agreement is often done by using fixed calipers on front wheels and floating calipers on the rear which fulfil cost and effectiveness requirements. Even if the pads moves in a floating caliper, they are always in slight contact with the rotor. A set of seals guarantees any leakage of pressure fluid and leaves the pads at their equilibrium position after braking. The pads might be pushed back by the disc naturally.

1.1.2 Disc

The brake disc consists of the friction ring, where the contact between brake pads and disc takes place, and the hat section, where it is mounted on the hub bearing unit.

Most discs are manufactured with pearlitic gray cast iron upon as the most widely used brake disc material, due to low cost, good machineability and well-balanced properties (high heat conductivity and vibration damping due to the flaky graphite, reasonable heat capacity and thermal stability). Disc thickness variation (DTV) has to be kept to a minimum. Too much DTV causes judder which can be felt in the steering wheel or the brake pedal.

The rotor is generally made of grey cast iron. It can be of either a simple solid rotor design or of a configuration with various vents for more effective cooling. A moving car has a certain amount of kinetic energy, and the brakes have to remove this energy from the car in order to stop it. Brakes convert the kinetic energy to heat generated by friction between the pads and the disc and this heat must be dissipated, mostly by the disc because the organic nature of friction pads doesn't allowed heat stocking.

Consequently, most disc are vented (fig. 1.2). They have a set of blades between the two sides of the disc which pumps air through the disc to provide cooling. A vented disc can be a solution to avoid heating up the pad too fast.
Another addition to disc heat-dissipation is cross-drilling or slotting the disc. The purpose of such machining is more dedicated to racing cars but the pad lifetime is significantly reduced because they are sources of stress concentrations which lead to cracks.

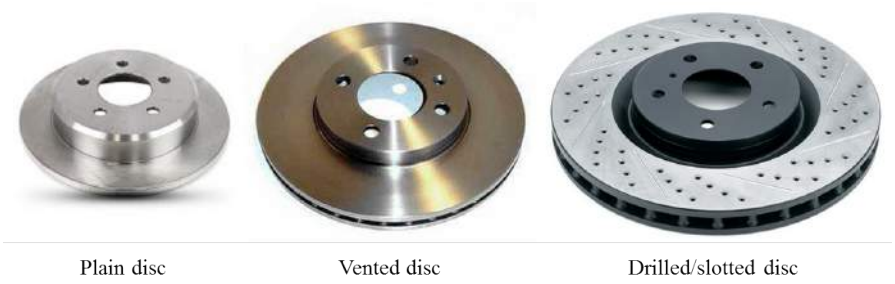

Figure 1.2: Types of disc brake

The following work will focus on tests done with vented discs which are the most customary.

The disc surface is a fundamental parameter which must be taken into account on braking applications. First, there is a natural waviness which cannot be entirely controlled at manufacturing state but reduced at mounting. Secondly, the roughness at macro- & micro-scale influences the quality of the contact surface with the pad. The non-planarity of the disc during high-energy braking enhances high temperatures and local hot spots/layers on the disc which deform the disc and modify consequently the disc surface. This phenomena can be found in automotive industry [Lee and Barber, 1994] but also in many areas as in railway [Panier et al., 2004] or heavy-duty trucks [Collignon, 2013].

At microscopic scale, the roughness driven by small defects is responsible in the tearing of the pad particles [Sallit et al., 1998]. Combined, these phenomenon add variability and complexity to the brake system performances and noise occurrence.

1.1.3 Pads

Brake pads are heterogeneous materials composed of several raw materials, usually in powder shape. Most pads are organic compounds but it can contains inorganic materials such as mineral fibers. Each raw material contributes and can significantly change the brake performances, the production process and the price of the brake pad. Since there are many confidential agreements surrounding the making of brake pads, there are few literature reference on the process of manufacturing. However, [Nicholson, 1995] has summarized the long history of this industry in a complete review.

The performance of a brake system in vehicles is mainly determined by the tribological interactions between the iron disc and friction materials. Friction materials used in the industry have a complex composition. There are often a score of different constituents, each with their function. They can be classified into 4 categories that reflect their respective functions:

- Binders & fillers: their role is to hold the components together. They provide low temperature and low noise. They are used to fill the pad in order to make it consistent with the lowest cost. Resin and barites are the binder commonly chosen but they have a stable behaviour at low temperature.
- Abrasives: such as aluminium oxide, their main goal is to give a high friction level (μ) and also low fading during the braking phases;
- Lubricants: the main goal is to obtain the smoothest contact when pressure is applied, raw materials like graphite and metal sulphide provides low wear of pad and rotor;
- Reinforcement: to give good mechanical strength and a good pedal feeling, inorganic or steel fibres are mixed with other raw materials because of their compressibility;

The proportion of each raw material is determined by proof of experience and by the intention of the manufacturer (more or less compressibility, good lubrication, etc.)

The process of pad production is done in six steps (fig.1.3):

1. Selecting raw materials: according to the performances searched, numerous raw materials are chosen to fill the requirements described previously
2. Weighing: each raw materials is weighted in order to respond to precise function on a certain amount; this step is empirically dependent (as the selection) and leaves in the experience of the formulator
3. Mixing: the raw materials are mixed together in a batch to give an homogeneous aspect to the pad
4. Moulding: the mixed raw materials are placed in a pre-heated mould and then pressed to form the pad shape. During this process, degasing is mandatory to not increase the porosity. Moulding can be "cold" (around ambient temperature), "warm" (below resin polymerisation temperature for resin-based formulations) or "hot" (over polymerisation temperature). Hot moulding implies degasing for reacting raw materials and so the moulding is done by steps. 80% of the pad is formed at this stage.
5. Curing: The pads are set in a oven on a cycle program adapted to not exposed them to high temperature gradient. The goal is to bind every materials together.
6. Grinding: The pads are machined at the contact surface to « initiate » braking at a similar temperature. It lower fading and increase the friction coefficient

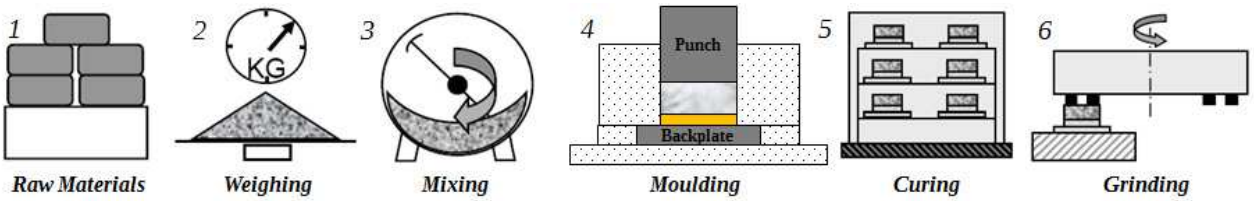

Figure 1.3: Brake pads common fabrication process

Pad shape can be chamfered, cutted-off, slottted. Putting additional part such as shims for example more damping, or moreover modifying the brake pad shape in order to smooth contact and change coupling with the disc ([Liu and Pfeifer, 2000])

Several requirements are demanded on the manufacturing of brake pads, regarding pad consistency, performances, cost, etc. Here is a short list which highlights these points:

- Friction coefficient: disc pads must have a friction level that isn't too high neither too low. High friction causes excessive wear and noise, while low friction leads to poor braking performance.
- Friction stability: the friction level has to be stable over a broad range of wear rates and temperatures (up to 700 °C).
- Pressure & speed sensitivity: the friction coefficient is supposed to be independent of pressure and speed.
- Shear Strength The material must be able to withstand large amounts of shear stress that are applied during hard braking.
- Hardness: harder material causes higher rotor wear and noise, while softer material wears faster.
- Wear: minimal wear of pad is desirable to extend the lifetime of the braking system.
- Noise: noise generation has to be kept to a minimum during braking.
- Environment factos: the influence of water, oil, sand or dust has to be minimized.
- Price: the formulation should be as cheap as possible.
- Pedal feel: pushing the brake pedal should result in a direct response of the brake system. A brake pad that is too soft or air in the hydraulic system will causes a bad response on the brake pedal. It is preferred that the pedal pressure is linear to the friction Force.
- Cracking: the brake pads should not crack, even under extreme braking conditions

These requirements, both asked by brake suppliers and customers, increase the difficulty to manufacture brake pad. It can explain why pad formulation contain numerous raw materials. Brake pad is a black box and leaves on the trial and error method, and so implies a great deal of variability from one pad to another. Also, these materials are subject to transformation due to sliding contact and so temperature. Therefore, it appears to be useful to look at threshold temperatures of these components, compared with manufacturing process temperatures and braking application.

1.2 Squeal noise: high-pitch noise enhanced by friction instabilities

1.2.1 Different types of noise

Noise on a disc brake system can appear on several conditions during drivers's experience. Most of them are classified by the car industry [Liu et al., 2007] and are frequently associated as a vibration problem which involves two major areas of vibration study:

- friction-induced vibration
- rotor/stator interactions

Thus, this section will focus on the type of noises known, especially squeal noise, and the mechanisms leading to it.

On a disc brake assembly, several type of noise can appear during use. Most of them are not lowering performances but they are the reflection of the modifying behaviour of the system and can become annoying for the driver ans its surrounding. Here is a short list of main noises which can be measured and classified.

The classification according [Akay, 2002] suggests there is two groups of noise: the low-frequency noises (below 1kHz) which are vibration-forced phenomenon, and higher-frequency noises which are self-excited excitations due to the contact interface (fig.1.4).

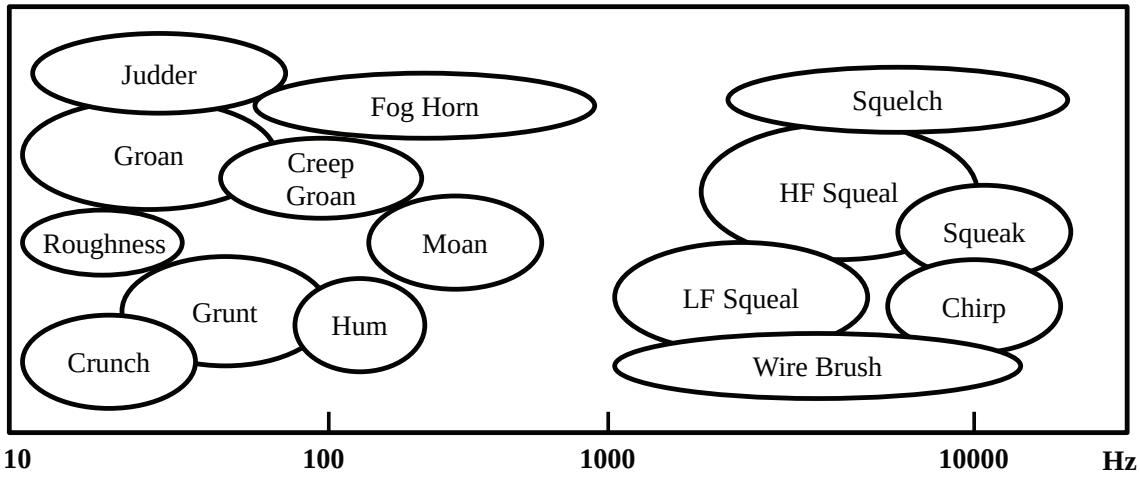

Figure 1.4: Noise classification during braking regarding frequency suggested by Akay [Akay, 2002]

The list below described some of the noises often encountered by the brake industry:

Judder Judder is a low frequency noise vibration (100Hz) which is link to the vibration induced to the pedal and steering wheel. It deals with a variation of braking torque which can appear at high speed (dynamic judder) and high temperature (thermal judder). At lower temperature, this noise might occur and it is called "cold judder". On the disc surface, several spots can be observed on the disc surface, however there is a low thickness variation of the disc (approx. 10 μm).

Grabbing Grabbing is a rare low frequency noise (around 100Hz) which is due to a high disc thickness variation or a high "disc run-out" (around 1/10 mm). This phenomenon can be classified as of stick-slip type according to [Oden and Martins, 1985].

Groan Groan is a low frequency noise (40 to 100Hz) on both front and rear brakes. After a heating and cooling cycle, when the car stops after a low speed travel (around 25kph in traffic to 0kph), this loud noise can be heard just before the stop and can be of a long duration (seconds). Low speed/pressure leads to a stick-slip situation and launch a switch between static and dynamic friction coefficient.

Hum A low frequency brake vibration that may occur with light brake dragging, usually at highway speeds.

Squeak A medium low-pitched noise of very short duration. It is a high-pitched sound, similar to rubbing a clean windows

Moan Moan is a noise which can come out with or without braking. It is a low frequency noise (100 to 450Hz) and it arises with low vibrations coming from a body resonance and are not felt by the driver. Low braking conditions (from 1kph), first stop after high humidity soak and forward and/or reverse braking can lead to moan.

Squeal Squeal is a mid-high frequency noise (from 1 to 10kHz). It can come out in braking or without braking. It is mostly induced by brake and disc vibrations. This kind of noise shouldn't impact the stopping/decelerating performances. Chamfering the pad, adding lubrication or maintaining the plain surface contact are solutions to reduce squeal, as modifying the pad geometry with slots or placing damped materials such as shim to the backplate. Cold temperatures as humidity can even cause more squeal noise. The cold weather combined with high early-morning humidity often worsens brake squeal, although the squeal stops when the lining reaches regular operating temperatures. Dust on the brakes may also cause squeal; there are many commercial brake cleaning products that can be used to remove dust and contaminants. Squeal can be of different type:

- Sustained squeal: A brake squeal characterized by long term (multiple wheel revolutions- several seconds duration) sound of essentially fixed frequency.
- Apply Squeal: A brake squeal that occurs with the initial brake application and generally lasts only a second or so in duration. Often occurs after a long period when the brakes were released, as with highway driving.
- Warble: A brake squeal that is characterized by several rapidly changing frequencies. Warble generally occurs at low speeds, and with very low brake apply pressures.

Wire brush Brake squeal characterized by several simultaneous very high frequency noises on a certain range (example: from 10 to 11 kHz, or 10-14kHz) due to multiple excitation sites on the brake linings. Wire brush noise sounds like a constant variable hiss and also a scraping or scratching sound which is caused by the linings lightly rubbing the surface of the disc.

It looks like squeal is covering the largest bandwidth. Therefore, the rest of this work will emphasize the squeal phenomenon and the physics which lead to it.

1.2.2 Squeal mechanisms

Commonly, when two bodies are in sliding contact, with friction, the tangential force is non-negative . In one hand, the friction force generates deformation energy to both solids. In another hand, there is an energy of dissipation due to the relative speeds of the two solids. When the amount of deformation energy is higher than dissipation, the system can be unstable at the contact interface, which can lead to system vibrations, and even acoustic radiancy. When squeal occurs on a brake system, experimental tests register peaks of frequency. (e.g. fig.1.5).

The entire brake vibrates periodically at discrete frequencies. The disc deformation at noise start is close to one of its own modes (a mode consisting on bending nodal diameters and/or a disc in-plane mode as in [Fieldhouse and Newcomb., 1993] fig.1.6).

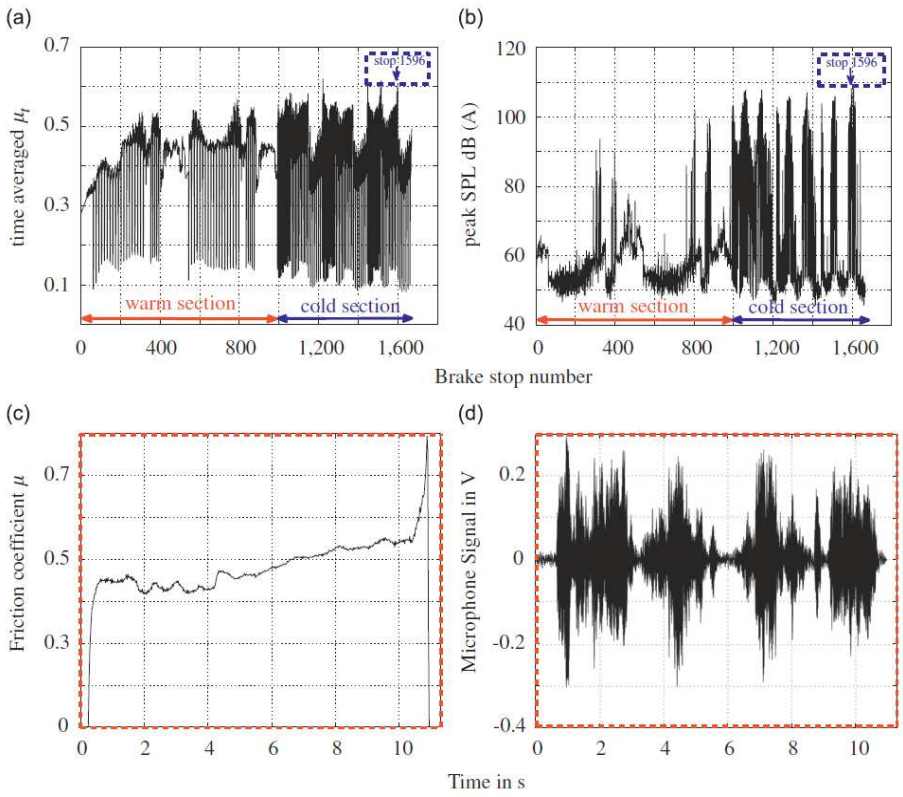

Figure 1.5: For a squealing brake stop: (a) time-averaged friction coefficients; (b) peak sound pressure levels in test matrix; (c) time series of friction coefficient ; and (d) time series of microphone signal [Oberst and Lai, 2011]

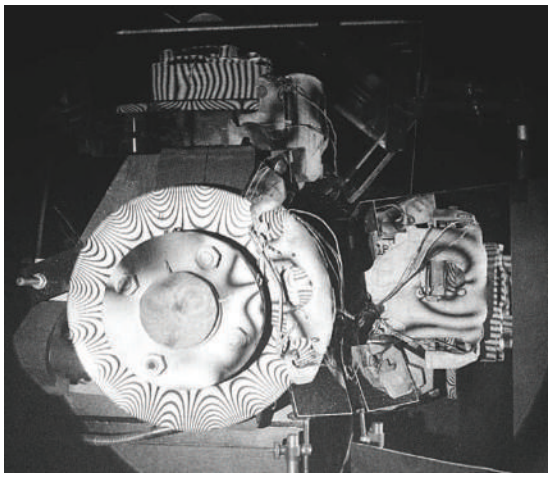

Figure 1.6: Interference fringes of a squealing system (10kHz) showing a 8 nodal diameter disc mode [Fieldhouse and Newcomb., 1993]

This subsection highlights the dynamic and theory built on sliding contact and thus squeal occurrence.

1.2.2.1 Negative gradient of friction velocity & Stick-slip theories

[Mills, 1938] attempted to examine various drum brakes and brake linings. It considers a contact law Coulomb, with a friction coefficient which is a decreasing function of the relative speed slip (fig.1.7).

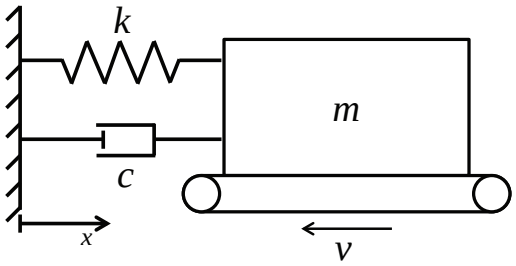

Figure 1.7: Mass (m) - spring (k) - damper (c) system with friction sliding contact at constant velocity (v)

According to H.R. Mills the motion equation of the system in figure 1.7 is:

$$m\ddot{x} + c\dot{x} + kx = F_f \tag{1.1}$$

If a law contact with a Coulomb coefficient of friction with decreasing speed is applied on ($\mu = \mu_1 - \mu_2 mg(v - \dot{x})$), it gives:

$$m\ddot{x} + (c - \mu_2 mg)\dot{x} + kx = 0 \tag{1.2}$$

with g the gravity force and F_f the friction force. If $\mu_2 mg > c$, the damping coefficient is negative and the vibrations are increasing exponentially. He hypothesised that squeal was associated with this negative gradient characteristics of dynamic friction coefficient against the sliding velocity. he thought that this mechanism was a necessary condition for a brake system to squeal. Besides, [Sinclair, 1955] observed this mechanism can lead to unstable oscillations and so self-excited vibration.

In [Fosberry and Holubecki, 1955] & [Fosberry and Holubecki, 1961], they suggested that the disc brake tended to squeal when either a static coefficient of friction was higher than the dynamic coefficient or a dynamic coefficient decreases with increase of speed present in the contact interface. The above mechanisms are also referred to as "stick-slip" and "negative damping" respectively in current terminology.

The stick-slip theory has not received much attention recently except for explaining some low frequency brake vibration problems such as creep-groan whilst negative damping theory still has its place in brakes squeal studies.

1.2.2.2 Sprag-slip

[Spurr, 1961] proposed a new theory of brake squeal called sprag-slip. He suggested the unstable oscillation in the system could also occur even with constant friction coefficient.

In describing this mechanism, Spurr developed a model (fig.1.8) that consisted of a rigid, massless rod pivoted at one end, and free to another end with an angle θ in contact with a rigid moving plane as shown in figure 1.8. An external force, L is loaded to its free end. The instability of the system depends upon the friction coefficient, the magnitude of the friction force, F_f and the normal force, N. These two forces then generates a resultant force that formed an angle θ which is important for the stability of the system. When the friction coefficient reaches the cotangent of the angle θ, the free end of the rigid rod would "sprag" or lock and the surface motion become impossible. Due to the stiffness within the system, it allows the rod free itself from the spragging condition. Once the spragging has been relieved, the original contact situation is re-established. This process could lead to a sprag-slip limit cycle.

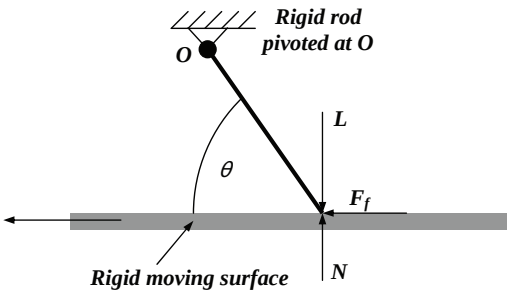

Figure 1.8: Sprag-slip according [Spurr, 1961]

In [Spurr, 1971], it has been attempted to confirm the sprag-slip mechanism through experimental investigation. He observed that squeal was associated with the position of the contact area between the pad and the disc and the nature of the contact between the cylinder and backplate.

[Earles and Soar, 1971] extended sprag-slip theory and used both experimental and analytical approaches to study squeal in disc brakes.

An experimental investigation was done based on a pin-on-disc combination system. They also developed a single-degree-of-freedom model to demonstrate the importance of non-linear coupling within the combined system. From the investigation they observed that within a certain range of angles of orientation of the pin, instability of the self-induced vibration motion appeared. This was due to the non-linearities in the system. In addition, they concluded that generation of squeal was dependent on the mean coefficient of friction, direction of disc rotation and on the presence of a torsional vibrational mode of the pin subsystem.

1.2.2.3 Mode lock-in

[North, 1976] proposed a theory of squeal where he developed a binary flutter model which more closely resembled disc brake assembly. An eight-degree of freedom model (1972) and later a two-degree of freedom model (1976) considered not only geometrical characteristics of the brake components but also took into account friction coupling and stiffness of the interactive components.

North's 2-DOFs model consisted of the disc layered between two flexible pads that had both translational and rotational stiffness. The distinctive features of this theory were the presence of the disc and the friction forces produced by pressure of brake pads, and the presence of two independent disc modes.

The novelty of this model was the friction forces between the disc and the layer of brake pad were incorporated as follower forces (forces which depend for their definition on the displacements of the body on which they act). In this theory, the model was bounded by immoveable planes, which meant that any axial displacement of the disc would cause a different pressure on one pad interface from that of the other pad interface. This variation could lead to friction forces to induce moment in the disc and subsequently if the fluctuation of the moment reached the natural frequency of the disc then it might be possible to induce instability in the system. The model was able to give good agreement in squeal frequencies, mode shapes and range of brake-line pressure with the experiment.

North's model was extended by [Millner, 1978], where he developed a six-degree-of freedom lumped parameter model of fixed caliper disc brake that coupled by a kinematic constraint. He stated that the conditions for disc brake to squeal were dependent on the friction coefficient of the pad, the mass and stiffness parameters of the disc brake assembly, and the contact configuration of the pad and the piston. He also concluded that a fairly good correlation was achieved between the observed trends and predicted results in squeal behaviour.

[Hoffmann et al., 2002] presented a minimal model (fig.1.9) for clarifying the physical mechanisms underlying the mode-coupling instability of self-excited friction induced oscillations. A conveyor belt with constant velocity v_B is pushed with a constant normal force F_N against a block m. The block is suspended by two linear springs with stiffnesses k_1 and k_2 and, in addition, a third linear spring with stiffness k_3 representing the normal contact stiffness between the block and the belt. A Coulomb-type friction force F_F with constant μ is assumed.

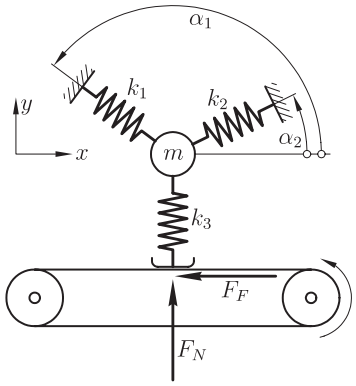

Figure 1.9: Minimal single mass two degree of freedom model by [Hoffmann et al., 2002]

Considering small perturbations around the steady sliding state and approximating a constant friction force by $F_F = \mu k_3 y$ the resulting equations of motion are:

$$\begin{bmatrix} m & 0 \\ 0 & m \end{bmatrix} + \begin{bmatrix} k_{11} & k_{12} - \mu k_3 \\ C & k_{22} \end{bmatrix} \begin{bmatrix} x \\ y \end{bmatrix} = \begin{bmatrix} 0 \\ 0 \end{bmatrix} \tag{1.3}$$

with:

$$\begin{aligned} k_{11} &= k_1 \cos^2 \alpha_1 + k_2 \cos^2 \alpha_2 \\ k_{12} = k_{21} &= k_1 \sin \alpha_1 \cos \alpha 1 + k_2 \sin \alpha_2 \cos \alpha_2 \\ k_{22} &= k_1 \sin^2 \alpha_1 + k_2 \sin^2 \alpha_2 + k_3 \end{aligned}$$

It is noticed the stiffness matrix is not symmetrical which is caused by the effect of the frictional contact, leading to a complex frequency eigenvalues: if the real part of the eigenvalue is positive then this mode will be unstable (figure 1.10). This model wasn't dedicated at first for comparison with brake squeal noise problematic. Although, many studies have used this theory as a model of understanding for pad-disc coupling.

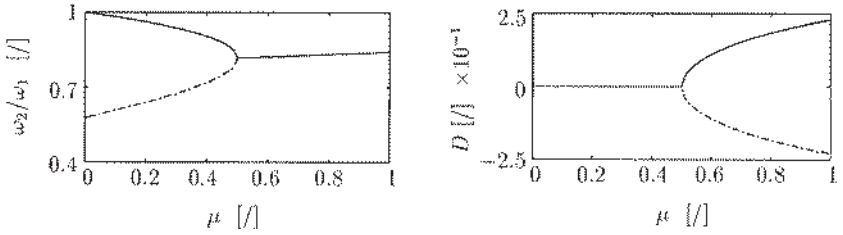

Figure 1.10: Mode-coupling phenomenon in terms of the merging of natural frequencies

[Murakami et al., 1984] examined squealing disc brakes using dual pulsed holographic interferometry. They believed that squeal was generated by coupled vibrations of the disc brake system. Supplementing the optical measurement technique, they used piezoelectric accelerometers which were mounted on several components of the braking system.

The experimental results concerned the vibration modes of the disc and pads.
They did not comment on the issue of whether or not the pads and caliper are the primary acoustic source of squeal but they noted the amount of squeal increased when the natural frequencies of the pads, caliper, and brake rotor were close to each other. They cautioned that closeness of these frequencies is not a necessary condition for squeal generation, however it is assumed squeal occurrence is due to a coalescence of the pad tilting with a out-of-plane disc mode. However, mode lock-in might not necessary be squeal noise.

1.2.2.4 Hammering

[Rhee et al., 1991] found the sprag-slip theories lacking in that they only described parameter spaces in which squeal might occur but not the actual mechanism exciting the squeal. Noting that the frequencies of brake squeal often correspond to natural frequencies of brake system components, the authors proposed a mechanical impact model they called hammering to explain the noise excitation. Several hammering mechanisms were proposed in [Rhee et al., 1991], among them, disc imperfections and spragging.

Hammering due to disc imperfections refers to the rocking of the pads of friction material over macroscopic waviness in the disc's surface (as may be caused by the local hot spots evidenced in [Abendroth and Wernitz, 2000]). This causes repeated impacts of the disc and can excite it into a state of vibration.

At first glance, the hammering theory appears to contrast the sprag-slip theory, where persistent contact between all components is assumed. However, Rhee et al. remarked that hammering was, in fact, compatible with sprag-slip instabilities. They argued that unstable interactions between various system elements (as in spragging) may cause hammering which leads to squeal. They also argue that stick–slip interaction associated with waves of detachment , can also be viewed as a series of impulses acting at the frictional interface. These impulses can, in principle, excite natural frequencies of the brake system components.

1.2.2.5 Conclusion

Several studies have applied the theories described above. Nowadays, the lock-in theory is one of the most accepted approaches as a necessary condition for squeal generation. Thus, particular attention is given to the dynamics of brake systems. The next chapters will mostly use this theory of unstable mode coupling.

1.2.3 Numerical simulation

Investigations into brake squeal have been conducted by various experimental and analytic methods. Experimental methods, for all their advantages, are expensive mainly due to hardware cost and long turnaround time for design iterations. Frequently, discoveries made on a particular type of brakes or on a particular type of vehicles are not transferable to other types of brakes or vehicles. Product development is frequently carried out on a trial-and-error basis. There is also a limitation on the feasibility of the hardware implementation of ideas. A stability margin is usually not found experimentally. Unfortunately, this produces designs that could be only marginally stable. Therefore, modelling brake squeal is a difficult problem to solve.

Analytical and numerical modelling, can simulate different structures, material compositions and operating conditions of a disc brake or of different brakes or of even different vehicles. With these methods (e.g. fig.1.11), noise improvement measures can be examined conceptually before a prototype is made and tested. Theoretical results can also provide guidance to an experimental set-up and help interpret experimental findings.

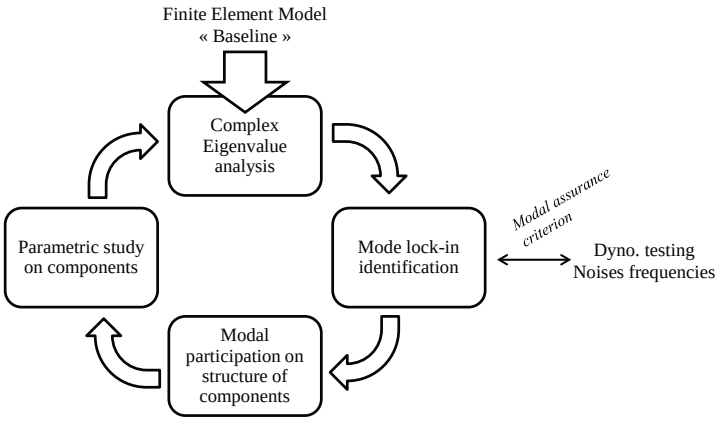

Figure 1.11: Approach to correlate brake squeal noise frequencies to unstable mode coupling in brake system complex eigenvalue analysis

Minimal models

Numerous models are simplified approach of the brake dynamic at the macro scale. Thus, only a small number of degrees-of-freedom are necessary for a basic understanding(e.g fig.1.12). In the literature a number of such models can be found, containing two or three degrees of freedom as in [Hoffmann et al., 2002] previously presented [Brommundt, 1995], [Shin et al., 2002], or [Popp et al., 2002]. This will not be covered here but several reviews as [Papinniemi et al., 2002] detail minimal models.

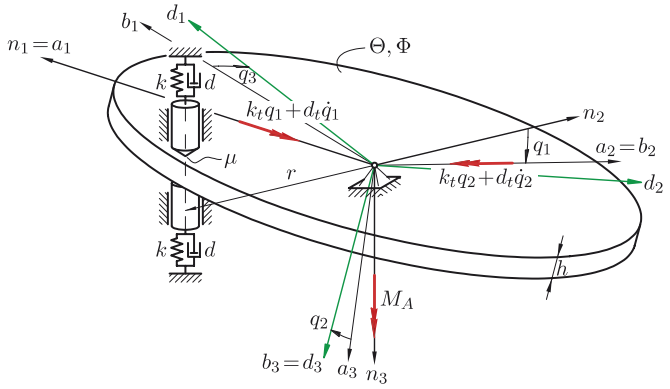

Figure 1.12: Disk brake model with wobbling disc [von Wagner et al., 2007]

Complete models

In the automotive industry, brakes are commonly modeled as multibody systems using finite element methods resulting in models with high numbers of degrees of freedom.

In the finite element modal analysis, many studies have been conducted in academic and industrial R&D but it can be quoted [Nagy et al., 1994], [Guan and Jiang, 1998], [Bae and Wickert, 2000], [Shi T.S. and Warzecha, 2001], [Baba H. and Takagi, 2001] and [Yang and Afeneh, 2004]. The list presented here is not exhaustive. Complete brake models with a large number of degrees-of-freedom are of interest in this work.

Most models cited above are complete (and complex) brake models as in fig. 1.13. It seems relevant to have a complete model to compare with for example experimental datas acquired, but the complexity leaves in the

modelling of bounding between components, as contact interfaces and so on.

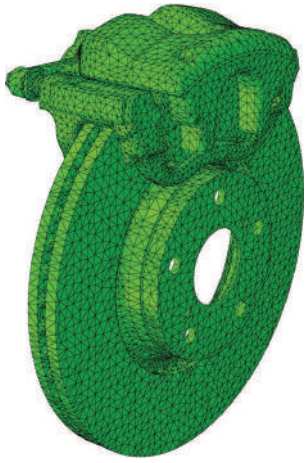

Figure 1.13: Complete brake disc for complex eigenvalue analysis [Renaud et al., 2012]

The finite element method, which is capable of analyzing complex systems, has been applied in brake squeal analysis. Simulation and analysis methods may be divided into two big categories: transient analysis in the time domain and complex eigenvalue analysis in the frequency domain.

Transient analysis

The transient results can be converted to the frequency domain by an FFT as in [Hu and Nagy, 1997]. In this approach, the dynamic responses in the time domain are calculated. If the responses diverge in time ([Adams, 1995]), the system is said to be unstable and squeal is said to occur. The major advantage of this approach is that no assumptions are needed to pre-define the contact condition and motion between pads and rotor during vibration. It also gives the ability to simulate the real brake system behaviour as in [Des Roches, 2011] (fig.1.14). That approach requires, in general, very large computer capacity and long computation time. The classic strategy to reduce computation time is is to use modal reduction[Loyer et al., 2012]. However, it has been shows non-linear interactions are difficult to represent in such extend. Moreover, even if a squealing condition is successfully detected, one may still have difficulty in selecting the effective parameters which are causing squeal.

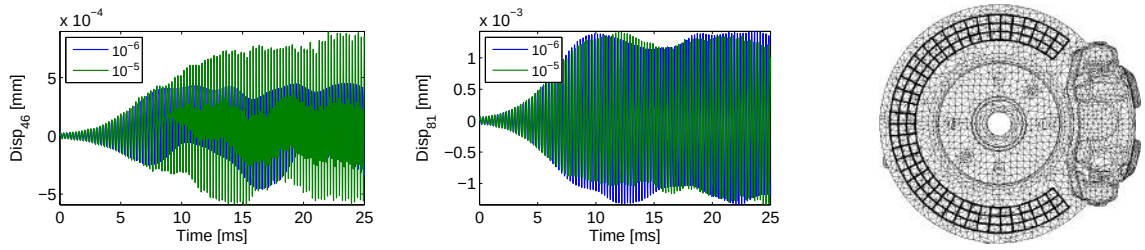

Figure 1.14: Transient analysis - Displacement results for sample points of the ODS grid, as function of the time step [Des Roches, 2011]

Complex eigenvalue analysis

An alternative to that is the complex eigenvalue analysis (CEA) method proposed by Liles [Liles, 1989]. In this approach, the friction coupling between the rotor/pad interface is introduced to the system by altering the system

matrices, leading to complex eigenvalues. The calculation is divided into two parts. First one is a quasi-static equilibrium of the system with pressure on pads and disc rotation. The second is the extraction of complex eigenfrequencies of the system state. The real parts of the frequencies gives an information on the stability of the system: if the real part of an eigenvalue is positive, the system is unstable and the corresponding eigenfrequency is assimilated as a possible squeal noise frequency. Many works as [Ouyang et al., 2005] or [Abubakar and Ouyang, 2006] used this method. More recently, [Bonnay, 2013] used this approach to implement material heterogeneities and contact properties such as bearing zone between pad and disc and assesed contact was more influent than brake pad heterogeneous properties.

CEA is the preferred approach for industry in terms of computing cost and calculation time, and permits design of experiment with parametric analysis to understand the influence of the system parameters on the squeal propensity.

In the end, the transient analysis is the richess approach. It gives a time-dependent evolution of the system stability. However, there are countless numerical parameters to set-up and the computation time is critical. The complex eigenvalues analysis appears to be the most comfortable to use in this frame of work: working on the whole brake structure with correct boundary conditions takes a lot of computation time with the transient approach. Moreover, the final step would be to implement pad/disc non-linear interactions which are difficult to apprehend with transient analysis.

1.3 Pad/disc interface: multi physics & multi-scale approach

This section is about the meso-/microscopic parameters at the contact interface and examines how deform, wear and tear the various components of materials during sliding, the nature of the contact interface, its topology, etc. The frictional contact phenomena committed to very different scales.

First, it is well assumed contact geometry at a global scale has an important impact on squeal noise occurence and so mode lock-in between pad and disc. Furthermore, many studies have shown a dependency of pad geometry into this coupling. In [Bergmann et al., 2000], it is shown chamfered or cut-off pad geometry modulates occurrence and frequency of squeal (fig.1.15), or more recently in [Duboc, 2013], the pad length also impacts these parameters.

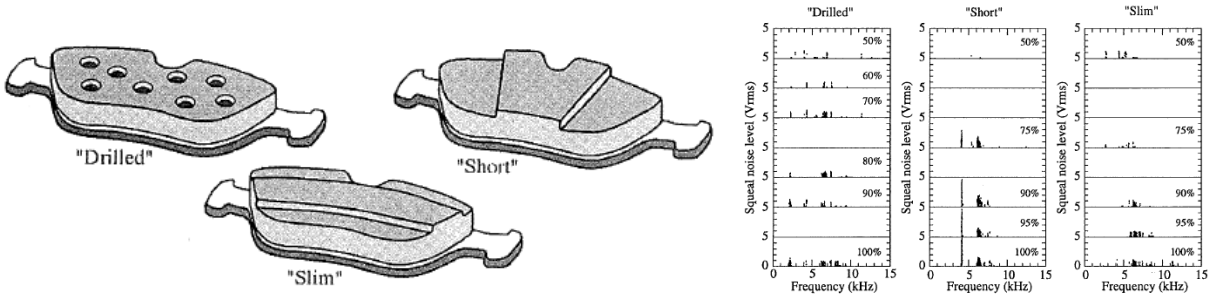

Figure 1.15: Different pad geometries and their associated frequencies/sound levels registered squeals for a NVH testing procedure [Bergmann et al., 2000]

But, in smaller geometry scales, the contact geometry influences also the mode lock-in. Thus, Akay defines five scales for considering the contact interface in figure 1.16. They all take into account the dynamic and physical transformation of materials.

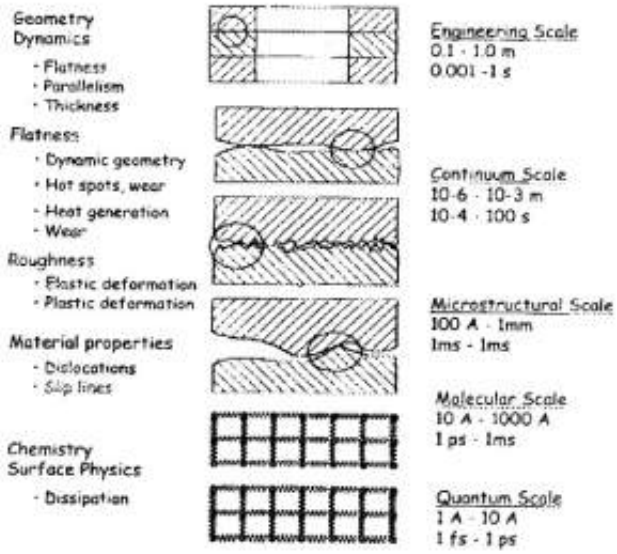

Figure 1.16: Contact scale according [Akay, 2002]

Through this section, friction interactions between pad and disc are shown in terms of mechanical degradation, thermal transformation and geometric evolution.

1.3.1 Surface evolution through sliding

Noise and vibrations are assumed to be friction induced, between the contact of two body with a relative speed. In order to understand the interactions between the disc and pad, [Godet, 1984] (followed by [Berthier, 1995]) suggested a concept around these two first bodies (in our problematic the pad and the disc) and the physics behind, suggesting a tribologic triplet. The third body concept applied to disc brake system was born. It takes into account the kinematic and also the material properties continuity.

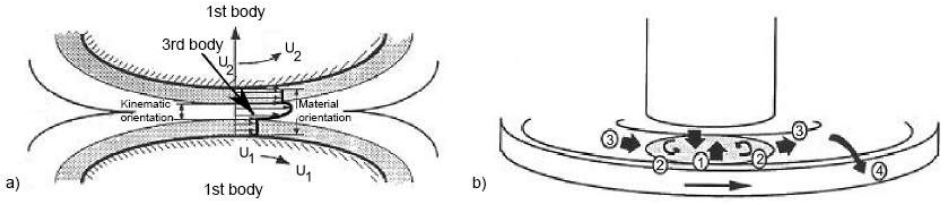

Figure 1.17: Contact interface - a) Tribological triplet; b) Tribological circuit & recirculation flow of third body [Berthier, 1995]

Between the pad and the disc, there is what is called a third body layer which can be on a liquid, gaz or solid state. This flux is composed of first bodies particles mainly which can be trapped between the contact.
Several roles are given to this layer: it bears the normal load due to the contact while adjusting the speed between the first bodies. Likewise, the friction generates high energies into the contact, so the third body layer is the lead dissipater of temperature.

In a steel disc/organic brake pad contact, it must be taken into account the friction material brings heterogeneities. Currently, discs are smooth and polished surface. However, the friction material is a rough surface. This rough surface is due to the numerous and various types of raw materials into the brake pad formulation. With friction, some materials are detached from the surface and flowing on the contact surface. This situation lead to create traps on the contact surface with the disc. Some materials, for example fibres which are hard materials, barely transform into debris and can emerge from the surface.

[Eriksson et al., 2002] described a schematic of the contact situation between an organic brake pad and a brake disc, involving contact plateaus with primary (lighter) and secondary parts, and a flow of debris, partly piling up against the plateaus (fig.1.18). A steel fibre constituting a stable primary plateau and a secondary plateau formed in front of the fibre, are visible in the cross-section. The frictional energy helps to compact and sinter the debris forming the secondary plateaus. It is interesting to note that Eriksson showed that brake pads which had many small contact plateaus were more likely to generate squeal than brake pads with fewer larger contact plateaus.

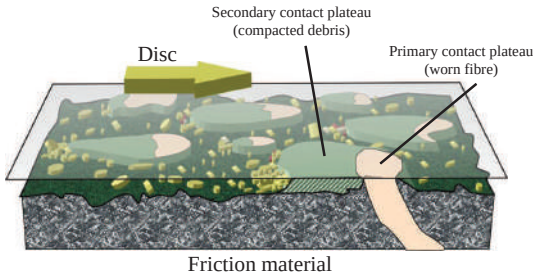

Figure 1.18: Contact situation between an organic brake pad and a disc [Eriksson, 2000]

[Roussette, 2005] has defined the tribological system on the pad/disc interface for the railway application. He observed the wear of the pad and disc particles forms a powder bed and the fibres are emerging with the debris flowing into porosities which form obstacles. Also, with friction, the plateaus can be enhanced through time and, with

recirculation of the debris, they can be fragmented or destroyed an so on. This can highly increase the generation of obstructions and can represent up to 50% of the contact bearing. Figure 1.19 from [Eriksson et al., 2001] shows cross-section SEM images of a worn friction material. The two primary areas of lift (fibers) and secondary (compacted powder) are clearly visible.

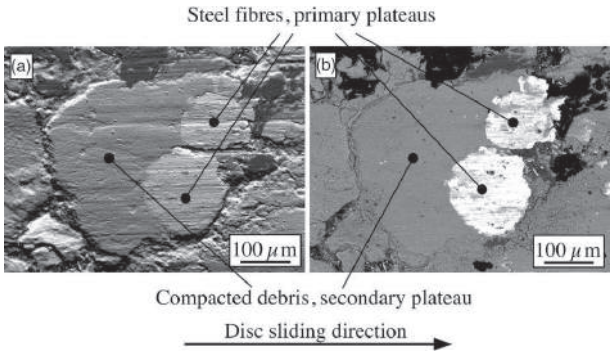

Figure 1.19: Contact plateau on an organic brake pad. Note the two primary plateaus, steel fibres, supporting the secondary plateau, compacted debris to their left (SEM). (a) Enhanced topographical contrast; (b) enhanced compositional contrast [Eriksson et al., 2001]

1.3.2 Tribologic circuit influenced by temperature

The pad-disc contact during the migration of the hot band is governed by strong interactions between localisation phenomena and the tribological circuit locally activated in the pad surface, fed by the recirculation flow in front of the hot band. This band corresponds to the site that bears the load and accommodates the sliding velocity, namely where the main part of the energy is dissipated, where thermal phenomena are localised. As a consequence, due to high loadings, the third-body band progressively breaks on the backside of the hot band, the detached debris forming a secondary source flow and further feeding the recirculation flow. More generally, the formation of compacted third-body results from a complex tribological circuit, implying coupling with hot-band localisation, heat dissipation and thermomechanical deformation contact. A compacted third-body band is formed from accumulation of particles trapped.

A schematic synthetic diagram of this coupling has been presented in [Desplanques and Degallaix, 2009] (Figure 1.20). It corresponds to a cross section of the pad-disc contact, perpendicularly to the sliding direction. Due to heat generation and first-body distortion by thermal expansion during the hot-band radial migration, friction occurs in a circumferentially-localised band of the apparent area of contact, implying high level of pressure and of power dissipation. At the same time, a gap separates pad and disc surfaces in the surrounding of this band, with an opening in the hot zone and a closure in the cold zone. Hence, in the hot-zone open area, powder layers carried by the disc rotation form the recirculation flow, while in the cold-zone open area, powders are trapped in the contact, sheared and compacted, leading to the formation of the compacted third-body band.

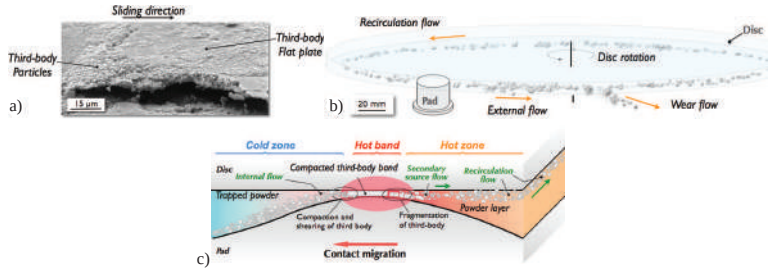

Figure 1.20: Tribologic circuit in braking [Desplanques and Degallaix, 2009]

1.3.3 Near-contact properties influenced by friction history

In most work done on pad contact surface, chemical composition of contact plateaus is mainly studied as [Eriksson, 2000]. Also, the geometric evolution is a area of reasearch thoroughly discussed in the literature, since it is well assumed it will modulate the contact coupling between instabilities, and with the asperities, enhance the instability due to debris flowing and plateaus formation. Research on contact pressure distribution in a disc brake system has been carried out by a number of people. The parameter is essential in the brake instability research area especially. Both numerical method, either complex eigenvalue dynamic transient analysis are used.

It has been well known contact heterogeneities are due mostly to the non-homogeneous portance of pad on disc. The plane-on-plane contact is not maintained because of the pad tilting on the disc and with wear, the planearity can't be assessed. The three orders of surface are impacted: shape, waviness and roughness. Also, the tribo-layer generates contacts plateaus which are in fact composed of several components which differents intrisic properties each. Thus, the combination results in difficulties to determine non-linear material properties and to take into account the complex geometric asperities.

In practice, sliding surfaces are never exactly plain and uncovered, but show a complex geometry of asperities, contact plateaus or a fissured tribological layer. In [Graf and Ostermeyer, 2011], this structure is understood as many small additional masses attached to thesurface of an elastic body. These masses are isolated from each other and are only coupled by the elastic body they are fixed on. To investigate effects that are larger than the dimension of single asperities, the inertia of those masses is distributed to a film of homogeneous inertia that corresponds to the average mass distribution on the surface (fig. 1.21). For the dynamics of this inertia layer no elastic properties and no spatial thickness are taken into account. A tribological surface is assumed that shows plateau-like flat structures of e.g. compacted wear debris, like it appears on organic brake pads.

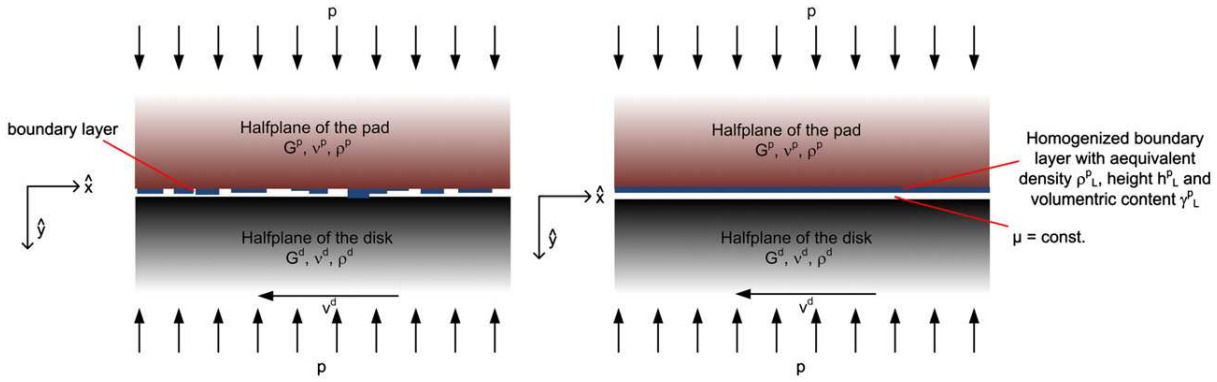

Figure 1.21: Homogenization of the inertias of the surface topography [Graf and Ostermeyer, 2011]

Another work from [Hetzler and Willner, 2012] deals with the friction coefficient and its stochastic properties which are calculated for a scanned surface of a worn brake pad. The data shows that the asperities can be approximated by paraboloids which allows to calculate the contact force and area with the Hertz contact model if the deformation is elastic. The friction force is calculated with the Bowden-Tabor approach which suggests that the friction force is the force to shear apart contacting asperities. This is considered to be the dominant friction cause in dry contact. The spectral decomposition is used to generate many surfaces with similar peak statistics.

An interesting approach is the work achieved in [Heussaff et al., 2012]. By measuring the brake lining he proposed to observe the micro-mechanical properties of the surfaces using indentation tests. The goal is to model the behaviour of the roughness and other non-linearities of the contact interface(fig. 1.22).

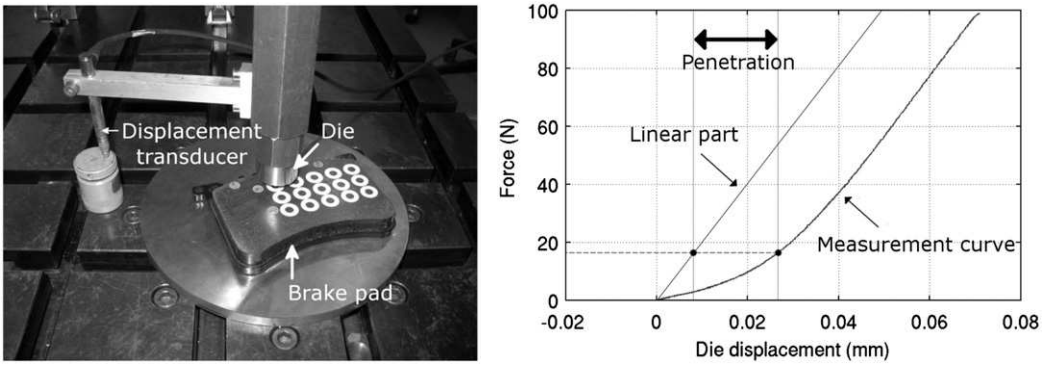

Figure 1.22: Measurement of the structural properties of linings, extraction of the non-linear part [Heussaff et al., 2012]

The breakthrough is the measurement and discretization of the contact geometry. The contact properties are modeled through a non-linear contact stiffness law which is usually not obtain experimentally but by empirical calculations. Accurate numerical contact pressure can be obtain (fig. 1.23).

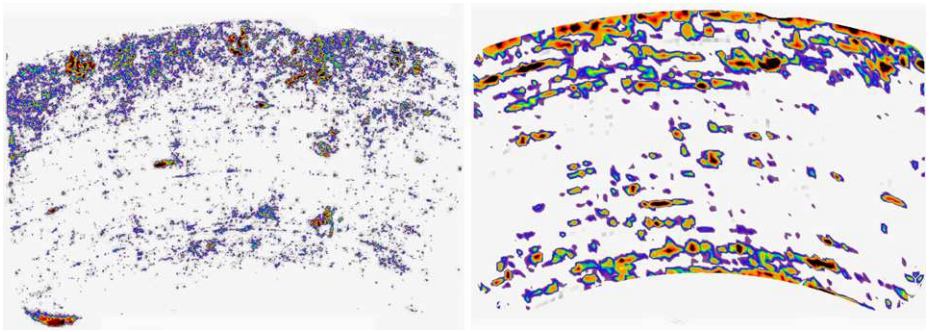

Figure 1.23: Measurement (left) and random computation (right)of pressure distributions [Heussaff et al., 2012]

[AbuBakar and Ouyang, 2008] have included in their numerical model a non-uniform distribution of the contact pressure from experimental static measurements. Furthermore, they have enhanced their model taking into account the wear of the material. They thus obtained good correlation between the experimental and the numerical term in wear of the contact and distribution. Similarly, the complex modal analysis performed with various distributions of pressure instabilities shows similar results obtained experimentally.

Through these kind of work, surface profile effect can be easily modeled. However, The literature shows the lacks of understanding and identification of mechanical behaviour of the tribo-layer. There is almost no multi-scale approach or at list a very few. These are mostly simple approaches and only few finite elements approach except for example Heussaff work, which is only focused on surface interface. The goal would be to take also into account the near-contact volumic properties.

1.4 Scope of the present work

The present literature review has displayed the multi-scale and multi-physics aspects regarding squeal noise.

Choice of components plays a major role into the occurrence of squeal noise. The most complex component is the pad. It has a formulation which contains more than a score of raw materials than, and is empirically designed. Moreover, the process of manufacturing is a multi-parameter process. Literature has shown the complexity of understanding material transformation, on pad side, which implies squeal noise. These parameters are countless and the combination of all makes the understanding more difficult. Thus, it seems mandatory to **simplify the composition and the manufacturing of friction material** to its necessary part. Thus, this thesis will focus on making simplified formulations with a known and fixed process which fullfil the industry requirements for a correct brake pad.

Breakthrough have been done in the literature to identify relevant mechanical & thermic parameters on the final pad product. The industry has even implemented these efforts in their process. Although **non-linear behaviour** is known in a global point-of-view, only few studies have quantified the **temperature and load-dependency** of friction material, even regarding **distribution through the pad**. These parameters have to be measured to understand the impact of formulation and manufacturing parameters on the pad out-of-manufacturing.

Aside the material characterisation, formulation impact on noise occurrence must be studied. The bibliography has shown the difficulty to analyse brake squeal noise because of the dynamic of components, especially on pad/disc contact. Therefore, in order to have a complete overview of impact of friction material on noise, **industrial and simplified brake systems** need to used, the first one for the global noise frequencies behaviour due to friction material and system, and the second one for focusing on pad material itself.

The direct consequences of sliding contact is the transformation of pad contact surface. The surface evolution is conditionned by the material intrinsic heterogeneities (raw components geometry & properties and physico-chemical reactions) and braking parameters (temperature, pressure, speed). The third-body approach is in adequation with these obsevations. A step forward has been done to consider profile evolution, but it lacks the identification of the non-linear behaviour at pad/disc interface and its modification through sliding contact & temperature. Thus, it is interesting to link surface transformations to appearance or not of noise. The evolution of pad materials properties through braking history is certain but unknown. The **identification of surface & volumic heterogeneities properties** (geometric & elastic properties) is a complex work which has been approach in many numerical studies but leaves as a challenge in term of quantification, which is this work's intention. The implementation of these datas in a complex eigenvalue analysis will assess the relevance of taking into account near-contact heterogeneities.

Chapter 2

Friction material: Characterization and Testing

Contents

In the aim of producing efficient brake pads, the industry has continuously developed new materials to gain better performances. In the improvement process of friction materials performance and NVH, there is a will of better understanding physical mechanisms hidden behind complex friction material formulations.

It is common to model pads as a homogeneous isotropic transverse material [Brecht et al., 2003]. However, brake pads are the result of a complex composition of various raw materials added to a specific production process which are both responsible for the performance of the final product. The sensitivity of performance to formulation- and process- variability can be here mentioned as well. The main difficulty is to acquire data that are representative of the friction material during braking applications.

Brake pads are complex heterogeneous materials which are considered as black boxes. In fact, most manufactures don't reveal their formulations but it well known most are designed by trial and error. Therefore, brake pads formulations can be composed of more than 30 different raw materials and each one has a specific functionality. Also, with the prohibition of asbestos use, a performant material for braking application but dangerous for public health, the stakes in finding the best materials for brake pads are tremendous.

In a matter of simplifying the problematic, it has been decided to work with a simplified formulation. Knowing the four function to fill into a brake pad (binder, abrasive, lubricant, reinforcement) only 10 components per formulations were chosen, and three formulations were designed. One industrial formulation (called "Ref." for reference), which composition and process are unknown, is used as comparison.

In the following sections, raw materials are described and measured to have a base of knowledge on the physical and chemical properties of each one. Then, the process of fabrication is described and stay the same for all three formulations. The final products are also studied chemically and then mechanically. Finally, to follow the complete protocol which is used in the brake system industry, the simplified friction materials are characterised as the industry requirements, furthermore with less conventional test devices, and then tested on a dynamometer bench test compared to an industrial formulation.

2.1 Formulations description

2.1.1 Raw components

2.1.1.1 Binder

Resin

Phenolic resin is obtained by the condensation of phenol, homologues of phenol or polyhydric phenols with aldehydes. Phenol-formaldehyde resins, which are obtained from phenols (mainly, phenol itself) and formaldehyde, have the greatest practical importance. Depending on the relative amounts of the reactants and the nature of the catalyst, the reaction produces either thermoplastic resins (novolacs) or thermosetting resins (resols). Thus, in the presence of acid catalysts (usually hydrochloric or oxalic acid) and an excess of phenol, novolac resins are obtained; in the presence of basic catalysts, such as sodium hydroxide or ammonium hydroxide, and an excess of formaldehyde, resols are formed.

Phenol-formaldehyde resins harden during processing upon heating; with novolac resins, however, a hardener is required (usually hexamine, in an amount equal to 6–14% of the weight of the resin). The hardening of resols involves an initial (A), an intermediate (B), and a final (C) stage. In the A stage, the physical properties of the resin (resol) are analogous to those of novolac resins since resol dissolves and melts. In the B stage, the resin (resitol) has the ability to soften upon heating and swell in solvents. In the C stage, the resin (resite) neither melts nor dissolves.

The hardened resins are characterized by high resistance to heat, water, and acids and good dielectric properties; combined with fillers, they have great strength.

The phenol-formaldehyde resins are used in the hardening of epoxy resins in order to impart higher resistance to heat, acids, and alkalies. The former are the resins most commonly used in the production of many types of plastics. Novolacs are used to obtain molding powders, and resols to obtain molding powders and plastic laminates.

Resin contains curing agents, which is important for the pad hardness. The amount of curing agent is precise because cracks can be observe if there is too much (the gas appearing during pressing cannot escape from the pad at moulding step) The second important property of a resin is flow; flow is the distance the resin will flow before hardening. Flow can influence the porosity of the pad. A typical preferred flow for the phenol-formaldehyde resin is 25-35 mm. The current resin used in the formulation is described in table 2.1:

Specifications	Melting point	Hexamine content	Flow at 125°C	Free phenol	Gel time at 150°C	Loss 135°C	Particle size 200µ	Particle size 100µ	Particle size
	°C	%	mm	%	mm	%	%	%	%
	85 - 95	% 8.5 - 9.5	25 - 35	0.2 - 0.8	1.2 - 2.2	0.5 - 1.2	0 max.	0 - 3	0 - 2

Table 2.1: Novolac Resin F129: ground phenolic resin, based on Novolak-Hexamine

Rubber
Rubber is a hyper-elastic materials which, as most elastic materials, stores energy when a force is applied, unless strain energy is stored thermally, and the resulting kinetic energy is released as heat. Rubber relaxation is endothermic, and for this reason the force exerted by a stretched piece of rubber increases with temperature (fig. 2.1.a).

Barites
Baryte is a natural Barium sulphate $BaSO_4$ and is used in applications such as friction linings, primers, putties and adhesives and as a filler in coatings, plastics, rubber and ceramics. In practice this is usually the mineral baryte (fig. 2.1.b).
Most baryte is grounded to a small, uniform size before it is used as a filler or extender, an addition to industrial products, or a weighting agent in petroleum well drilling mud.

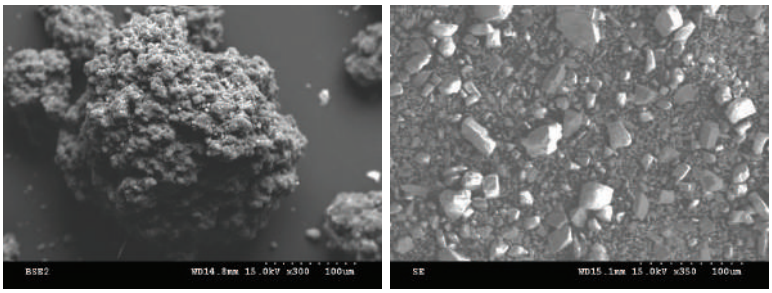

(a) Rubber (b) Barites

Figure 2.1: Binders and fillers observations

2.1.1.2 Abrasives

Aluminium oxide
Aluminium oxide is used for its hardness and strength. It is widely used as an abrasive, including as a much less expensive substitute for industrial diamond. It has a low heat retention and low specific heat.
Aluminium oxide can be grown as a coating on aluminium by anodising or by plasma electrolytic oxidation. Both its strength and abrasive characteristics originate from the high hardness (9 on the Mohs scale of mineral hardness) of aluminium oxide.

Synthetic hydrated calcium silicate
Synthetic hydrated calcium silicate (or Promaxon-D, the commercial name) is an open inner structure surrounded by an outer shell of close knitted needle-like crystals. The chemical structure of Promaxon-D corresponds with the known mineral Xonotlite $Ca_6Si_6O_{17}(OH)_2$. By means of a special crystallisation process and controlled crystal growth, particles are produced with a more or less spherical morphology.

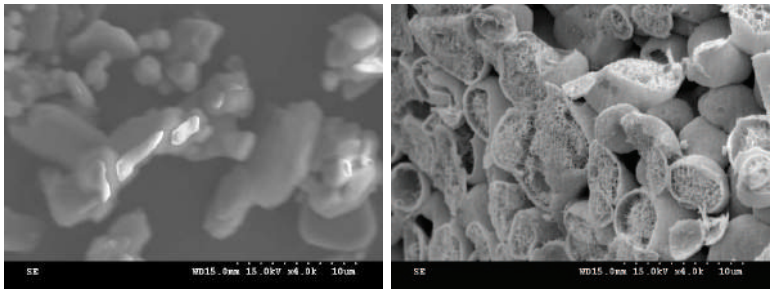

(a) Aluminum oxide (b) Synthetic hydrated calcium silicate

Figure 2.2: Abrasives observations

2.1.1.3 Lubricant

Braking is a high-energy mechanism and so it must not be felt rough by the driver. So, lubricant materials are used to smooth in order to have a progressive braking phase.

Two raw materials are used to obtain a lubrication function in the friction materials: synthetic graphite and tin-sulphide. Synthetic graphite is comming in two shape: the smaller size is dedicated to lower temperature and the higher is effective in high temperature (higher than 200°C).

Element	Min %	Max %
Sn	60	-
S	19	24
C	-	1.8
Fe	-	1

Table 2.2: Tin-sulphide composition

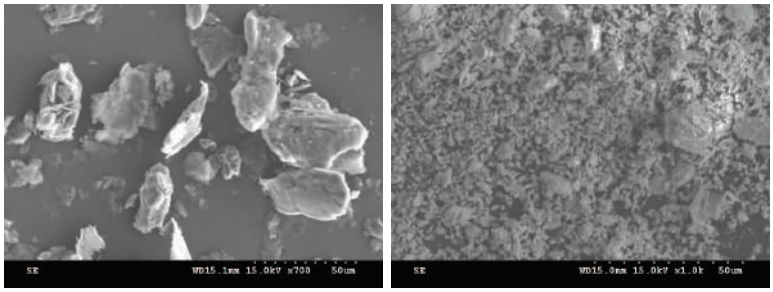

(a) Graphite (b) Tin Sulphide

Figure 2.3: Lubricant observations

2.1.1.4 Fibres

There are mainly two-types of fibres in friction materials and both are used in the formulations tested. The first type of fibre is short steel fibre in opposition of the second type, mineral fibers which are inorganic materials issued from rock as coke, lime or diabase. Their mechanical behaviour and surface treatment result in better reinforcement properties under extreme braking conditions. It is a chopped mineral formed at high temperature (1400°C) in continuous fibres for application in friction materials. The product is designed to maintain its dimensions during dry mixing but must not at high speed. Mineral fibres can be implemented into the formulations as single fibres, or in matrix-coated fibres (figure 2.4). There are many advantages of using these kind of geometry:

- Easy processing
- High reinforcement
- High temperature resistance (softening point > 800 C)
- Stable friction performance
- Reduced noise generation
- Alternative for other reinforcement fibres (e.g. steel fibres)
- Non-corrosive material

Fibre orientation is important into friction material production. With natural gravity, the fibres will lay down in the mould/pad transverse direction. This will impact consequently the orthotropy of the final pad. Both types of mineral fibres and steel fibres are used in the simplified formulations.

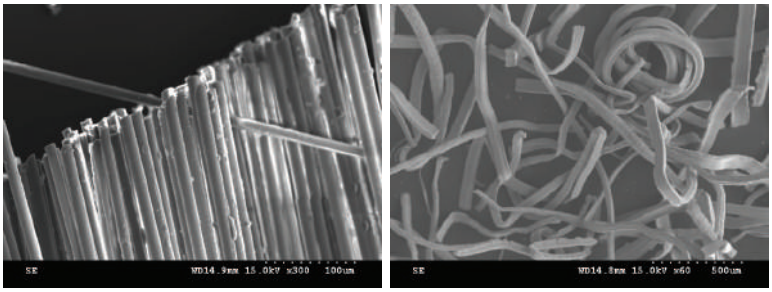

(a) Matrix-coated fibres (b) Steel fibre

Figure 2.4: Fibres observations

2.1.1.5 Granulometry

Size and shape of raw materials are key parameters in the product compaction at production stage. It will condition the overall porosity and further on brake application, the debris generation and tribo-layer nature. It must be controlled and known. Table 2.3 describes the geometry of each raw materials. The granulometry and hardness values in Moh of each raw materials. give a hint of the general dispersion which will be encounter thereafter, as far as the natural heterogeneity of the final product.

	Type	Industrial reference	Granulometry (µm)	%	Diameter (µm)	Length (mm)	Hardness (Moh)
Raw Materials	Binder	Novolac resin	<200	0	<25	-	-
			<100	2			
			<75	3			
		Rubber	<40	98	250	-	-
			<80	80			
	Abrasive	Aluminum oxide	<45	95	<25	-	9
	Lubricant	Synthetic graphite (Fine)	<75	96	<25	-	1.5
		Synthetic graphite (Coarse)	500-2000	90	1000	-	1.5
		Tin Sulphide	-		<25	-	1,5
	Inorganic fibres	Mineral fibres	-		5.5	230±50	6
		Matrix coated mineral fibres	-		14	9	6
		Steel fibre	<1000	1	60	0.8	6.5
			<500	5			
			<250	10-20			
			<125	20-30			
	Filler	Barites	<45	99	<25	-	3-3,5
			<32	96			

Table 2.3: Raw materials granulometry used in the three simplified friction material formulations

2.1.2 Process

In figure 1.3, it has been seen fabrication process can be sum-up in 3 principal steps: mixing, moulding & curing which are described in this subsection. The process used here is the same for all 3 formulations.

2.1.2.1 Mixing

In order to produce a homogeneous mixture of the materials, the compounds of the selected formulation are mixed. Before mixing, a bag containing the raw materials is prepared. Each raw material is quality-controlled and weighted according the formulation, then the bag is stored. After one night storage in the laboratory (humidity: ±50%, room temp.: ±23°C), all the materials are added into the mixer and totally mixed for 2 minutes at 2000rpm. This mix cycle is divided into two steps of 1 minute because constant mixing for 2 minutes will cause the mix to get too warm, which causes the resin to start flowing. The temperature rises up slowly during mixing. Mixing speed can be adjusted while pouring fragile materials as mineral fibers if it is necessary to not have them chopped off.

2.1.2.2 Moulding

Moulding is the production step where the mixed powder are compacted into a pad shape. There are two types of moulding:

- Hot moulding which always takes place above the curing temperature of the phenolic resin. In order to minimize the hot moulding duration, it is desirable to maximize the temperature. However, a too fast curing of the resin will cause blistering. The applied pressure depends on the formulation (binder content, thermal conductivity) and its desired porosity. Due to some internal reaction with and/or between some raw materials, degasing several time during the process might be necessary.

- Cold/warm moulding takes place below the curing temperature of the resin. To reach the desired porosity the pressure needs to be significantly higher than pressures applied during hot pressing. Because the resin doesn't need to cure during the pressing, the press time is very short compared to hot pressing. Warm pressing typically lasts longer than cold pressing to give the heat time to penetrate into the material. Heat will make the resin sticky and improve the quality of the warm pressed materials.

Warm moulding is used in the following work. During moulding process, pads are pressure controlled at 93MPa during 2 minutes. Since the temperature is below 90°C, most materials might not transform consequently. It must be noticed that 80% of the friction material is shaped at the moulding stage.

2.1.2.3 Curing

The curing process follows after the pressing cycle, which plays an important role in forming the pads. During curing, resin gets enough time and temperature to flow and react. Generally, a short moulding process should be combined with a relatively longer curing.

Pads that are cold moulded, can be very brittle before curing because the resin might not fully react during moulding. This means that the pads need to be handled carefully from the moulding to the curing process. After curing however, cold moulded pads have comparable hardness and strength to hot moulded pads.

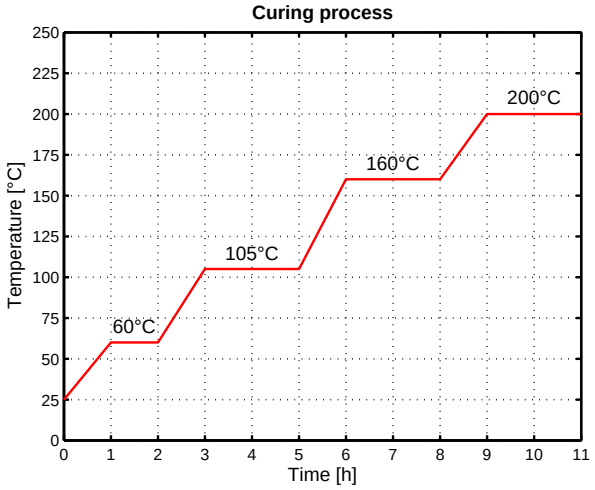

Figure 2.5: Curing program used for simplified formulations A,B & C

2.1.3 Current process & variations on formulations

A reference material, identified as Ref., is chosen as a referee in term of properties and performances. It is a commercial unknown formulation which is currently used in Chassis Brakes products.

Table 2.4 sums-up the process of manufacturing simplified brake pads used in this work. For the need of this study, several formulations have been designed by the friction material supplier with only 10 components for each one and 3 formulations were retained. Table 2.5 describes the percentage in volume on the total volume of the pad for each raw materials.

Process step	**Mixing**				**Warm Moulding**				**Curing**		
Variable	Temperature	Time	Speed	Humidity	Mould Temp.	Pressure	Time	Degassing	Time	Temperature	Pressure
Unit	°C	minutes	RPM	RHm	°C	MPa	minutes	cycle	hours	°C	bars
Current	90	2	2000	50	90	93	2	no	11h	200	5

Table 2.4: Current process parameters of simplified formulations A, B & C

Raw Materials % in volume/total volume	Binder				Abrasive		Lubricant			Inorganic fibres (strength)		
	Novolac resin	Rubber Coarse	Rubber Fine	Barites	Aluminum oxide	Synthetic hydrated calcium	Synthetic Graphite Coarse	Synthetic Graphite Fine	Tin Sulphide	Mineral fibres	Matrix coated mineral fibres	Steel Fibres
Formulation A	15	x	10	37.6	0.4	x	12	2	3	12	4	4
Formulation B	15	x	10	41.6	0.4	x	12	2	3	12	4	x
Formulation C	15	10	x	38.6	0.4	3	12	2	3	12	0	4

Table 2.5: Formulation variations in term of raw materials proportions (in volume percentage of total volume)

One can notice formulations Form.A and Form.B are really close, the main difference leaves on the steel fibre missing in the Form.B formulation which is compensated by barites. The evolution with theses formulations and the Form.C is the type of fibre used and the type of rubber. The matrix coated fibres are removed and the rubber is changed for a coarse one. The aspect of formulation C is more regular than formulation A and B, which suggests a more homogeneous material in term of size of raw material. Also, synthetic hydrated calcium is added. Figure 2.6 shows the macroscopic differences regarding visual aspect. Formulations A & B have more coarse particles comparing C.

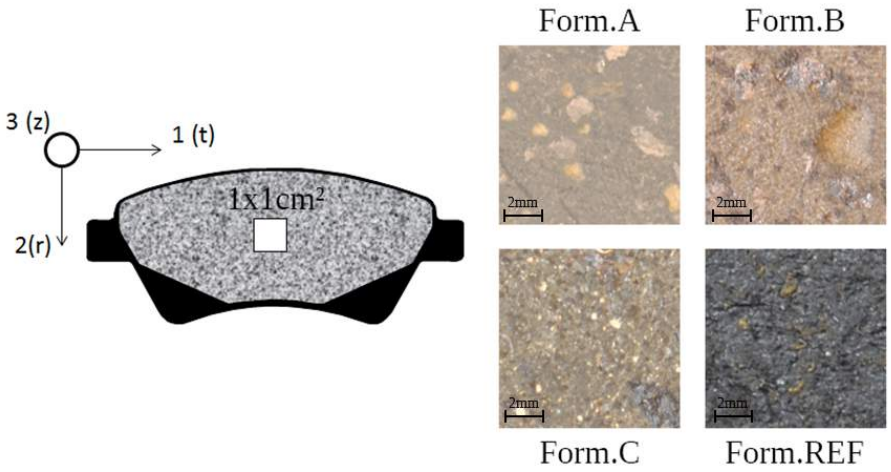

Figure 2.6: $1 \times 1cm^2$ macroscopic picture of 4 pad with differents formulations

2.1.4 Simplified brake pads properties regarding industry requirements

Compressibility testing The compressive strain of a brake lining is an important design parameter in the evaluation of brake-fluid volume displacement, brake-pedal travel and the propensity for judder or noise.

Most brake system suppliers uses the [ISO6310:2009, 2009] norm. It is still the standard compressibility test which is considered as robust to compare pads from one batch after manufacturing. Compressibility test according to ISO 6310 is performed on a heating plate, simulating the rotor. Various forces are applied (from 20 to 160 bars) to the support by means of a stamp representing a brake piston. The type of piston depends on the targeted brake system in term of shape, contact area, etc.

The test is about measuring the relative thickness reduction during a cycling compressive test at two different hot plate temperatures, 20 and 200°C. By representing the hysteresis cycle load/deformation, the viscoelastic behaviour of the friction material is displayed and an elastic modulus can even be estimated. For example, a low thickness variation suggests a rigid brake pad.

As a quality control, formulations have been tested regarding compressibility. Chassis Brakes requirements are between 150 to 200μm. Only test at 20°C is studied. Figure 2.7 shows these results and thus justify the choice of formulations. Form. A & B compressibilities are mean values on 10 samples, as for form. C & Ref. (with additionnal deviation). Simplified formulations are almost equivalent, with a little more compressibility from the formulation C which might be due to the synthetic hydrated calcium presence which is a highly porous material. Ref. material has a higher compressibility which can be explain by one main possibility: between the backplate and the friction material, there is glue (as in simplified formulations) but also an underlayer (only in Ref. formulation) which can increase compressibility subsequently. Studies as [Matozo et al., 2006] as shown the impact of such addition versus material without it. In a more general analysis on material C & Ref., the compressibility deviation is important, even for a commercial formulation, and this measurement has to be taken into account with caution.

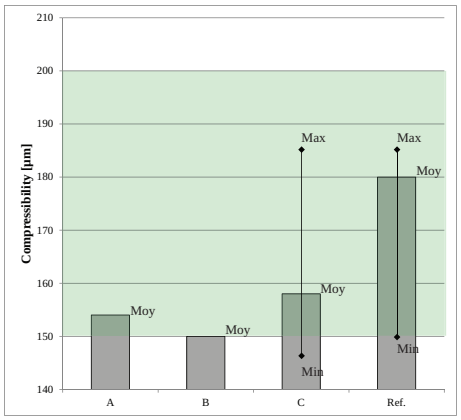

Figure 2.7: Compressibility value for each formulations versus formulation Ref.

In order to verify if a pad responds to industry requirements, interesting measure for the industry is frequency response and damping of components. It provides understanding of structural dynamic characteristics of the components and brake system. Also it gives a "Quality Control" of components regarding their dispersion from a batch to another, as far as compressibility testing of brake pads.

The easiest and most accurate for the frequency list of modes of a structure method is measured by impact. The structure will be affected at different points referenced via a hammer (for effort) and the resulting displacement will be increased by an accelerometer. Depending on the direction and the position of the impact and the accelerometer response mode is more or less strong. It is therefore necessary to perform measurements on these points in three directions, if possible.

Thus , the frequency response of the component $H(\omega) = \frac{X(\omega)}{F(\omega)}$ can be plot: with X the displacement and F the force given by the hammer. The frequency response (or FRF) gives the free modes of the structures (represented by stable poles on the FRF curve) and the equivalent damping. This method of measurement provides a comprehensive list (if you have the good points of excitation and response) and particularly precise view of structure natural frequencies. It is quick and inexpensive. Component modal test measures natural frequencies, modal damping ratios, and/or mode shapes of pad, rotor, insulator, caliper, anchor bracket, knuckle, etc.

Chassis Brakes requirements are approx. 0.8 for frequency response/damping. Results regarding this data is shown in table. 2.6

	Damping				
	3.2kHz	4.8kHz	6.7kHz	9.8kHz	10.3kHz
Form. A	0,9	0,93	0,92	0,83	0,7
Form. B	0,92	0,95	0,86	0,92	0,73
Form. C	0,91	0,83	0,82	0,76	0,61

Table 2.6: FRF response of pad and damping per frequency range

2.2 Physico-chemical testing

Friction material is known to be transforming under temperature generated by friction. Gradient of temperature can be easily important in few seconds of contact with the disc. It has been seen in the literature transformations on contact surface such as compacted plateaus. composed of raw materials debris. This section is showing the transformations under temperature for raw materials and those of the complete pads. Correlation is intended to check the main components unstable during friction. Several tests are used for this analysis:

- Thermogravimetry gives an information on the weight loss (and gain) of the material tested through temperature (all samples which are $50mg$ of reduced powder are tested in oxygenated atmosphere, near to braking conditions from 25 to 800°C). Main signal gives weight loss with temperature and the derivated signal is also studied in order to get transformations peak temperature.
- Dilatometry measures the linear elongation of the material through temperature. Samples are cylinder of $\phi 8mm$ and $15mm$ long, and their elongation is measured through 3 cycles from ambient 4 to 400°C.
- Dynamic Mechanical Analysis tests the friction material intrinsic mechanical properties (normal and/or transverse) but with frequency and temperature (in the atmosphere environment)

2.2.1 Raw materials evolution with temperature

Resin The resin used for the pads is a phenolic resin moulded at 90°C and cured at 200°C. It is assumed the resin as already begin polymerisation at moulding stage and not yet finished at curing. Figure 2.8 compares the two states of the resin with thermogravimetry test by tracing the weight loss in percentage (blue) and its derived signal so it is easily to find the key temperatures.

It appears resin which has already seen 200°C doesn't react until it passes this temperature level. Then it continues its transformation. After, a certain level of temperature (>450°C) the resin starts to degraded and loses more than 60% of its initial weight.

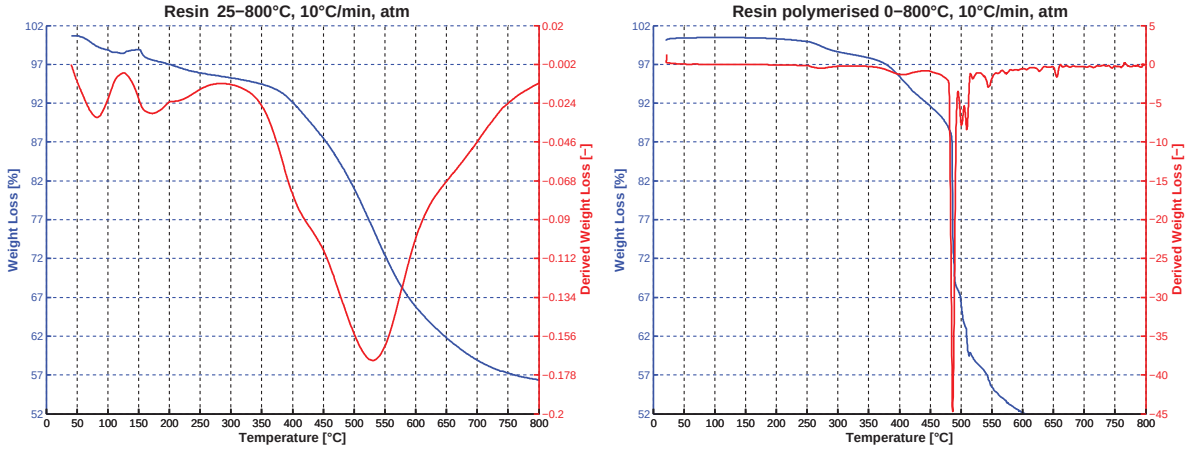

(a) Resin

(b) Polymerised resin (at 200°C)

Figure 2.8: Thermogravimetry of resin w/o and with initial polymerisation

Rubber The thermogravimetry of rubber is shown in figure 2.9. The rubber starts to react and lose weight at 200°C. After, a certain level of temperature (>450°C) the rubber starts to degraded and loses more than 50% of its initial weight and seems to be destroyed with temperature.

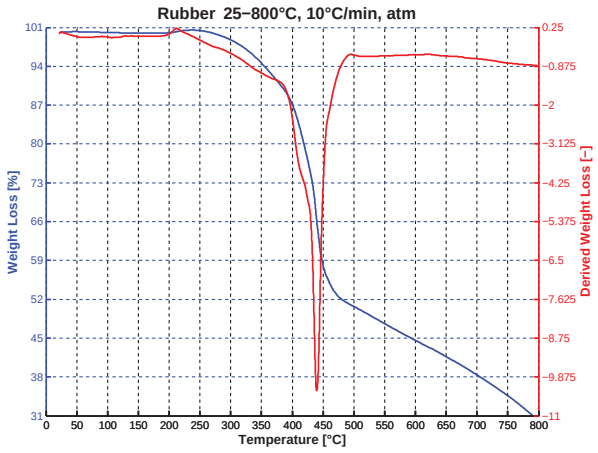

Figure 2.9: Thermogravimetry of rubber

Less impacted raw materials Figure 2.10 shows other materials which are susceptible to react but the measurement shows temperature doesn't impact them significantly. Looking at the weight scale of these figures, there is almost nothing going on for graphite, steel fibre and tin sulphide. Barites and mineral fibres are not tested because of their fusion point higher than the bracking application (>1400°C).

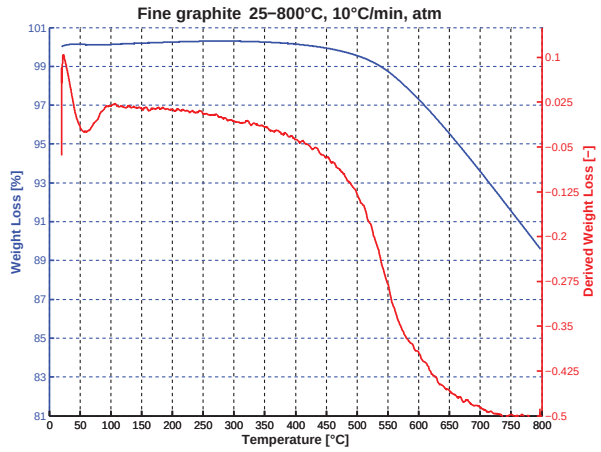

(a) Fine graphite

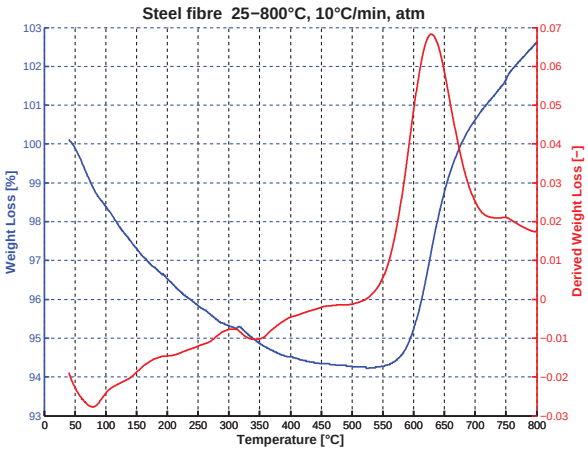

(b) Steel fibre

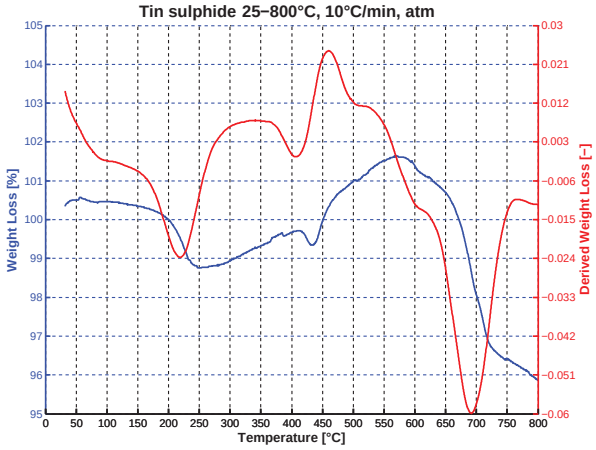

(c) Tin sulphide

Figure 2.10: Thermogravimetry of other raw materials

2.2.2 Complete friction materials

Thermogravimetry

Following the raw materials weight loss under temperature measurement, the same has been done on complete friction materials. Figure 2.11 shows the same cycle as raw materials. Key temperatures appears for both simplified formulations (A & C) at 250°C and 450°C which are closed to the temperature seen for resin and rubber degradation. Ref. material seems to have the same temperature behaviour which suggests raw materials equivalent to resin and rubber into its formulation.

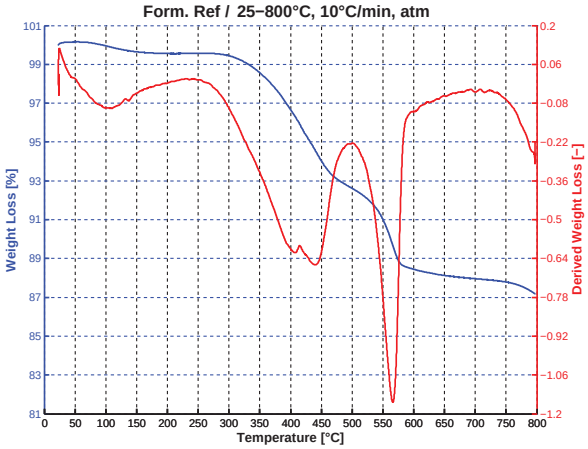

(a) Form. Ref. (industrial form.)

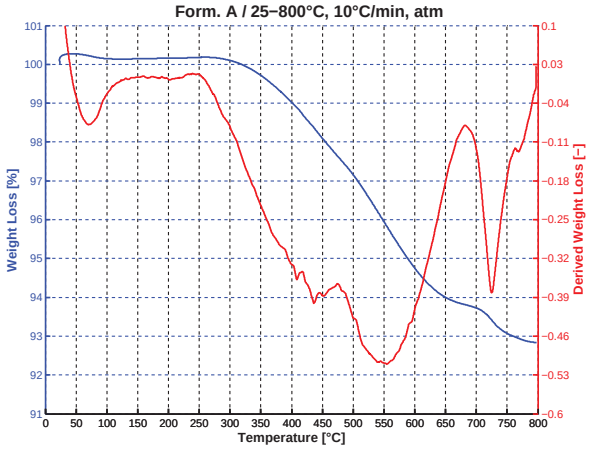

(b) Form.A

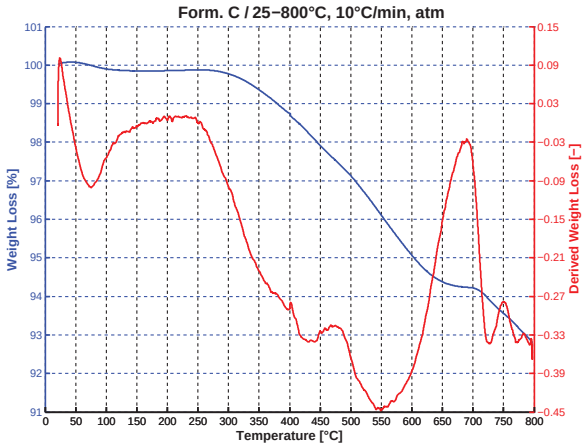

(c) Form.C

Figure 2.11: Thermogravimetry of friction material formulations

Dilatometry

Samples from friction materials Ref. and C are tested via 3 successive cycles from ambient to 400°C, under azote atmosphere. Only temperature rising parts are shown (see figure 2.12).

During first temperature rising, the samples (especially formulation C) are shrinking after 200°C. The shrinking might be due to the polymerization reactivated above what has already seen the material. The shrinking appears only between certain temperature and then takes over the expansion which leads to a negative $dL/dL0$. Thereafter, shrinking loses in intensity because the chemical transformations must have been stabilized and non-reversible, and the expansion takes over leading to a positive $dL/dL0$. Cycle after cycle, the material is less dilated with temperature and seems more stable: there is a kind of history effect. Looking at thermal expansion, Ref. and C have the same trend but the proportions are higher for formulation C.

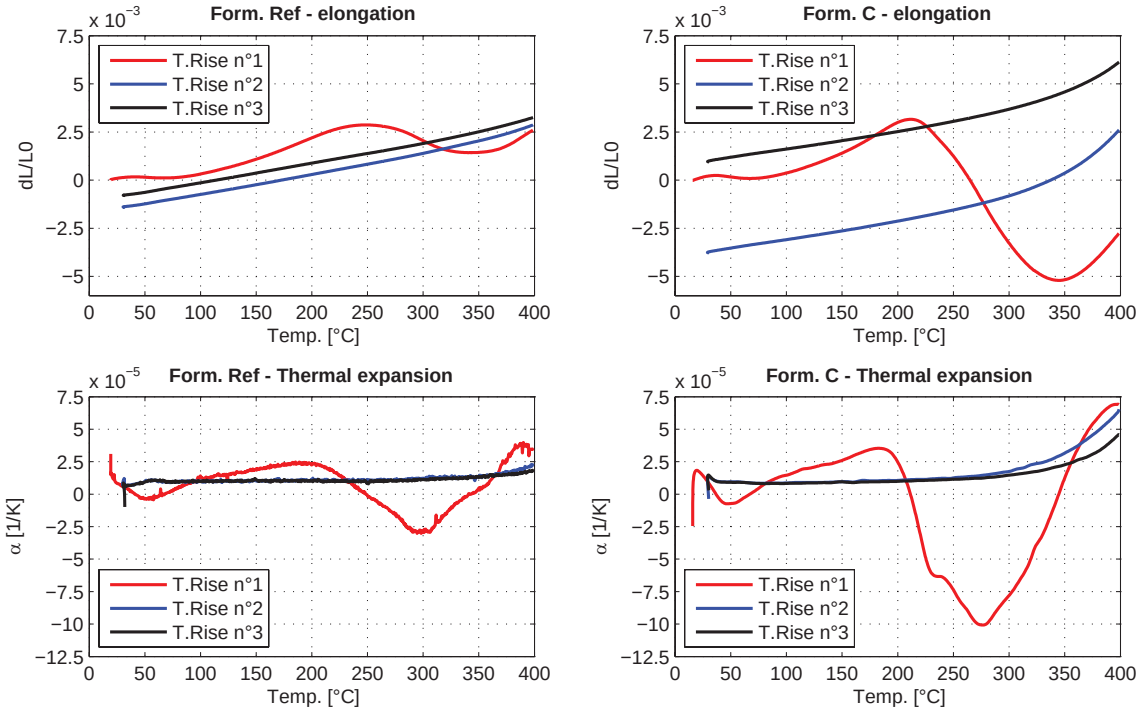

Figure 2.12: Thermal elongation & expansion of Form. REF vs. Form.C

Dynamic Mechanical Analysis

In order to have an overview of the viscoelastic behavior of the simplified formulations, Dynamic Mechanical Analysis has been performed to measure the formulation Form.C. This measurement is useful in the identification of the rheologic behaviour of materials, coupled with temperature effect.

The device apply, under ambient atomosphere, an oscillating force in 3-point-bending sollication and record an oscillating sample response. Modulus is calculated from the elastic response; e.g. sample response "in phase" with applied oscillatory stress. Loss factor is calculated from the viscous response; e.g. sample response "out of phase" with applied oscillatory stress. The friction material has been sampled from $\phi 70mm$ round pads (fig. 2.13). These samples have been measured in 3-point-bending mode with a free bending length of $40mm$ on the normal direction (axis of moulding): the samples were prepared in a way that the stress during bending is applied perpendicular to the brake pad thickness. 4 tests have been done at 4 differents frequencies.

The applied force was limited to a maximum of 1N and the dynamic amplitude to $10\mu m$ (approx. 0.01% of strain). The measurement parameters are listed below in table 2.7.

Sample Holder	Temperature range	Heating rate	Atmosphere	Max dynamic force
3 point bending	25 to 600°C	3K/min	air	1N
Max. deform.amplitude	**Frequency**	**Free bending lenght**	**Sample Width**	**Sample thickness**
±10µm	[1; 3.33; 10 ;33.3] Hz	40mm	10mm	2.4mm

Table 2.7: DMA - Measurement parameters

In figure 2.14, the multifrequency measurement is shown for sample Form.C in a temperature range from 25°C to 600°C. It can be observed that after a decrease in storage modulus E', the slope changes at around 250°C and the modulus increases again until 480°C. The increase in E' is accompanied by a decrease in the loss factor (tan δ) of the material.

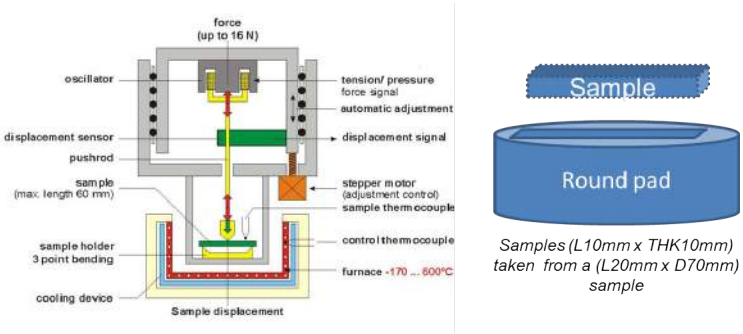

Figure 2.13: DMA - Schematic design of test device and sample preparation

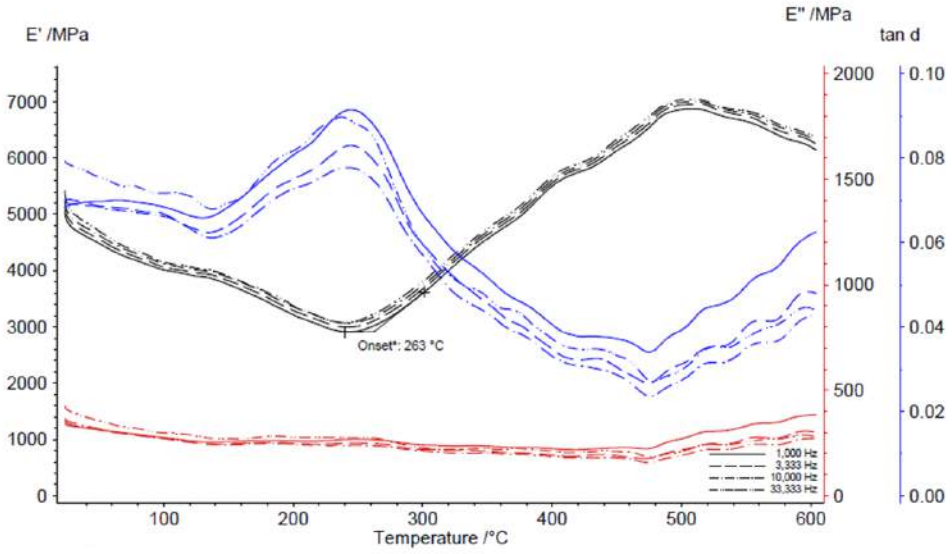

Figure 2.14: Multifrequency measurement for sample Form.C: storage modulus E' (black), loss modulus E" (red) and loss factor tan δ (blue).

One can notice the Form.C thermogravimetry diagram has shown the same peaks of temperature: a peak at 250°C and one around 450°C. This in turn corresponds to the mass loss step in the enclosed thermogravimetry curve and can be interpreted as decomposition or oxidation of organic resin in the brake pad matrix. Comparing with dilatometry, there is also a stiffness loss around 250°C, which is recovered and even increased passed this step of temperature.

2.2.3 High temperature influence on organic friction material: conclusions

It this section, it has been shown the friction material dependency to process temperature and its conditioning for further application. The final product will only be stabilized below maximum temperature seen in its whole manufacturing. The simplified formulations are designed and processed below 200°C. Also, raw materials are sensible to characteristic temperatures. Hence, there seems to be two threshold temperatures for the three simplified formulations:

- at 250°C: it is mostly due to the resin which has not finished is polymerization at the end of curing
- at 450°C: the resin and rubber are starting to be degraded at this temperature level and these peaks are seen

on all three materials thermogravimetry.

Even if the reference formulation is clearly not the same, the threshold temperatures are the same.

One can imagine what will be the consequences on friction material behaviour during first braking applications: on dilatometry, shrinking appeared after 200°C but the whole sample was heated. On a brake system, the temperature gradient is applied on the contact surface with the disc, so the material transformation won't be uniform. There will be a non-homogeneity of structure along the material. Also, heat conservation is influenced by conductive raw materials. Steel fibres which are only into formulations A and C make the materials conductive.

Finally, it has been seen friction material has a strong dependency on history. Cycling temperature increases, the material response is different from a cycle to another (as seen with dilatometry measurement). Thus, it can be foreseen the same subsequent braking will have a different response than the previous one. Since braking applications are passing by these tempartures threshold, these conclusions must be taken into account.

2.3 Stiffness of friction materials using static and dynamic measurement techniques

Throughout the years, to obtain mechanical properties, methods based on compression tests offered the ability to have static/quasi-static behaviour regarding the loading. International standards as [ISO6310:2009, 2009] evaluate compressive strain on the brake lining (pad+backplate) with preload and can give material constants to feed models.

Linking the material properties to the dynamic behaviour during braking is a complex problem and many studies have been done to study the dependency of loading and frequency on brake pads as [Wegmann and Stenkamp, 2012] or [Sanders et al., 2008] showed. [Hornig and Von Wagner, 2013] analysed the stiffness dependency on static and dynamic loading, and observed there is a large influence of preload on stiffness. In many experimental and numerical approaches, pads have often been considered with transverse-isotropic homogeneously distributed elastic properties. If some experiments deal with the heterogeneity of friction material elastic properties, few have shown it on a static and dynamic scale and the influence on finite-elements brake systems stability analysis is hardly known.

To screen the nonlinear viscoelastic frequency- and load-dependencies, the present investigation goes through the study of heterogeneity by confronting three methods: a classic compression test, a mapped compression test and a non-destructive test using ultrasonic propagation.

2.3.1 Preliminary testing

Preliminary compression tests have been done on cylinder shape samples (diameter $\phi 10mm$, length $20mm$) for the three simplified formulations. Contact surfaces are polished. The samples are taken in normal and transverse direction of the pad. Each sample is tested on a compression cycle up to 1000N 3 times ($\sigma_{max} \approx$ 20MPa). Force/displacement are measured. Set-up and results are presented in figure 2.15. Formulation C is stiffer in transverse direction than formulation A and B which are almost similar. The trend is different regarding normal direction. A is stiffer than B which can be explain by the removal of steel fibres. Also, C is softer than A and B. The lack of matrix-coated fibres might be the main reason. The non-isotropic behaviour is highlighted, in accordance of many research, as in [Brecht et al., 2003]. At last, non-linear behaviour is shown and might be caused by porous materials as synthetic hydrated calcium or rubber.

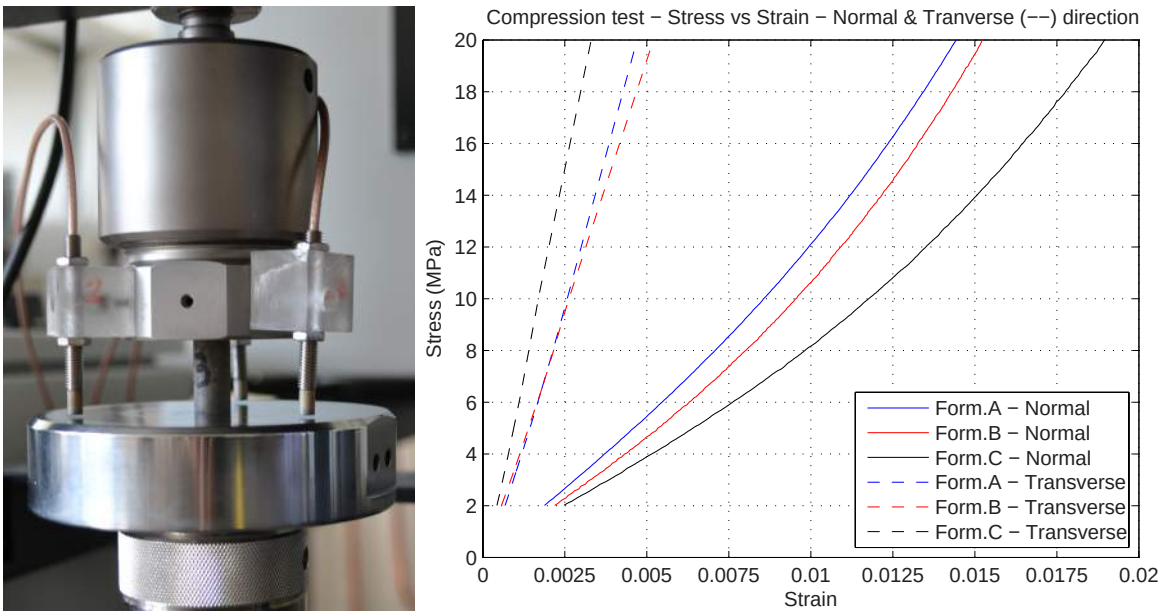

Figure 2.15: Compression test on cylinder samples - Normal and transverse responses

With these datas, a normal elastic modulus load-dependant can be estimated, taking the tangent slope of the $\sigma = f(\varepsilon)$ curve. In figure 2.16, a tangent value of the elastic modulus is determined from $\sigma = f(\varepsilon)$ (cf. fig.2.15) according 1-D Hooke law. It is observed modulus increase-rate through loading is almost the same for all three simplified formulation. It is confirmed formulation C has the lowest modulus with 750MPa (at $\sigma = 4$MPa), B is following with 900MPa and A is the highest with 1100MPa.

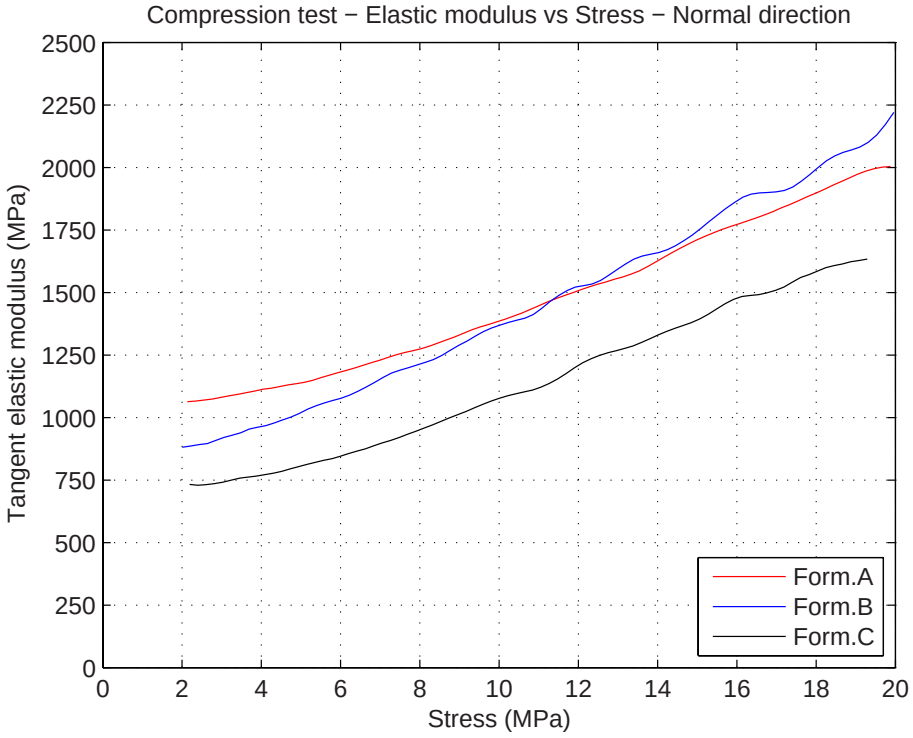

Figure 2.16: Evaluation of normal elastic modulus regarding load

2.3.2 Mapped compression test

For the following investigation of friction material properties distribution of brake pads, quasi-cubic $15 \times 15 \times 11 mm^3$ (r,t,z described in fig.2.17) friction samples are prepared on several locations of the pad following two different procedures. Samples are machined are machined and detached from the backplate and underlayer. These samples are investigated with static and ultrasonic methods. Directions 1, 2 and 3 define respectively the tangential, radial and normal directions. For each formulations, four pads are tested.

The test runs in a classic Instron compression machine with a special tool designed to charge one square sample.

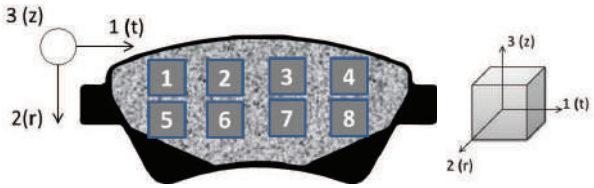

Figure 2.17: Friction material samples conditioning for compression test - First cycle

One force cell measures the axial force and three capacitive sensors measure the z-axis displacement. Two additional capacitive sensors are put in the transverse x-axis direction to read the Poisson ratio, which is not presented in this

work. The sensor setup is used for samples with and without backplate as shown on figure 2.18. Only tests without backplate are studied.

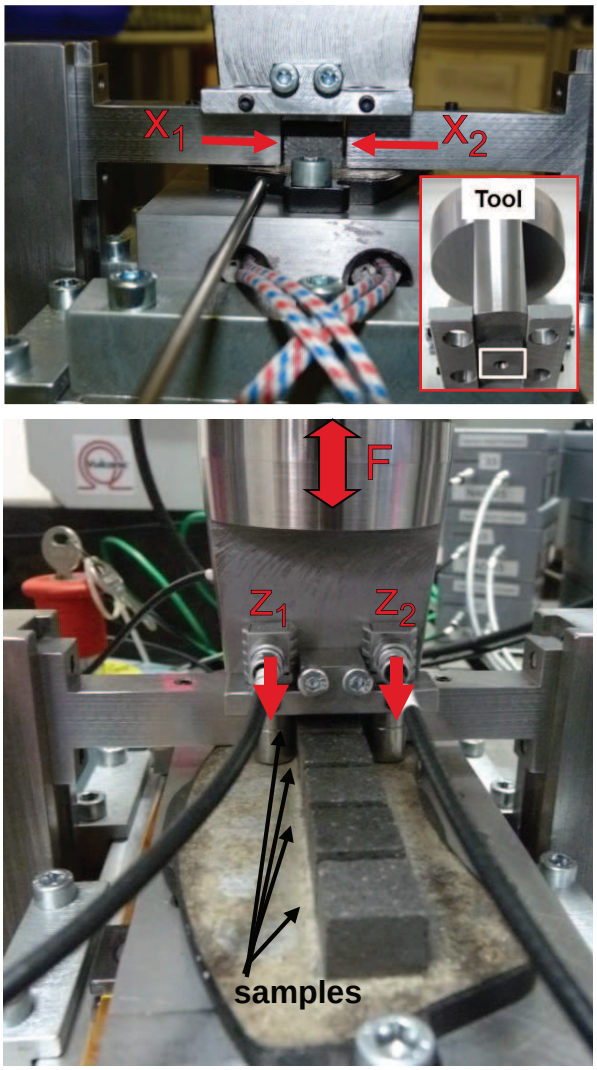

Figure 2.18: Compression test setup and sensors orientation

It is well established that friction materials have a strong load-dependency, which makes them non-linear. Therefore compression tests screen friction material under 0.5MPa, 1MPa and 1.5MPa preloads which are representative for average brake pressure application conditions at 10bar, 20bar and 30bar ([Yuhas et al., 2006]). For each preload condition, the sample is compressed with a 0.25MPa amplitude sinusoidal force at 0.5Hz during ten cycles. After a few cycles, creep effects can be neglected.

In order to confirm the comparison with a classic compression test, figure 2.19 shows the same trend regarding formulations in fig.2.15.

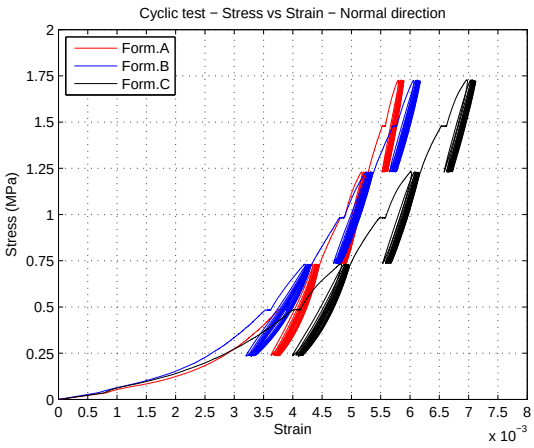

Figure 2.19: Compression cycle test - $\sigma = f(\varepsilon)$

Elastic modulus is identified using 1D-Hooke's law. For normal elastic modulus, it states:

$$E_z = \frac{k_z \times L_z}{L_x \times L_y} \tag{2.1}$$

with k_z the normal sample bulk stiffness and L_x, L_y, L_z the sample dimensions. For in-plane directions, it states with u being the x- or y-axis:

$$E_u = \frac{k_u \times L_u}{L_u \times L_z} \tag{2.2}$$

The mentioned cycle-patterns are programmed on the compression machine and dedicated in-house software is developed in Matlab environment for an automated post-processing. The identification focuses on elastic modulus in this study. For more robust results, all elastic parameters are identified with 1/4-Cycle overlapping e.g. forty values are extracted from ten cycles. elastic modulus is deduced from material stiffness, itself calculated by least square fitting on force-displacement hysteresis. Additionally, uncertainty analysis is performed and guaranties an uncertainty for elastic modulus estimated between 2% and 20%. The worst case happens when the material is stiff and the applied force is low, which implies very small material strain. The elastic modulus for each sample are lower than those in the preliminary tests due to the geometric difference of the samples and the set-up/cycle.

2.3.3 Ultrasonic test

The ultrasonic test consists of measuring wave travel-duration through the material square-sample by two transducers. The first one is used as an emitter and plays an ultrasonic wave, the second one is used as a receiver and listen to the ultrasonic wave as mentioned in figure 2.20.

For dynamic compression properties testing, the technique uses longitudinal wave propagation at 1MHz. This frequency ensures a wavelength which lies between $1mm$ and $2.5mm$ depending on material stiffness and size. Consequently, at least four wave-oscillations happen while the wave travels through a $10mm$-thick sample. Besides, the ultrasonic wavelength never reaches the fibers- and porosity-scale below $1mm$ and ensures a material averaging effect.

Ultrasonic testing identifies the wave travel-duration t, from which the longitudinal wave velocity v_l is deduced. The material stiffness C_{ii} in the i-direction is proportional to the square velocity of the wave traveling along length l_i through area $l_j \times l_k$ and material density ρ:

$$C_{ii|i=1,2,3} = \rho.V_L^2 \equiv \frac{m}{t^2}.\frac{l_i}{l_j l_k} \tag{2.3}$$

which leads to elastic modulus $E_{ii} = k_{ii}.C_{ii}$. k_{ii} is a weighting function of all Poisson ratios and its mathematical expression depends on transverse isotropic material structure hypothesis. For the purpose of this study, Poisson

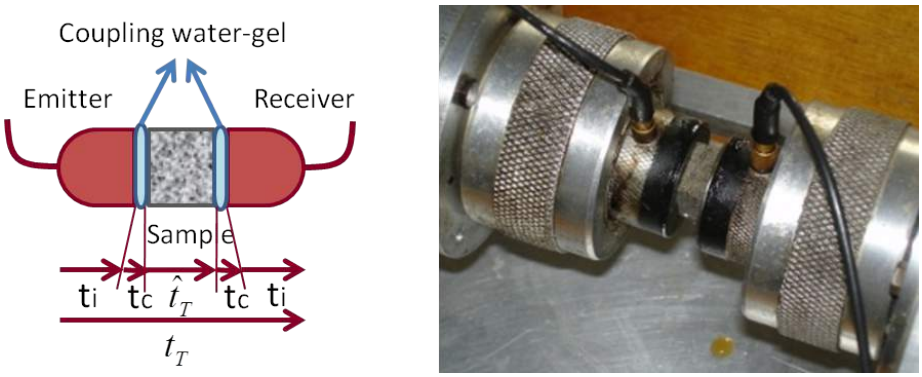

Figure 2.20: Ultrasonic testing transmission setup

ratios are taken from [Brecht et al., 2003]. Poisson ratios and weighting functions k_{ii} are presented in figure 2.21. The knowledge of this function allows defining the ratio between stiffness coefficients C_{ii} and elastic moduli. In-plane tangential- and radial-moduli are bounded between 75% and 100% from the stiffness. Normal modulus is bounded between 92% and 100% from the normal stiffness.

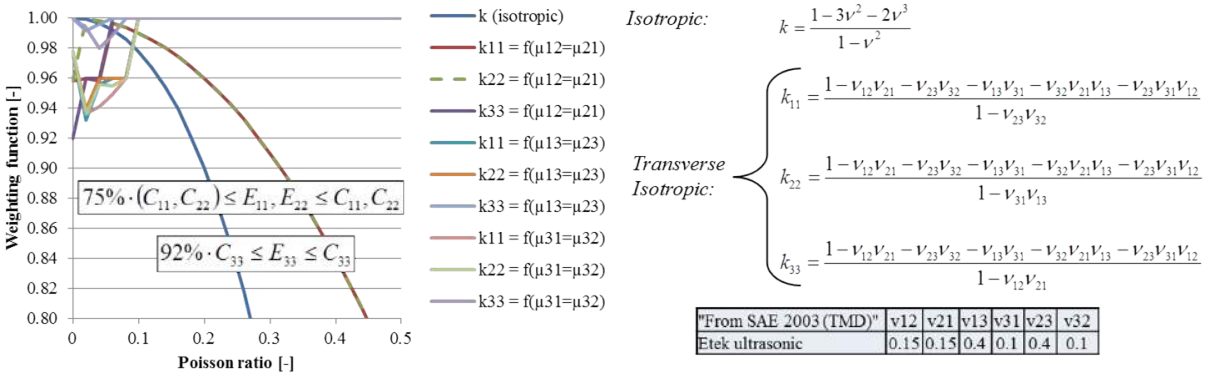

"From SAE 2003 (TMD)"	v12	v21	v13	v31	v23	v32
Etek ultrasonic	0.15	0.15	0.4	0.1	0.4	0.1

Figure 2.21: Weighting functions k_{ii} evolution with Poisson ratios

2.3.4 Results at pad scale

Static and ultrasonic measurements are made on sixteen cubic samples taken on two pads (8/pad) for each formulation. Figure 2.22 presents elastic moduli average results for each material direction on samples with neither backplate nor underlayer.

Left- to right-bars show different formulations. For each bar-group, one sees respectively elastic moduli in tangential- (E1), radial- (E2) and normal-direction (E3). The quasi-static moduli show a strong load dependency in all directions for all formulations. The material is clearly stiffer for higher preloads. The high-frequency Moduli from ultrasonic testing are much higher than the static values with a ratio close to ten between 0.5MPa quasi-static values and 0MPa ultrasonic values. Regarding transverse isotropy assumption, one can notice that it is relatively true, since the in-plane moduli E1 and E2 are close in value for the same formulation. Moreover, these values are twice to three times stiffer than the normal moduli E3. As said before in chapter 2, looking at the formulation aspects, small raw material changes are brought between A, B and C.

Nevertheless, consequent stiffness changes can be obtained. For example, B is the same as A, except it has no steel fibers, which decreases the elastic modulus E1 in tangential direction. C, which has much lower modulus-values

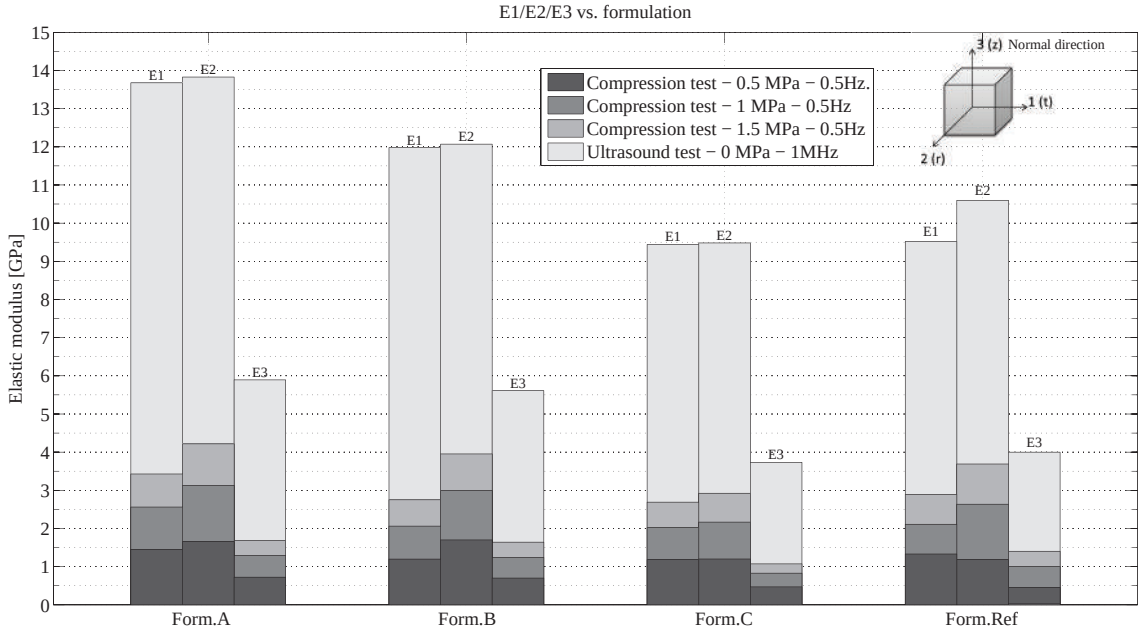

Figure 2.22: Elastic modulus per direction/preload/formulation

than A is different by the organic fibers content and replacement of fine rubber (for A) by coarse rubber (for C). C has also more abrasives than A, but lubricants and fillers are the same for both.

The analysis of elastic behavior versus preload shows that elastic moduli always increase with preload. The increase rate is about 1.5-2.5GPa/MPa for in-plane modulus. It is about 0.5-1.5GPa/MPa for out-of-plane modulus increase. A is most sensitive material to load, Indu.1- and C-formulations are least sensitive. Since the process is the same for A and C, the elastic modulus increase rate can be tuned by modifying formulation. This behavior is strongly implied in non-linear properties of friction materials. The tests in figure 2.15 have shown the same response even though the samples don't have the same shape.

Regarding ultrasonic results, the trend is similar: C is the less stiff material. Also, transverse isotropy is confirmed. It lacks intermediate measures in term of frequency (0.5Hz for compression, 1MHz for ultrasonic testing). Since the gap is too high, conclusions can't be made on the influence of frequency on the stiffening of friction material.

2.3.5 Distribution of elastic properties through the pad

For the study of friction material stiffness distribution, samples are taken from brake pads meshed into two rows and four columns. Each of in-plane and out-of-planes elastic moduli are identified on quasi-static compression- and ultrasonic measurements. Figures 2.23 & 2.24 presents synthesized results for each formulation, direction and test. The grayscale colormap deals with elastic modulus deviation compared to the average value of the pad. It reaches $\pm 20\%$ variation depending on formulation, direction and test (the figures shows $\pm 15\%$ colorbar in order to be more convenient to analyse). Each variation value is an average of two measurements. Global modulus distributions show coherent results between quasi-static and ultrasonic testing for each direction and formulation. It demonstrates that brake pads stiffness distribution pattern depends from the formulation and production process.

It is difficult to comment on a possible organized distribution since the heterogeneity is different from pad to pad. Although, the in-plane distributions pattern is usually different in radial and tangential directions, which underlines non-symmetric fibers and porosities concentrations and orientations even if average modulus values are close. A first analysis focuses on radial variation and a second one focuses on tangential variations. For example,

formulation Ref. shows stiffness increase on inner radius for in-plane moduli E1 and E2, whereas formulations A and B show stiffness decrease for tangential modulus E1. Formulation Ref. has the most homogeneous distribution, contrary to formulation C where all directions are highly disturbed. In fact, formulation C is clearly stiffer on outer radius if one look at the out-of-plane modulus E3.

The analysis shows also a tangential distribution pattern for all cases. For example, formulations A and C show opposite tendencies. For in-plane moduli, A is stiffer on the center of pads compared to leading and trailing edges, contrary to C.

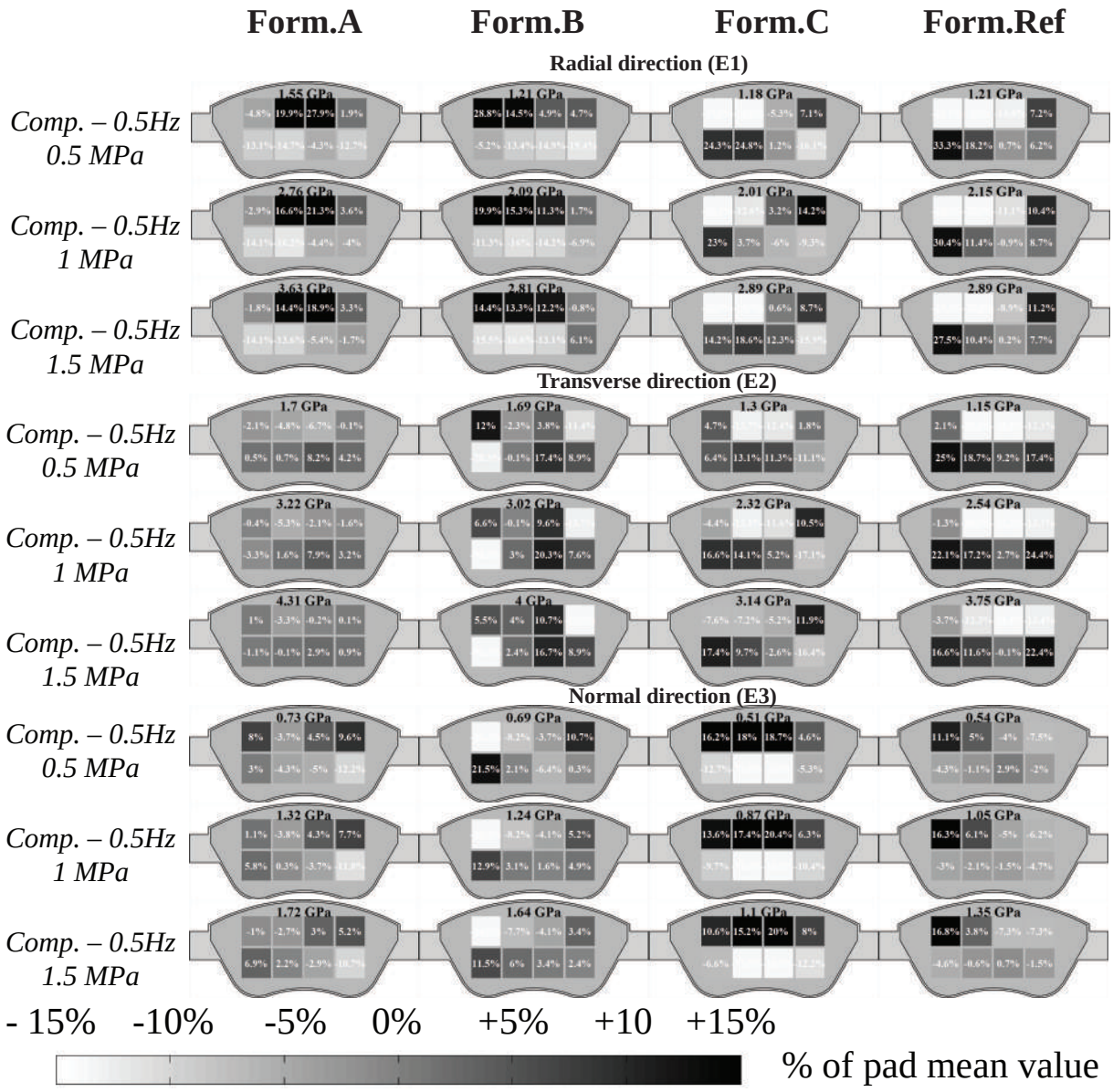

Figure 2.23: Elastic modulus distribution per direction/formulation for compression test

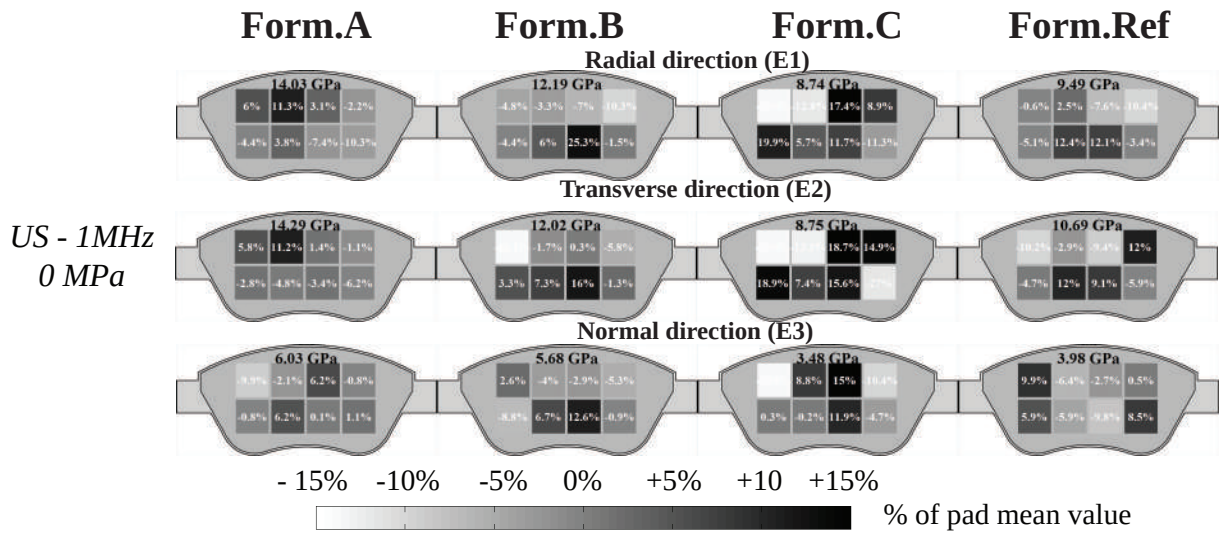

Figure 2.24: Elastic modulus distribution per direction/formulation for ultrasonic test

2.3.6 Conclusions on elastic properties

Brake pad stiffness is evaluated by identifying elastic moduli in different directions. Comparing with classic compression tests on cylinder shape samples, the friction material behaviour is similar, e.g. the non-linear behaviour of materials is highlighted. Also, non-linear behaviour of raw components is seen by the stiffening of the material through load. However, there are small differences between the two techniques which might be due to the samples geometry. The transverse isotropy is less marked for cubic compressions tests, it is more anisotropic. The geometry coupled with the composition of raw materials of this elementary volume should play on the material properties (for example, amount of fibres and their orientation).

There are little differences between both tests due to the samples geometry (cylinder versus square), but the evolution with loading, regarding formulation is the same: A & B are similar (with A slightly higher than B due to steel fibres) and C is the less stiff friction material (the raw materials are more homogeneous in term of granulometry, there are no matrix coated fibres and it contains porous materials as synthetic hydrated calcium). In a global point-of-view, Reference formulation is quite similar to A and B. Even if the formulation are surely different, the elastic response is merely the same. Regarding formulations, fibres orientation is directly translated with the transverse isotropy found between measurement directions.

This investigation has been broadened to the study of transverse isotropy. The elastic assumption of transverse isotropy is mostly verified even if friction material formulation can influence significantly the elastic properties of brake pads. The influence of formulation and process is different for in-plane and out-of-plane modulii. Each material combined with its process has a specific stiffness level and distribution signature. Some materials are stiffer on edges in-plane & out-of-plane (Form. REF) whereas some materials are softer on edges in-plane & out-of-plane (Form.A & Form.C).

The preparation of several cubic samples taken from the same pad allows studying the elastic moduli distribution aspects along one pad geometry. The measurements performed during this study confirm that the stiffness distribution is strongly dependant on the friction material formulation and on the production process itself. There is a certain variability from pad to pad (here $\pm 20\%$). It seems there is no organized distribution of elastic properties.

At last, it has been also shown the dependence of preload on quasi-static techniques, and the influence of test type and excitation frequency on results. It is confirmed that elastic modulus has a strong dependency on frequency and preload. It is confirmed friction materials are heterogeneous and non-linear transverse isotropic materials.

2.4 Friction material testing: effect on NVH properties

2.4.1 NVH procedure to analyse noise

Brake squeal can be identified and classified subjectively or objectively (processing microphone and accelerometer data). Not every up and down on the FFT spectrum curve can be considered as a squeal event. However, brake squeal has a distinctive peak with possible harmonics displayed in its FFT spectrum.

In the achievement of reproducing noisy situations on road and having a rightful idea of what are the mechanism which lead to squeal noise, it is mandatory to develop a test as accurate as what sees the brake on real car situations.

Basically two approaches can be followed when designing dynamometer brake noise procedures. The first approach leans toward duplicating vehicle-driving conditions. The brake is tested on vehicle and the noise performances are measured under conditions related to road tests such as the Los Angeles City Test (LACT) or the Mojacar Test ([Mody et al., 2002]).

The second approach is less environment dependant. The brake is tested on a dynamometer bench by systematically increasing or decreasing pressures and temperatures. Using this test method, it is less likely to miss noise events. The procedure is to use controlled fixed speeds (it usually covers only low fixed vehicle speeds such as 3 to 10 km/h) during braking which enables a systematic search for squeal conditions by covering varying test parameters such as temperature and pressure.

In the early 90's, a European working group including car manufacturers, braking system suppliers, and friction material companies, developed a dynamometer test procedure known as the AK noise in order . This procedure uses the two main modes:

- drag mode at low speed with a pressure application profile meant to induce instability and squeal noise,
- deceleration braking at moderate speeds at constant brake pressure.

The drag mode procedure gives a broad view of the noise events occurring at the tested brake system. Also, stop brakes are performed in the same frame of parameters. Both emphasize the replication of vehicle road test.

Lately, the SAE J2521 (1999) combines both braking modes to satisfy the strong need for a global standardization of squeal noise dynamometer tests. The main optimization leaves in the addition of inertia stops. The test include three main schedules:

- standard test sections with deceleration, drag, and forward/reverse sections at various temperatures and speeds,
- optional schedule looking at noise during cold modules to assess noise propensity below 50C and at or below freezing level of zero degrees,
- optional schedule looking at noise after fade to assess the influence of high temperature excursions on the noise propensity of a given brake.

The main result is the noise frequency and pad temperature versus stops through time.

The mechanical and thermal properties of the simplified friction materials are identified at the macroscopic scale. It leaves the possibility to test the friction pad regarding perfomances and noise. In the industrial process of testing brake pads, NVH tests are performed. The classical test is based on the SAEJ2521 procedure which is dedicated mostly to squeal. It is a temperature-driven procedure which sweeps different pressure and velocity. Drag and stop brakings are experienced and mesured. Friction coefficient and noise frequency/level are the signature of the brake pad and will condition the brake supplier choice for one formulation to another. This section describes the braking procedure done on friction materials to test their actual noise behaviour under several stress conditions (speed, temperature, pressure).

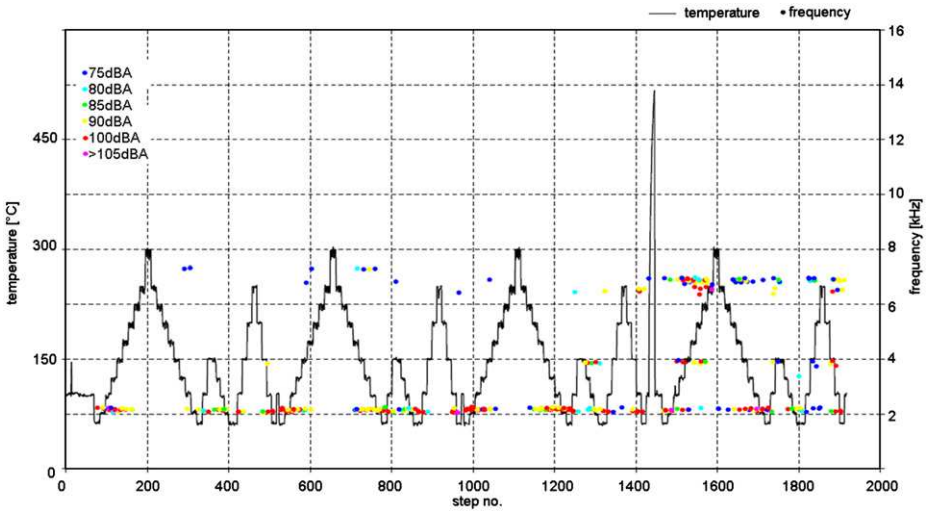

Figure 2.25: Temperatures and radiated sound in a SAEJ2521 test procedure. Colored dots represent registered noisy stops [Graf and Ostermeyer, 2011]

2.4.2 System description

The brake system used is a front-wheel disc brake referenced as ZoH3.3.1. It is has been developed on the floating caliper principle. Bolt loading is minimized by the symmetrical arrangement towards the center of the disc. As the pad-sliding has stainless-steel springs, the ZoH (for zero offset harmonized)provides permanently low sliding forces. This ensures minimum residual drag and differential lining wear. The brake is of a graphite cast-iron manufacturing.

The brake disc is a grey cast-iron ventilated disc which can support extreme loads because of its high temperature conductivity, low thermal tension and high resistance to thermal cracks.

The floating caliper and disc are mounted on an inertia dynamometer. which is fully instrumented:

- A microphone for measuring incoming sounds is placed at $10cm$ from the disc surface, and at $50cm$ height from the disc axis.
- Accelerometers are used to launch the test measurement for a certain level of vibration. They can be exposed to high temperatures due to the brake sequences. So the accelerometers must be placed on the pad housing.
- The temperature measurement is taken on both pads at their centers and at 5mm from the contact surface with the disc.
- Pressure into the caliper, disc speed and torque are also recorded.

2.4.3 Test procedure & industry requirements

The NVH3505 procedure is an adaptation of SAE J2521 programmed and used at Chassis Brakes. It determines the propensity of a given friction material, under normal or extreme temperature conditions (between zero and 550°C), to generate squeal noise on a given brake configuration, selecting and evaluating different brake configurations (friction material size and geometry, noise shims, brake hardware, etc.) related to noise in the hearing range development of noise reduction measures using prototype materials or configurations.

In order to have complementary contact surfaces between pads and disc, high energy friction sequences are set up at the beginning:

Figure 2.26: Floating caliper brake adapted on an inertia dynamometer bench

- Rod07 – Break-in
- Rod05 – Conditioning, bedding

A test is dedicated to evaluate global performances:

- Eff01 – Friction characteristic (deceleration)

3 tests are repeated at different stages of the procedure

- AK07 – Drag Module
- AK12 – Backward/forward drag module
- AK08 – Deceleration module to 0kph

Some other tests expose the brake to specific conditions to modify friction characteristics:

- Ech150D – Intermediate warm-up
- Fade01 – Temperature fade module
- Recov01 – Recovery (equivalent to Rod05)

The disc velocity values are [-3; 3; 5; 10; 50; 80; 100]kph. The pressure is set at 5, 10, 15, 20, 25, 30, and 35 bars. The temperature into the pad at 5mm from the contact surface is set at [100; 150; 200; 250; 550]°C.

The measurement is triggered by accelerometers located as close as it can be regarding the thermal stresses (the amplitude of vibrations launches the measurement). The temperature is measured at the center of the internal pad (motor side) at 3mm from the contact surface.

The complete NVH3505 procedure is described in table 2.8. It must be noted, for having a longer test and to see the history effect of braking, the NVH3505 is followed by a procedure called NVH3505R: a reduced version which is stopped before fading phase (task N°19)

Task N°	Type	Cycle number	Init. speed max (kph)	End speed max (kph)	T (°C)	P (bars)
1	Rod07 - *Break-in*	30	80	30	100	30
2	Rod05 - *Bedding*	32	80	30	100	30
3	Eff01 - *Friction characteristic*	6	80	30	100	30
4	AK07 - *Drag module (normal)*	266	10	10	300	30
5	Ech150D - *Intermediate Warm-up*	24	50	0	150	30
6	AK12 - *Backward/forward*	50	3/-3	3/-3	150	20
7	AK08 - *Deceleration module*	108	50	0	250	30
8	Eff01 - *Friction characteristic*	6	80	30	100	30
9	AK07 - *Drag module (normal)*	266	10	10	300	30
10	Ech150D - *Intermediate Warm-up*	24	50	0	150	30
11	AK12 - *Backward/forward*	50	3/-3	3/-3	150	20
12	AK08 - *Deceleration module*	108	50	0	250	30
13	Eff01 - *Friction characteristic*	6	80	30	100	30
14	AK07 - *Drag module (normal)*	266	10	10	300	30
15	Ech150D - *Intermediate Warm-up*	24	50	0	150	30
16	AK12 - *Backward/forward*	50	3/-3	3/-3	150	20
17	AK08 - *Deceleration module*	108	50	0	250	30
18	Eff01 - *Friction characteristic*	6	80	30	100	30
19	Fade01 - *Temperature fade module*	15	100	0	550	30
20	Recov01 - *Recovery*	18	80	30	100	30
21	AK07 - *Drag module (normal)*	266	10	10	300	30
22	Ech150D - *Intermediate Warm-up*	24	50	0	150	30
23	AK12 - *Backward/forward*	50	3/-3	3/-3	150	20
24	AK08 - *Deceleration module*	108	50	0	250	30
25	Eff01 - *Friction characteristic*	6	80	30	100	30
		1917				

Legend

X	Measured braking
Y	Deceleration braking
Z	Drag 10"
XX	Constant pressure

Table 2.8: NVH3505 procedure: braking applications (NVH3505R stops at step 18)

2.4.4 Noise results

In figure 2.27, noise occurrence is described in percentage of total braking for each procedure and formulation, e.g. if 10 brake stops out of 10 of procedure i are noisy, there is an occurence of 100%.First thing to note, regarding noise, all formulations are noisy. A, B C & REF are noisy.

During NVH3505, there is a similar behaviour to noise for all simplified formulations (A, B & C) until $fade01$: the percentage or noisy braking is almost the same for each steps and upper 30%. There seems to be a pattern regarding type of braking. It appears decelerations brakings (AK08 & Eff01) are noisier than AK07 and AK12 (backward/forward, -3/+3 kph), so stop tests are noisier than drag tests. Reference formulation seems to be less noisy (around 20-30% max.) but it begins to make more noise after fading until reaching to 100% at beginning of NVH3505R. During NVH3505R A, C & Ref. are getting noisier, unlike B which noisy behaviour is decreasing. Fade01 has clearly modified noise behaviour for all three formulations.

Looking on squealing frequencies per formulation, table 2.9 describes noise occurrence per bandwith and by comparing first procedure (NHVH34505) with second procedure (NVH3505R):

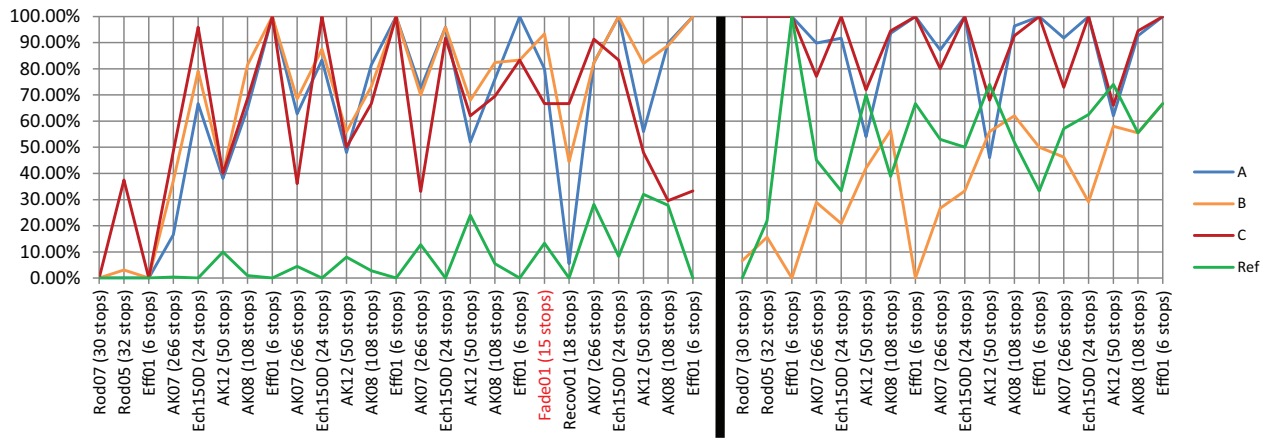

Figure 2.27: Noise occurrence regarding procedure history

- Form.A: Noisy around 6-8kHz and 10-11kHz, noise shifting around 6-8kHz during second procedure, fading decreases the squeal frequency.
- Form.B: NVH3505 is noisy around low frequencies (from 2 to 8kHz) shifting to 10-13 kHz during NVH3505R, the material is more influenced by initial temperature test than fading (a "squeal pattern" according temperature appears)
- Form.C: Noise always around 10-11kHz, appearance of 13 kHz noise in second procedure, the material is barely influenced by fading.
- Form. Ref.: Low frequency noises around 2-2.5 kHz, appearance of 10-13 kHz during NVH3505R, fading is lightly influencing the material and only accelerates high frequency emergeance which already appeared before fading.

Form.C is not influenced by the brake stops and is stable around high frequency noises. Form.B & Form. REF provide low frequency noises, although Form.A & Form.C are generating high frequency.

Regarding wear, regular formulation should lose maximum around $0.7mm$ materials, as for material Ref. Simplified formulations are highly wearable, up to $2mm$ for formulation C which might be caused by the simplification of raw materials number. Also, formulation C is composed of mostly small components which permit a high recirculation of particles and thus enhances wear. It must be noticed between formulation A and B the steel fibres are removed. friction coefficient is lowered and wear has increased.

Formulation	μ	Wear (mm)	Noise Occurrence (NVH3505/NVH3505R) (%)													
			Global		*2-2.5kHz*		*3.6kHz*		*6.4-8kHz*		*10-11kHz*		*13kHz*		*15-16kHz*	
Form.A	0.5	1.44	61	88	0	0	0	0	21	56	27	4.5	1.4	4.1	3	4.9
Form.B	0.4	1.51	55	40	9	0	13	0	14	7.8	0	10	5	8	0	0
Form.C	0.4	2	67	82	0	0	3.76	0	5.3	4.5	48	57	1	2.8	0	3.7
Form.Ref	0.5	0.7	11	52	4	24	1	0	0	0	0	8	2	14	1	0

Table 2.9: Noise occurrence regarding procedure (NVH3505 vs. NVH3505R)

The figure 2.28 shows peak frequency, and figure 2.29 shows friction coefficient, both vs. initial temperature and section/stop number for all the individual brake events which had at least one peak above the $70dB(A)$ threshold.

All formulations are only a bit noisy at the beginning. With brake stops cumulating, the formulations A, B & C are becoming more and more noisy and sensible to high frequencies. The friction coefficient is increasing with sliding contact. However, whenever a peak of temperature is achieved (from up to 300°C), the friction coefficient decreases dramatically, even more at fading phase. At these high temperature stops, the brake environment is silent. The friction coefficient is highly correlated to temperature. On form. B, the friction coefficient is decreasing a lot after Fade01 and the next task is noisier. All materials responds as so except formulation C which doesn't seem to be impacted by temperature regarding noise but mostly on friction coefficient.

Material A & B are highly influenced by fading. Especially form.B which after several braking seems to get back to its initial noise behaviour. This might be due to the lack of steel fibre which make it an insulating material. There is a "recovery" phenomenon. Form.C and Ref. are slightly influenced by fading. The occurence is more due to an history effect, e.g. the high frequencies ($> 12kHz$) already appeared before fading and kept increase all along the procedure.

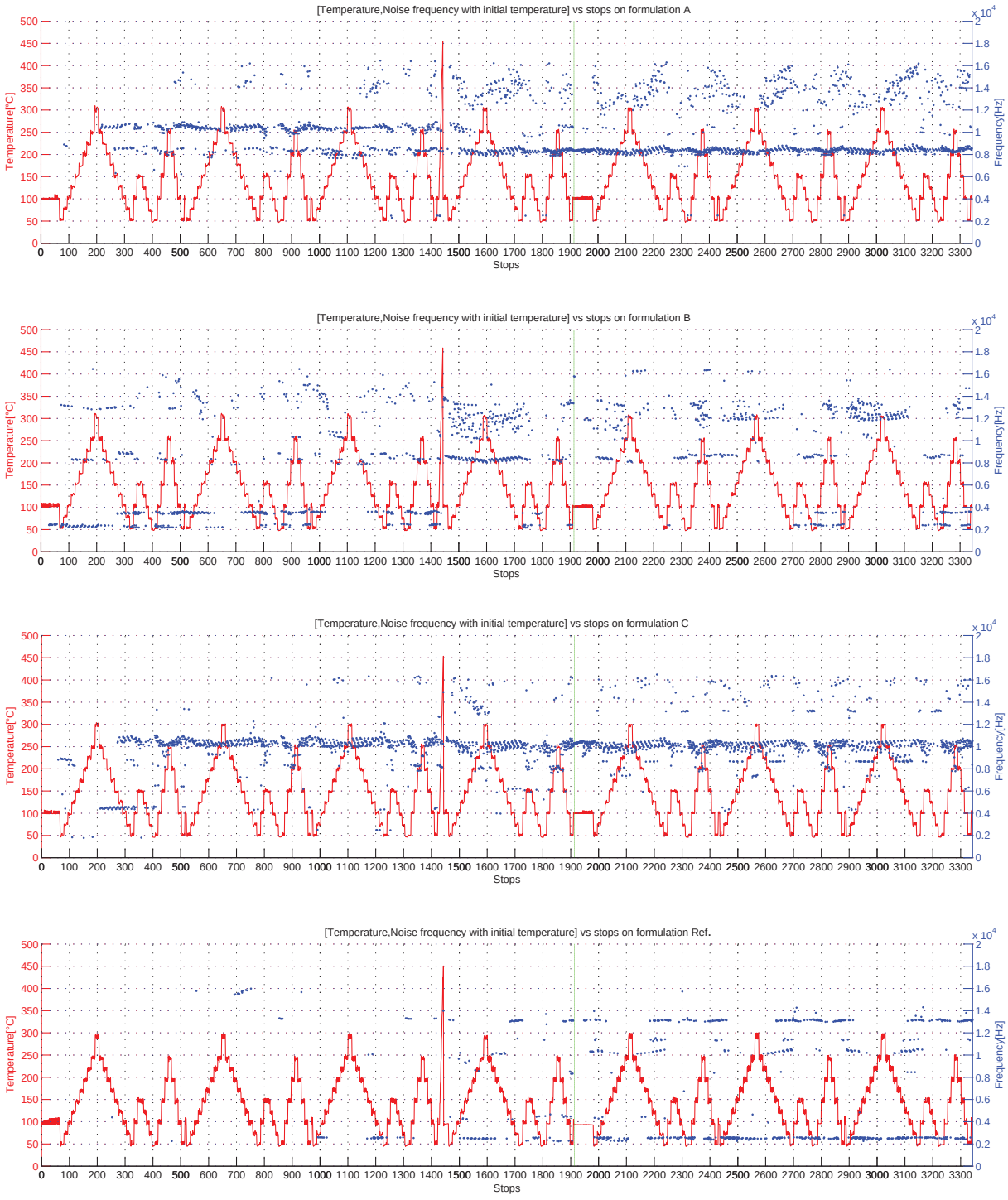

Figure 2.28: Noise occurrence and equivalent temperature/frequency according formulation

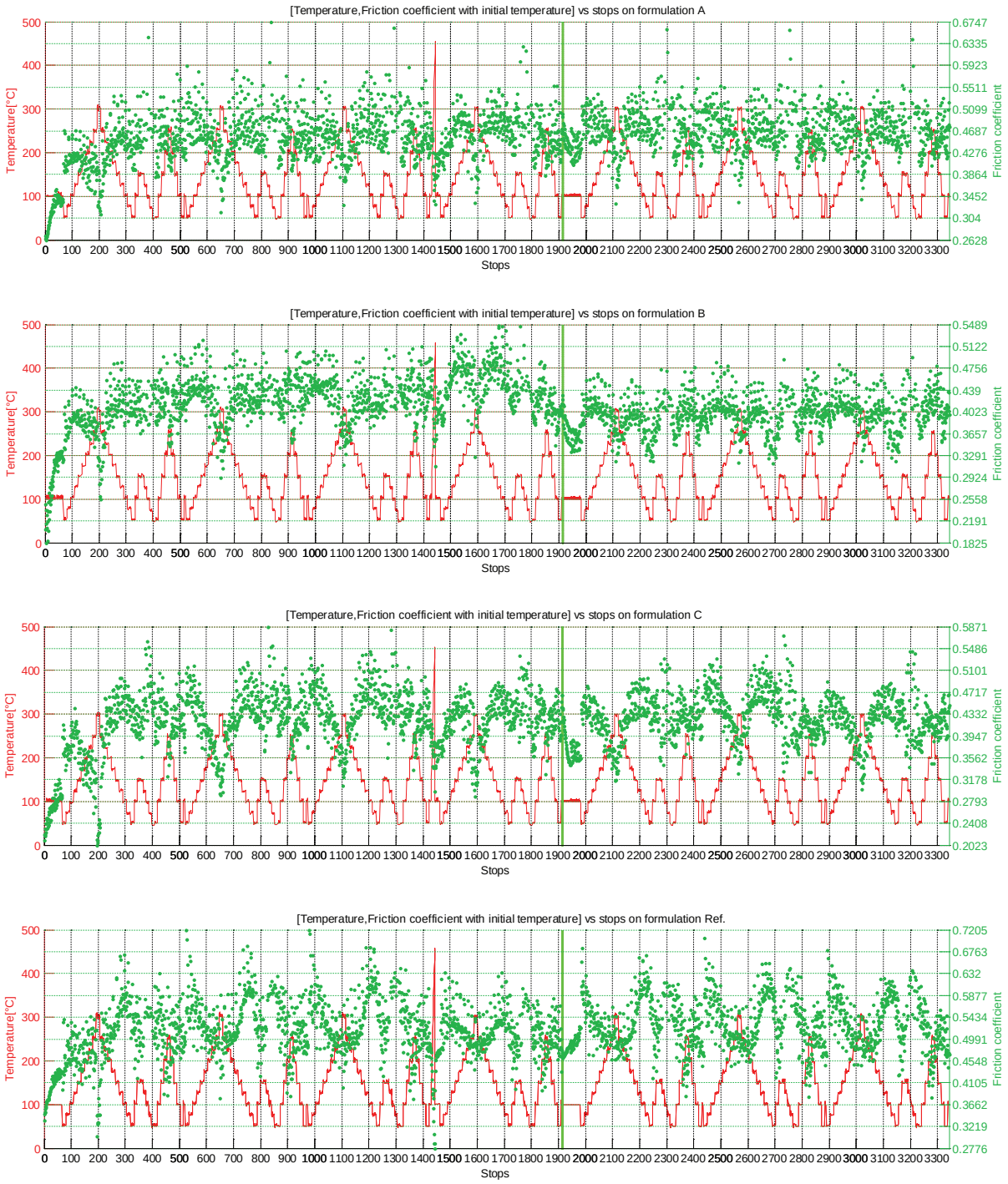

Figure 2.29: Noise occurrence and equivalent temperature/friction coefficient according formulation

In order to investigate on repeatability of test, a second campaign (detailled in chapter 4) has been performed. The results are shown for formulation C and Ref. in figure 2.30. For formulation Ref., results shows the repeatability between the two series regarding global noise occurrence history and frequencies emergence. Ref. formulation seems more stable than formulation C. Before fading, the brake response is much noisier and after fading, the frequency involved are differents (8kHz here instead of 10kHz for the first campaign). It suggests from pad to pad, formulation C has a more important variability than formulation Ref. Further testing should be done to confirm it.

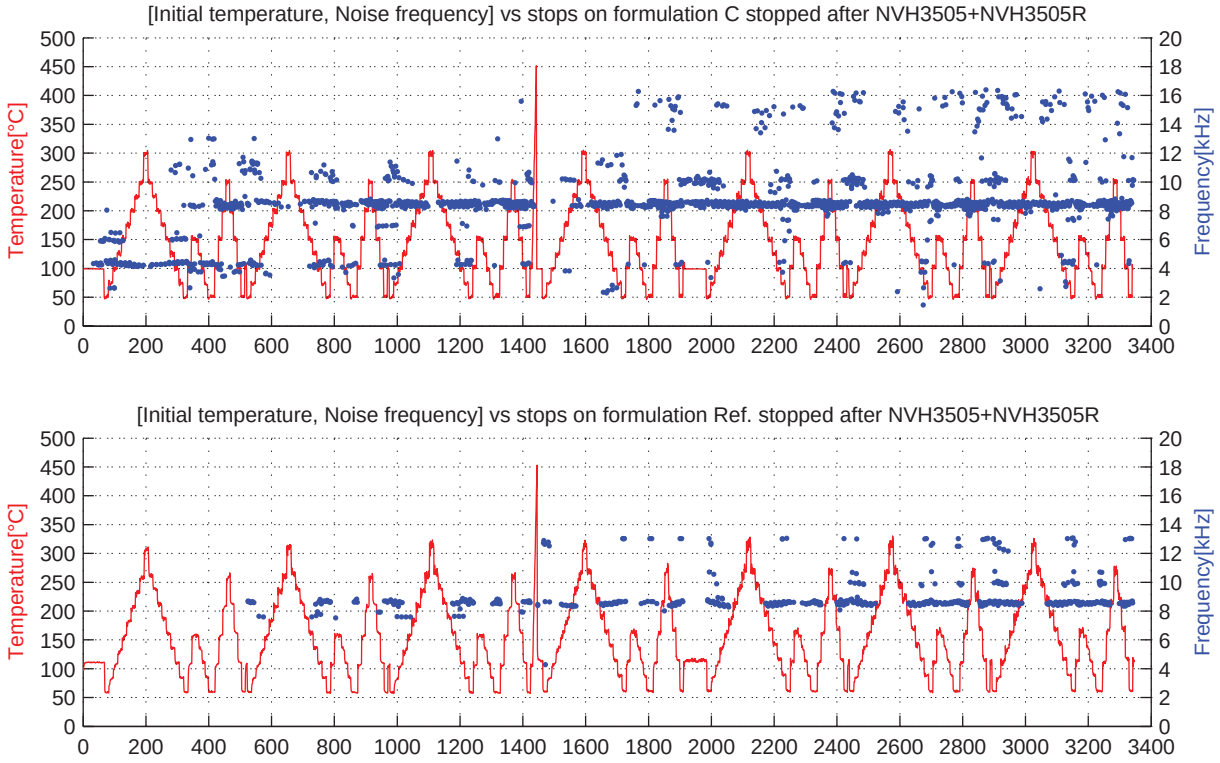

Figure 2.30: Second test series on formulations C and Ref. for repeatability

2.4.5 Comments on influential parameters

First of all, the materials (except C) are strongly sensitive to temperature. At 250°C (which is a threshold temperature for all materials), the friction coefficient is always lowering as the noise is vanishing. There is clearly a temperature effect. Formulation Ref. seems to be the more disturbed by temperature increases.

Secondly, the effect of fading is the same for all materials: the noise is more or less vanishing and the frequencies above 14kHz are activated and are durable. Hence, it means permanent materials transformations are enhanced at 450°C (the second threshold temperature), no matter is the formulation. Friction material is more or less sensitive to fading as function of raw components and manufacturing parameters. There is especially a hidden link with transformation temperatures. For instance, A,B and C have threshold temperature at 250°C and 450°C. When these temperatures are reached, the pads are degraded. In this NVH study, noise response is changed.

Speed won't be commented here since the test is not sweeping much this parameter. Looking at figure 2.31 which details the whole procedure regarding pressure/temperature versus noise frequencies involved, pressure influences range of frequency. Low pressures will activate low and high frequencies for formulation A and C. It appears to be the same for formulation B but it's less clear. Mid-frequencies (8-10kHz) are activated by high pressure (from 10 bars) for all formulations. It can be noted for every noise rays regarding pressure, there is a slight effect of

temperature: for high temperature braking, the frequency involved for the same pressure but at lower temperature decreases a bit. The temperature appears to modulates by decreasing the frequency around a certain pressure.

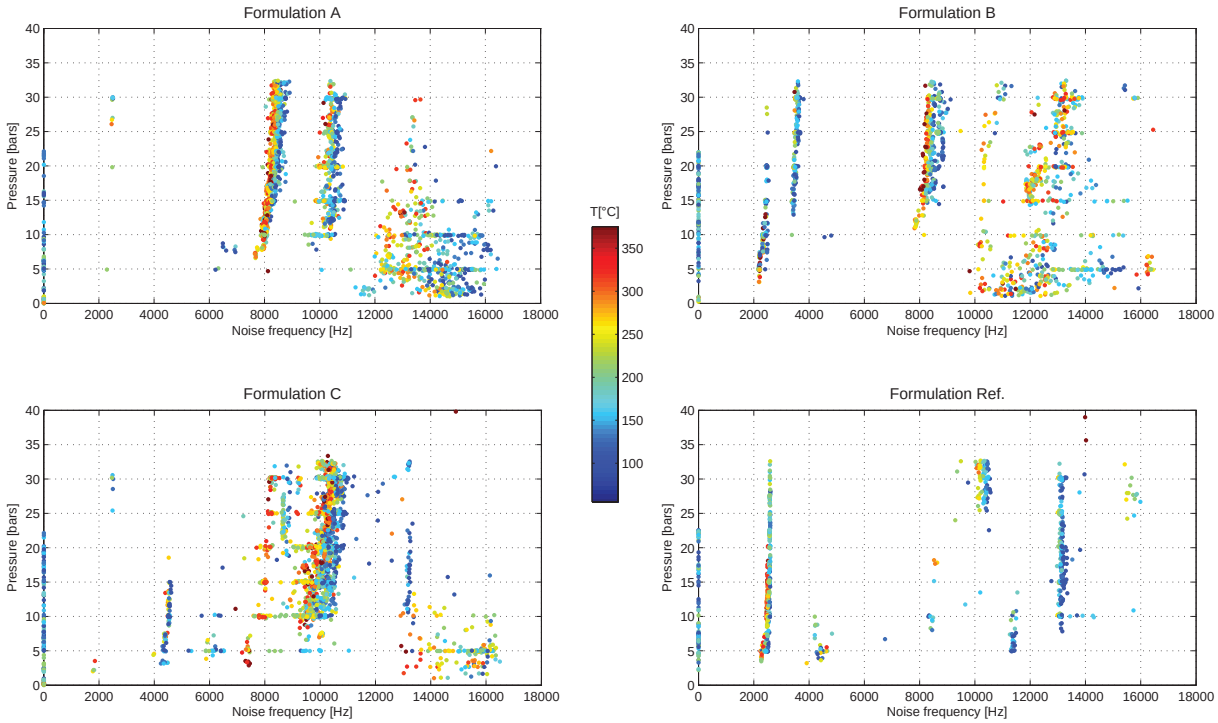

Figure 2.31: Pressure/Temperature versus Noise frequency per formulation (first tests series)

2.5 Chapter synthesis

In this chapter, three simplified formulations have been designed and compared to an unknown industrial formulation. From raw materials state to final pad shape, the in-temperature behaviour has been shown. Manufacturing process has been detailed and taken into account into material transformations. Therefore, the brake pad intrinsic properties is conditionned by the raw materials structure and furthermore by the manufacturing. Threshold temperatures have been brought to light (at 250°C and 450°) and these are conditionned by resin and rubber content into the simplified materials, and furthermore by the curing stopped at 200°C. Also, composition plays its part into the transverse isotropy of the material. Fibres types (matrix coated or singles) and orientation impact the normal/transverse elastic ratio. Hence tranverse direction is stiffer than normal direction.

Compression and ultrasound tests have underlined heterogeneity given by the composite structure of friction materials. Even if the measurement is macroscopic, the materials properties are inequally dispersed from a location to another on the brake pad. In addition, the natural dependency on loading of friction material has been emphasized and is influenced by the formulation itself. The diversity of raw materials is the reason of the non-linear response of the pad through loading. Further tests shall be made on different loads and frequencies with temperature on values near the real braking applications. Hence, numerical approaches of brake pads will be fed with realistic databases.

Noise tests have drawn attention to the variability of frequencies induced by braking sequences. Three effects have been emphasized:

1. Formulation effect: from a formulation to another, the frequencies involved are different at procedure start, so the intrisic properties conditionned by raw materials and manufacturing will influence the noise response. For instance, comparing formulation A to B, the lack of steel fibres into B seems to lower noise frequencies. It can be well understood the material is less stiff, so the coupling at contact is more heat conservative and the material is more alterable regarding transition temperatures.

2. Temperature effect: from the consequences of manufacturing, the material will be stable at a certain temperature. Above this temperature, the material will transform and its behaviour will be change temporarly and/or permanently, function of wear conditions coupled to the temperature gradient into the pad. Looking deeper into formulations transformation temperatures, the 250°C step linked to curing procedure at manufacturing is seen for all 3 simplified materials, as noise is decreasing after this step of temperature. Thereby, the material is strongly reacting, especially resin and rubber, and the natural transformations coupled with sliding contact enhance the disappearance of noise. However, some materials are not influenced by temperature. This is the case for formulation C. Even if friction coefficient is lowered with temperature, no changes are seen regarding noise.

3. History effect: at different steps of the procedure, each stops noise response is different. The previous braking will influence the following. Hence, the surface topology and properties must evolved in time. One can notice with frequency reponse through time for every formulations, with wear increasing, with punctual phases as fading, noise is modulated and might be not of the same nature as in the beginning. Thus, pad topology seems to be one of the relevant parameters in the occurrence of noise to study.

As a matter of fact, these conclusions naturally ask several questions.

A design of experiment on both raw materials (choice, quantity & shape) and friction material production is a way to understand deeper the role of each step of manufacturing in the intrisic pad material properties and the consequences on NVH.

The results show an industrial brake system with a complex dynamic behaviour coupled with simplified (or not) friction material increases the difficulty to analyse noisy or silent state. Repeatability of noise performances is a uncertainty and must be confirmed by more tests. Paradoxically, the richness of frequencies also allows to distinct different types of coupling. Therefore, coupling these results with the same frequency study on a simpler braking device could be a way to understand what is the contribution of friction material formulation to noise occurrence.

The three effects (formulation, temperature & history) must be quantified in a practical way. The most obvious is tracking the surface evolution through friction stages, at different set of parameters (mostly temperature). Therefore, understanding of friction material noise response might be link to surface microscopic evolution.

Chapter 3

NVH testing on a simplified brake system

Contents

3.1 Motivation

In the previous chapter, it has been seen experimental processing on an floating caliper disc brake of squeal noise can be difficult. The complex geometry and dynamic of the brake system lead to numerous noise frequencies. Some works as [Massi et al., 2006] or [Duboc, 2013] are based on test rigs with known dynamic and simplified geometry. The friction material is a bar in the case of Massi, and a cube in Duboc system. Some results were found regarding pad geometry, contact surface evolution and noise generated.
In the optic to study the influence of friction material on another system, this chapter is dedicated to look at the same friction materials and their influence on a system which is a fine transition between a tribometer and a complete industrial brake. Geometry is also investigated. A numerical model is built in parallel of experimental testing.

3.2 Experimental set-up

The pin-on-disc setup developed at Chassis Brakes Intl. is a simplified system that simulates the behavior of a disc brake system with a U-shape fixed caliper (figure 3.1). The friction force applied on the disc is provided by two round pads on both sides of the caliper in order to have a symmetric pressure (figure 3.2). The system is similar to a pin-on-disc system because of the simplified pad shape (a $\phi 30mm$ cylinder). This pad shape, assimilated as two pin-on-disc contacts as proposed by [Earles and Soar, 1971] and in [Earles and Badi, 1984]. The coupling between both surfaces is weaker than in an industrial brake system but it simplifies the understanding of the dynamics of each component in squeal mechanisms.

It also has a short tribological circuit. To have the less coupling into the system, the moving links between components have been limited to the pad-housing/caliper and the piston/caliper. The looseness is minimal for both liaisons, and can be adjusted for the contact pad-housing/caliper. The simplified brake has been designed to accept sensors informing on static and dynamic behavior (mainly acceleration/force). This setup is an agreement between a fine tribometer and an industrial brake system.

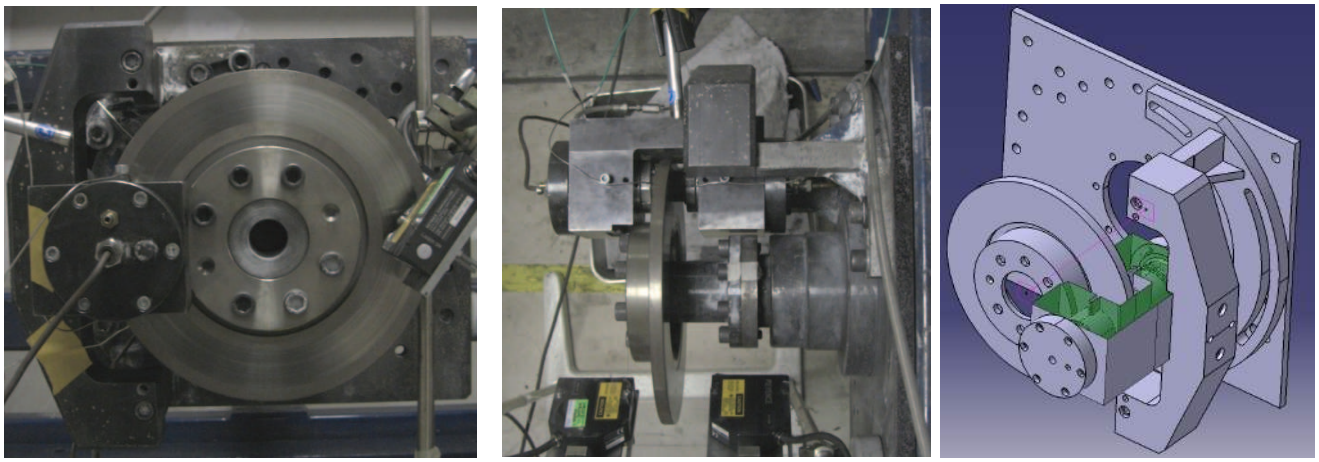

Figure 3.1: Fixed-caliper symmetric pin-on-disc system and associated CAD design mounted on axle bench

The hydraulic pressure is entering by the two lids fixed on the caliper and pushes the pistons against the pad-housings. They are both guided by two screws that prevent from their rotation around the pressure pads axis (fig.3.1). These screws have also the function to permit more or less the tilting of both pads. It has been shown that the noise occurrence can be clearly reduced if the tilting is annihilated. There is room between caliper and both pad-housings ($150\mu m$ on the diameter).

The system has the particularity to generate one clear noise frequency during braking sequences. This noise is measured between 3.5 and 3.7 kHz, depending of the functioning conditions (pressure, disc speed, temperature) friction material formulation, and pads shape.

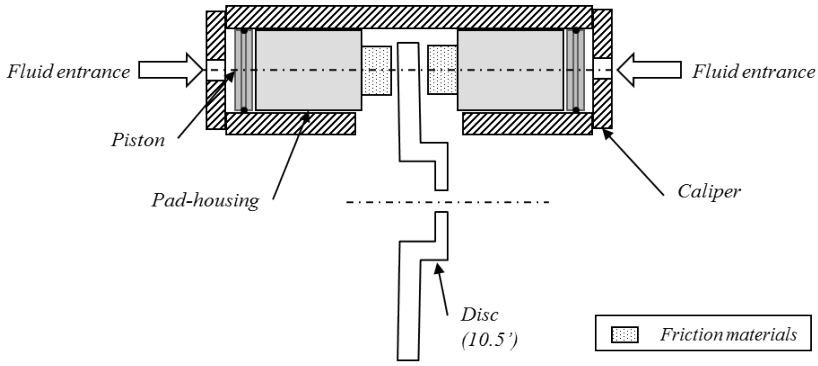

Figure 3.2: Schematic of the simpified brake set-up

In figure 3.3, it is shown the time/frequency graph of the sound pressure response for a continuous brake sequence at $100rpm$ and $20bars$. The main excited frequency (and only) is around $3.6kHz$ for a friction coefficient up to 0.4. Noise appears here $75s$ after the beginning of braking.

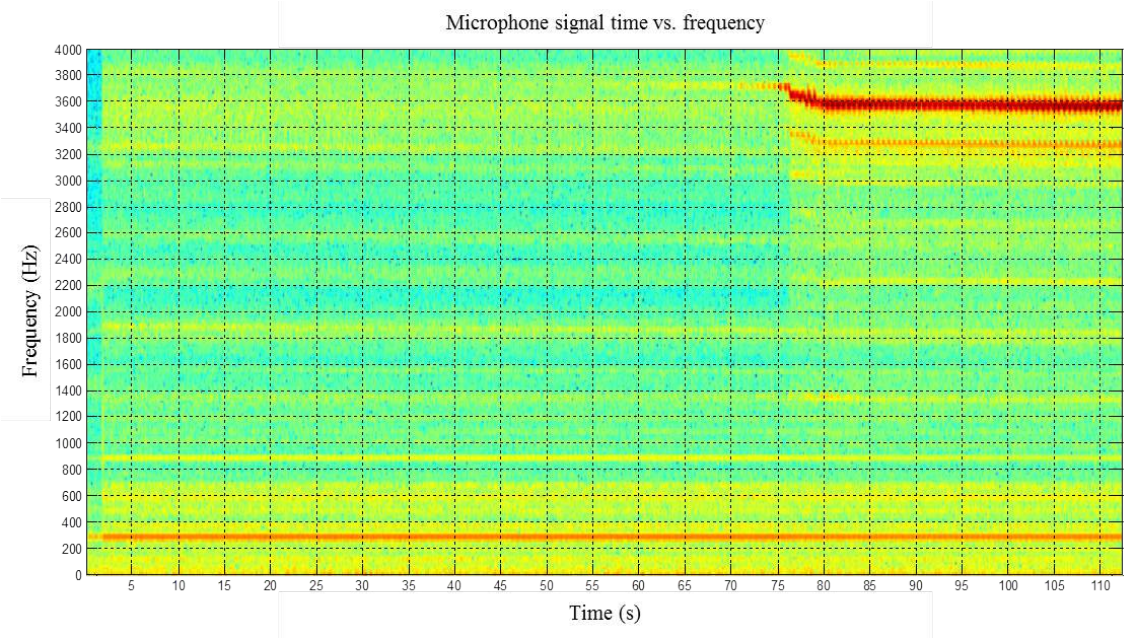

Figure 3.3: Measurement of sound pressure/frequency of microphone during maintained pads/disc contact

3.3 Test procedure

This test procedure has for main goal to simulate classic urban conditions on a dynamometer. The main purpose is to measure noise occurrence with different pad formulation & geometry on the hybrid brake. Also, noise occurrence will be correlated to other parameters measured in order to establish a link. The time-history effect will also be taken into account. This procedure is used elements of the NVH3505 test procedure (which is based on the SAEJ2521), i.e. drag tests mostly referenced as AK21. All tests in this chapter (4 formulations with different geometries) are performed with this procedure.

The disc is full unventilated $\phi 254mm$. Before testing, the disc is rectified to obtain a roughness value around 0.6 and $0.8\mu m$ in order to limit disc thickness variation during braking.

For each pad, a compressibility test is done before any further experimentation and the compressibility must be in accordance with industry requirements (approx. $150\mu m$). The test is performed according to the [ISO6310:2009, 2009] and the procedure B is used, only at ambient temperature.

Then, round pads are machined in the classic pads shape according to the hybrid brake pad-housing dimensions. The height of pin (not counting the height of the plate) should be $9.5mm$ with a diameter of $30mm$.

In order to transmit energy during braking optimally, a uniform contact surface between the disc and the pads is required. A bedding phase is performed before each test. The bedding procedure is detailed below.

N°	T (°C)	**Vi** (kph)	**Vf** (kph)	P (bars)
30 times	75	50	0	7,5

Table 3.1: Simplified brake bedding procedure - Deceleration test (total brakings: 30 stops)

After the bedding phase, a drag procedure (called AK21) sweeps 9 temperature rises described in table 3.2 up to 150°C. The AK21 procedure is repeated 2 times in order to obtain a braking history but at a temperature always below 150°C (at $5mm$ from the contact surface into the pad). The temperature is below threshold transformation of the friction material, previously seen in chapter 2. The complete procedure is summarized in the table 3.3 below:

N°		*1*	*2*	*3*	*4*	*5*	*6*	*7*	*8*	*9*	*10*	*11*	*12*	*13*	*14*	*15*	*16*	*17*	*18*	*19*	*20*	*21*	*22*	*23*	*24*	*25*	*26*	*27*
T° up	(°C)	T°C = [50;75;100;125;150;125;100;75;50]																										
Vi	(Kph)	3	5	10	3	5	10	3	5	10	3	5	10	3	5	10	3	5	10	3	5	10	3	5	10	3	5	10
Vf	(Kph)	3	5	10	3	5	10	3	5	10	3	5	10	3	5	10	3	5	10	3	5	10	3	5	10	3	5	10
P	(bars)	0	0	0	15	15	15	1	1	1	13	13	13	3	3	3	11	11	11	5	5	5	9	9	9	7	7	7

Table 3.2: Simplified brake procedure AK21 - Drag test for several temperature (total brakings: 9 temp. $\times 27 = 243$)

1 – Bedding – 30 applications		
T=75°C	V= 50 to 0 kph	P=7,5 bars
2 - AK21 matrix (drag) – 243 applications		
T=[50;75;100;125;150] °C	V=[3;5;10] kph	P=[1:2:15] bars
3 - AK21 matrix (drag) – 243 applications		
T=[50;75;100;125;150] °C	V=[3;5;10] kph	P=[1:2:15] bars

Table 3.3: Complete braking procedure: bedding is followed by two AK21 phases

3.4 Simplified brake system complex eigenvalue analysis

In this section, a numerical model based on the simplified brake is built in order to investigate mode lock-in through a complex eigenvalue analysis (CEA) described in figure 3.4. The first step is modelling each components according to its geometry and mass both measured by classical ways (weighing, interferometry). The modal behavior of each component is measured by combination of force transducer hammer and vibrometer laser measurements. The experimental mode frequencies and shapes associated are compared to their FE model related by the modal assurance criterion (MAC) [Allemang, 2003]. The main parameters to work with for correcting the modal error are the materials properties (Young Modulus, Poisson coefficient). The same process and criterion are used for sub-assembly and boundary conditions.

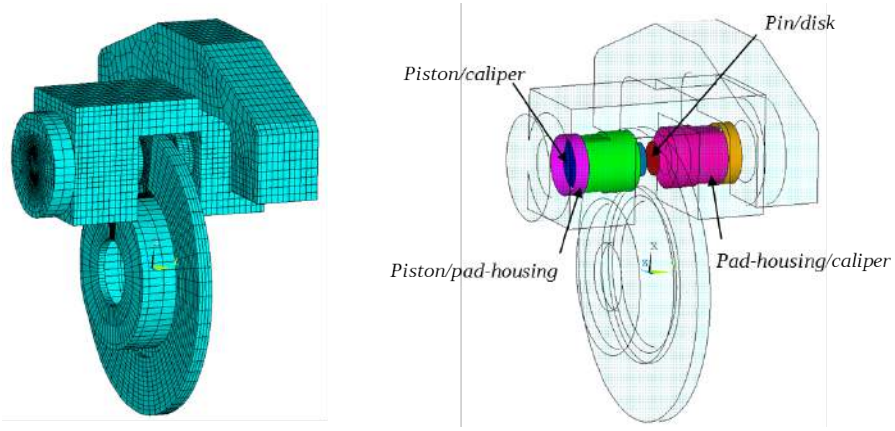

Figure 3.4: Simplified brake system - FE model and contact zones

It must be noticed that the friction material has an isotropic transverse model in the numerical study, and it is well known that it might has a more complex behaviour. For a first study, the FE results are shown with this behaviour for formulation A. The numerical model is based on a two-steps calculation between 0 and 10 kHz [Ouyang et al., 2005]:

- a nonlinear quasi-static stress analysis (including the pressure on pistons and disc rotation)
- a nonlinear pre-stressed modal analysis to determine the complex eigenfrequencies

The real parts of the frequencies gives an information on the stability of the system: if the real part of an eigenvalue is positive, the system is unstable and the corresponding eigenfrequency is assimilated as a possible squeal noise frequency. The contact algorithm is the augmented Lagrangian method and initial penetration is included. The contact detection is done at Gauss integration point. The friction is modeled by classical Coulomb law. Table 3.4 presents the default parameters (friction coefficient and contact stiffness). Friction coefficient between pads and disc has been verified experimentally, and sliding surfaces as pad-housings and pistons into the caliper are set at 0.22 (steel-on-steel contact).

Contact	Target	Contact algorithm	Friction coefficient	K (contact stiffness, N/m)
pin	disk	Augmented Lagrange method	0.45	8.18E+13
pad-housing	caliper	Augmented Lagrange method	0.22	9.58E+13
piston	caliper	Augmented Lagrange method	0.22	1.48E+15
pad-housing	piston	Augmented Lagrange method	0.22	5.07E+14

Table 3.4: Contacts definition in the FE model

3.4.1 Dynamic behaviour

Considering the macroscopic phenomena, the finite element model has been fully correlated to the experimental set-up. Determining the free-free components behavior, the boundary conditions and the sub-assemblies into the FE model rests on experimental measurements that can be easily obtained. For each contact, the input parameters are the friction coefficient and the contact stiffness induced by both contact and target components. The friction coefficient between sliding components is considered as a simple steel-on-steel contact (0.22). For the pin-disc contact, the measurements done on the rig have given an average coefficient around [0.4; 0.45].

To compare with the experimental analysis, the numerical model must simulate the same analysis. It is has been demonstrate in complex modal analysis that a complex mode with a positive real part is consider as an unstable mode. Therefore, the objective is to correlate the unstable complex modal shapes and frequencies obtained in the finite element model with the results of the operational deflection shape measurement (ODS) done during noise appearance in the experimental rig.

Mode lock-in appears when two modes vibrate at very close frequencies until they merge and become one unstable mode. This phenomenon may be the major reason of squeal occurrence in brake systems. This is why an operational modal analysis has been done to identify the modal shape of the brake system at noise frequency.
A 3-heads laser vibrometer system has been used to perform the measurement and trigger at around the squeal noise generated by the simplified brake. It captures the velocity of disc, caliper & arm and pads (as in figure 3.5, 3.6 & 3.7) at noise frequency. The bending mode captured for the disc involves an out-of-plane mode of the disc with nodal diameters. The experimental modal shape of the pad-caliper assembly is more complex:

- a torsion mode around the axis of the caliper
- a torsion mode on the length of the arm
- an out of phase pads tilting

The correlation between the ODS and the FE results will be only qualitative (MAC correlation demands a mesh as fine as in the FE model and hasn't been done). The experimental measurements were done at $P = 20$bars, $\omega_{disc} = 100rpm$. It appears that the numerical unstable mode at 3.7kHz has the same shape as in the experimental set-up.

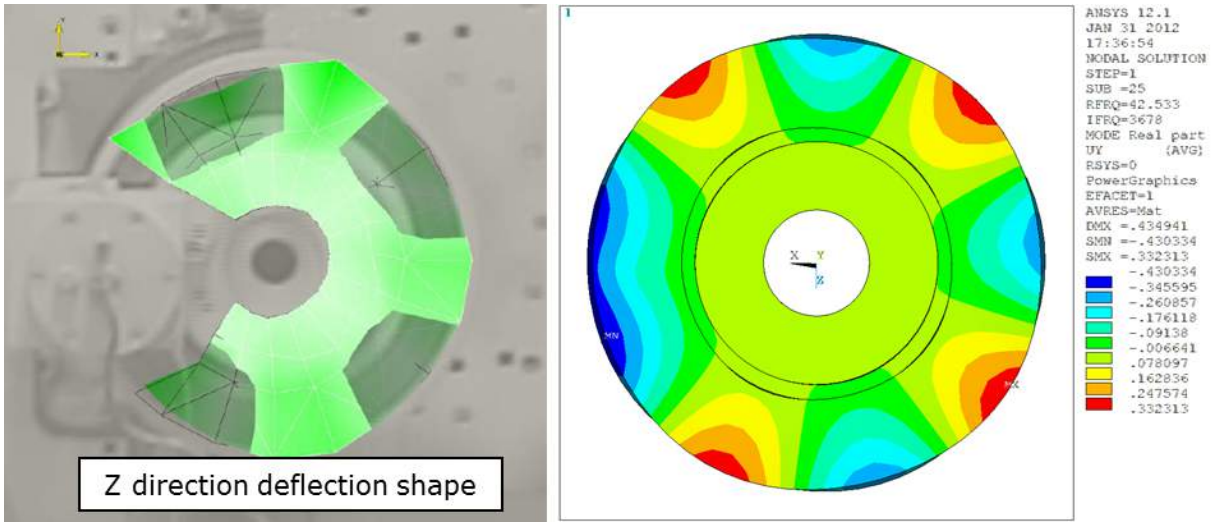

Figure 3.5: Comparison between operational deflection shape of disc VS. FE model results at 3.6kHz

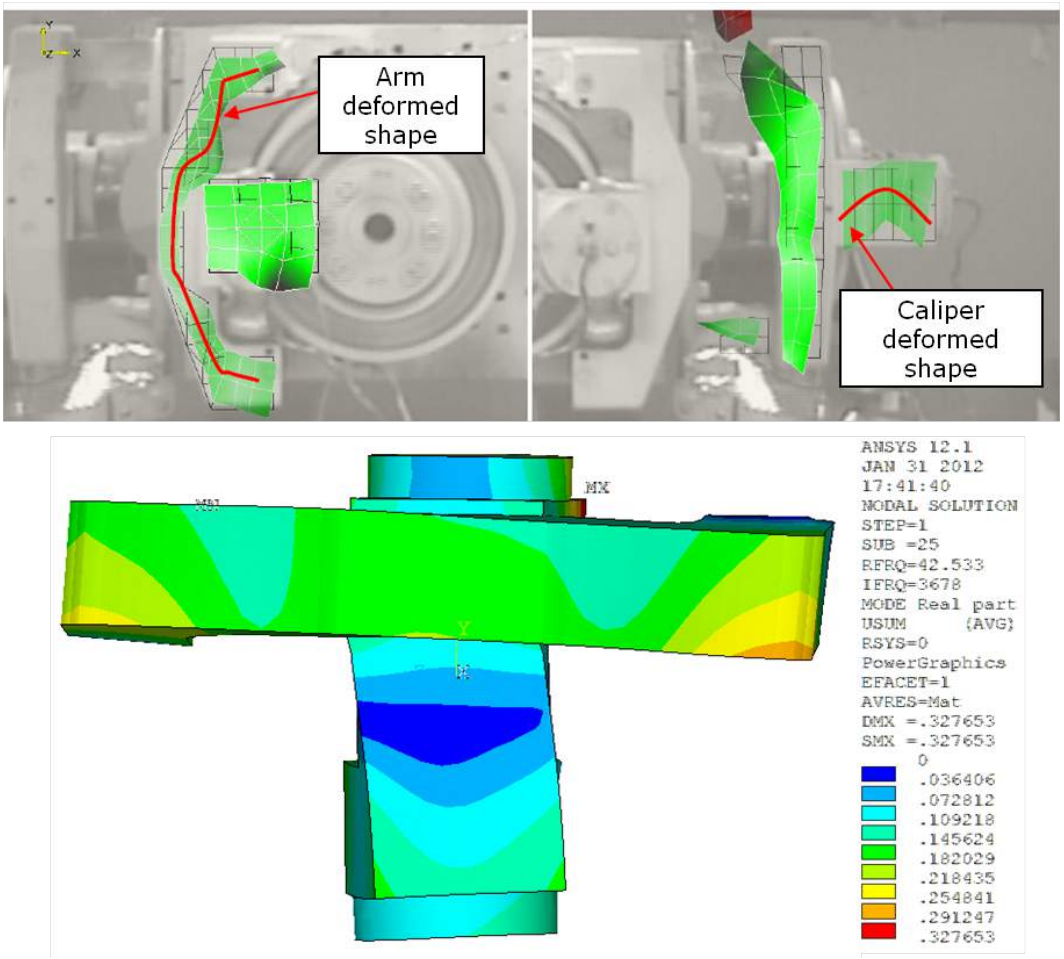

Figure 3.6: Comparison between operational deflection shape of arm and caliper VS. FE model results

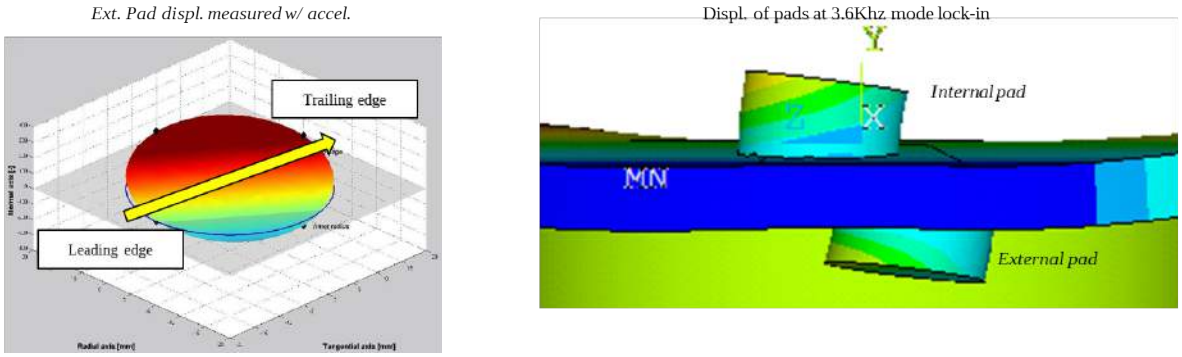

Figure 3.7: external pad-tilting measured during squeal versus numerical instability

3.4.2 Evaluation of the contact stiffness: a parametric study

The simplified brake has a simple tribological circuit to focus on the pads/disc contact. However, it is well known that the whole dynamic of the brake system plays its part on the appearance of noise, and moreover the contacts between moving components. The main difficulty in building a macro-scale finite element model is the choosing of a contact algorithm.

There are only few methods to determine the contact stiffness between two solids such as the power balance method described by [Triches-Jr et al., 2008] but it is always focused on pad/disc contact (and mostly flat surfaces). In our case, it is needed that contact stiffness between cylinder parts to be defined (i.e. piston/caliper, pad-housing/caliper, piston/pad-housing). In the automotive industry, the most used method on these matters is a parametric study on the FE analysis: a range of realistic contact stiffness values are swept in order to approach the experimental modal shapes and frequencies, the unstable modes staying the aim. For the parametric study, we will not focus on the pad/disc contact, preferring to have the surrounding of this contact well correlated before analyzing the main contact.

Disc brake squeal models in complex eigenvalue analysis give information on the deformed shapes stability. It is assumed that a squealing mode can be related to an unstable mode in the FE model (there is a positive real part in the eigenvalue). However, it must be keep in mind that an unstable mode is not necessarily a squealing mode, but the reciprocity is satisfactory even though it cannot describes the intensity of the vibrations and noise level.

It has been shown the contact stiffness between the pad-housing and the caliper (in both rooms) is the parameter the most sensible above all others. This is why a parametric study has been done. The contact is a steel-on-steel contact with a functional clearance between both surfaces ($150\mu m$ on the diameter). The contact algorithm is the augmented Lagrangian method and initial penetration is included. The contact detection is done at Gauss integration point. The friction is modeled by classical Coulomb law. The stiffness is evolving around $[9.88.10^9; 6.91.10^{13}]N/m$ and the unstable frequencies are studied in table 3.5. Below $9.89.10^9 N/m$ the contact stiffness might be not representative and upper $6.91.10^{13} N/m$, the contact is too stiff and the calculations do not converge.

Pad-housing/caliper					
Contact stiffness (N/m)	9.88E+9	9.58E+10	9.58E+11	9.58E+12	1.92E+13
Unstable frequencies (Hz)	729;1578	1578	1580;1887;2347	1586;3629	3677
Contact stiffness (N/m)	2.96E+13	3.95E+13	4.96E+13	5.75E+13	6.91E+13
Unstable frequencies (Hz)	-	-	770	-	

Table 3.5: Evolution of mode coupling versus contact stiffness on pad-housing/caliper

This sensibility study shows that the mode lock-in around 3.7 kHz that involves the same deformed shape during squeal noise is unstable at a pad-housing/caliper contact stiffness between $[9.10^{12}; 2.10^{13}]N/m$.

For a complete analysis of the mode lock-in evolution, a study showed in figure 3.8 on near frequencies that might lock around unstable frequencies has been done. The interpolation between points is only here to follow the mode lock-in and has no other goal. The red cross is the default stiffness value used for most numerical captures in this study.

There are 5 possibilities of mode-coupling varying the pad-housing contact stiffness in the field described in table 3, but not all might be related to squeal noise. A fine study on deformed shape is expected. However, by comparing frequencies and deformed shapes around these frequencies, even though they don't coalesce, we can suppose that some modes evolve regarding figure 3.8. They seem to merge around low frequencies.

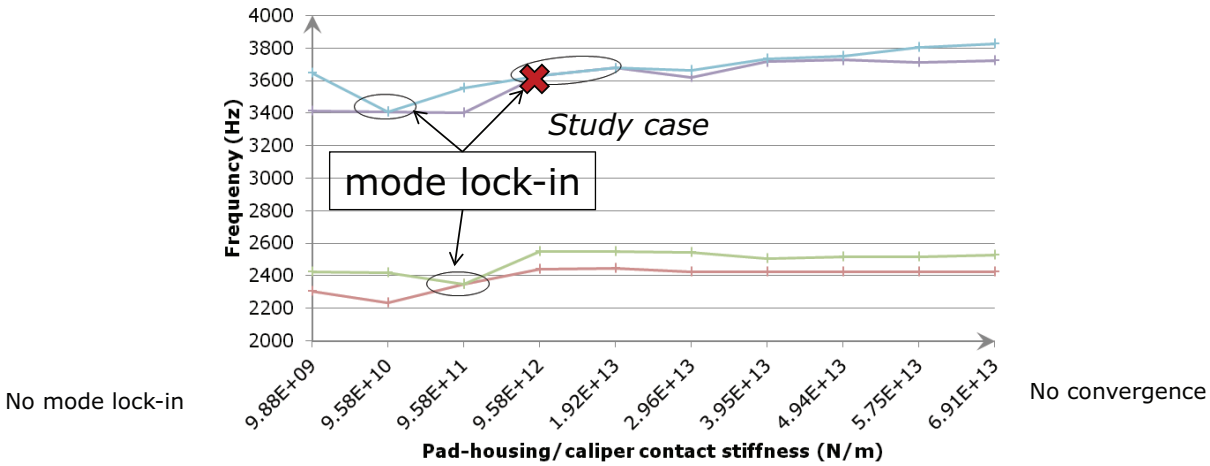

Figure 3.8: evolution of coalescing modes according to pad-housing/caliper contact stiffness

It is assumed that the tilting of the pad is one of the factors that lead to squeal noise. In our case, the tilting is driven by the pad-housing/caliper's stiffness between both parts. One might think that other contacts zones are minor factors. Table 3.5 shows the influence of varying the contact stiffness of piston/caliper and pad-housing/caliper. The model is considered symmetric, so the contact stiffness is the same on both sides. The contact stiffness between pad-housing and caliper is set at $1.92.10^{13}$N/m, a case the mode at 3.7kHz appears, which is logic because this bonding directly drives the pad/disc contact. It seems that varying the contact stiffness of these two contact zones influences the mode coupling in the model. These are not the key parameters, so they will be fixed in order to drive the model by only tuning the contact stiffness between the pad-housing and caliper.

It still miss a complete understanding on how behave the numerical model through different sets of parameters but besides the contact pad/disc, it seems the pad-housing/caliper contact is driving the instability appearance around 3.7 kHz.

3.5 Effect of pad geometry on squeal noise

One parameter that influences squeal noise occurrence is the pad geometry. Several tests have been performed on the experimental set-up for different formulations in forward brake sequence on different pressure, temperature and speed conditions. Three geometries have been tested: a cylinder shape, then 10 mm & 15 mm removed from leading edge of pad. The tests have been performed for the 4 friction pad formulations. Results in terms of noisy braking are shown on table 3.6.

Formulations		***Form. A***			***Form. B***		
		cylinder	*-10mm*	*-15mm*	*cylinder*	*-10mm*	*-15mm*
% of noisy brakings	*2.0-2.8 kHz*	0	0	0	1.4	0	0.4
	3.1-4.2 kHz	33.1	0	0	33.2	0.4	0

Formulations		***Form. C***			***Form. Ref.***		
		cylinder	*-10mm*	*-15mm*	*cylinder*	*-10mm*	*-15mm*
% of noisy brakings	***2.0****-2.8 kHz*	0.6	0	1.83	0	0	0
	3.1-4.2 kHz	22.5	0	14.1	29.7	0.6	0

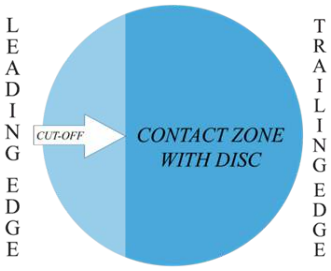

Table 3.6: Results on NVH tests regarding noise occurrence versus pad shape & formulations

All cylinder shapes are making noise around 3.7 kHz, even though the formulation is not the same in each case. When the contact geometry is reduced, a 2 kHz noise appears and the 3.7 kHz noise merely vanished. Calculations on the FE model have been performed to confirm the influence of geometry on mode lock-in. Results are displayed on figure 3.9.

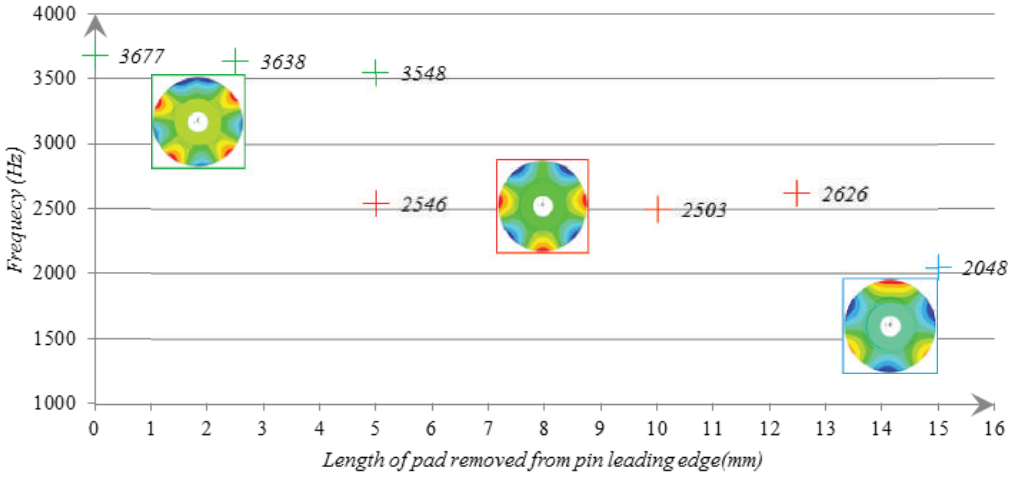

Figure 3.9: Modes coupled according to size of pad cut-off

Using contact parameters defined in table 3.4, the mode lock-in, involving an out-of-plane disc mode and tilting of pads, is the same for all unstable modes in the FE model, whatever the frequency is. It must be noticed the nodal diameters are different regarding the frequency locked-in (4/5 around 3.7 kHz and 3/4 around 2-2.5 kHz). However, the 3.7 kHz mode vanishes after removing more than $5mm$ of the pad and unstable modes around 2-2.5kHz appear. It has the same general tendency observed on experimental tests. Some additional measurements on intermediary geometries might be necessary to confirm this hypothesis. Such results have been already seen on work such as [Duboc et al., 2010]: the contact geometry influences the system stiffness and most of all the dynamic behavior of the pad-housing, which enhances a lock-in modification and therefore instabilities). The mode lock-in under 2 kHz for a 12.5mm cut-off might not be related to noise problem if it appears to exist. That would explain why this mode was not measured during tests.

3.6 NVH tests for different formulations

Four friction materials with different formulations (the simplified formulations versus Form. Ref.) have been tested on the simplified brake system. It has been observed that, during most experiments, the main frequency for the different formulations is always around 3.7 kHz (according to table 3.7).

Friction mat.	**Percentage of noise around frequency (%)**				
Formulation	2.0-2.8kHz	3.1-4.2kHz	10.-11.8kHz	12.6-13.5kHz	Total
Form. A	0.0	33.1	1.0	9.9	44.0
Form. B	1.4	33.2	0.0	0.0	34.6
Form. C	0.6	22.5	0.0	0.0	23.1
Form. Ref.	0.0	29.7	0.0	0.0	29.7

Table 3.7: Noise freq. appearing during NVH tests on the experimental rig with different friction material formulations

Noise results are developped in NVH history results fig. 3.10. There is globally low formulation effect regarding noise. Temperature is influent: at every peak of temperature (150°C), noise is almost vanishing. This result is similar in the industrial floating caliper seen in chapter 2. Comparing in details formulations, noisy situations appear for Form.A, Form.B & Form.C at low temperature (under 150°C). Around 30% of braking are noisy for formulation Ref. Form.B starts silent & becomes noisier with procedure, contrary to Form.A & C which are starting noisy & become silent with procedure.

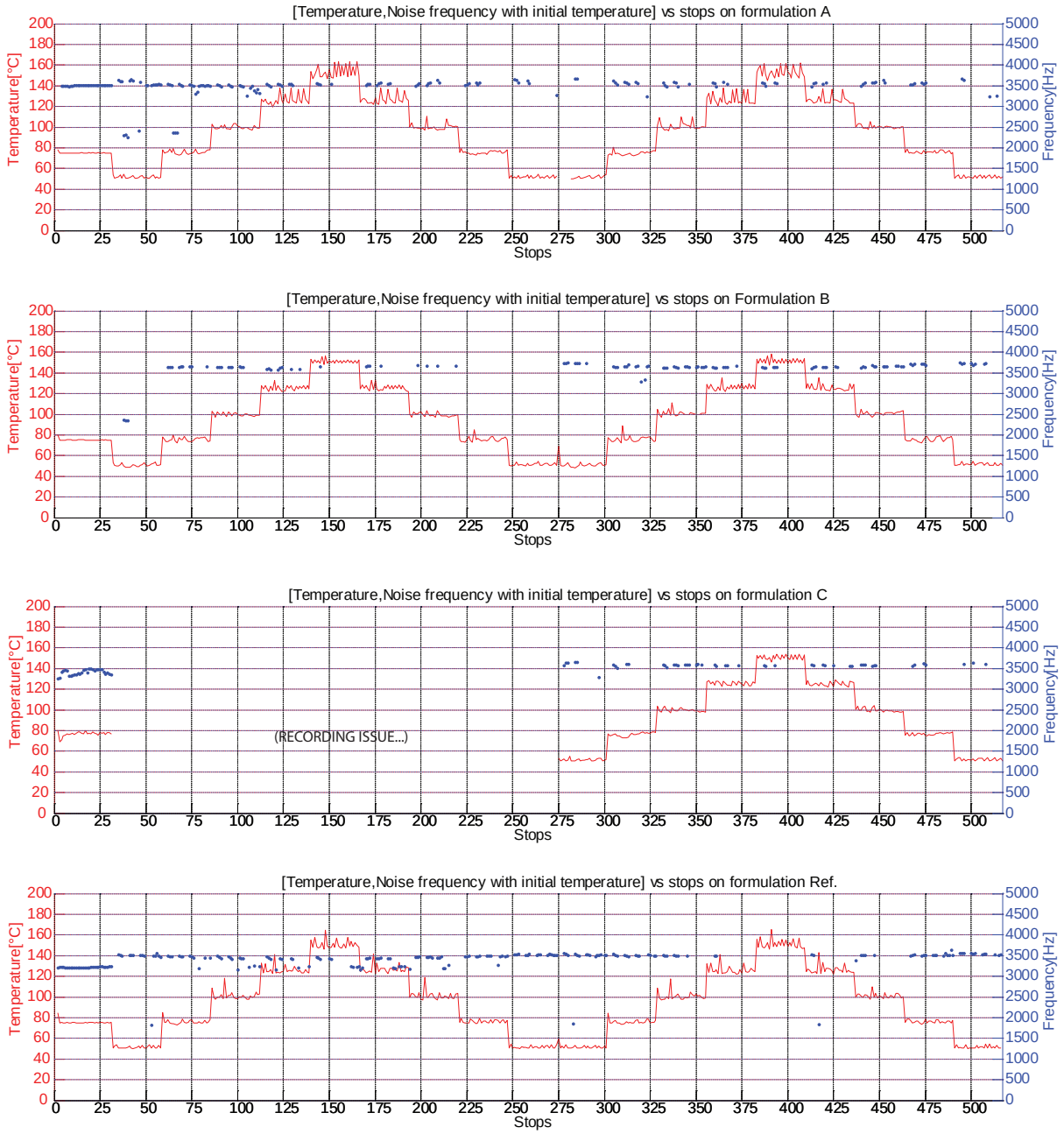

Figure 3.10: NVH results on simplified brake - Cylinder shape

3.7 Pad surface evolution with temperature influence & history effect

The sample used for test in table 3.3 are analysed by SEM measurement in order to track the surface evolution. At 3 step of one procedure for each formulation, the same samples are taken from the brake and measured then put back on.

Figure 3.11 describes the evolution from virgin state to third repetition of AK21 phase. The pad leading edge is shown, even if all surface has the same aspect in each cases (see Appendix B for more pictures). Firstly, it can be seen the surface at virgin state seems rough for the three formulations and through sliding contact, the surface changes a lot but differently depending formulation.

Looking per formulation, formulation A and C are quite similar in terms of evolution: the surfaces are getting more uniform in terms of composition, shots of carbon are smoothing, but the overall surfaces are still rough. For formulation B, the surface is getting smoother and smoother, as there is no rough particles. Also, the virgin surface is quite similar to the used surface for this formulation: with sliding and particles recirculation flow, the pad surface doesn't seem to be covered by any layer. For all formulations, it is noted the graphite particles are visible. The graphite is considered as a lubricant from friction material suppliers and this might explain why the third body layer is not maintained on these coarse particles.

The main conclusion of this study is the sliding contact is of course modifying the surface and transforming the surface, even enhance circulation of particles. However, depending the formulation, the contact surface might respond differently. In the case of formulation B, the formulation is known as less conductive, regarding heat capacity measured in chapter 2. Thus, the accumulation of heat at initial temperature braking of 150°C might be much higher. The chemical reactions above 200°C must be activated and so physical transformations such as glazing. This phenomena is appearing directly after first AK21 for formulation B but it is appearing much later for A & C (at second AK21).

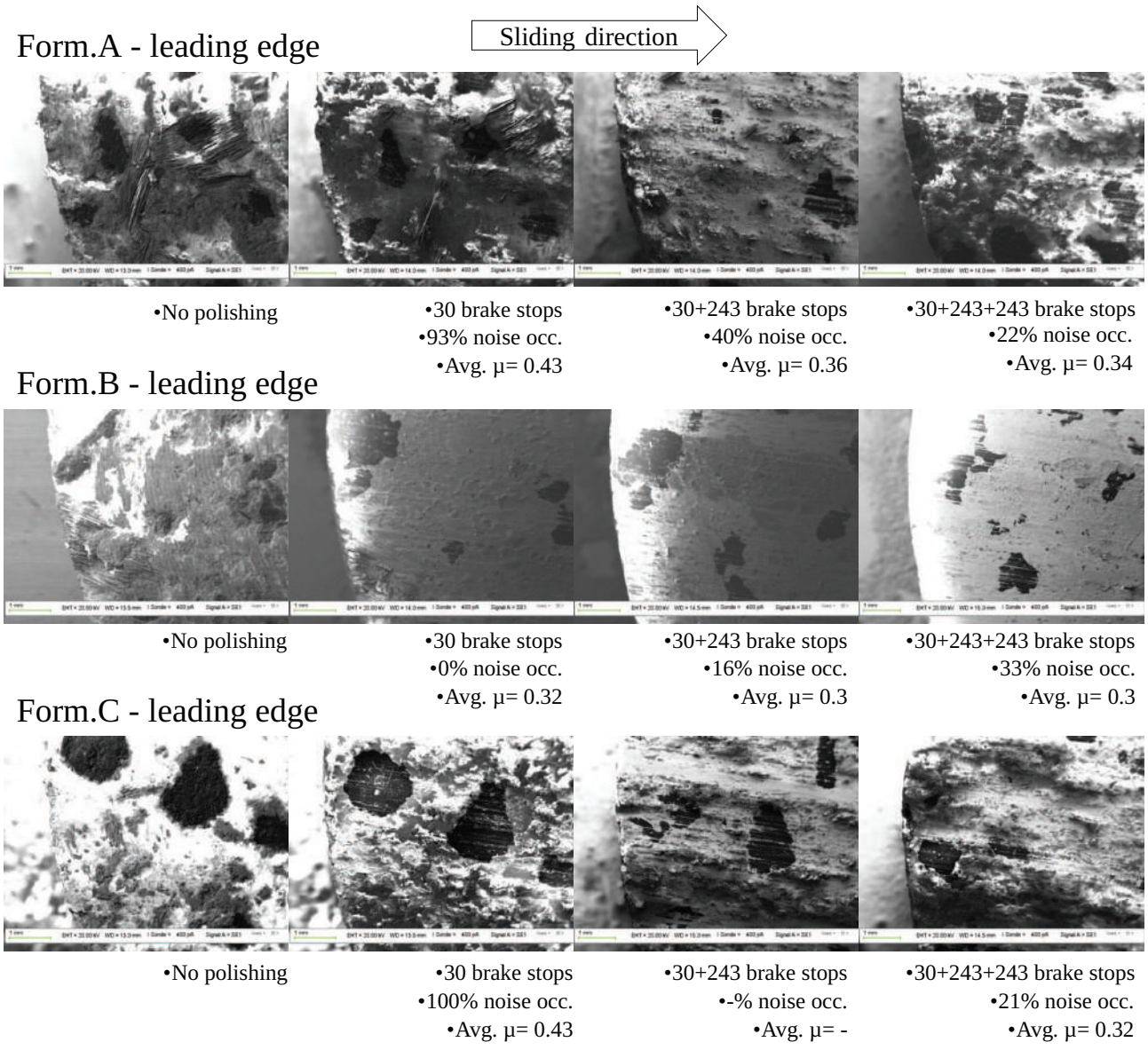

Figure 3.11: History effect on different pad formulations - Leading edge SEM observations

3.8 Chapter synthesis

An experimental set-up designed for studying brake squeal noise has been presented. It has the main feature to generate mainly one frequency band of noise around 3.7kHz.

A finite element model has been developed in order to analyse mode-coupling and determine the influence of each parameters on the model instability. Concerning pad-housing/caliper interface, it seems the contact stiffness is a complex parameter to evaluate since there is no clear method to measure it experimentally. The tuning of this linking has a strong impact on the system stability and highlight a weakness of such experimental device. However, by fixing secondary components and varying relevant ones such as the pad-housing/caliper that drive the pad tilting, good correlation may be obtained between the squealing frequencies and the unstable frequencies. The same modal shape for the disc and the caliper has been identified.

Then, fixing all contact stiffness in an unstable mode for a cylinder shape at 3,7 kHz, the influence of the pad shape with cut-off geometry from a full pad to half-pad at the leading edge, has been investigated experimentally and numerically. The same trend has been observed for both. The 3.7 kHz noise vanished when the pad is reduced, leaving small occurrence of 2 kHz noise. Regarding the FE model, the mode coupling at 3.7 kHz leaves place to 2kHz instability. There is a strong impact of contact geometry on mode lock-in. With the simplified brake system, geometry is the most influential parameter on noise occurrence, and the interfaces between components are sensitive. It suggests the need of a bigger contact surface to solicitate more the material and more stable bondings.

The interesting part of this numerical study is the fact the friction material properties themselves won't impact the stability but mostly the contact geometry. Thus, it appears unstable frequency, and supposedly squeal, is mostly induced by contact geometry, from a macroscopic point of view. Thus, at a microscopic scale, it is also assumed the contact geometry is not idealistic and plane as the numerical study shows. The bibliography as suggested contact plateaus and this is enhanced by materials properties. So, it is necessary to understand the generation of tribo-layer regarding geometry as far as mechanical behaviour.

The major influence would be on the friction coefficient and/or noise occurrence & frequency. There seems to be a close link with material transformations and surface. However, the tests described here are unsufficient to complete the understanding. Temperature threshold are not seen as much as in a classic NVH test, also the formulation effect is hidden due to the system simple geometry. Therefore, a new strategy is set up in the next chapter and all the effort are focused on the study of surface and volumic evolution of pad properties with sliding history.

Chapter 4

Effect of sliding history on pad surface & volume properties

Contents

4.1 Investigation on history effect on a NVH test

4.1.1 Motivation

Through the previous chapters, it has been seen the impact of friction history and temperature on noise occurrence. The resultant surface of the brake pad seems to be the response of a noisy (or silent) situation. In this chapter, a complete investigation is done on influences of history effect through normalized test on an industrial brake system (fig.4.1). Four situations of friction will be studied: each pad is quantified geometrically and local material properties at near-contact volume are estimated.

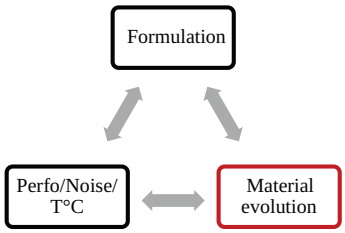

Figure 4.1: Link between pad formulation and its response to braking: surface evolution

The tests done on the simplified brake in chapter 3 gave a hint of the local transformations of friction material through sliding contact. It might have been interesting to analyse profile and mechanical properties of such surfaces. However, difficulties to distinguish friction material impact on noise on the simplified brake have been encountered. Also, profile evolution and local heterogeneities are of interest. Since, it is needed to have the most measures it can be made on a sample in order to have an accurrate stochastic analysis, it quickly appears the cylinder pad shape is not sufficient for such analysis.

Therefore, it has been decided to work with classic pad shape on the industrial brake, the ZoH3.3.1. Moreover, working on the NVH3505+NVH3505R procedure which has been described in chapter 2. Key phenomena have been shown such as temperature effect & history effect and specific steps of this procedure are of interest, specifically the fading step. Hence, 4 tests are programmed with the same procedure but stopped at differents steps in the test sequence. Two tests are stopped before and after fading (task N°19) since it has been seen the impact of high temperature in chapter 2. This is made for two formulations: C and Ref. Each situation will be completely studied regarding noise behaviour.

4.1.2 Experimental set-up

The NVH3505 + NVH3505R procedure, as in section 2.4, is used once again on the same industrial floating-caliper brake system. This system is employed instead of the simplified one because of the net area available to be analysed on an industrial brake pad contrary to a cylinder shape. The procedure is repeated 4 times but each one is stopped at a particular moment of the procedure and withdrawn from the bench. A new pad is used for each test and begins from task N°1 according table 2.8. All tests are performed on formulation C, with the formulation Ref. for comparison. Here is a description of each test (fig. 4.2):

- Test 1 (stopped after task 18): the test begins with NVH3505 but stops just before the beginning of Fade01. The pad won't see an elevation of initial temperature higher than 300°C (at 5mm from the contact surface, into the pad center).

- Test 2 (stopped after task 19): the test begins with NVH3505 but here stops just after task Fade01. At the end of this step, the pad has seen 550°C (minimum). The goal of this step is to compare two pads at different temperature level (test 1 vs. test 2)

– Test 3 (stopped after task 25): The complete NVH3505 is done. The pad has seen 1917 brake stops, with a "fading" phase and some stops after.

– Test 4 (NVH3505 + NVH3505R): All tasks from NVH3505 followed by NVH3505R are executed, so the pad has seen the same tasks as previous tests, with an additionnal procedure. The purpose is to see effect of history and wear on mechanical properties.

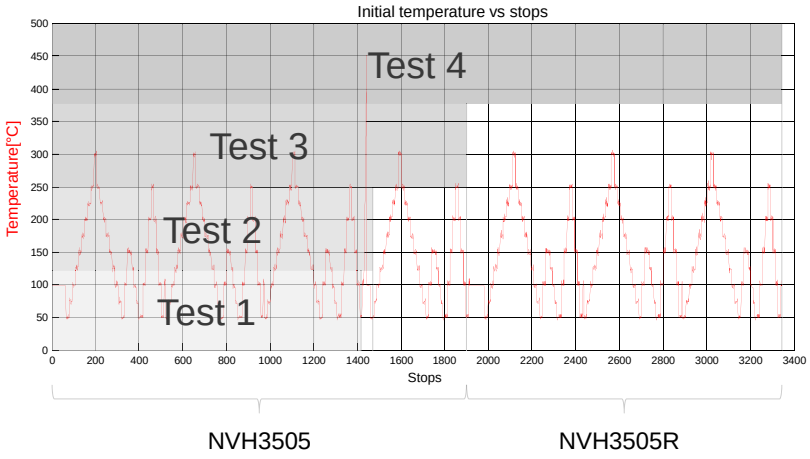

Figure 4.2: Test procedures descriptions regarding complete NVH3505+NVH3505R procedure

4.1.3 Noise results

In figure 4.3, noise occurrence is described in percentage of total braking per procedure for formulation C & Ref., e.g. if 10 brake stops out of 10 of procedure i are noisy, there is an occurence of 100%. First remark is the global repeatability in terms of noise occurrence evolution for all tests (taking into account common procedures from test to test). However, test 1 for formulation C is clearly different from others. Formulation C is noisier than Ref., and noise is increasing with history. Comparing to chapter 2 results, the global trends are similar.

Figures 4.4 and 4.5 show the frequencies evolution and associated final surfaces after each test for both materials C and Ref. The evolution of friction material surface is displayed in parallel of noise frequency history versus temperature. Red dust is rust from the disc due to the climatic room.

First of all, regarding chapter 2 tests and comparing one test to another for each formulation separately, it seems test repeatability is here in every test even if there is slight differences. These might be caused for example by the pad mounting on the caliper or the manufacturing variability. Brake pads are heterogeneous materials and this must be taken into account in this "variability" issue. The noise frequency ranges are equivalent and, even the history and activation of high frequencies are alike. Both formulations generate mostly one frequency range and are either more or less stable around it all along the procedure. C material is noisier than Ref. It must be noticed Test 1, 3 and 4 last stops are in a noisy state, whereas **Test 2 has stopped silent for both materials C & Ref**.

For material C, surface is drastically evolving from virgin state to test 4. Surface is getting darker regarding a new pad, sign of the heat spreading into the materials, and so material chemical transformations. It must be noted the surface seems relatively rough for all tests, except for test 2 which is stop at the end of fading phase. The surface has a kind of mirror aspect. Glazing is almost uniform from leading to trailing edge. The temperature is above 450°C into the material and regarding thermogravimetry/dilatometry measurement, the material will transform significantly over 250°C. There, this second threshold has been crossed and thus implies material transformations, and moreover degradation. It can be noticed the noise behaviour after fading changes a lot looking at test 3 and 4. Thus, the material transformations enhanced a different coupling, which suggests a modification of the tribo-layer

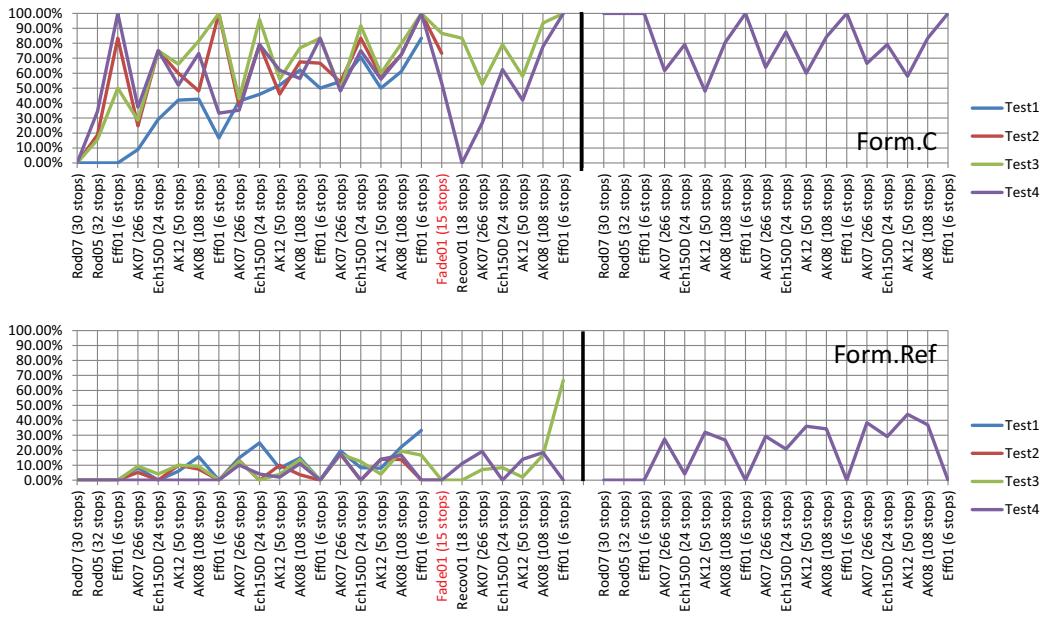

Figure 4.3: Noise occurrence regarding procedure

nature, to the volume itself.

The frequency range is wide for formulation C. However, low frequencies are disappear with stops, and even more after fading. The temperature has a low effect on other frequencies, they appear durable along the history. Also, high frequencies ($>$ 10kHz) emerge permanently and don't cease their propensity. The material transformations emerge not only on the surface but also in the pad volume. Hence, one can expects the gradient of mechanical properties into the materials has evolves according to the heat level and dissipation.

Regarding formulation Ref., even if the raw materials and manufacturing process are different, the observations are almost the same: the material is getting noisier with stops cumulation. Also, fading increases the emergeance of high frequencies (around 13kHz). The 8kHz noise is more and more present. The glazing effect is also appearing after fading (test 2). The main difference between form. C and form. Ref. is the noise overall percentage which is lower for the industrial material.

From top to bottom (inner pad):
0 - unused pad
Test 1 - NVH3505: stopped before fading
Test 2 - NVH3505: stopped after fading (450°C)
Test 3 - NVH3505 completed
Test 4 - NVH3505 +NVH3505R
Left: leading edge / Right: trailing edge

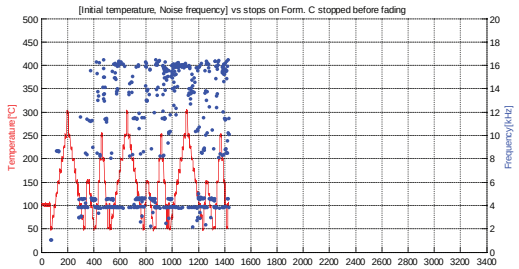

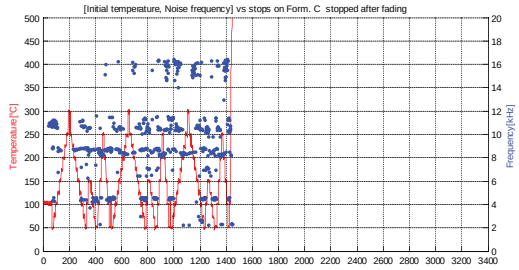

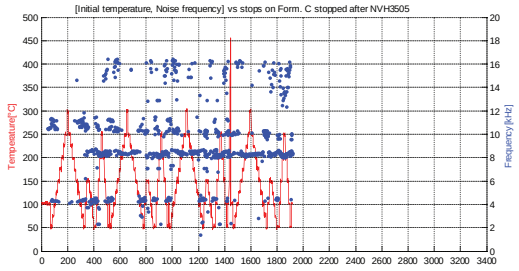

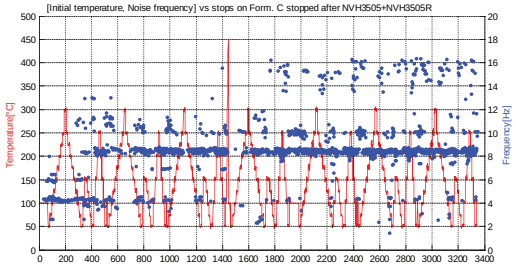

Figure 4.4: Comparison of pad surfaces (internal pad) from form. C and their associated noise response through 5 different friction states

From top to bottom (inner pad):
0 - unused pad
Test 1 - NVH3505: stopped before fading
Test 2 - NVH3505: stopped after fading (450°C)
Test 3 - NVH3505 completed
Test 4 - NVH3505 +NVH3505R
Left: leading edge / Right: trailing edge

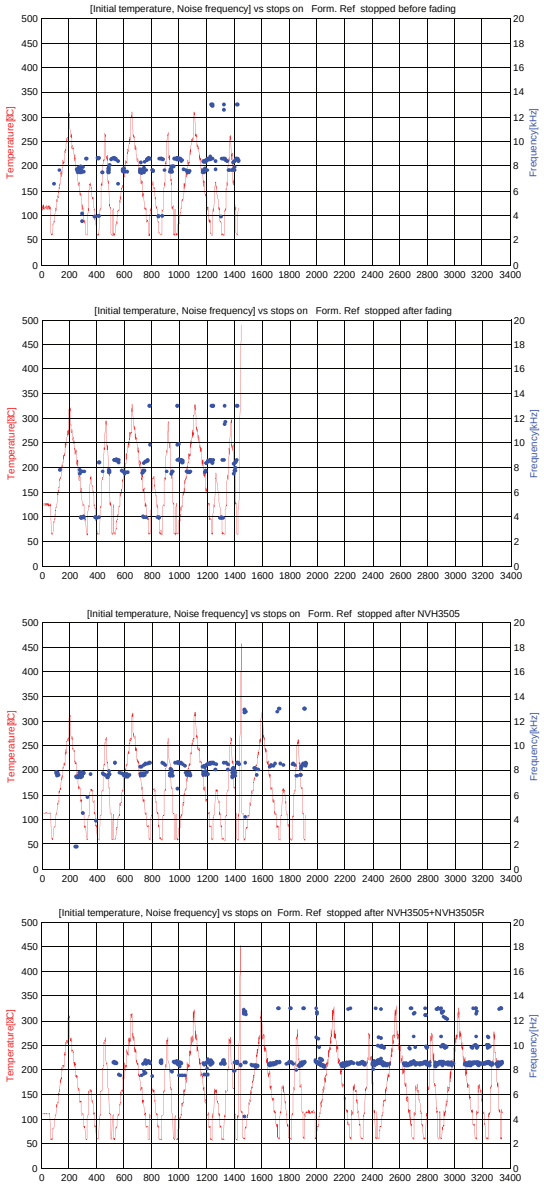

Figure 4.5: Comparison of pad surfaces (internal pad) from form. Ref. and their associated noise response through 5 different friction states

4.1.4 Conclusions on NVH tests

Noise tests have been performed on brake pads from formulations C & Ref. stopped at different states of friction on the same procedure. Common steps for every tests per formulations are almost repeatable. Regarding formulations, C is noisier than Ref. Both are generating 8kHz frequencies all along the procedure. Moreover, 10-12kHz noises are appearing with friction and become more and more present. Temperature is a key parameter: at each peak of temperature (above 300°C), the brake stops become silent. Fading is a noise suppressor for material C.

Concerning surface evolution, used pads (test 1,3 and 4) are similar and have an highly different aspect comparing to a new pad. The surface is darker and shiny. After fading (test 2), the surface is covered of glazed material which is appearing on both formulations. Further brake stops at lower temperatures remove this layer and the material regains its previous aspect. High transformations of the material C occur after 200°C and even degradation above 350°C, especially for resin and rubber (cf. chapter 2). Moreover, for material C & Ref., permanent modifications in term of frequencies are appearing after fading (mostly high frequencies above 10kHz). It suggests a material transformations not only on the surface but also into the volume.

Thus, the combination of the noisy/silent state and the chemical transformations or the material lead to think the link between both is the surface (cf. chapter 2). The topologic evolutions and the local properties behind them must be analysed and understood for each state of friction, from the surface to the volume, taking into account the natural heterogeneity of the material (formulation) which might be increased with friction (plateaus and tribo-layer). A profile study coupled with observations is critical before trying to quantify the local mechanical heterogeneities.

In order to strengthen the study, it might be of interest to launch longer tests. It appears the noise occurrences are not stable. Also, repeatability is not entirely attested, therefore each test should be done several times.

4.2 Geometric surface analysis

In this section, the innerpad surface profile of each NVH tests is measured. Classic methods decompose the profile into three orders: shape, waviness and roughness. Then, microstructure analysis is performed.

4.2.1 First order profile - Shape & wear

To determine the first order profile (Shape), a three-dimensional measuring machine is used . With this test in addition to the default form, the friction plane orientation relative to the backplate reference plane are known (see Figure 4.6). Backplates appear to have a natural tilting which has been offset with steel shims. The reference plane is the backplate in order to avoid this tilting into the measure and focus on friction material surface.

The reference plane is the same on each pad and the friction material thickness (for form.C) is only measured, thus the wear for each friction stage can be determined. 140 points are measured on the surface (every 5mm). All results are summarized in Figure 4.7. Tapered wear is naturally observed for all samples which is link to the brake kinematic: the pad is pushing on the disc surface and also tracted by the disc rotation. Thus, the fact the leading edge (left side of pad) is more wear than trailing edge is coherent.

New: almost flat surface, some irregularities, maybe positionning or backplate tilting (not a plane surface obviously)

Test1: High wear rate especially on the leading edge of pad (left side), ascending level from upper leading edge to lower trailing edge

Test2: Very high wear rate (only 16 stops diffence between test 1 and 2 with a $10\mu m$). The resultant deflection is different from test 1, 3 and 4. A concave shape appears on the upper left side of the pad. The suggested hypothesis is the pad is heat conservative during fading phase (450°C) at his center and when the brake is cooling down, the

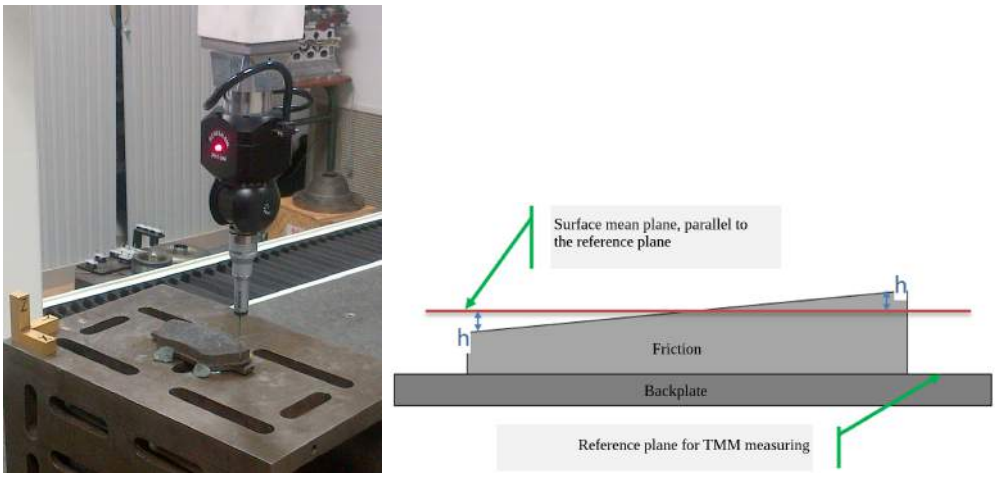

Figure 4.6: Three-dimensional measuring machine reference planes

borders of the pad are cooled before the center. The center offset of the deflection shape might be due to the the leading edge being hotter than trailing edge. The contact area is then reduced and it has been noticed a silent situation during last stops. It suggests a link between both.

Test 3 & 4: The wear rate seems to be lower than for test 1 and 2 but the wear shape is clearly the same as in test 1.

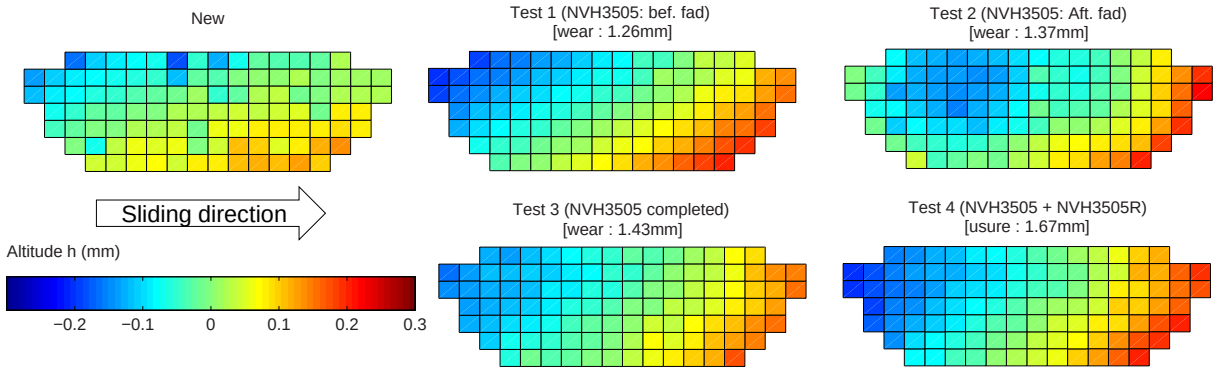

Figure 4.7: Evolution of form. C pad profil & wear - Tridimensionnal measurement

A same trend can be observed for material Ref. in fig.4.8. However, the material is affected in a minor way. For example, fading doesn't seem to affect significantly the surface and the wear is more progressive regarding the global history.

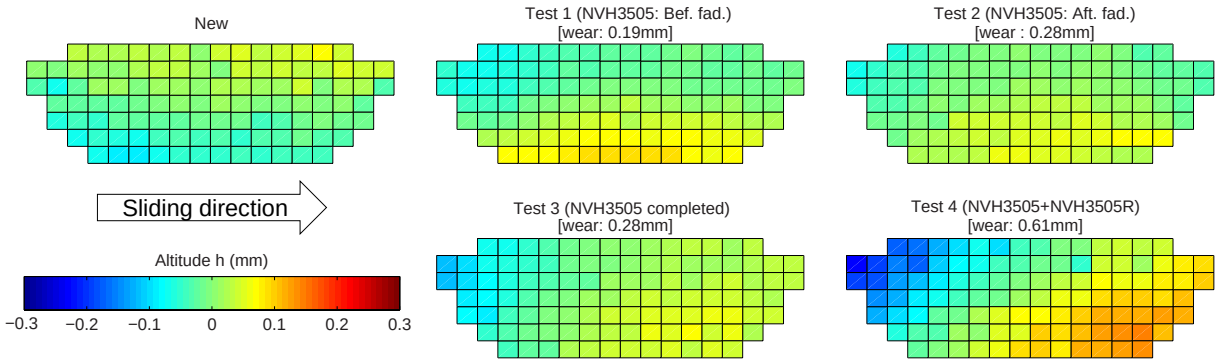

Figure 4.8: Evolution of form. Ref. pad profil & wear - Tridimensionnal measurement

In theses results, it can be summarized:

- New pads are almost plane surfaces, even if form. C has a higher planeity defect regarding Ref.
- Used pads have the same shape due to the kinematic positionning during braking (leading edge is in-contact while trailing edge contact is open).
- Fading modifies the plane itself to a concave shape: the material thermic inertia combined with high temperature gradient might have caused a "hot-spot" at pad center.

4.2.2 Waviness & roughness

To determine the waviness and roughness defects, the profiling is used. In addition, the studied material being the result of several compounds assembling, so there are very heterogeneous optical properties, thus the contact profilometry is used. The choice of using contact instead optical profilometry has been decided by the lack of a working device. The pressure applied on the material barely scratches the surface. Previous studies has shown the slight impact of such measure on friction materials as in [Baklouti et al., 2013] (fig.4.9).

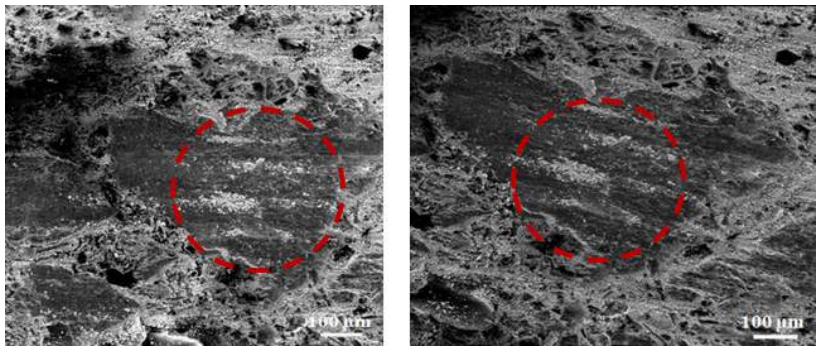

Figure 4.9: Before (left) and after (right) contact profilometry [Baklouti et al., 2013]

The machine KLA-Tencor P16 + is used (figure 4.10). The pad center is observed with a rectangle of 14 lines spaced $2.5mm$ and $60mm$ length. This distribution takes into account the capabilities of the machine and allow to see the parameters evolution in function of the disc radius.

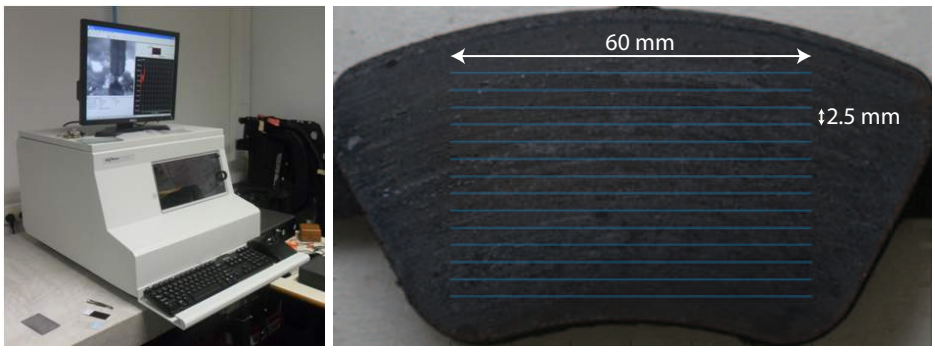

(a) KLA Tencor P16 + (b) Profilometer lines observation

Figure 4.10: Mechanical profilometer device

Other test parameters are:

- The force applied by the probe on the surface: $5mg$
- The measurement resolution: $2\mu m$ (that is to say a speed of $200\mu m.s^{-1}$ acquisition rate $100Hz$)

The determination of these parameters is a compromise between measurement accuracy, material damage and measurement speed.

Tests give a rough picture of the surface profile, to extract characteristics, post-processing is based on the standard ISO16610-31 which use the Gaussian filtering. This filter is used to calculate each point of the profile in terms of its close neighbors with a Gaussian weighted (fig.4.11) as follows:

$$G(x) = \frac{1}{\alpha \times \lambda_0} \times \exp^{-\pi \times \frac{x}{\alpha \times \lambda_0}} \tag{4.1}$$

with

$$\alpha = \sqrt{\frac{\ln 2}{\pi}} = 0.4697 \tag{4.2}$$

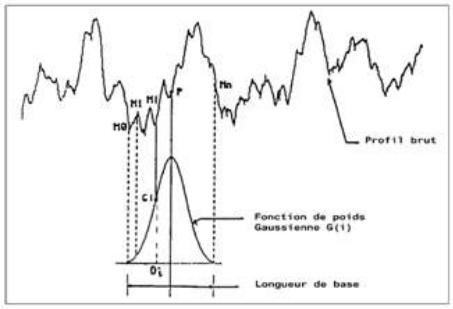

Figure 4.11: Gaussian weighted

Where λ_0 is the cutoff wavelength of each order (eg, λ_c called "cut-off" to determine the boundary between roughness and waviness), they allow by applying successively to extract each profile as shown in figure 4.12. It must be noted the shape cutoff wavelength ($\lambda_f = 6$mm) is similar to three-dimensional measurement (5mm). However, here the pad tilting is not given, therefore it is difficult to conclude on the shape by the contact profilometer.

Parameters	λ_0 filter	Base length
Shape	$\lambda_f = 6$mm	$L_f = 6$cm
Waviness (W)	$\lambda_c = 2.4$mm	$L_c = 6$mm
Roughness (R)	$\lambda_s = 2.4\mu$m	$L_s = 1.2$mm

Table 4.1: Base length for 1, 2 and 3^{rd} geometric orders

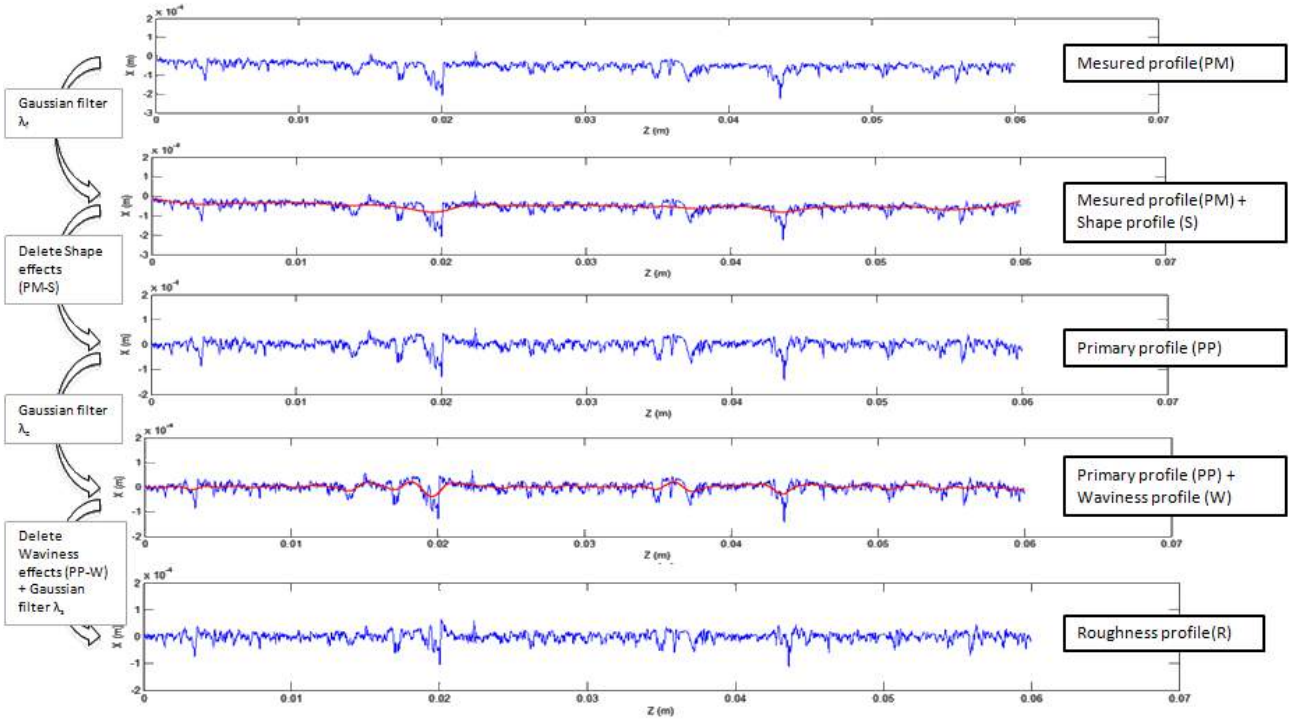

Figure 4.12: Example of profiles extraction method (shape, waviness, roughness) on Test1 innerpad, line 8

By this method, the waviness defects (Wa) or roughness (Ra) are determined on a line to know the mean default on a pad a defects average is done per measurement line. One result on the center line of pad formulation C is shown regarding waviness in figure 4.13 (roughness signal frequency is too high to conclude on). The main result from this graphic is the waviness is lowered with friction from virgin to sliding state. From test 1 to test 4, the waviness has globally the same order.

At this stage the three profiles are extracted, and the arithmetic mean deviation (Wa for waviness and Ra for roughness) can be evaluated. The generic equation to calculate an arithmetic mean deviation is presented in figure 4.14. Shape deformation is calculated but it can be altered by the inaccuracy of the pad positioning on the machine plate. Also, the filter (6mm) is almost equivalent to the one used for three-dimensional measuring machine (5mm). Hence, the shape results with contact profilometry will be not regarded and only three-dimensional measuring machine results will be used for shape.

$$X_a = \frac{1}{n}\sum_{1}^{n}\left(\frac{1}{i}\sum_{1}^{i}(\mid Z_i - Z_{moy_i} \mid)\right) \tag{4.3}$$

with :

– X = W (Waviness), R (Roughness)

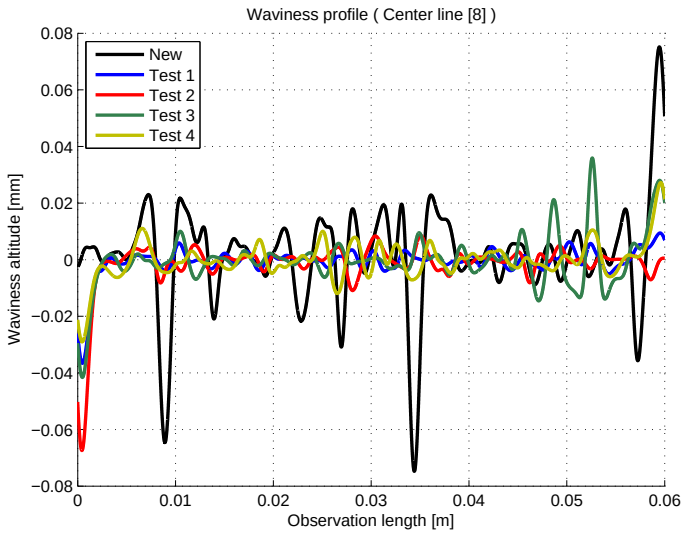

Figure 4.13: Waviness profile: Test1/Line 8 on pad formulation C

- n = number of base length
- i = points per base length
- Z_i = profile altitude at the point X_i
- Z_{moy_i} = average profile altitude at the least squares sense to the point X_i

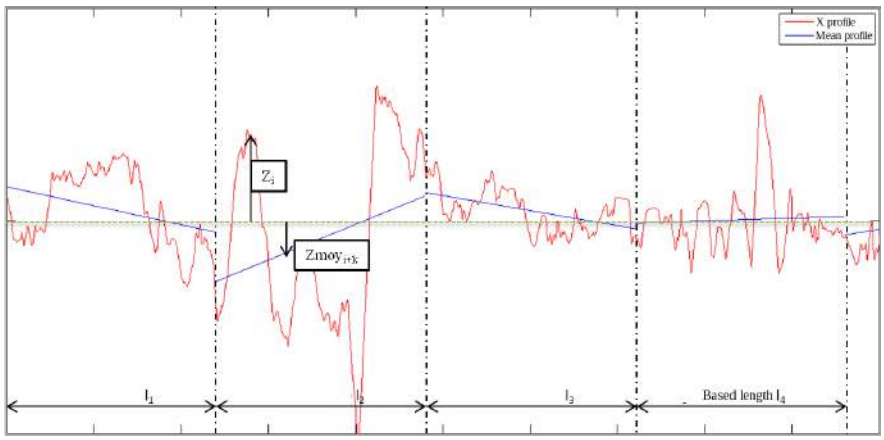

Figure 4.14: Parameters for determining the arithmetical mean deviation

Mean waviness and roughness results over all the lines for both formulations C & Ref. are shown in figure 4.15 and 4.16, in addition with maximum and minimum of mean values. A change of state between a new and worn pad can be already seen: friction lowers significantly the Wa and Ra. However, deviation from test to test is the same (approx. $4\mu m$). Moreover, on waviness and even more on roughness, fading (test 2) smooths the profile. From an observator point-of-view, the surfaces have been glazed for both materials on test 2 and seem more regulars. Thus, this measurement quantifies this observation.

Comparing formulations, formulation C with sliding contact has a "stabilized" roughness and waviness for new, Test 1, 3 & 4. Fading has a smoothing effect (Test 2). Formulation Ref. is more influenced by braking history: fading (Test2: temp.> 450°C) reduces the surface profile but with numerous stops after (Test3&4), the material recovers his previous state (as in Test1) and even more increases for both Wa and Ra.

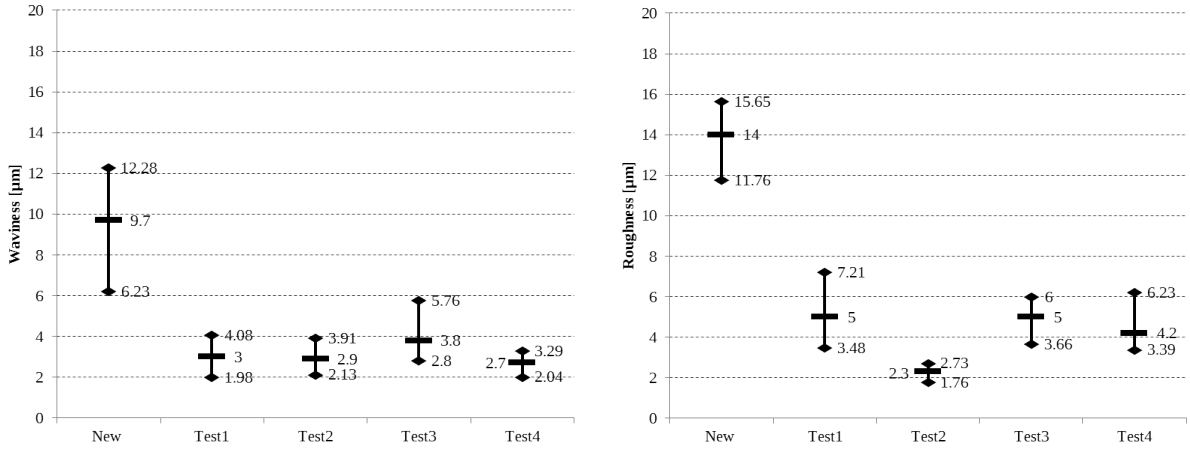

(a) Waviness (b) Roughness

Figure 4.15: Mean deviation of waviness and roughness results for material formulation C

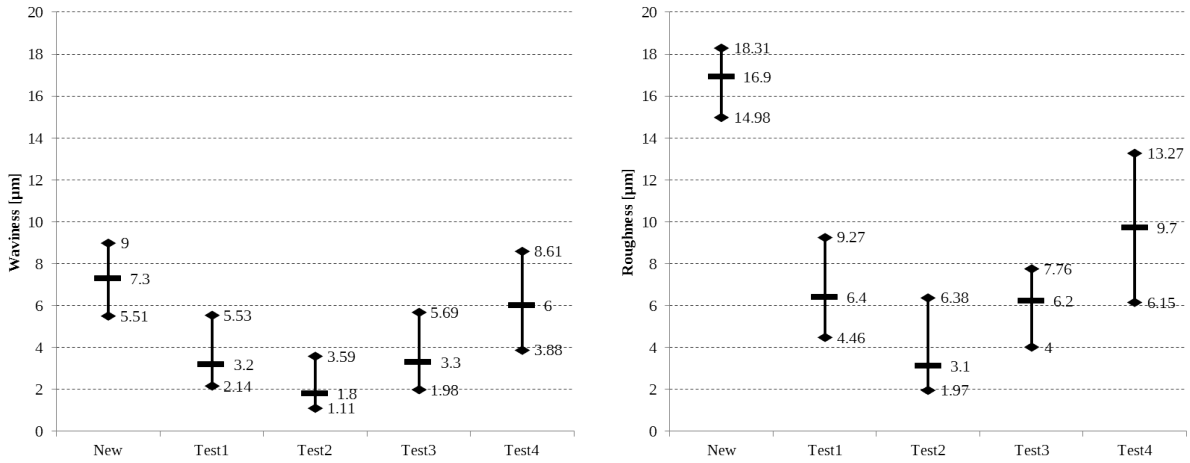

(a) Waviness (b) Roughness

Figure 4.16: Mean deviation of waviness and roughness results for material formulation Ref.

4.2.3 Microstructure observations

Brake pads are composites of materials with very different properties. The weakest components, such as resins and solid lubricants, have a hardness of 200 MPa, while the abrasive particles and fibres in some cases may have a hardness of up to 20 GPa. Further, the components show a wide spectrum of wear resistances. These differences result in a complex contact situation with unevenly distributed wear and compaction of wear debris which results in a surface characterised by flat plateaus rising above the rest of the surface, as identified in works as [Eriksson and Jacobson, 2000]. The plateaus can be spotted with the naked eye as shiny spots against a dark background. The present subsection is focused on exploring the pad surface from formulation C at different sliding state using scanning electron microscopy (SEM) coupled with x-ray detection. Virgin, before & after fading states are analysed.

At end of manufacturing, the pad seems only covered by resin and carbon at first sight: a grey surface shadows the most raw materials (in fig. 4.17). However, global x-ray detection on the studied area shows the elements presence in the materials. All elements of the formulation are found.

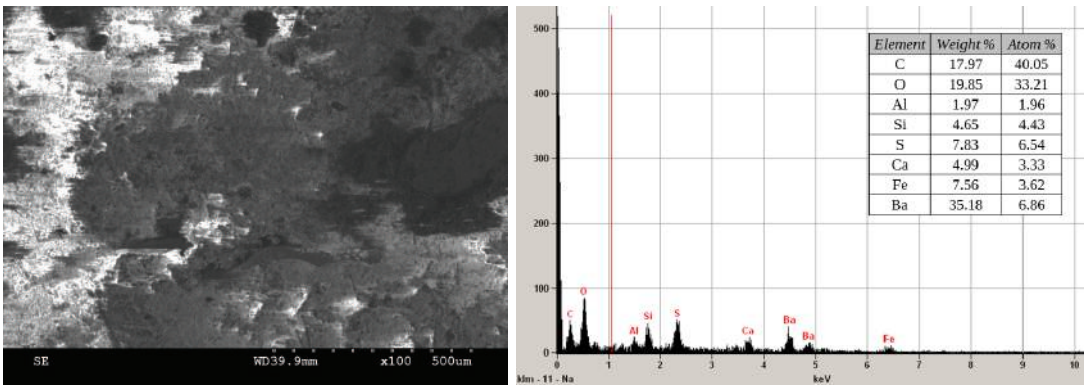

Figure 4.17: Microscopic observation of new pad from formulation C

Figure 4.18 shows the formulation C inner pad after Test 1 (before fading). "Left-side" (a) is located around pad leading-edge, in opposition to "right-side" (d) is the trailing edge. "Upper-center" is the upper-radius of the pad from pad center, in opposition to "lower-center" which is the lower-radius. First thing to say is plateaus (c) are emerging from surface (b,c & d). They are around $500\mu m$ large and there are wide carbon spots (a and c) around $200\mu m$ large all along the surface. One thing to notice is there are a lot of powder particles as in (b).

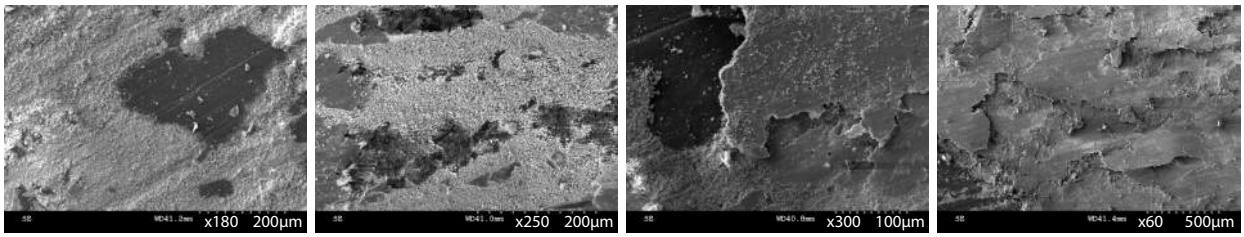

(a) Left side (b) Upper-center (c) Lower-center (d) Right-side

Figure 4.18: Before fading (Test 1) for formulation C

Comparing with figure 4.19 after fading, the surface has bigger and continuous plateaus all along the pad (b). The surface seems more glazed as in (a) and the contact plateaus seem thicker (c and d). Particle powders are less present which suggests a "cleaning" of the tribo-layer(c). Only particles found are more as debris from contact plateaus (d).

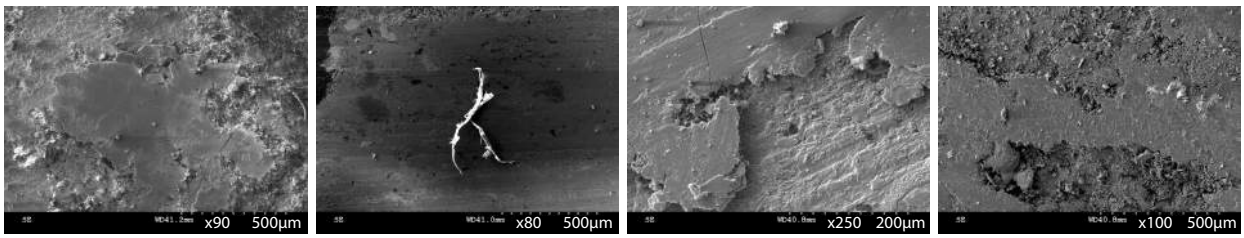

(a) Left-side (b) Upper-center (c) Lower-center (d) Right-side

Figure 4.19: After fading (Test 2) for formulation C

A transverse cutting (into pad volume) has been performed at pad center (fig.4.20) and shows the heterogeneous composition of the pad at virgin state and after fading (test 2). It must be noted for test 2, there are a lot of small components trapped between fibres near sliding contact (upper-left corner), and the compaction is decreasing near the backplate, the compounds seem much bigger. The virgin state appears to be compacted homogeneously from surface to backplate. This must be due to the degradation gradient: in test 2, the surface is heavily loaded in term of stress and temperature at surface and less near backplate.

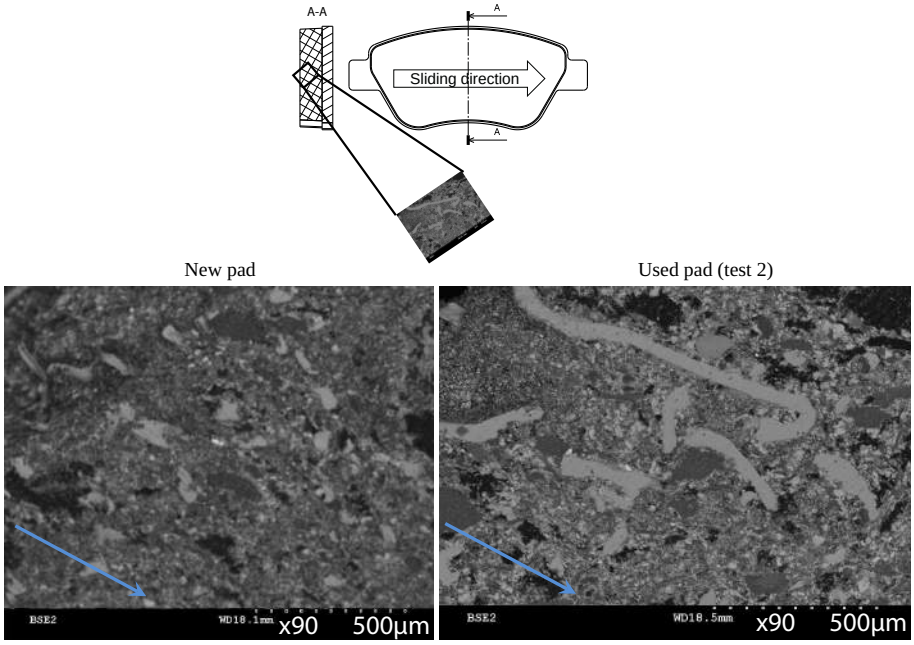

Figure 4.20: Transverse cut of innerpad after fading (arrows indicate from pad surface to backplate direction)

4.2.4 Conclusions on geometric analysis

In this section, it has been shown the brake stops consequences on surface profile. Three main conclusions emerge from it.

Wear/shape Regarding global profile, new pads are rough surface comparing to used pads which are smoothed with friction. Also, kinematic contact geometry conditions the pad wear: the wear profile is plane for test 1,3 & 4 whereas, with fading (450°C), the profile becomes concave, certainly due to thermal dilatation coupled with wear. This might influence the contact area significantly and thus modify the noise frequency, or even appearance.

Important wear rate is seen for both materials, even more for form. C. Fading enhances this phenomena comparing to other brake stops.

Waviness & roughness Comparing new pad and used pad, the waviness and roughness are deeply lowered. Test 1, 3 and 4 are almost identical for formulation C, whereas form. Ref. tends to go back to its virgin state at test 4. For fading test, the mean values for both are the lowest, the profile is almost flat. Particle size impacts roughness as waviness (confirmed for formulation C regarding granulometry in chapter 2). Contact plateaus sized which are amassed particles can be also related to waviness.

Influential events With high temperature gradient as fading, material surface is smoothing. The third body layer is more homogeneous and smooth, as wear is increasing. Formulations C and Ref. are keen on this behaviour. After fading, with cumulation of brake stops, contact surface come back as before fading due to the circulation of particle and wear. The particles and debris behind the surface, which were not affected by fading, recirculate and generate a surface similar as in test 1.

4.3 A methodology to evaluate local material properties

4.3.1 Motivation

Profilometry has shown the geometric evolution of surface with sliding contact. SEM analysis has drawn attention to the chemical and physical transformation of the particles and plateaus at the contact. It leaves the mechanical behaviour evolution from a friction state to another. The difficulty is in the scale to study the phenomena. Works has [Heussaff et al., 2012] described in chapter 1 are the rudiments of identifying the local stiffening. The surface rigidity is measured by a flat indenter and the whole non-linear behaviour is translated into a non-linear stiffness. In the literature, breakthroughs have been done on identifying films or small particles by indentation. Therefore, it seems interesting to use this method to characterise local heterogeneities on the pad surface.

4.3.2 A brief history of indenting materials

Most measurement only considers bulk material properties such as compression test. Contact mechanics is more dedicated to understand the surface and geometrical constraints. Hence, theories has been exposed through the last centuries.
Geometrical effects on local elastic deformation properties have been considered as early as 1880 with the Hertzian Theory of Elastic Deformations ([Hertz, 1882]). This theory relates the circular contact area between two spheres to the elastic deformation properties of the materials.

Rheological models have been developped based on Hertz contact theory. Devices invented around this theory lay on probes brought into contact with the material of interest, measuring properties such as hardness, wear rates, etc. Indentation measurement is based on this concept. A tool of a certain shape is force- or displacement- controlled into the studied material, and then released from contact. A loading-unloading curve can be traced in the force-displacement domain.

Its main purpose is to connect the load P (N) with the indent dimensions to define the hardness, resistance to plastic deformation. The hardness number is defined as:

$$H = \frac{P}{A} \tag{4.4}$$

with A_P the projected area or A_T true contact area.

With Hertz theory, contact pressure can be estimated from contact surface to a certain deformed volume limit. Thus, elastic properties can be identified from material tested. To incorporate the effect of adhesion in Hertzian contact, [Johnson et al., 1971] formulated the Johnson-Kendall-Roberts (JKR) theory of adhesive contact using a

balance between the stored elastic energy and the loss in surface energy. The JKR model considers the effect of contact pressure and adhesion only inside the area of contact, which can be approximate to:

$$P = \frac{4a^3 E_r}{3R} \tag{4.5}$$

where P is the load applied, R the ball radius, $a = \sqrt{Rh}$ the ball imprint radius on the material and E_r the elastic modulus resultant of both materials in contact:

$$\frac{1}{E_r} = \frac{1-\nu_{ind}^2}{E_{ind}} + \frac{1-\nu_{mat}^2}{E_{mat}} \tag{4.6}$$

[Johnson, 1987] has extended this theory by developping the special cases, and moreover the one interesting in this work problematic: the sphere-plane contact.

Hertz and later JKR theory used the loading part of indentation curve.Other theories used the unloading part of the curve. It deals with the fact hertzian contact hypothesis considers:

- area of contact is smaller than the characteristic radius of the body,
- the surfaces are continuous and non-conforming,
- the strains are small and within the elastic limit,
- the surfaces are frictionless.

Thereby, most contact are non-hertian. From this observation, [Oliver and Pharr, 1992] has developped a new theory on the unloading part of the indentation curve. During unloading, it is assumed that only the elastic displacements are recovered; it is the elastic nature of the unloading curve that facilitates the analysis. They assessed there are three important quantities that must be measured from the $P = f(h)$ curves: the maximum load, $P_{max}[N]$, the maximum displacement, $h_{max}[mm]$, and the elastic unloading stiffness, $S = dP/dh$, defined as the slope of the upper portion of the unloading curve during the initial stages of unloading (also called the contact stiffness).
The accuracy of hardness and modulus measurement depends inherently on how well these parameters can be measured experimentally. Another important quantity is the final depth, h_f, the permanent depth of penetration after the indenter is fully unloaded.

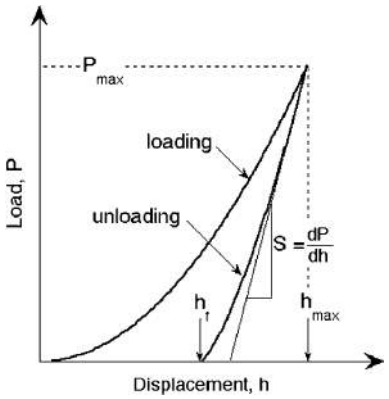

Figure 4.21: Schematic illustration of indentation load–displacement data showing important measured parameters

The indentation field is quite wide and in this frame of work, the aim won't be to make a design of experiment of the indentation measurement. Many studies have shown for example the effect of indentation size effect which assess the hardness is less dependant of the load with the indentation size growing [Nix and Gao, 1998]. Also, phenomenon as creep effect during indentation measurement [Chicot and Mercier, 2008] or pop-in/nucleation during

loading [Lorenz et al., 2003] are important to look for but it won't be the purpose here. A more complete and recent review of indentation achievements can be found in [Mendoza Delgado, 2009] PhD work which is a good introduction to the many difficult aspects of measurements.

The loading part of the indentation measurement will be studied and exploited with the Hertz contact theory extended by JKR work. In fact, the loading part of the curve is the interesting part in this study because it deals with the beginning of contact and it takes into account the surface behaviour which won't appear in the unloading part because it is supposed entirely volumic and elastic. Macroscopic scale indentation will be used due to the millimetric nature of some raw materials. In addition, in order to study materials in specific friction states, hence not loosing surface history, the samples will not be prepared (no polishing or flatness / parallelism).

4.3.3 Indentation testing parameters

The $10mm$ Brinell indenter shape has been chosen in accordance with the brake application: the raw materials are of a millimetric size and the contact must be considered as plane as possible. The flat indenter is too restrictive regarding the edges but the ball geometry of $10mm$ as a radius sufficient and is a good compromise. After a sensitivity analysis for each parameters (which will not be detailled here), it has been noticed that the choices for load speed and ball size are correct.

All the indention tests for this study are performed with 2.5 ZHU Zwick device (fig.4.22), whose main features are listed below:

- Crosshead speed : 0.001 to $50mm.min^{-1}$
- Load range : 5 to $2500N$
- Measurement travel : $4mm$
- Resolution travel : $0.02\mu m$

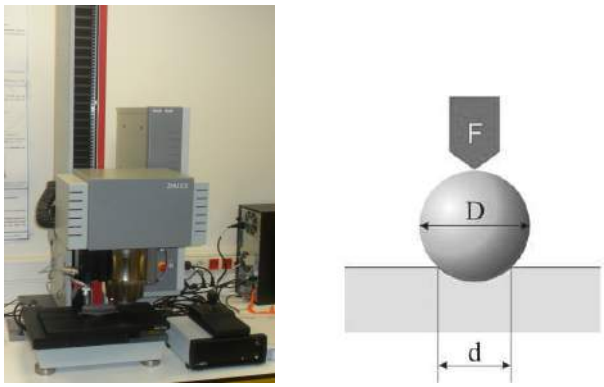

(a) Indentation machine (b) Brinell Indenter

Figure 4.22: Indenter device and tool shape

The probe is affecting the tested material in its volume. Commonly, between to indented spot, there must be a distance of two times the probe diameter, hence here $2 \times 10mm$. However, the current study uses an elementary volume of $\phi 5mm^2$. The methodology which justify this choice will be described in chapter 5. Also, a max load of 300N is applied.

Knowing this elementary volume, the brake pad is divided into 140 square areas of $5mm$ side (figure 4.23). Thus, this cutting permits to emphasize a potential heterogeneity of material behaviour without impacting the surrounding.

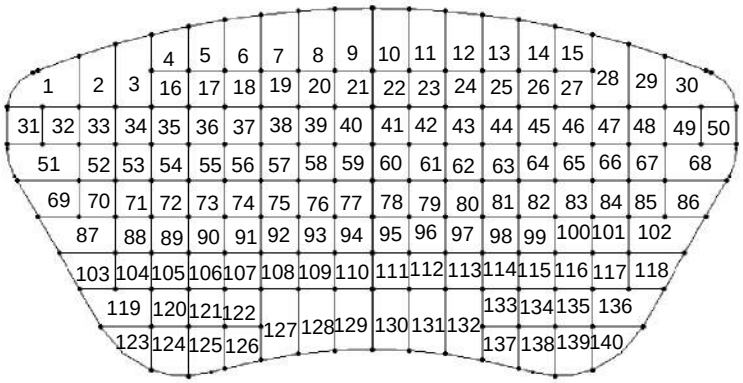

Figure 4.23: Indentation tests mapping

4.3.4 Material response to indentation measurement

In this subsection only some representative results of each sample are presented. The different curves figure 4.24 shows a wide dispersion of results depending on the indent location. Also, the loading curves slope is different (and globally lower) for new pad compared to used pad: with friction the pad is stiffening.

For each material state, the unloading part between 90 and 40% of maximum loading seems similar - i.e. found approximately the same elastic behavior in this area-, although the load profile is very remote. Methods such as [Oliver and Pharr, 1992] should be avoided because the maximum load is to high compared to the application and it does not retransmitted heterogeneity.

Regarding the loading part. The beginning of the curve is flat: this might translates a surface "effect". In addition, the material heterogeneity is visible through the dispersion curves: comparing one curve to another, the slope is different and evoluting with loading. Hence, load curve highlights the stiffening material and surface diversity.

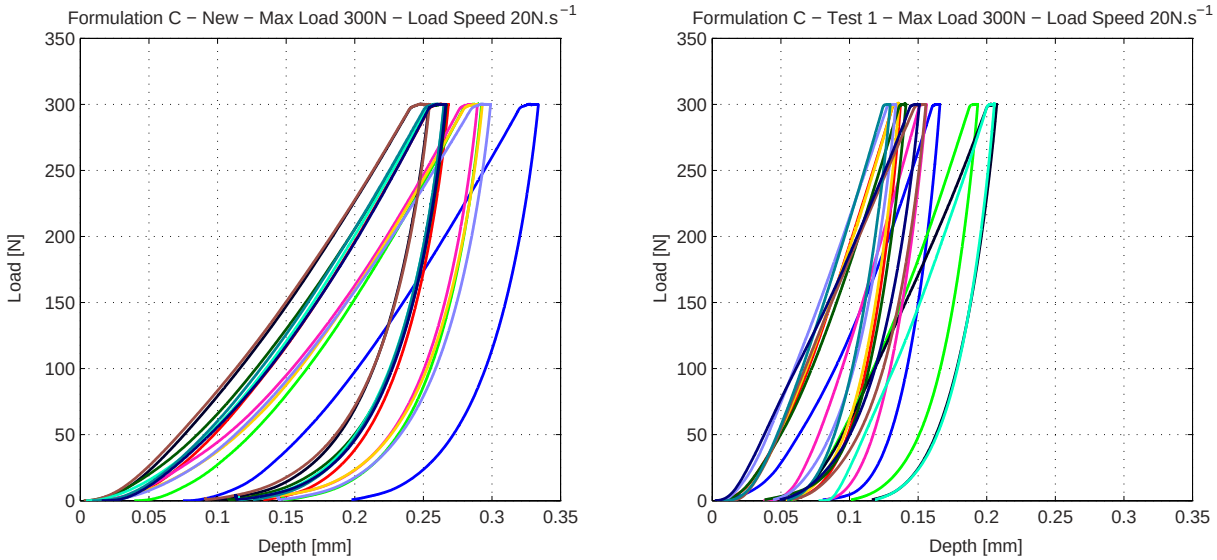

Figure 4.24: Load-Depth curves on formulation C - New pad versus used pad (Test 1)

For this first approach, standard Hertz theory is used to calculate elastic modulus, which are given at $150N$. This choice is justified in chapter 5.

4.3.5 Elastic modulus distribution analysis: sliding history comparison

Considering measurement mapping in figure 4.23, 136 indentations out of 140 are done on **innerpads** from each test (New, 1,2,3, and 4). 4 test located at positions [4;15;123;140] are not measured due to the inaccessibility of these points with the indenter probe, therefore the mean elastic modulus is attributed there. Each curve is post-processed with standard Hertz contact theory at load 150N (tangent elastic modulus is calculated). The histograms in figures 4.25 and 4.26 shows the statistical dispersion of elastic modulus for formulation C and Ref. A strong difference is shown between new and used states: the new pad is more homogeneous, whereas slided pad properties are more distributed. Regarding new pad, the elastic modulus is centered around 830MPa for form.C and 1500 MPa for form. Ref. On used pad (Test 1 to 4), results emphasize that each pad has a strong heterogeneity of their elastic modulus with a standard deviation close to 2000MPa. With sliding contact, the material is strongly stiffened.

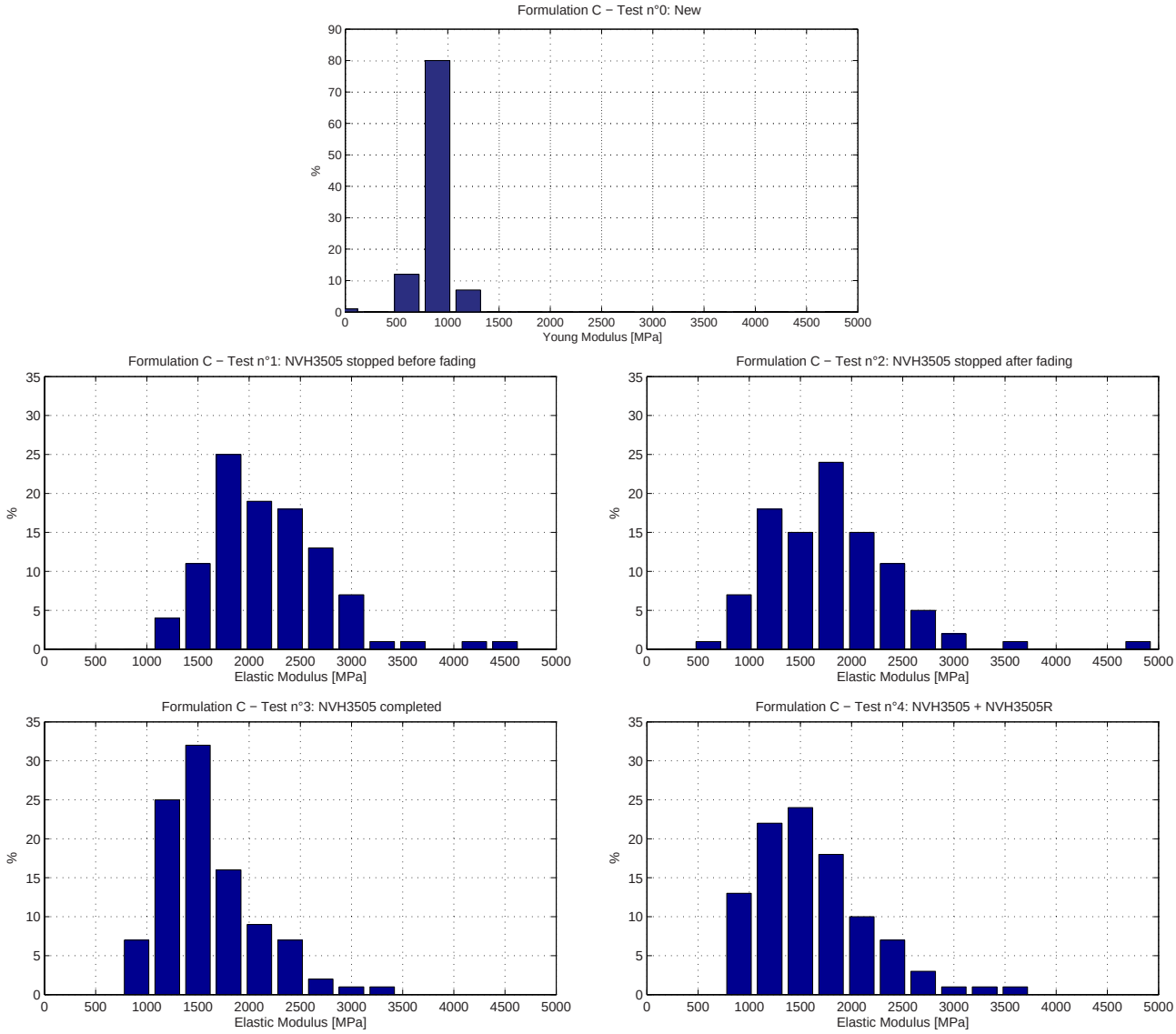

Figure 4.25: Form. C - Clusters of elastic modulus per sliding state identified for load up to 150N

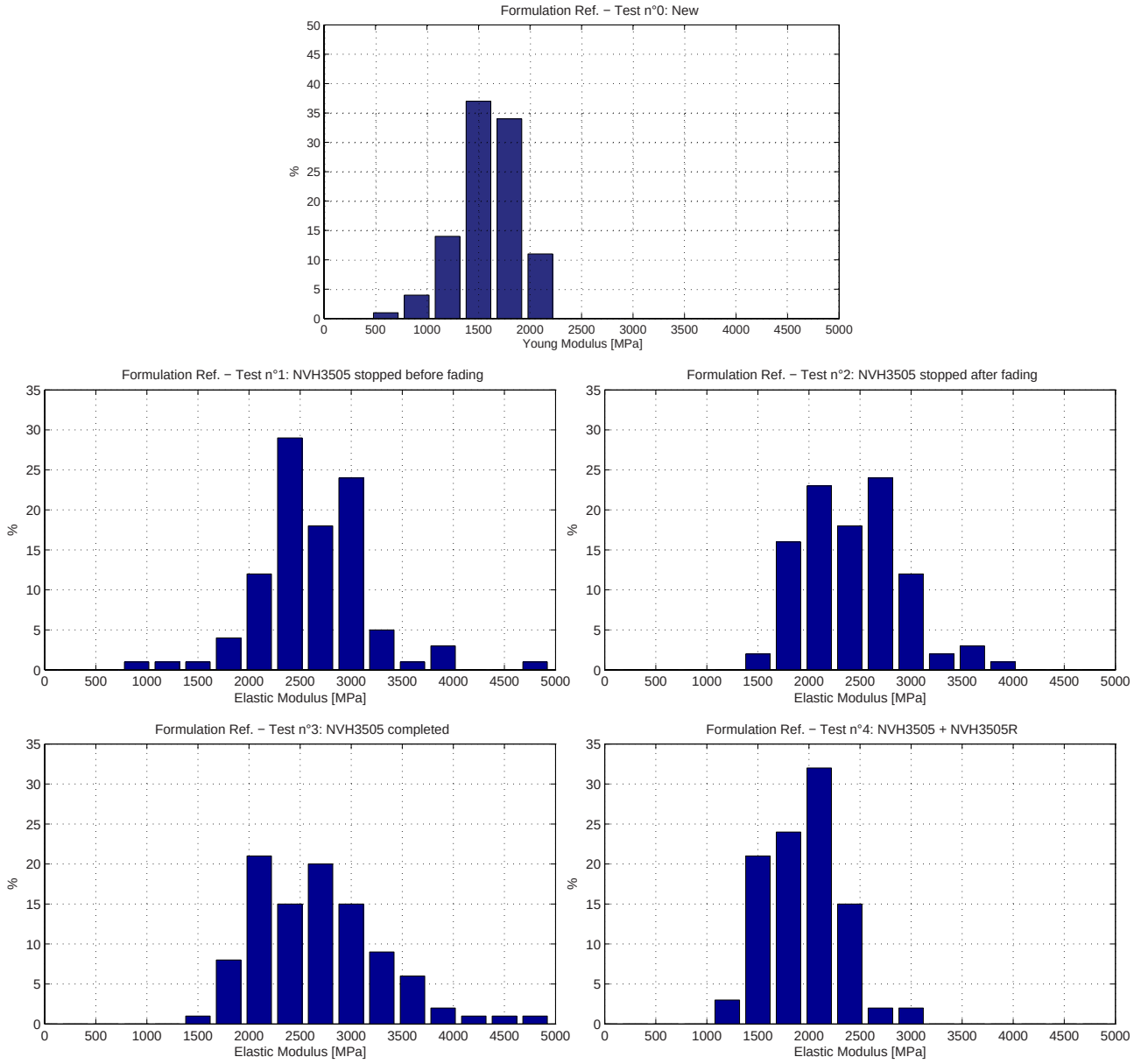

Figure 4.26: Form. Ref. - Clusters of elastic modulus per sliding state for load up to load 150N

The second approach locates each modulii on pad and highlights several results for both formulations (fig.4.27 & 4.28) The edges seem stiffer than the center. The cracks & holes of thermocouples are visible (e.g. at pad center fig. 4.27 in test 4 for formulation C), indicating the important wear (thermocouples are drilled at 5mm from pad surface) and also that the material is characterized in its volume.

On formulation Ref., the modulii appear to be stiffer around leading edge than trailing edge, and moreover than pad center. Comparing with shape measurement in section 4.2.1, the wear orientation looks clearly similar to elastic modulus distribution. This might be caused by compaction of leading edge during sliding which might lead less porosity, material homogeneisation, wear and plateaus formations (particles agregates around fibres),etc. It is less visible for formulation C: the modulii have a very heterogeneous and unprivileged location.

Regarding mean elastic modulus for each test, formulation C stiffness is decreasing with brake stops from test 1 to test 4. The same behaviour is less clear for form. Ref: the mean elastic modulus is more constant and decrease only between test 3 and 4.

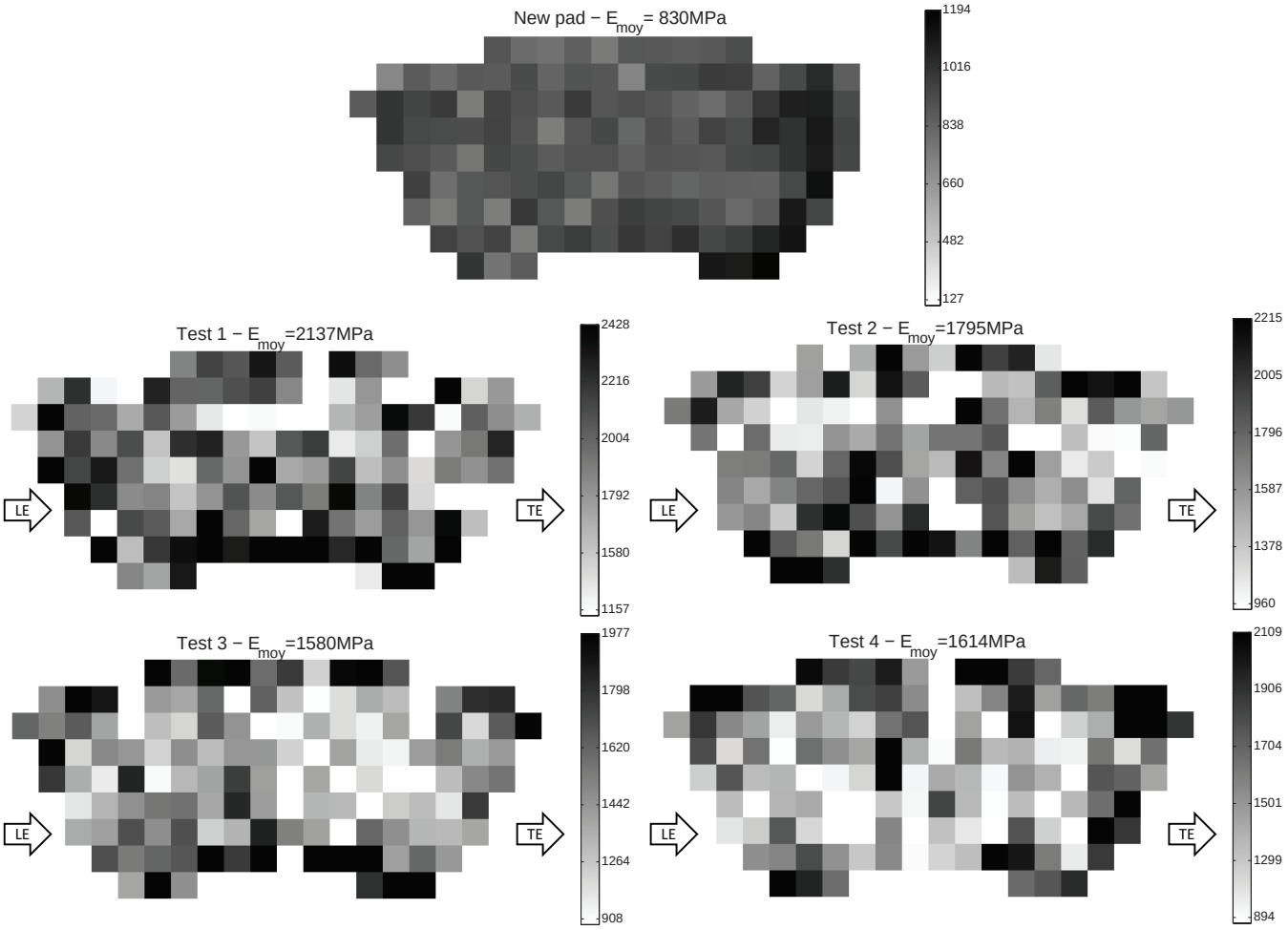

Figure 4.27: Form. C - Elastic modulus mapping measured by indentation for load up to 150N

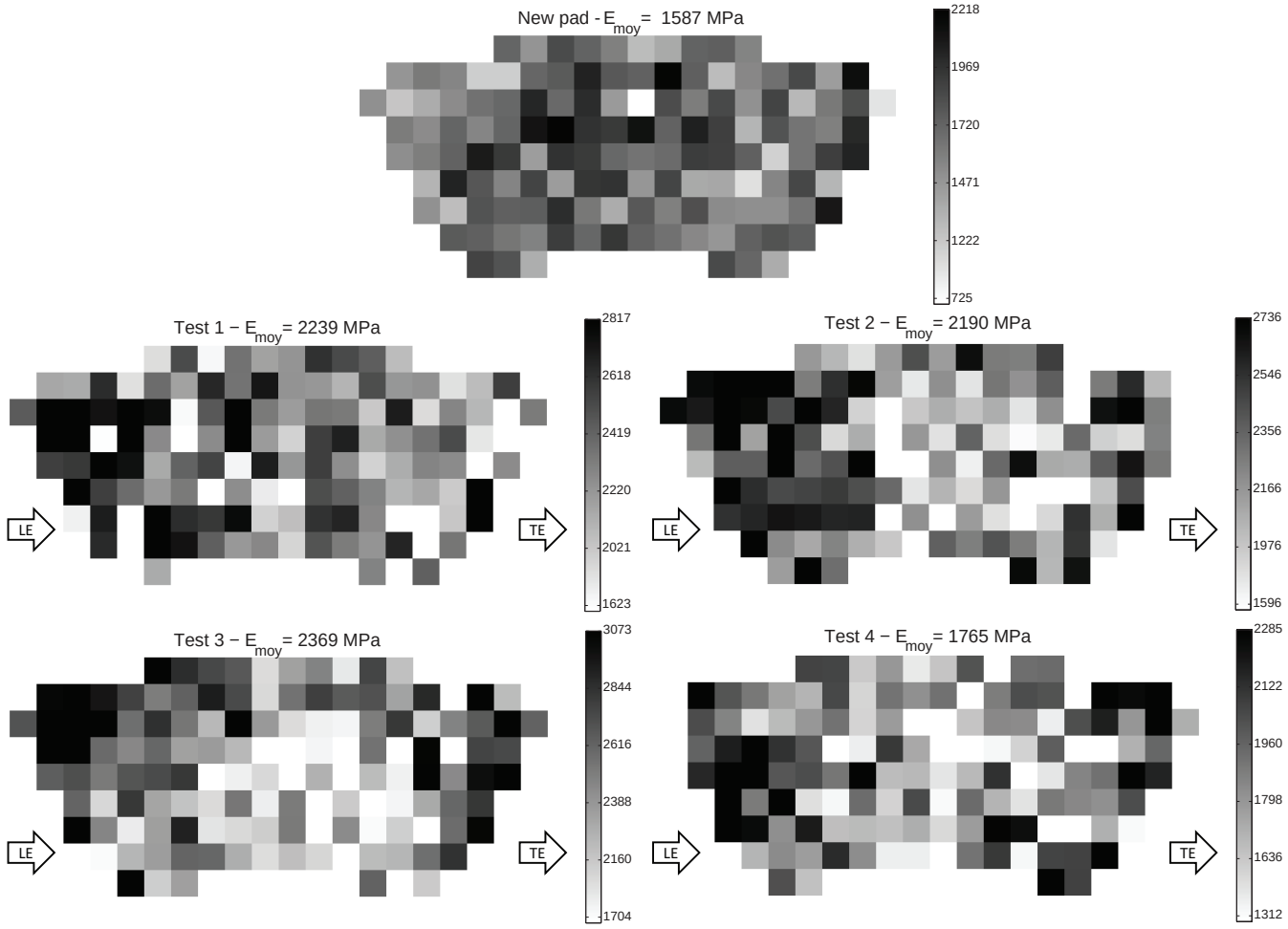

Figure 4.28: Form.Ref - Elastic modulus mapping measured by indentation at load for load up to 150N

Finally, whether the histogram or mapping representation, both materials present a certain homogeneity when they are new. But, it disappears whenever sliding contact is operated.

Having shown that the friction material is very heterogeneous - in its volume and its surface condition -, the first approach is not complete. The difference between the curve (h, P) experimental and numerical is important, the both diverge (see fig 4.29). The end slopes seem to be parallel, thus this method characterises the material in its volume. It shows the choose to determine the elastic modulus at 150N is too high and doesn't reflect the curve beginning. It lacks the surface effect which "offset" the load-depth curve.

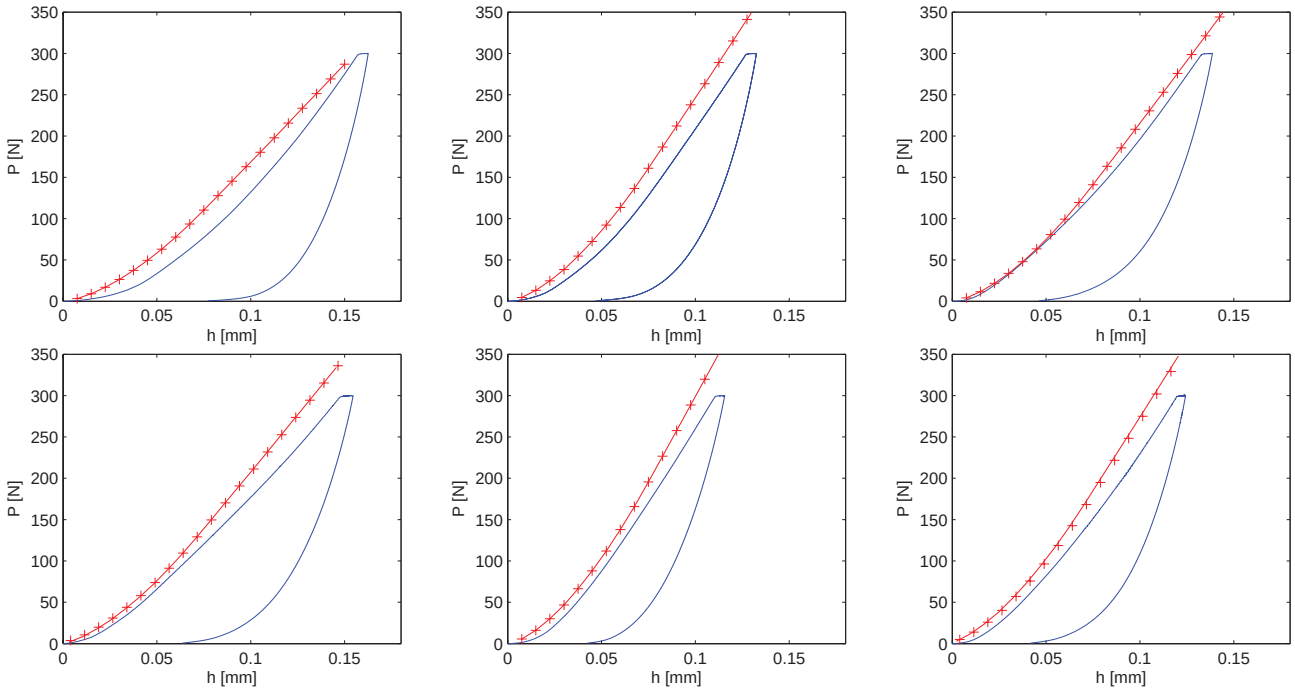

Figure 4.29: Comparison between experimental data (-) and numerical results (+)

Thereafter, the development of a method which characterize more accurately each of these phenomena will be established in order to introduce them in a finite element model and to evaluate their part in the occurrence of noise-braking.

4.4 Chapter synthesis

In this chapter, a noise occurrence test campaign has been performed in order to obtain characteristic friction surface state regarding temperature and history effect. Every tests were stopped at a noisy state except the one with highest temperature peak (test 2: fading at 450°C). It has been noticed between virgin and used state an important change of surface aspect.

Considering surface evolution, profile analysis has been performed in order to quantify surface defects according loading. It has been seen the shape is the most significant in terms of wear and surface orientation, due to kinematic positioning. Waviness and roughness are second order parameters which are characteristics regarding loading: Ra and Wa are high for new pads but decrease with friction, and even more for fading test (test 2). Both formulation C & Ref. are reacting as so. Therefore, three types of surfaces can be counted: "new", "used" and "fading". Looking at microscopic observations, the difference between "used" and "fading" is the type of plateaus and debris at pad surface: they are more continuous and homogeneous after a high elevation of temperature. Thereby, the severe chemical transformations of constituants has given glazed and "melted" plateaus (mostly resin and rubber for formulation C). This might explain the smoothing on profile seen after fading.

In order to understand the link between the state "noisy/accidented surface" and the state "silent/glazed surface", it has been decided to focus on elastic properties. Brinell indentation has been chosen to evaluate an elastic modulus in the sense of Hertz theory on 140 points of pad interface, for each test. Therefore, a stochastic distribution of elastic modulii has shown the strong heterogeneity of friction material which is stronger after friction. The heterogeneity is less visible for new pads. For fading tests, modulus deviation is less important than for other friction tests. This correlates with observations by profilometry and SEM observations.

Summarizing with compressibility and compression tests performed on various samples through this work, indentation modulii obtained seem in good accordance (see table 4.2).

		A	B	C	Ref.
Compressibility (µm)		154	150	158	180
Elastic modulus (MPa)	cylinder ø10mm (@1.5MPa)	1085	875	750	/
	cubic 10x10x15mm^3 (0.5/1/1.5MPa)	730 | 1320 | 1720	690 | 1240 | 1640	510 | 870 | 1100	540 | 1050 | 1350
	indentation ø10mm New pad (150N)	/	/	835	1471
	Indentation ø10mm Test1 (150N)	/	/	1850	2239
	Indentation ø10mm Test2 (150N)	/	/	1591	2190
	Indentation ø10mm Test3 (150N)	/	/	1402	2369
	Indentation ø10mm Test4 (150N)	/	/	1438	1765

Table 4.2: Compressibility and elastic properties summary regarding test device

The link between noise behaviour, pad formulation, profile and mechanical properties is yet to be found. However, it appears a smooth surface coupled with a concave shape is a less noisy surface. The link with mechanical properties is more uncertain since no important differences are shown with standard Hertz approach. Having shown that the friction material is very heterogeneous - in its volume and its surface condition - but the first approach is not complete. It misses the surface effect relative to low load values of the indentation load-depth curve. In fact, on the preliminary work it has been proved that characteristic changes according to the load applied and parameters evolve with the history. The elastic modulus evaluation at 150N is too stiff and unsufficient. In addition, the equivalent stress for 150N is above 100MPa, which is above braking application. A static measurement of 10 bars pressure application on innerpad backplate has been performed (NVH tests are between 0 and 30 bars). A pressure film between pad and disc measures the contact pressure between both (fig. 4.30). The results are showing a maximum of 20 bars for 10 bars application. Considering that rotation is not considered here, and the bonding effect at pad leading edge would increase this value, but still lower than 100MPa.

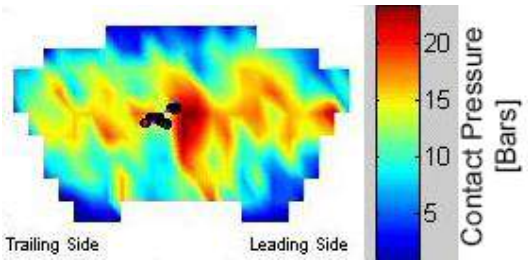

Figure 4.30: Pressure film measurement between innerpad and disc of static normal pressure between disc and pad for a 10 bars fluid pressure application

Thereafter, the development of a method which characterize more accurately each of these phenomena is required before introducing them in a finite element model and to evaluate their part in the occurrence of noise-braking.

Chapter 5

Heterogeneous material properties: impact on mode coupling instabilities

Contents

5.1 Motivation

Earlier, the Hertz contact theory with a "classical" approach has given an initial elastic modulus evaluation but at $150N$ load. In this section, to take into account the modulus evolution as a function of the applied load, as observed with compression results in chapter 2, the Hertz contact theory is adapted as a function of load. Also numerical contact parameters reproduce surface heterogeneities as seen on chapter 4. Thus, the same indentation tests done in previous chapter are post-processed with a different approach for formulation C. The goal of such modelisation is to implement these materials heterogeneites and contact stiffnesses into a complex eigenvalue analysis of a brake system and look at their influence on mode lock-in.

A more complex modelling is done. It takes into account the volume, but also the material surface. This new analysis, also based on the Hertz contact theory breaks down as follows:

- discretization of the Hertz theory for $E = f(P)$
- taking into account the material side effects, by the introduction of coefficient C which is the ratio between actual and theoretical depth in order to deduce a non-linear stress-strain law
- introduction of numerical parameters to compensate the surface effects. $(K_n\text{-}TOLN)$

This modelling intention is to transcribe the material behaviour more precisely, taking into account surface interactions and load-dependency, and then improving brake pad non-linearities and heterogeneities.

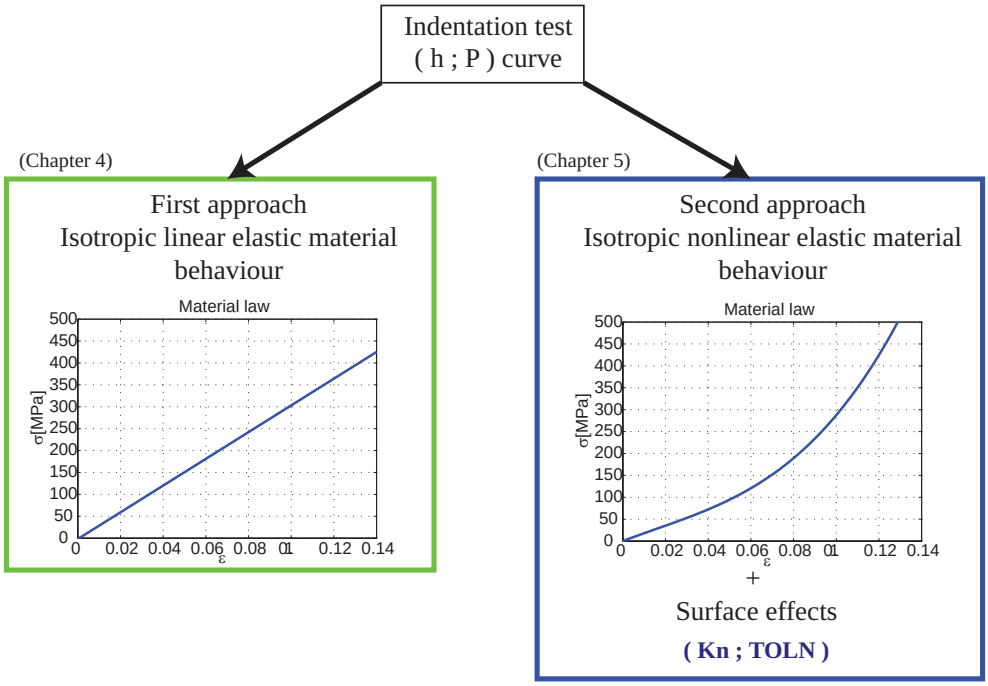

Figure 5.1: Material modelling of friction material - Methodology overview

5.2 Approach to identify friction material & contact properties through indentation test

5.2.1 From indentation test to volumic & surfacic behaviour modelling

Affected volume by indentation A finite element static analysis based on the test is designed. In a first approach, parameters are defined by empirical estimation, then refined if necessary. Thus, the test parameters used

are a maximum load at $300N$ and a ball size (Brinell geom.) of $10mm$.

The studied material is meshed roughly in the volume. Asides, the contact interface with the ball is meshed more precisely. Only one layer of the ball is modelled (the one in contact) in order to avoid contact singularities but also reduce calculation time. In addition, the following hypothesis are made:

- Axisymmetric model on y-axis
- Isotropic material (after comparison between an isotropic and a transverse isotropic model, error can be quantified of $4\mu m$, see details in Appendix C)
- Mesh size: ball=0.1mm, material surface=$67\mu m$, material volume=0.2mm
- $E_{indenter} = 318GPa$ & $E_{mat} = 1GPa$
- Elements type: quadratic elements

Taking into account all previous choices, the indentation test model is established in fig.5.2.

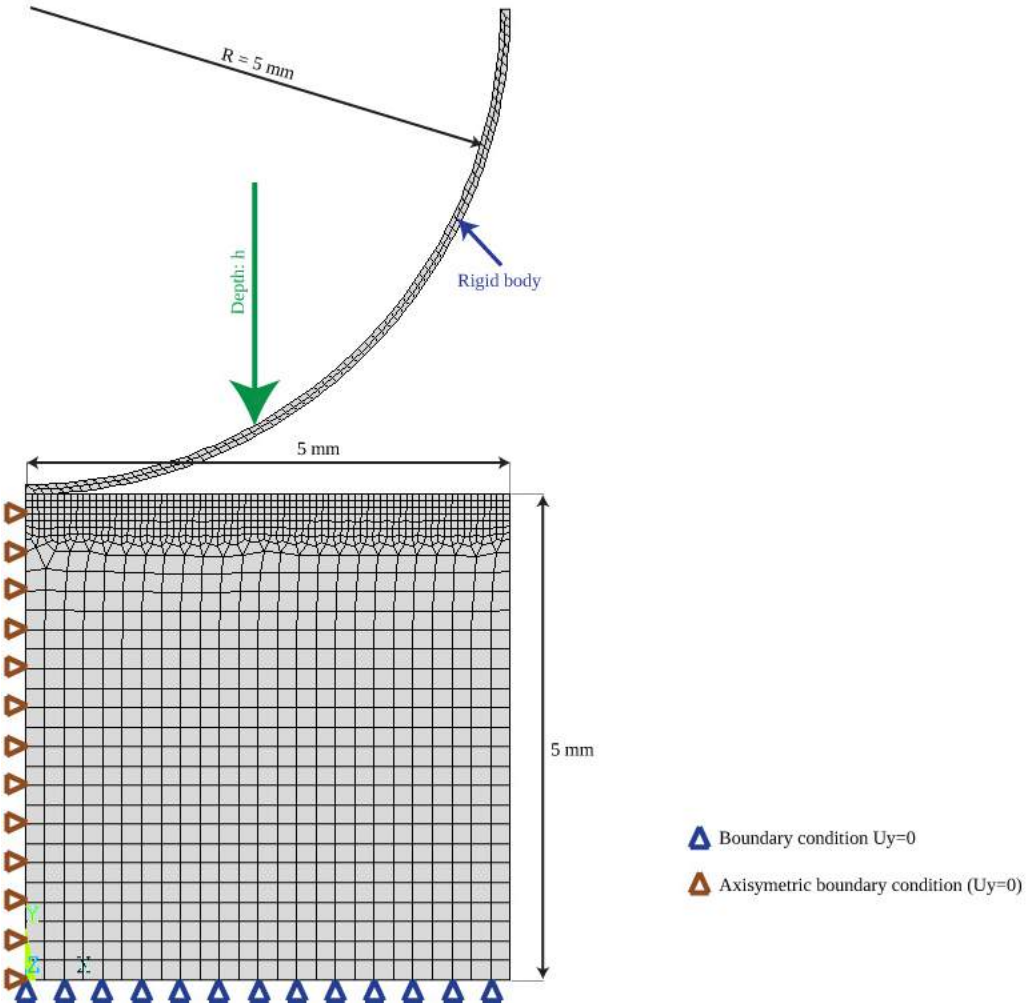

Figure 5.2: Finite element static analysis of Brinell indentation test

The model permits to estimate the affected volume which is below a cylinder of $\phi 4mm$ and $2.5mm$ high (cf. fig. 5.3). This justifies the use of a $5 \times 5mm^2$ indentation mapping in chapter 4.

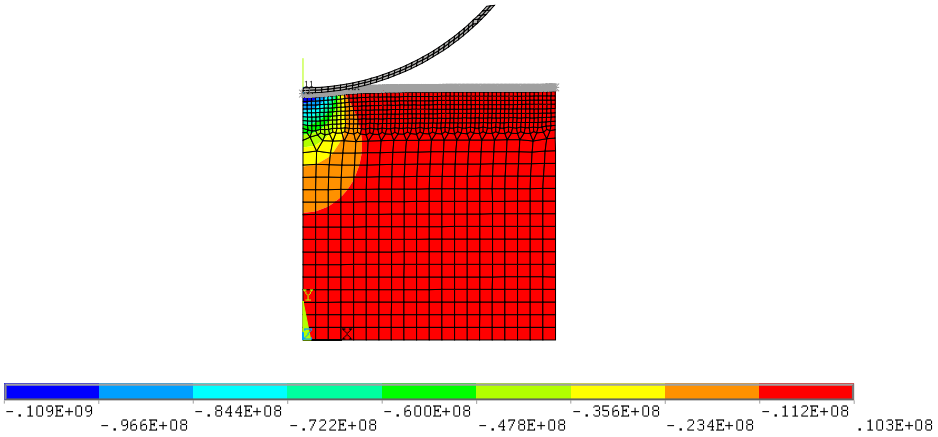

Figure 5.3: Numerical estimation of affected volume by indentation of formulation C (applied load 150N) - Normal stress

Knowing constant elastic modulus of friction material at one spot (identified in chapter 4), the indentation test is simulated and compared to load-depth experimental curve in fig. 5.4. The curve $P = f(h)$ numerical versus experimental are not correlated. The numerical model is too stiff, even at the very beginning of the curve. Thus, the FE indentation model lacks of parameters regarding contact and volumic behaviour definition. It suggests the problem can be decoupled into two features:

- Phenomena linked to the surface: profile asperities described by waviness & roughness on approximation of $20\mu m$, a maximum value for both, which can be modelled by contact stiffness and penetration tolerance. Also, sensor is accurate above $5N$. At this load, the asperities are compressed and the material is sollicitated in its volume.
- Volume properties: the h-P curve shows a non-linear behaviour of material which cannot be reproduced by a constant elastic modulus. Therefore, a load-dependant modulus must be evaluated above $5N$ (stopped at $150N$ for this frame of work).

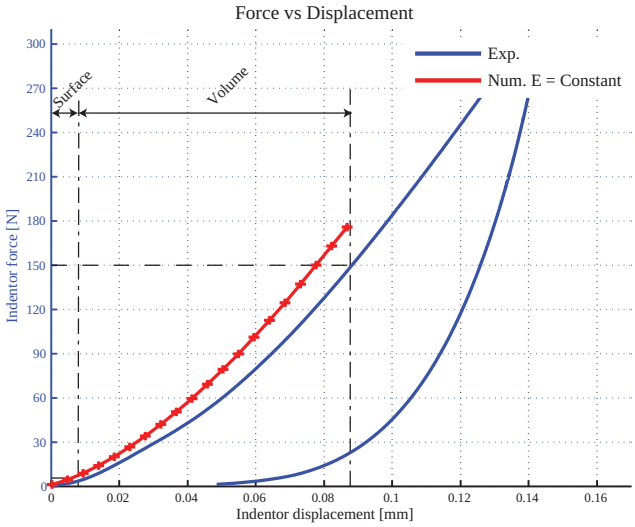

Figure 5.4: Assumption on "surface" and "volume" effect - Form.C indentation curve (Test 1 - Point N°10) and numerical result for E=constant

5.2.1.1 Volume properties

Hertz contact theory applied per load

It has been previously seen the non-linear evolution of material elastic behaviour. A similar trend as been identified in chapter 2 regarding compression test. Thus, an elastic modulii is calculated for each load point using Hertz contact theory. To do this, the presented approach in the previous chapter is used but the $h = f(P)$ curve is discretized for $E_r = f(P)$ determination. The discretisation gives a value of E_r for each pair $(h; P)$, so the Hertz equation becomes:

$$P_i = \frac{4}{3} \times E_{r_i} \times \sqrt{R} \times h_i^{\frac{3}{2}} \tag{5.1}$$

In the field $h^3 = P^2$ the slope is defined by:

$$\Delta_i = \left(\frac{3}{4} \times E_{r_i} \times \sqrt{R} \right)^2 \tag{5.2}$$

with Δ_i, the slope of the straight line between points $(i-1)$ and $(i+1)$ in the sense of least squares.

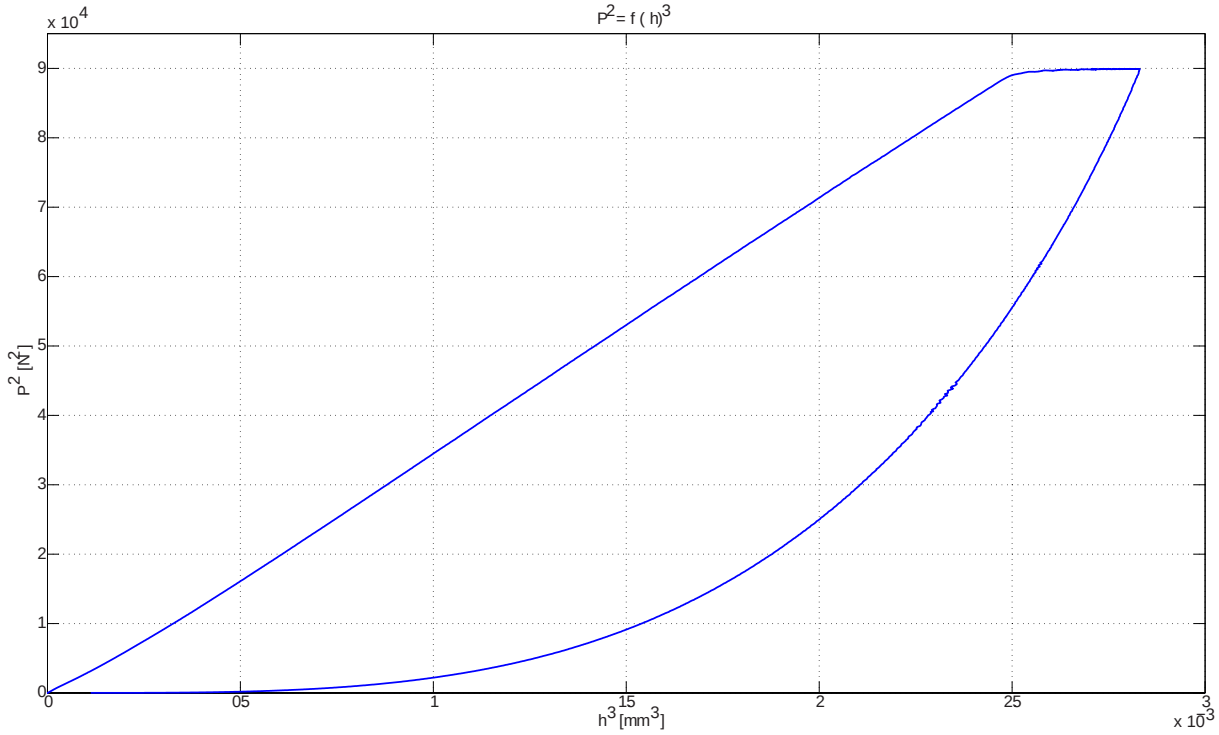

Figure 5.5: Representation in $(h^3; P^2)$ field - Form.C (Test 1 - Point N°10)

Then, the reduced module can be obtained for each step by:

$$E_i = \frac{1 - {\nu_{mat}}^2}{\frac{1}{E_{r_i}} - \frac{1-{\nu_{ind}}^2}{E_{ind}}} \tag{5.3}$$

At this stage, the Hertz approach is discretized, which allows to observe the elastic modulus evolution as a function of applied load as in figure 5.6. It suggests a non-linear behaviour of the material which is stiffening with load, as seen in chapter 2.

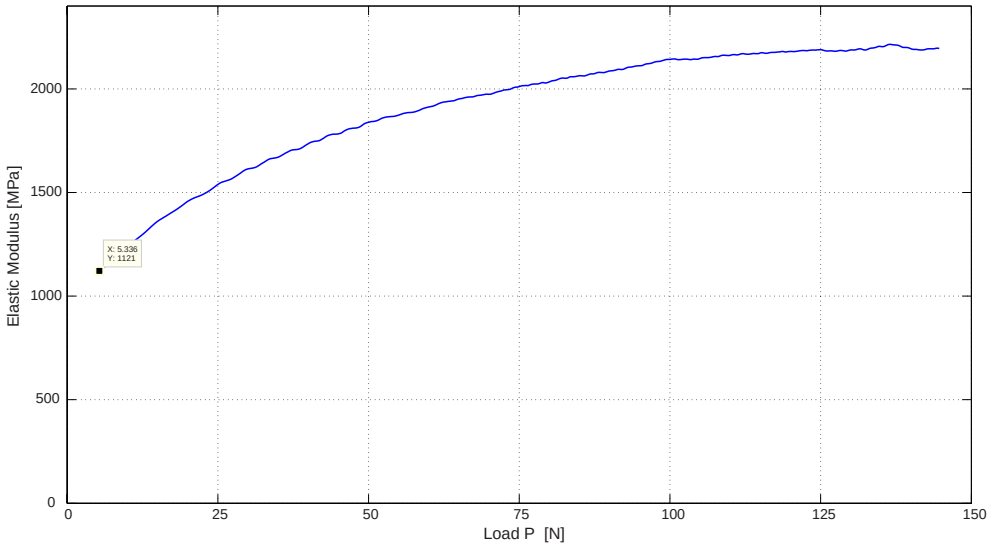

Figure 5.6: Elastic modulus versus load identification by Hertz contact theory (Test 1 - Point N°10)

To supply the indentation FE model, the volumic identification must be moved in the stress/strain field, the [Hertz, 1882] work is used which defines as follows the maximal stress:

$$\sigma_{max_i} = \frac{2E_{r_i}Rh_i}{\pi a_i} \tag{5.4}$$

with a_i the contact radius between the probe and the material at load P_i. The global strain definition is determined by:

$$E = \frac{p_m}{\varepsilon} \tag{5.5}$$

with p_m the mean pressure applied by the Brinell indenter, and it gives:

$$\varepsilon_i = \frac{4a_i}{3\pi R} \tag{5.6}$$

At this point, this new approach allows to reproduce the rigidifying material behaviour. But one point should be further discussed: in fact the contact area definition between the probe and the material must take into account the edges effects, this problematic is tackled in the next subsection.

Correction of contact area estimation

Figure 5.7 represents the contact projected area between the indenter and the material surface. Considering only geometric features, the radius contact area would be:

$$a = \sqrt{2Rh - h^2} \tag{5.7}$$

However, profilometry fig. 5.7(b) has shown that when applying a force on the indenter, the friction material deforms and edge effects appear. Furthermore, the imprint left by the ball on the pad surface is not symmetrical.

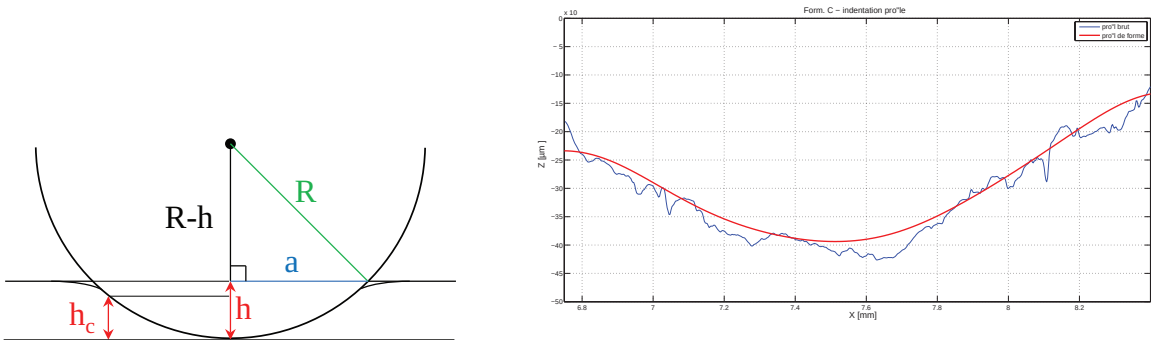

(a) Indentation schematic

(b) Indentation shape profilometry - "sink-in"

Figure 5.7: Indentation shape analysis

To account for the difference between theoretical (h) and actual (h_c) penetration contact, a C coefficient is introduced which is the ratio between both. Similar approaches have been done in [Johnson, 1987] or more recently in [Bartier et al., 2010]. Contrary to these works, the coefficient is considered here as constant.

$$h_c = C \times h \tag{5.8}$$

It means if $C = 1$, the measured depth is correct and the Hertz theory hypothesis are filled (plane contact), and if $C \cong 0$, the depth measured is far from the real contact depth and the contact is non-regular. Thus, the contact radius with the probe becomes:

$$a = \sqrt{2RCh - (Ch)^2} \tag{5.9}$$

with $C \in]0, 1]$.

The choice of C coefficient has been done because the material deformation to "sink in" is not an axisymmetric profile and depends on the near-surface components. So, the conventional relations of edges effects compensation could not be used. Moreover, $h \ll R$ so:

$$a = \sqrt{2RCh - (Ch)^2} \cong \sqrt{2RCh}. \tag{5.10}$$

In this way, stress (eq. 5.4) and strain (eq. 5.6) may be described by:

$$\sigma_{max_i} = \frac{2E_{r_i}Rh_i}{\pi\sqrt{2RCh_i}} \tag{5.11}$$

$$\varepsilon_i = \frac{4\sqrt{2RCh_i}}{3\pi R} \tag{5.12}$$

The C coefficient value needs to be determined. Thoroughly, coefficient should evolve during testing but in a first approach, it is considered constant. A specific factor is calculated for each indentation point. This one is difficult to determine experimentally, so a numerical approach is chosen to do this. This specific point is extended in subsection 5.2.1.3 after developing all method parameters.

5.2.1.2 Surface modelling : introduction of contact stiffness and penetration tolerance

The above subsection presented volumic properties identification with load. The lower 5N part of the (h, P) curve (fig. 4.21) must be also identified.

Phase called "transitional" or "surface effects" is composed of the following phenomena:

- material detachments (particles, debris)
- third-body layer
- wear shape, waviness, roughness
- etc ...

This part is very complex in view of the parameters diversity; it deserves a separate detailed study. But here in this frame of work, the phenomenon is compensated numerically by a normal contact stiffness, denoted K_n, and penetration tolerance to be applied on the surface normal direction, denoted $TOLN$.

$TOLN$ is a thin surface layer, in the sense of finite elements, in which the indenter can enter the material without deforming it (i.e. not solicit any of the material characteristic). But in this area, the indenter is still opposed to an effort introduced by the contact stiffness which is modelled by a spring of K_n stiffness (fig.5.8). When the consumption of the total contact flexibility (hence the penetration tolerance) the volumic properties, the non-linear elastic law, is used.

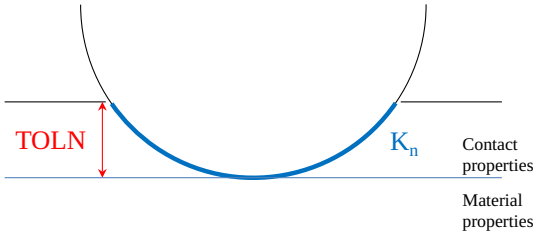

Figure 5.8: Contact stiffness and penetration tolerance schematic

The influence of each parameter on $(h; P)$ curve is represented on fig 5.9. Elastic modulus is supposed as constant. TOLN gives an "offset" to the displacement with a force conditionned by K_n stiffness.

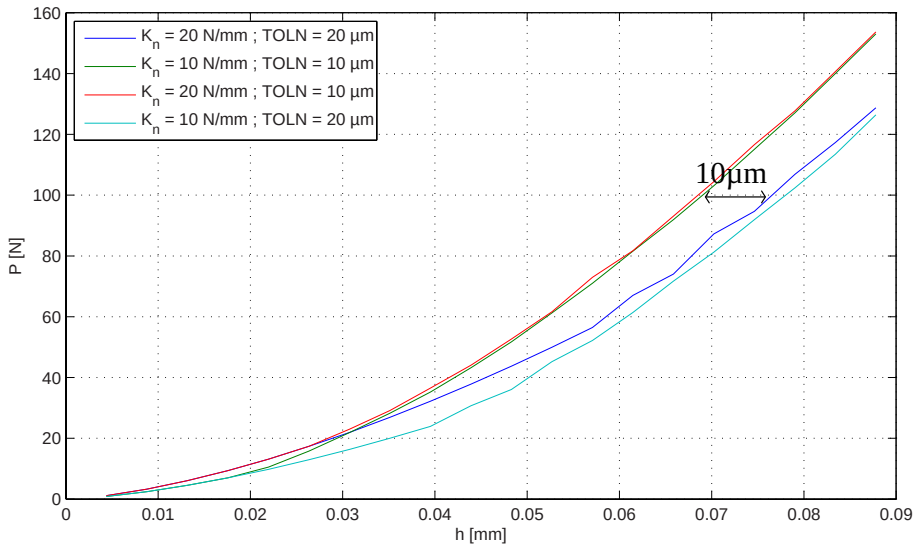

Figure 5.9: Sensitivity analysis results on K_n and $TOLN$ behaviour (Test 1 - Point N°10)

By successive iteration, a criteria at 1N to approximate these variables has been found. K_n and $TOLN$ are

fixed with the following definition, for N nodes in contact:

$$K_n = \frac{F_0/h_0}{N} \tag{5.13}$$

$$TOLN = h_0 = h_{(F=1N)} \tag{5.14}$$

It is a first approach to model uncontrolled phenomena. It would be more convenient to calculate these parameters ($TOLN$, F_0) instead of fixing them. However, the method used here is sufficient to establish a model of the friction material.

5.2.1.3 Loop algorithm on contact area correction factor

At this stage, all the parameters are determined to supply our FE model except C. The simulated indentation curve is calculated with different values of C. The absolute gaps between each numerical point versus experimental is determined and a mean gap value is given. The numerical curve with the minimum mean gap is selected as the best approximation (fig. 5.10).

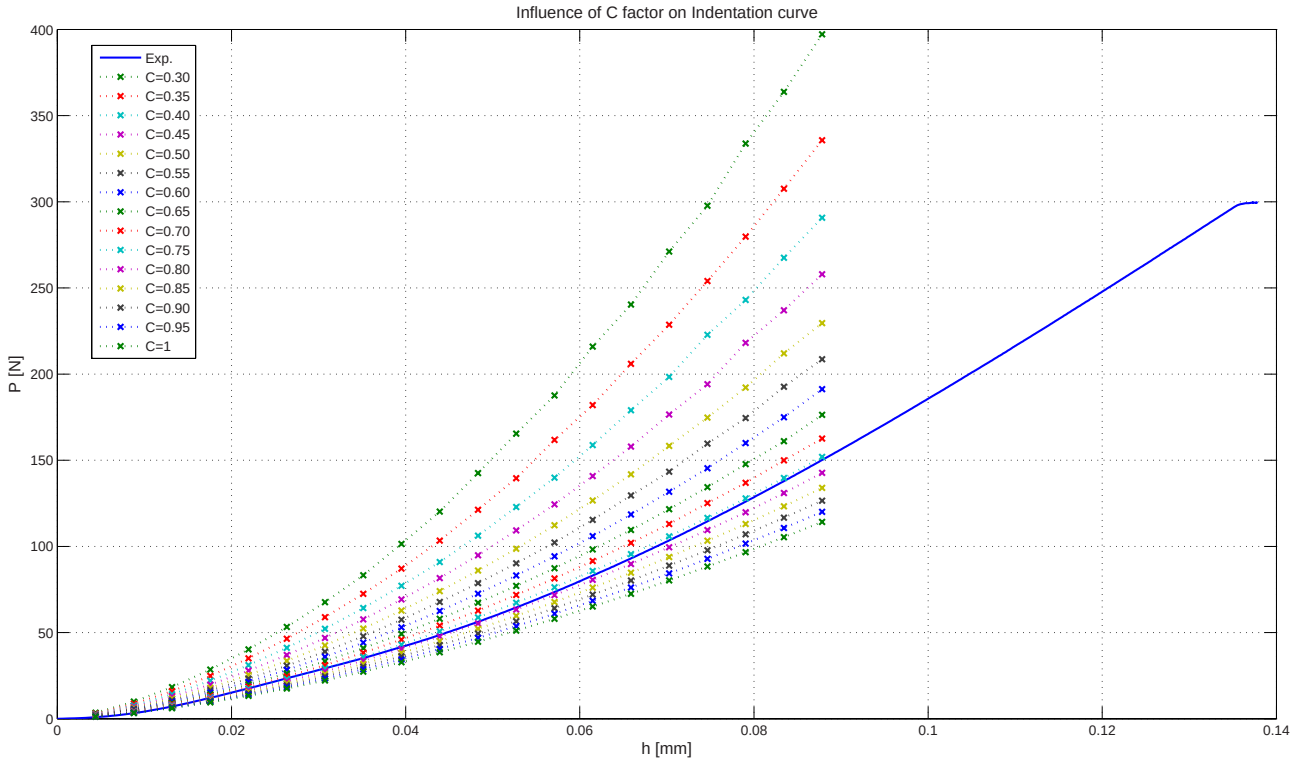

Figure 5.10: Comparison of numerical $h - P$ curve depending on C coefficient with experimental measure (Test 1 - Point N°10)

To reduce the computation time, the C coefficient is limited to 5% accuracy. The C determining method is sufficient for a first approach to the material law. In chapter 4, the elastic modulus for each indentation measure was identified at 150N. The simulation was correct in a first approach (fig.4.29) but was imprecise. The new method developped here is more accurrate. An example highlights this in figure 5.11, from measure to numerical comparison by implementing the right non-linear material law coupled with identified contact properties.

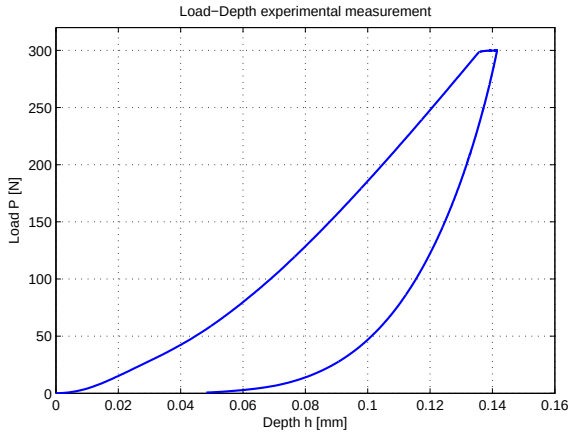

(a) Exp. load-depth curve

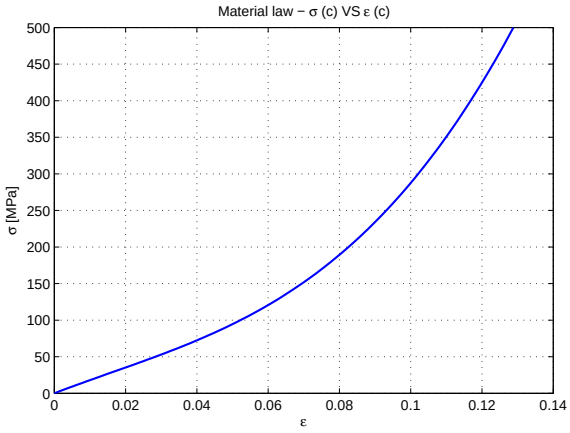

(b) Stress-Strain curve (corrected with C)

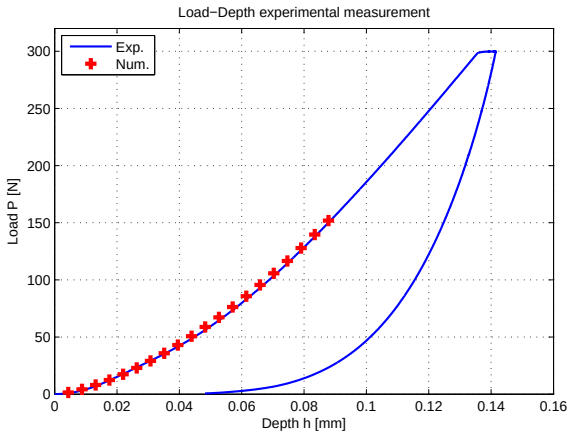

(c) Exp. vs. Num. load-depth curve

Figure 5.11: Indentation post-processing: from measure to estimation (Test 1 - Point N°10)

In conclusion, it is possible to numerically reproduce an indentation test to identify a material behavior by providing consistent material law for modelling the volume and a normal contact stiffness, plus a penetration tolerance for modelling surface phenomena.

This method has been applied on inner brake pads (form.C) from chapter 4 (new and test 1 to 4), so it represents 136 curves times 5 tests. It is relatively efficient, on average, it has a error rate below 5% per pad, which is satifying (table 5.1).

Form.C	Successful post-processing
New	71,6 %
Test 1	97,78 %
Test 2	99,2 %
Test 3	95,59 %
Test 4	97,79 %

Table 5.1: Post-processing accurracy

At last, the complete identification methodology sum-up in figure 5.12 gives these parameters, which are input into the FE indentation model:

- σ_{max}, the stress seen by the material with the probe
- ε, the strain undergone through loading
- K_n, the contact stiffness between probe and material
- $TOLN$, the penetration tolerance

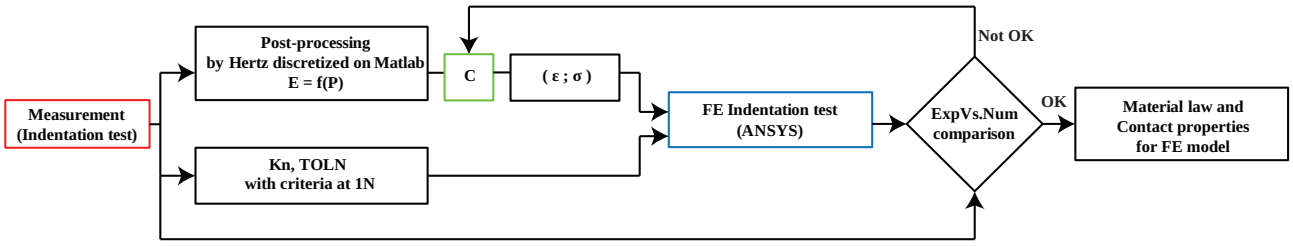

Figure 5.12: Identification methodology summary

This methodology gives quite satisfactory results as some examples in figure 5.13. Comparing with results of previous approach (fig.4.29), the contact properties add the necessary offset at curve beginning, and the non-linear law minimizes the gap with the experimental data.

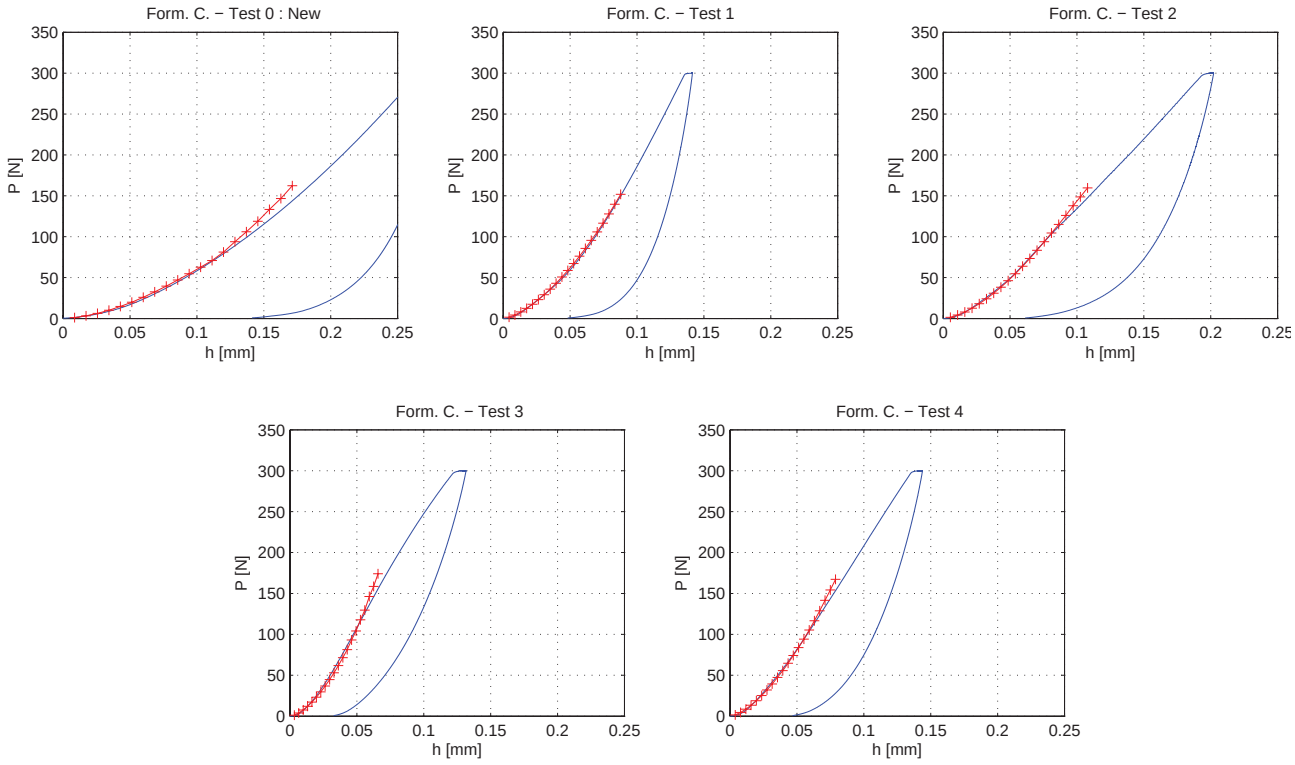

Figure 5.13: Indentation tests: Comparison experiment vs. numerical result for five different sliding situations on form. C

In view of the tests number, subsequently only analysis results are presented, but Appendix D contains all the comparison between experimental and numerical for formulation C test 1.

5.2.2 Results

In figure 5.14, non-linear elastic modulus is compared to min/mean/max values identified in chapter 4. First remark is the dispersion for used pads (tests 1 to 4) is higher than the virgin case. It appears the min/max modulii identified in chapter 4 cover the non-linear laws at high loads (100MPa). However, looking at low loads (below 20MPa) the comparison is uncertain. In addition, the braking application is under 30bars (approx. 20bars at pad interface, fig.4.30). Therefore, it is more convenient to compare with lower constant modulii as in figure 5.15 where they are identified at 10MPa.

In both figures, a mean estimation of non linear laws is traced (in magenta). It appears the linear modulus well estimates the behaviour at high loads, whereas, at low loads (below 10MPa) the begining of the curve is clearly non-linear and the linear modulus is overestimating this part. The non-linear is mainly seen at low loads. It explains why the classic Hertz determination of elastic modulus at 100MPa appeared to be correct at high loads in chapter 4.

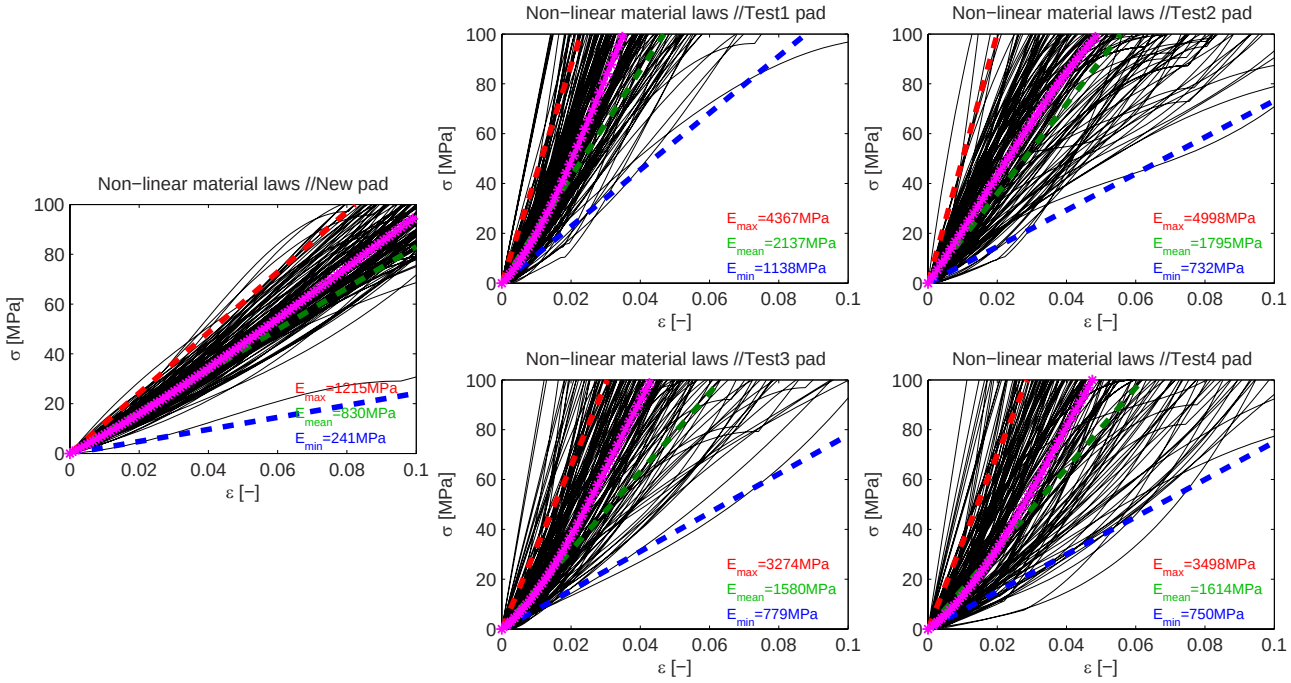

Figure 5.14: Non-linear material laws for 5 friction states - Comparison with min./mean/max. elastic modulus determined at 100MPa by classic Hertz Method and "mean" non-linear law (in magenta)

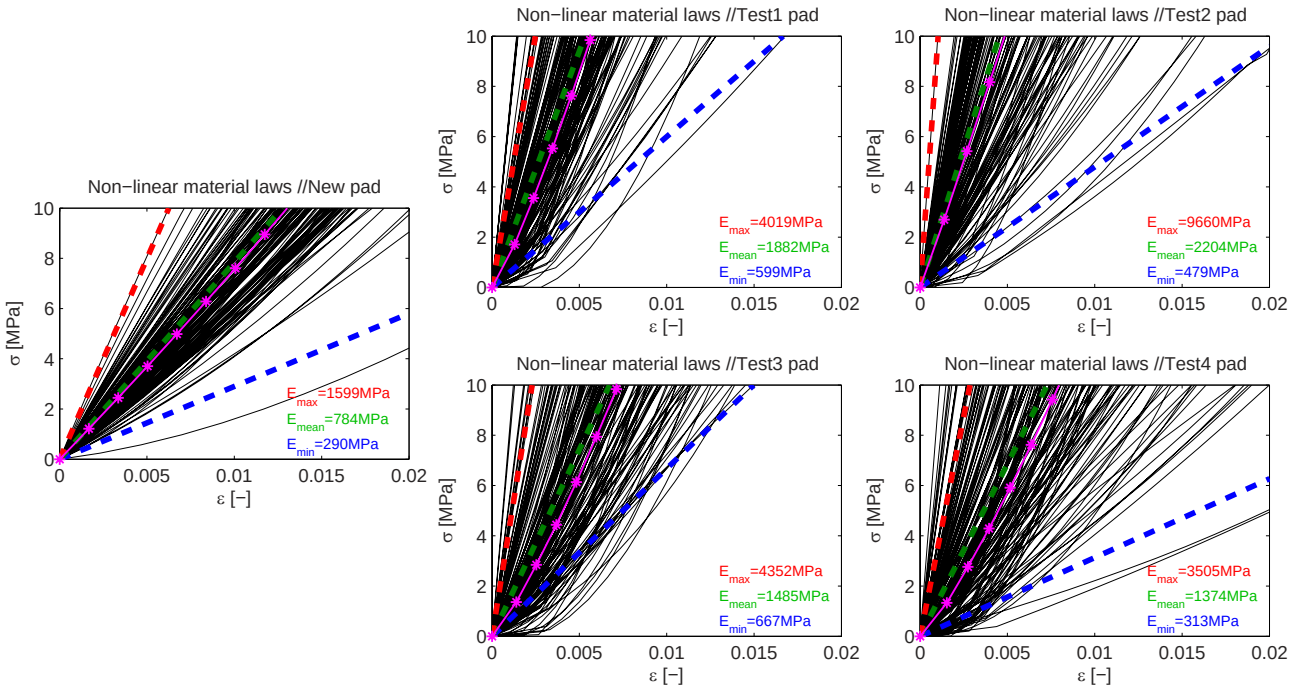

Figure 5.15: Non-linear material laws for 5 friction states - Comparison with min./mean/max. elastic modulus determined at 10MPa by classic Hertz Method and "mean" non-linear law (in magenta)

The statistic repartition of $TOLN$ (fig. 5.16 and 5.17) shows no particular trend except the range is between 0 and 50 μm but mean value is centered around 5 and 20 μm.

K_n range (fig.5.18) is between 0 and $5.10^6 N/m$. Mean value is also centered $1.10^6 N/m$ for test 1, 3 and 4. Contact stiffness dispersion is wider for new pad and especially test 2 ($]0; 5.10^6] N/m$).

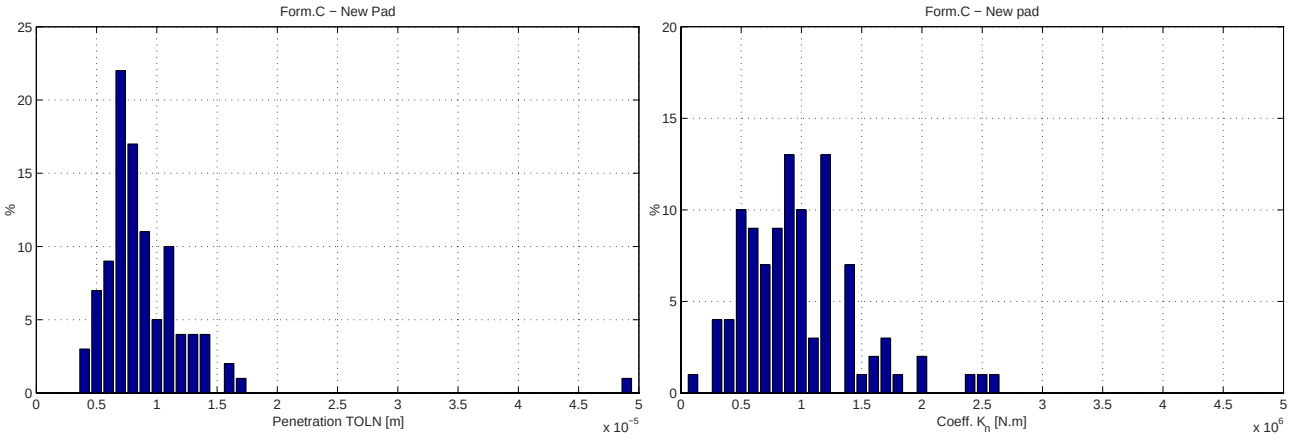

Figure 5.16: Penetration tolerance and contact stiffness occurrence for new pad (form.C)

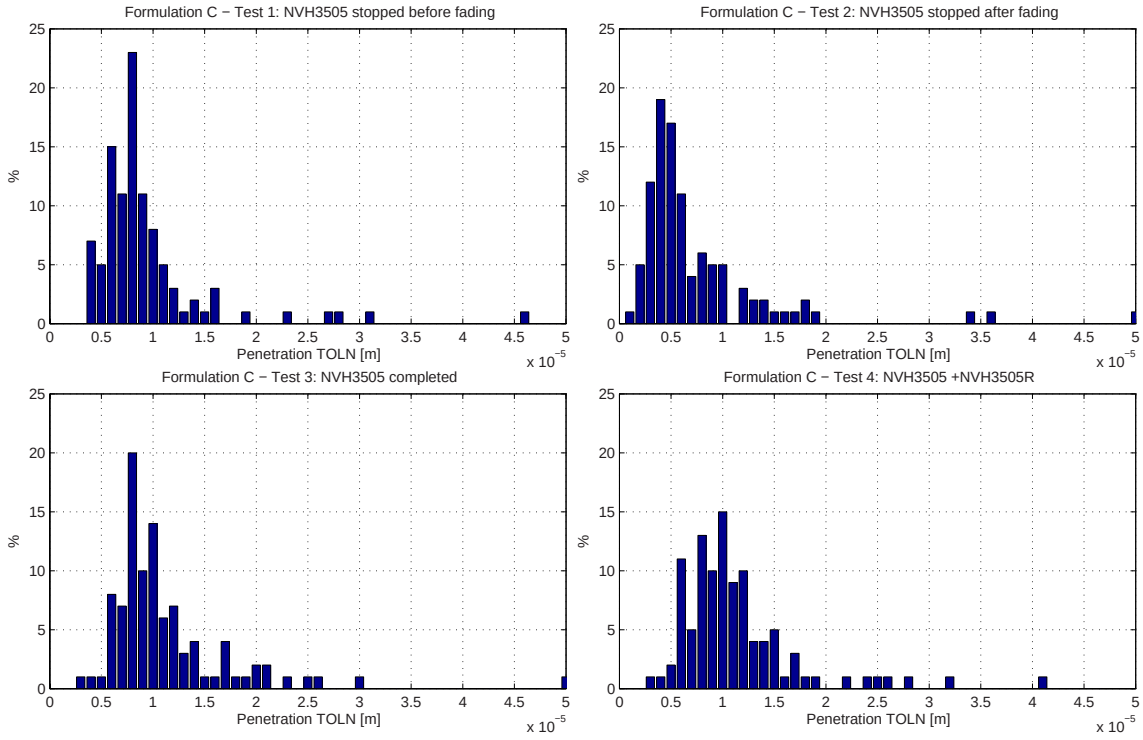

Figure 5.17: Penetration tolerance for used pads (form.C)

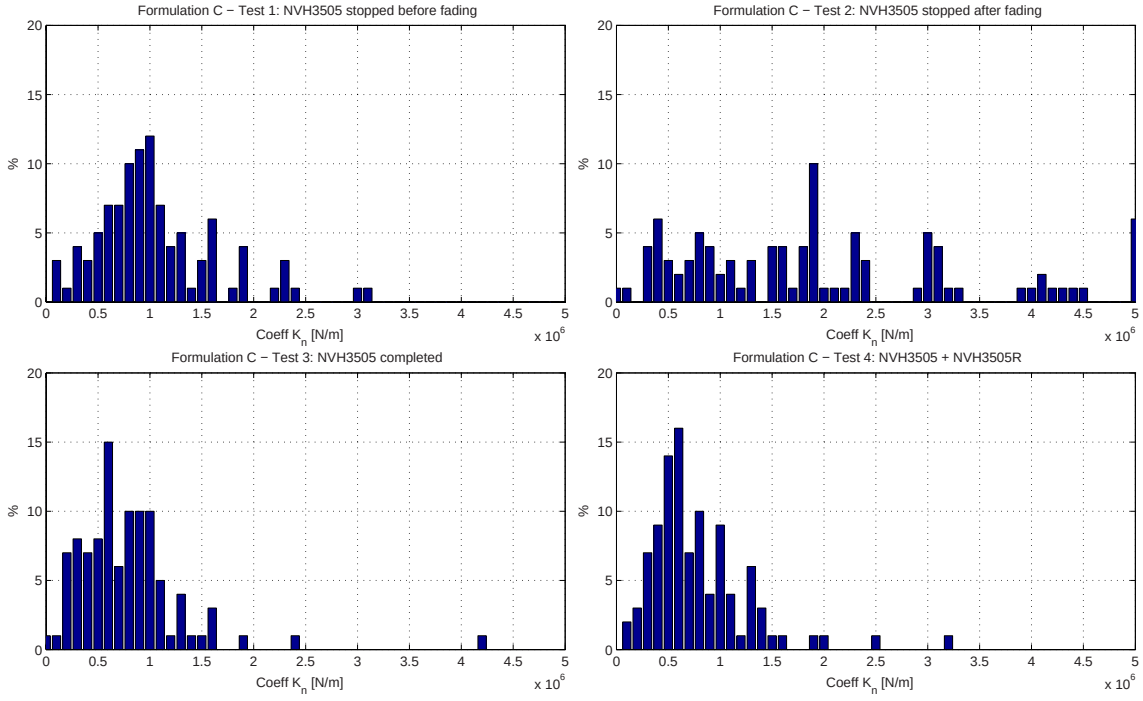

Figure 5.18: Contact stiffness occurrence for used pad (form.C)

The difference between test 2 and the rest is difficult to interpret. Though, it could be the response of severe contact surface heterogeneities (material detachment, plateaus, cracks, etc.). Moreover, mean value of K_n increases and $TOLN$ decreases after fading. It has been seen in profile measurement the general waviness/roughness is lowering after fading, which is in accordance with contact stiffness and penetration evolution. Figures 5.20 & 5.19 present the penetration tolerance and contact stiffness distribution on the pad.

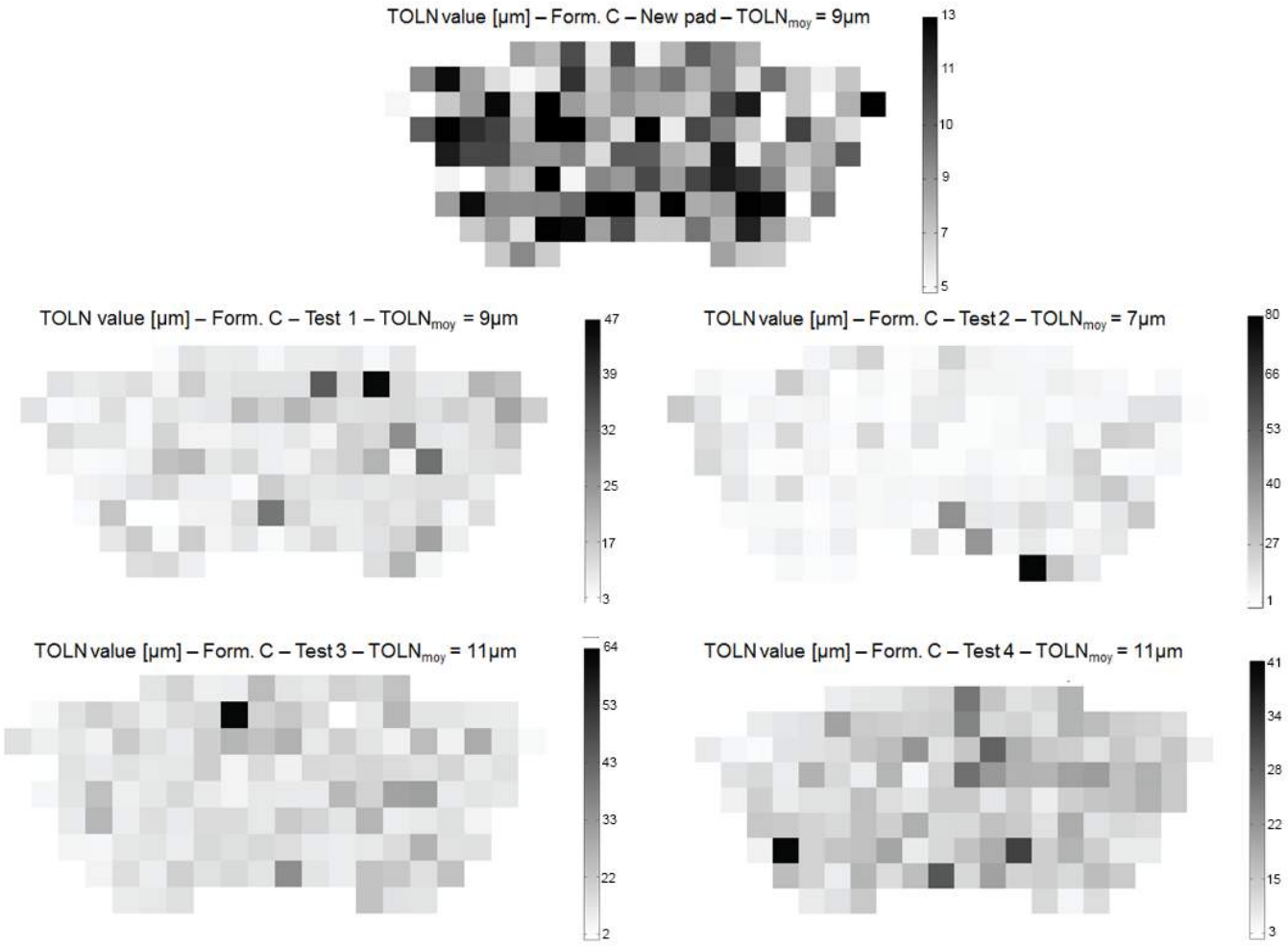

Figure 5.19: Penetration tolerance distribution for innerpad new, test 1, 2, 3 and 4

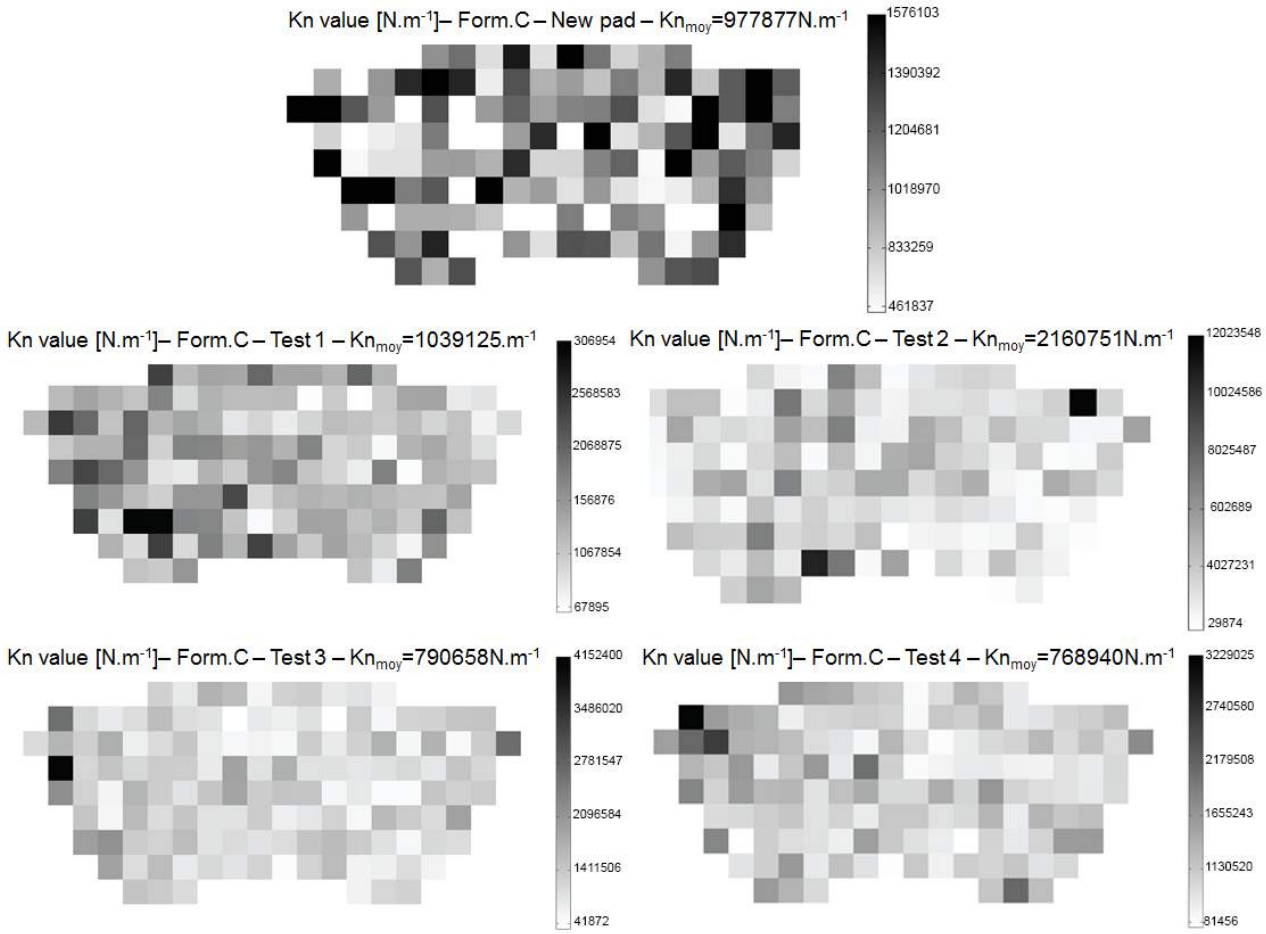

Figure 5.20: Contact stiffness distribution for innerpad new, test 1, 2, 3 and 4

To compare the numerical parameters according to their friction states, the average value of each is calculated and summarized in 5.21. In general, the various parameters are highly variable for test number 1 and 2 but they are stabilized on longer cycles (after undergoing the fading). The elastic modulus is given at 10MPa loading. With friction, E increases and is almost twice higher than at its virgin state. With fading, the elastic modulus reaches 2.2GPa (0.8GPa for virgin state).

Analysis of the results on K_n, $TOLN$ shows fading seems to affect each parameter. It can be noted the mean penetration tolerance $TOLN$ given in this approach is superior to waviness Wa and roughness Ra (except for virgin material). There seem to be a correlation between K_n and $TOLN$: when $TOLN$ decreases, K_n is increasing (e.g. test 2). Reverse phenomena is seen for tests 1, 3 and 4. Linking with noise, there is no particular values for all tests regarding profile (waviness & roughness). However, for test 2 (stopped after fading), the elastic modulus and contact stiffness (which has the widest dispersion for this test) are at the highest value, and noise occurrence around this test is decreasing. No direct conclusion can be made based on these parameters, but implementation into a calculation would allowed to make assumptions.

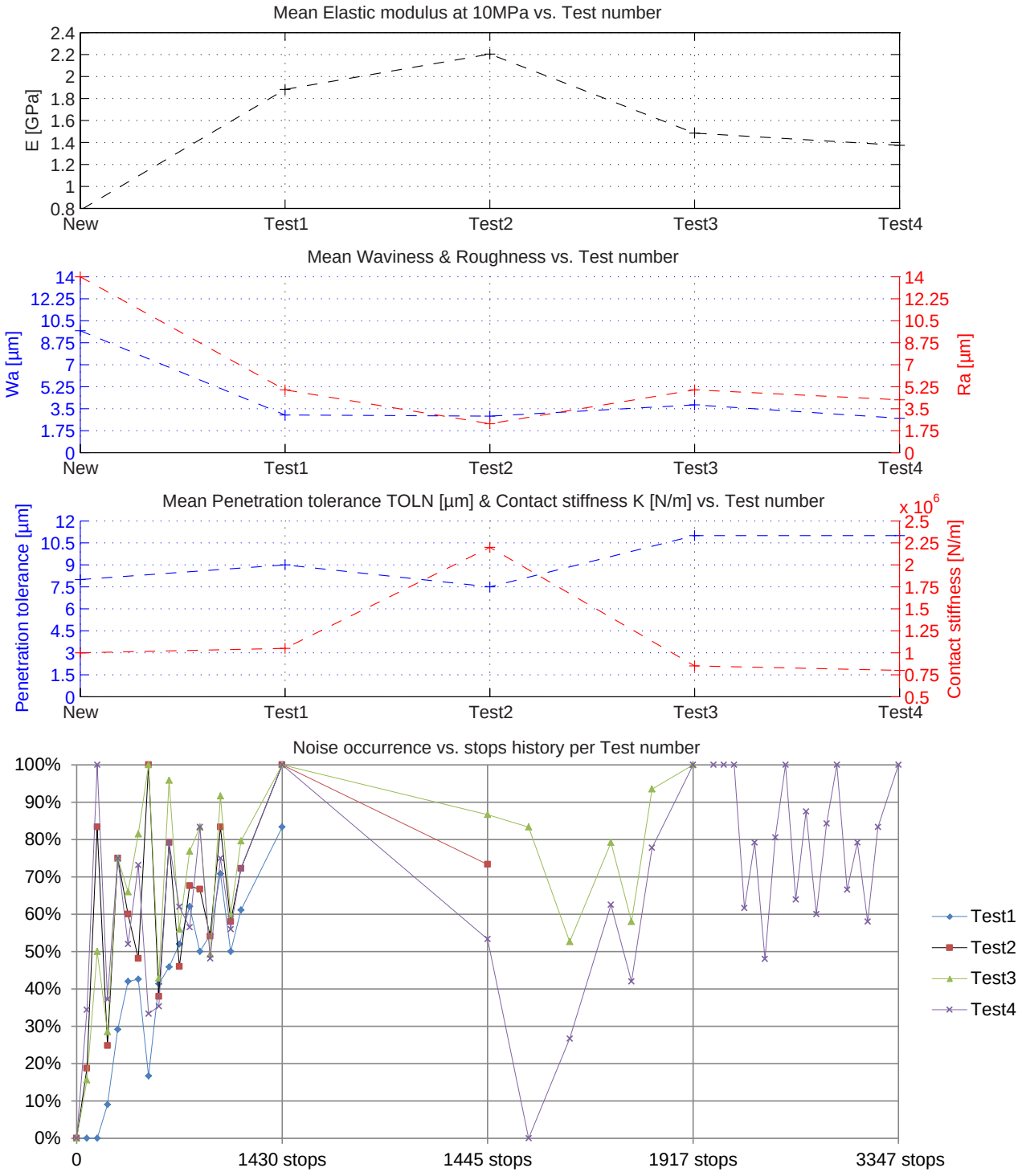

Figure 5.21: Mean evolution of mean constant E at 10MPa, Wa, Ra, K_n and $TOLN$ regarding friction state for formulation C

5.2.3 Conclusions

A new approach for friction material characterization has been developed. The material behaviour has been modelled around an indentation static simulation versus the experimental test. It is based on the assumption that the material behaviour is decoupled into two part:

- the contact surface which represents a few μm and is compensated by a contact stiffness and a penetration tolerance. The two compensate the profile asperities
- the subsurface of the material regarding contact interface. The material is affected in its volume and due to the temperature gradient, the mechanical properties are non-linear. A material law has been build on the stress-strain response. It takes into account the stiffening with loading with Hertz theory determination of Hertz modulus, associated to a correction factor which takes into account the material deformation non-uniformity.

With the implementation of these parameters, the indentation simulation of used pad gives a satisfactory equivalent to the experimental test. On a complete brake pad, this methodology improve the existing method by adding new features: non-linearity of material volumic properties and surface stiffnesses, associated with distributed properties through the pad.

Although the model gives satisfactory results, improvements are possible to be more precise in predicting phenomena. Here are given some possible future research:

- The K_n and $TOLN$ coefficient are effective to compensate the surface effects but they do not represent reality. Both options can be proposed to improve this aspect:
  - The first is to provide a coefficient K_n could be non-linear and so recreate the non-linearities surface effects.
  - The second solution would delete these coefficients and taking into account profiles directly in the FE models (it will also have an impact on mesh sizes and therefore seems unlikely except for shape)
- The evaluation of the affected volume may also be improved to increase the number of tests per brake pad and so have a higher heterogeneity resolution. it could be done by creating a law linking indentation depth and affected volume.
- Indenting with different size of indenter or even shape would permit to consider more the surface profile. A good agreement between a flat indenter with smoothed border is a way to get closed to the braking application.
- The isotropic material assumption is a strong assumption, it would be possible to create models with a transverse isotropic material in the future.

5.3 First implementation into a brake squeal analysis

Previous section has supplied a methodology to estimate local heterogeneities mechanical properties from pad surface to its volume:

- non-linear elastic modulus (load-dependant material) law (volume)
- contact stiffness and penetration tolerance (surface)

Here, the effort is made to implement these properties into a numerical brake pad. The effects and contribution of each volumic and surfacic heterogeneities is discussed. A complete complex eigenvalue analysis of a simplified brake application is used in order to draw attention to which of these parameter is the most critical on mode lock-in.

Material heterogeneities through the pad has been shown in the previous section. Elastic distribution per state of friction is known at 150N. Thus, following model of brake pad in figure 5.22 can be simulated with a localised distribution. Patches on the pad volume are distributed according to indentation mapping as in chapter 4.

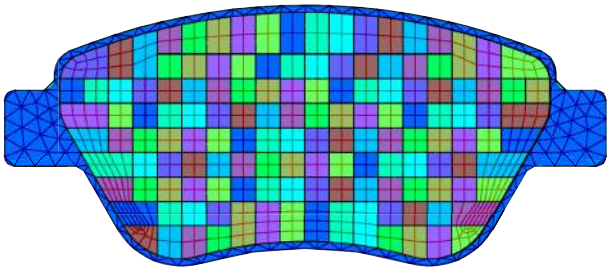

Figure 5.22: 140 patches distributed on the pad: each patch has his own material and contact properties

5.3.1 Model presentation

In the literature review, it has been seen squeal noise occurrence is commonly link to mode lock-in between components, consequently pads and disc. This method is one relevant way to understand squeal, but it has its limits (cf. literature review in chapter 1).

An industrial brake system is a complex device to model: the components have their own behaviour which are not easy to figure out due to their geometry (e.g. caliper or anchor) and furthermore, there are a lot of sliding contacts to consider. Pads and disc obviously but also between the piston and the inner pad, the anchor and the small columns guiding it into the caliper, etc. In order to analyse the influence of pads volumic and surfacic heterogeneities on mode lock-in before even considering these complex geometries, it appears to be more convenient to work on a simplified model. So, the impact (or not) of material properties depending on loading and contact parameters will be more visible.

In this frame of work, a simplified two pads with disc model has been designed (fig.5.23). Classic pad shape and plain disc are used. The plain disc is a grey cast-iron disc with an elastic modulus of $118GPa$, a Poisson ratio of 0.25 and density of $7200kg/m^2$. The disc is rotating aroung y-axis and is blocked on the bowl regarding x- and z-axis. Boundary conditions are also applied on pad extremities (x- and z-axis) and pressure of $10bars$ is applied on both backplates($E_{backplate} = 210$GPa). Regardless the industrial brake pad, this choice has been made to have a symetric behaviour on both side and limit eventual difficulty on mode shape analysis.

Elements used for meshing are quadratic elements which are 3D 20 nodes structural solids. They have three degrees of freedom per node: translations in the nodal x, y, and z directions.

Contact interaction between pad and disc is a surface-to surface contact solved by augmented Lagrange method. Contact detection is done at Gauss integration point. Contact stiffness by default is equal to $1.3.10^{14}N/m$ with an initial friction coefficient $\mu = 0.5$. Contact interface mesh is refined on 60° sector of the disc.

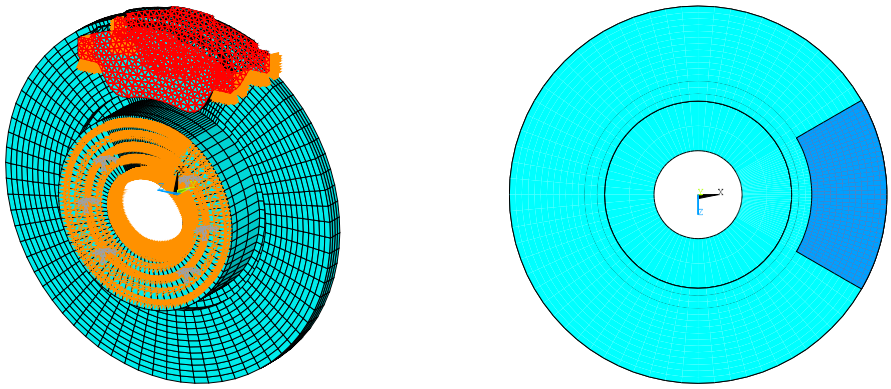

Figure 5.23: Pads/disc FE model: in red, 10*bars* pressure is applied on both pad backplates, in orange, 0-displacements boundary conditions (on x- and z- axis), disc contact zone is in dark blue

The analysis is a complex eigenvalue analysis. It is divided into three steps:

1. static equilibrium with pressure applied on both backplates (10bars)
2. quasi-static calculation implying a rotation of the disc
3. extraction of complex eigenvalue with the use of unsymmetric stiffness matrix

It must be noticed the present model can't be compared to the experimental results found in chapter 4 Here, the disc is unvented and the boundary conditions are differents.

5.3.2 Reference calculation

Before implementing heterogeneous material laws, a isotropic mean elastic modulus for formulation C (830MPa). Contact pressure is shown at pad interface in figure 5.24. Contact covers all the pad from leading to trailing edge (left to right). There is an overpressure at leading edge which covers 1/8 of the pad surface (2 to 6 MPa), as a low pressure zone in trailing edge (0.1 MPa). This might be smoothed by wear profile implementation (the leading edge of the pad is sharp at virgin state).

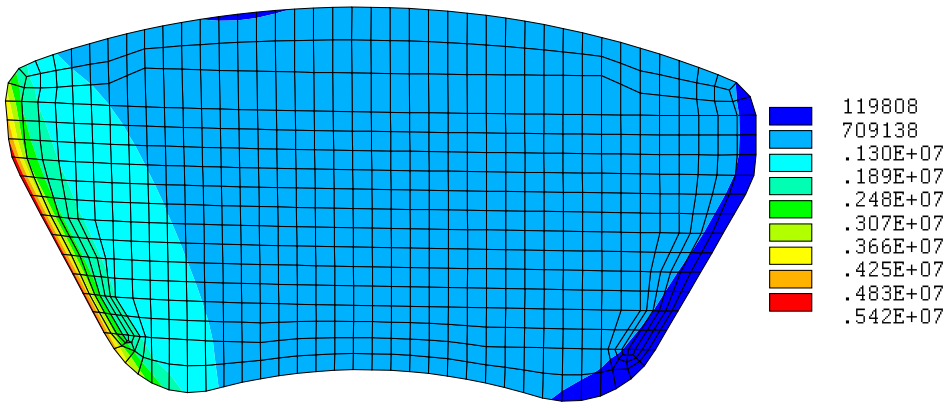

Figure 5.24: New pad - Contact pressure (Pa) - Homogeneous isotropic modulus (830MPa)

Concerning complex eigenvalues showed in figure 5.25, there are 5 unstable mode out of 40 (in red). Figure 5.26 displays associated deformed shape. Mode M1 is an out-of-plane disc mode with the pad following the disc

deformed shape. M2, M3, M4 and M5 are pad contributed and moreover contact related. These results suggests the contribution of contact between pad and disc for the system stability.

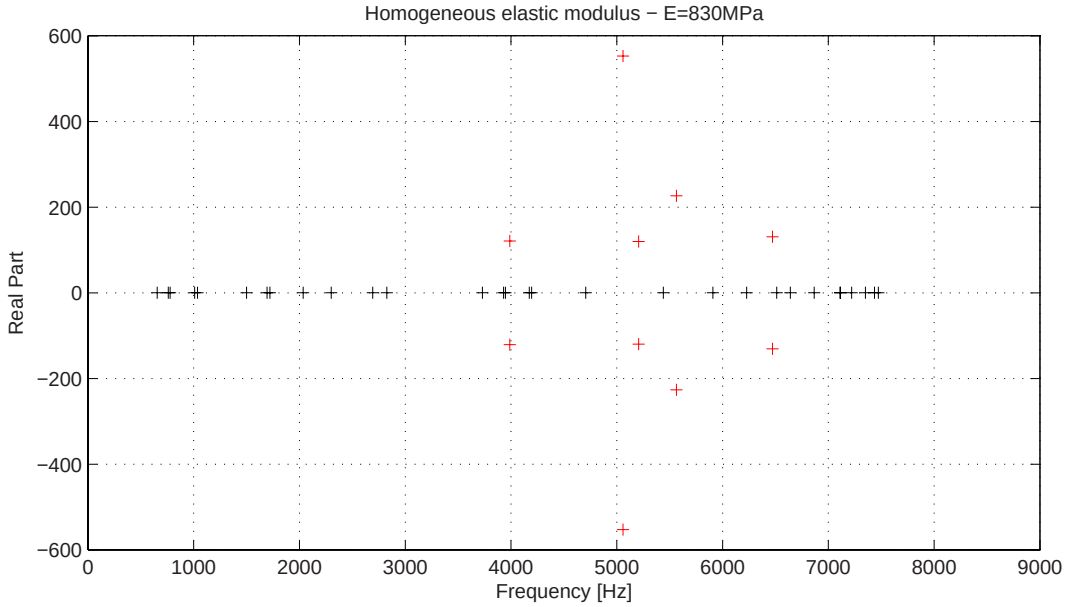

Figure 5.25: New pad - Homogeneous elastic modulus 830MPa, eigenfrequencies versus real part analysis

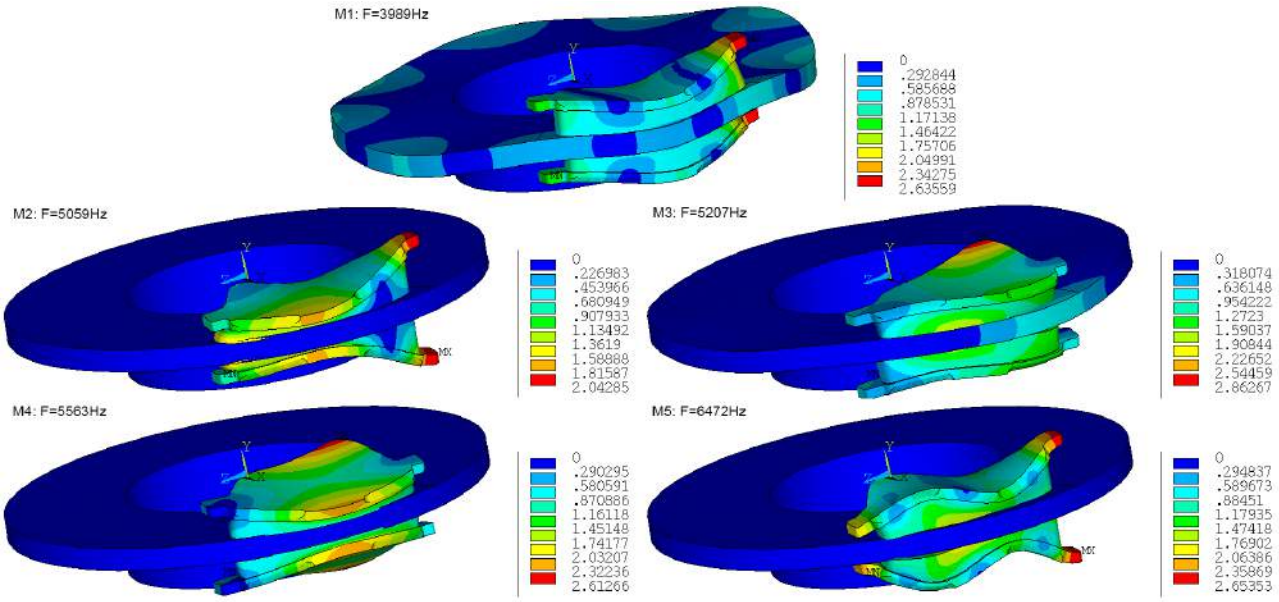

Figure 5.26: New pad - Deformed shape for unstable modes - Homogeneous elastic modulus 830MPa

5.3.3 Contact & volumic non-linearities impact on mode lock-in

In this subsection, heterogeneous non-linear material properties with surface linear contact stiffnesses (& penetration tolerances) are implemented into the finite element model. 5 mappings are studied: new pad, test1, 2, 3 and 4. Figure 5.27 shows contact pressure on innerpad for all 5 situations. There seems to be only few differences except for test 3 which leading edge is highly loaded regarding other tests.

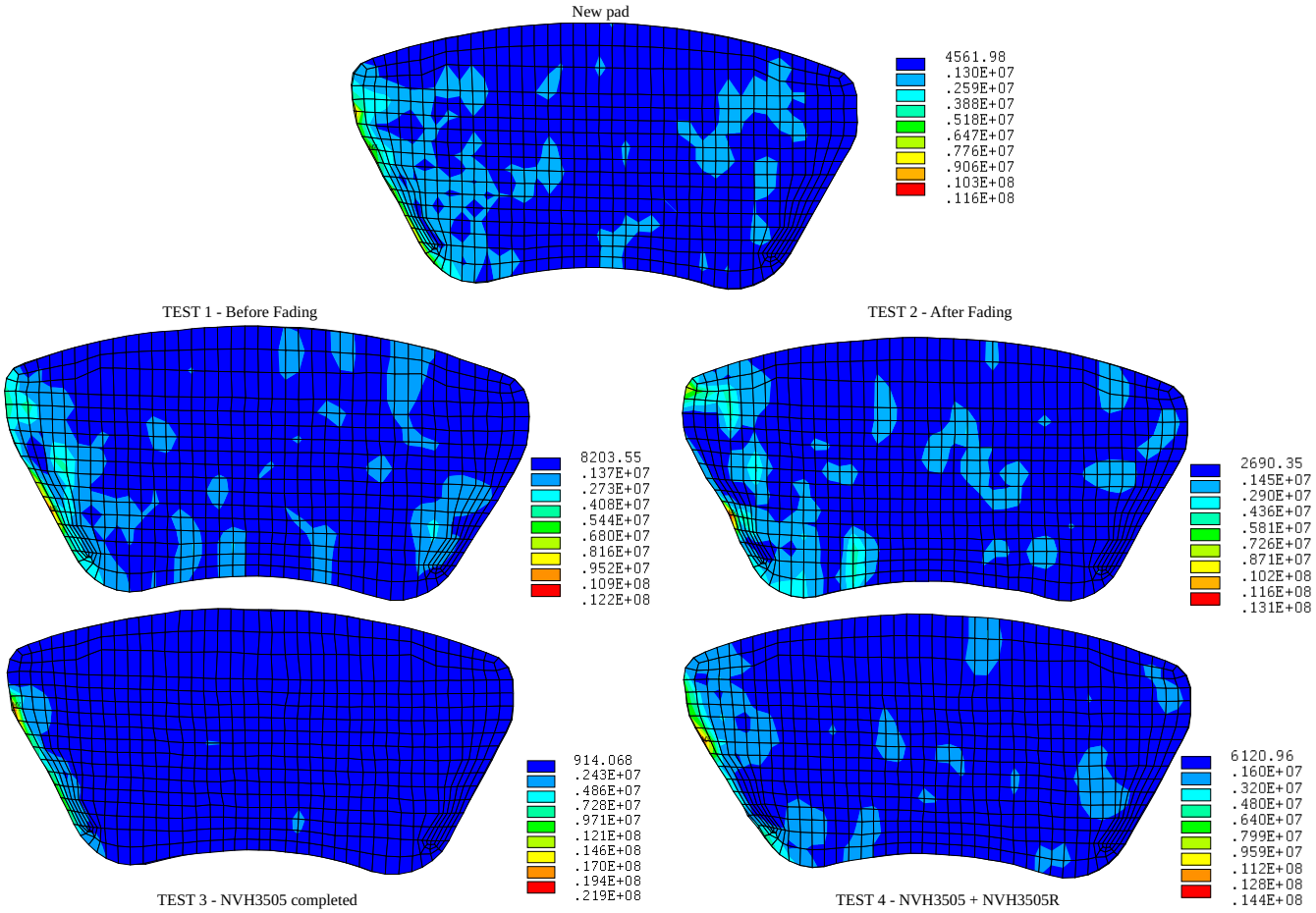

Figure 5.27: Test 1 - Non-linear heterogeneous modulus & contact properties - contact pressure (Pa) - Four braking situations

Figure 5.28 describes eigenfrequencies versus real part. Red crosses are unstable modes. First result is the same eigenfrequencies (by extension same deformed shapes) are involved for all cases. Three modes at 2.1, 2.3 and 8.2 kHz are unstables. However, some of them don't appear in every test. In test 1, 3 and 4, the three unstable modes emerge. Regarding new pad, only mode 3 is appearing, which is mostly a disc out-of-plane deformed shape. The two other modes are more contact related. In test 2, there is no unstable modes. Comparing with reference calculation (fig.5.25), material heterogeneities are "filters" since there are less unstable modes as in the homogeneous case.

These numerical results, coupled with stiffness bar graphs 5.16, 5.17 and 5.18, shows a minor propensity to become unstable for highly heterogenous contact surface stiffness , which has been seen for new pad & test 2. Also, it has been observed surfaces are less accidented and more regular for these two situations.

The volumic properties (figure 4.25) might play the same part in the mode lock-in occurence. The elastic properties seem more homogeneous for new pad than test 2, and one mode does appear for new pad and not for the other.

As a results, surface heterogeneities distribution might plays an important part in the occurrence of mode lock-in, but cannot be dissociated to volumic properties distribution which seem to also influence different modes. Also, pads parameters which didn't make noise at their ending (test 2 and of course new pad) have shown no propensity to become unstable in the FE model and confort the idea squeal is linked to mode lock-in.

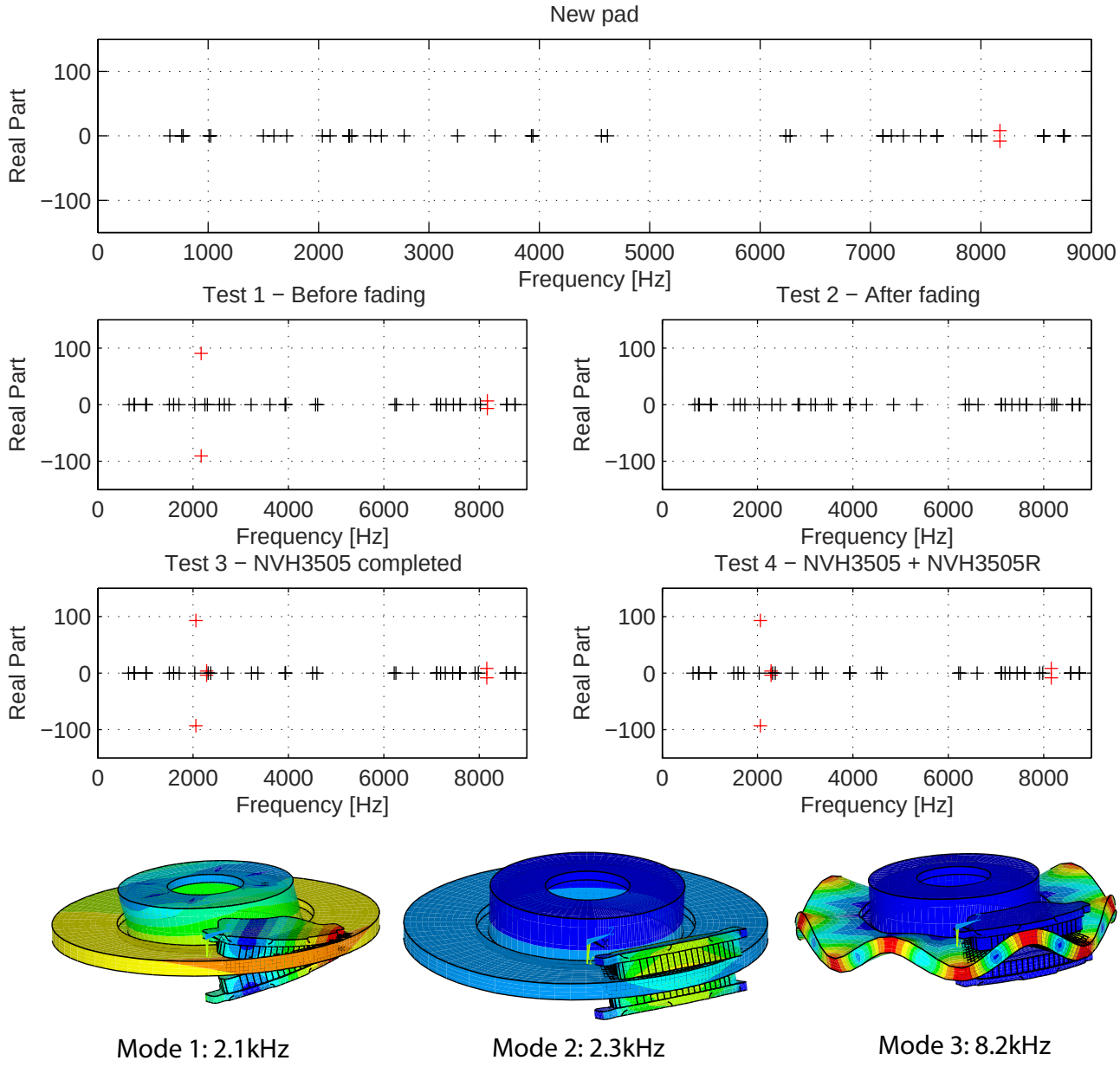

Figure 5.28: Non-linear heterogeneous modulus & contact properties, eigenfrequencies versus real part analysis - Comparison between 5 elastic properties mapping corresponding to new pad & 4 NVH ending situations

Comparing with homogeneous case (fig.5.24), the contact pressure is less localised on the leading edge and more distributed on the surface. The maximum pressure (around 13bars) is more realistic regarding application (maximum of 20bars for real braking application). Regarding unstable modes, there are less in the heterogeneous case. The real parts for unstable modes are less important (±600 for homogeneous case versus ±100 for heterogeneous).

In a second analysis, the purpose of is to see the impact of contact stiffness heterogeneities regarding the

volumic heterogeneities. The contact stiffness and penetration tolerance are imposed at their default values ($K_n = 4.8.10^{14} N/m$ and $TOLN = 280\mu m$) as homogeneous datas, and only heterogeneous non-linear material properties are taken into account. In figure 5.29, shows the contact pressure for all 5 friction situtations. Firstly, the contact pressure regarding figure 5.27 is more homogeneous.

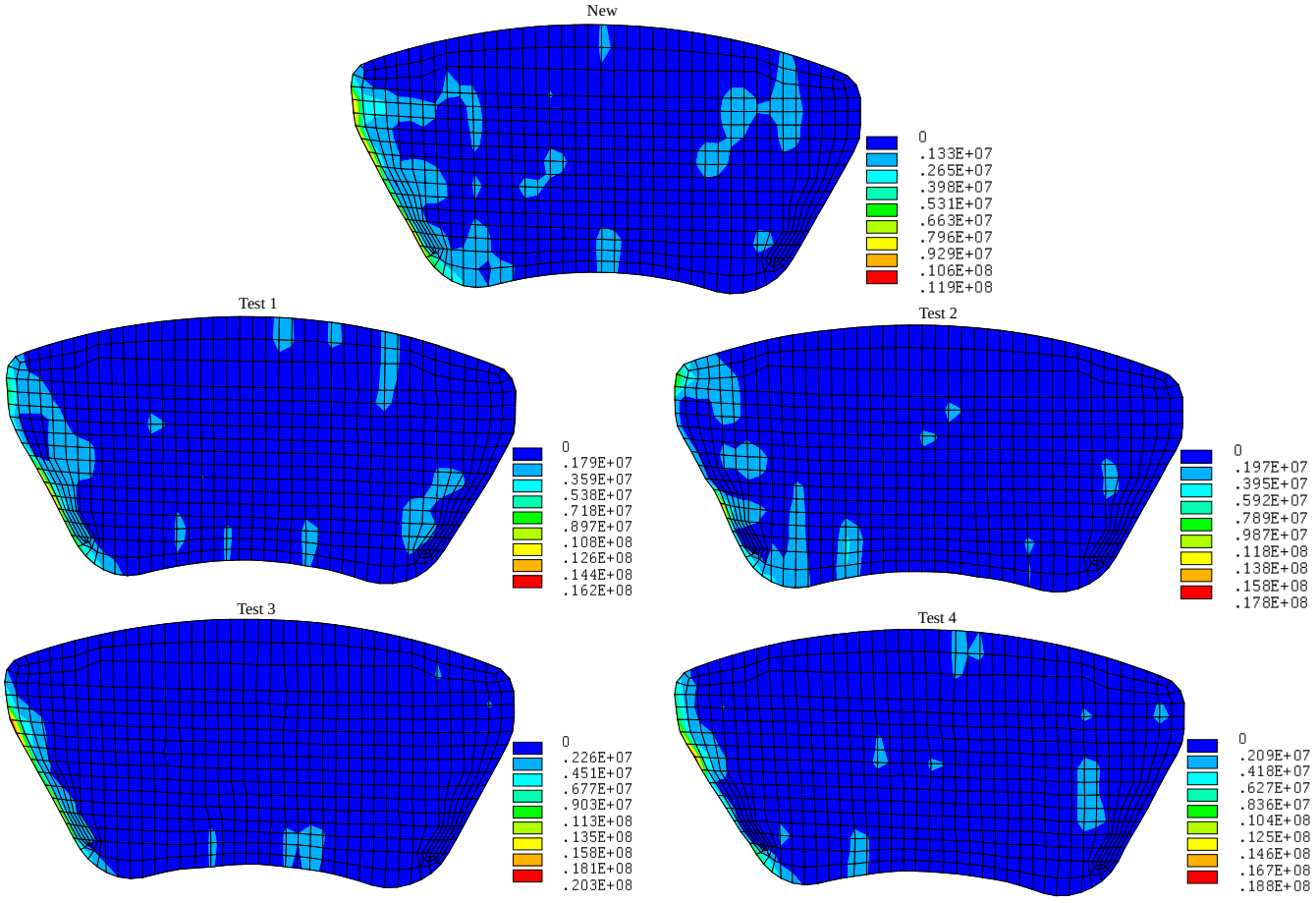

Figure 5.29: Test 1 - Non-linear heterogeneous modulus contact pressure (Pa) with homogeneous contact properties - Four braking situations

In figure 5.30, the unstable eigenfrequencies involved are completely differents (two modes at 7kHz and 8.6kHz) and the real part are even less important (below 20). Hence, contact stiffness distribution and heterogeneity have a strong impact on mode lock-in.

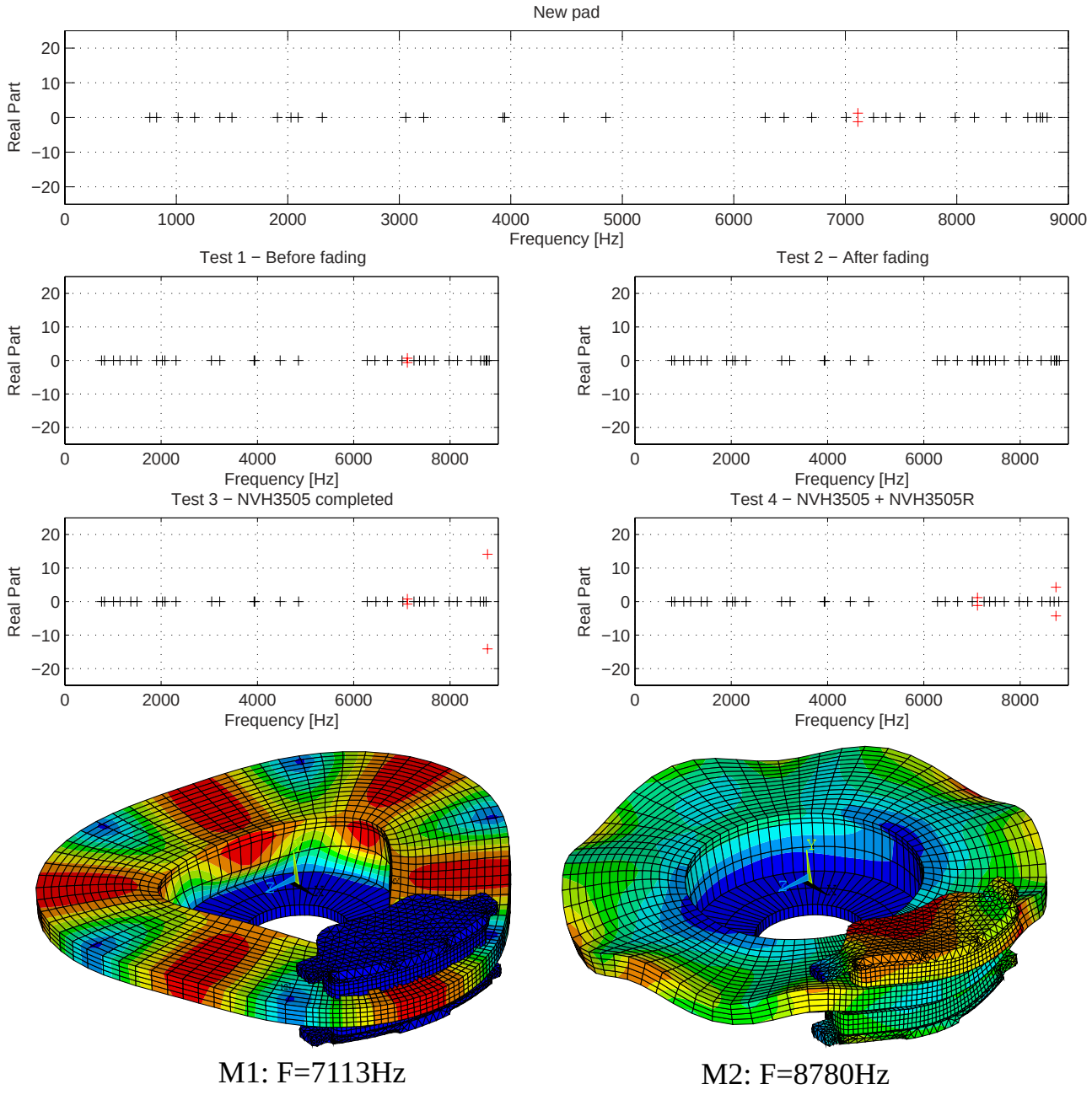

Figure 5.30: Non-linear heterogeneous modulus with homogeneous contact properties, eigenfrequencies versus real part analysis - Comparison between 5 elastic properties mapping corresponding to new pad & 4 NVH ending situations

5.3.4 Bondary conditions and profile influences

In the previous brake simulation, the caliper is not taken into account. Therefore, the forces applied on the pad are symmetric and don't relate the real brake application. It has been seen in chapter 4 the shape is a first order parameter. With the current simulation, it can be expect there won't be an effect of implementing the shape. Thus, it is interesting to add coupled displacement conditions (here called coupling BCs) on both backplate ears to simulate a normal application of pad regarding disc axis (fig.5.31): the backplate displacement is supposed parallel

to the disc, guided by the caliper.

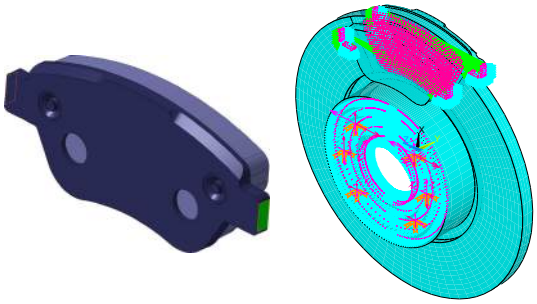

Figure 5.31: Coupling BCs on backplate ears nodes (linked in green): the displacements of backplate ears are identical regarding y-axis (disc axis)

Figure 5.32 shows contact pressure with implementation of profile for two cases: one without coupling BCs, and a second with. The profile introduced here is coming from the shape three-dimensional measurement from test 1 and implemented with a least square method. Without coupling, the contact pressure is similar to the homogeneous case. Adding displacement coupling, the contact pressure field is different: the pressure applied is more homogeneous.

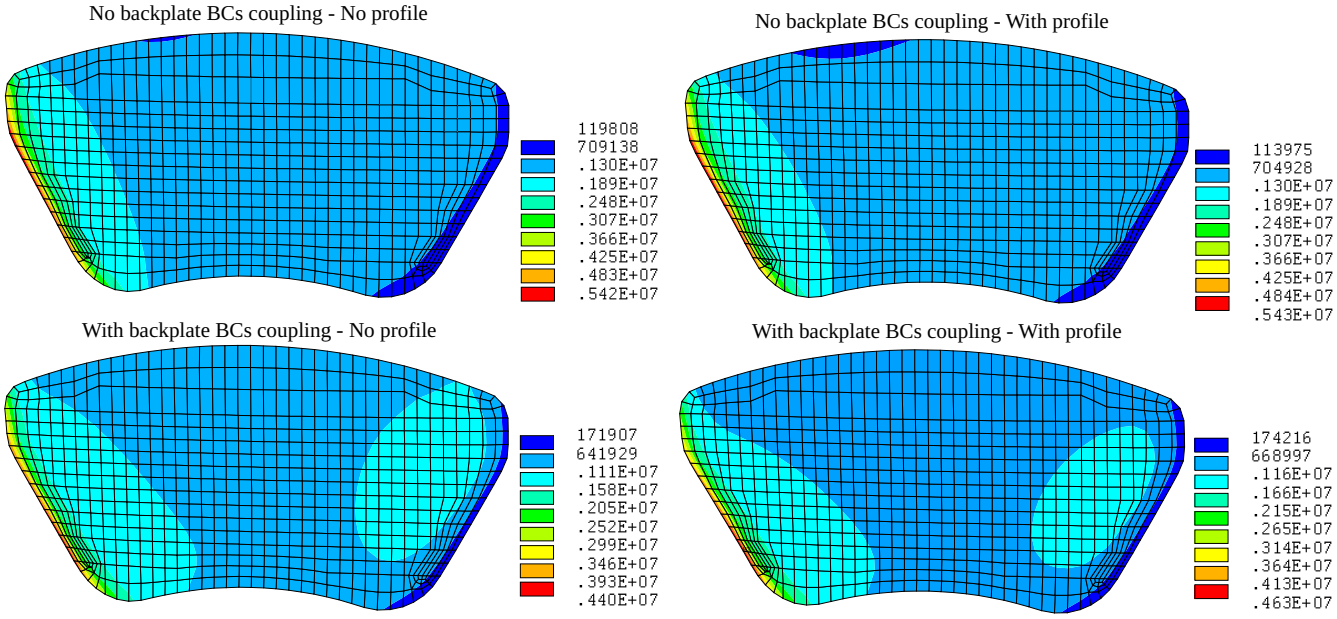

Figure 5.32: Homogeneous modulus (830MPa) contact pressure (Pa) - Implementation of backplate boundary conditions coupling & innerpad profile comparison

In figure 5.33, complex eigenvalues results are shown. Implementing profile won't change the frequencies and moreover the instability. The deformed shape are stricly identical to the reference calculation modes. However, adding coupling BCs modifies deeply the modal response. Figure 5.34 shows the associated mode shapes for unstable frequencies (three modes).

This study shows the impact of boundary conditions, linked to the structure. This simulation lacks the other components and highlights the brake squeal problematic can't be only focused on pad and disc contact, but also with the complete system.

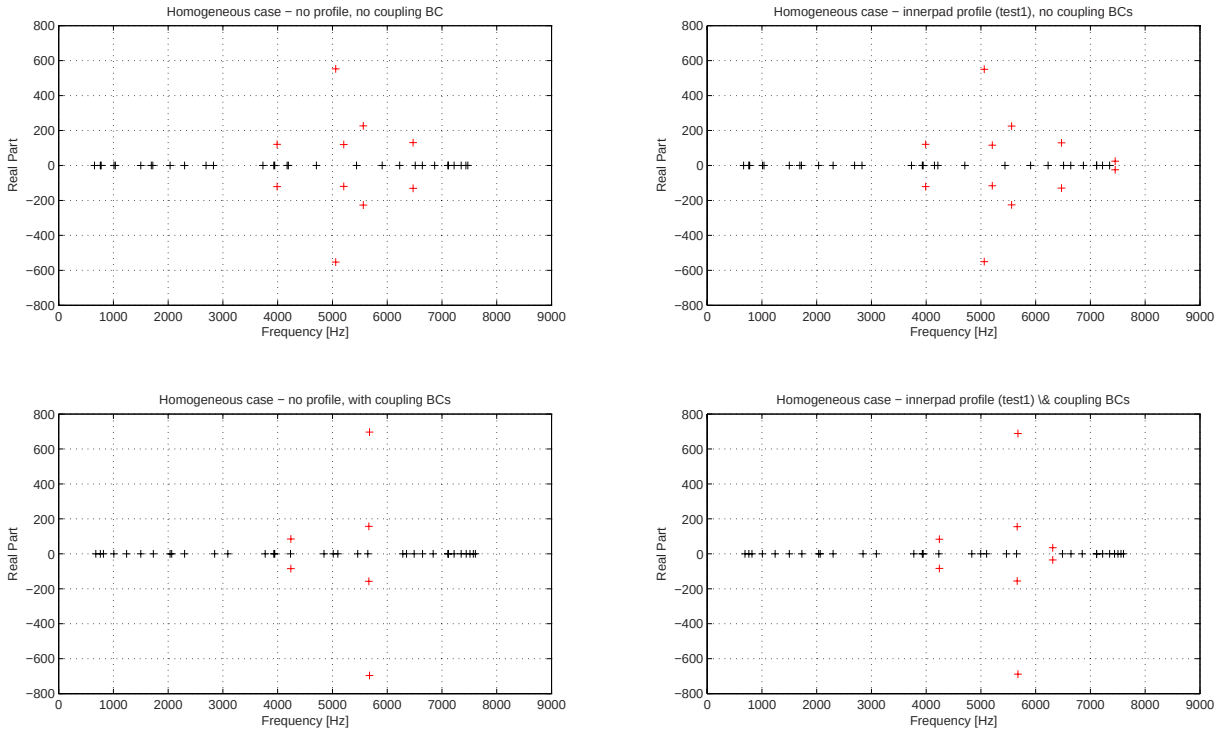

Figure 5.33: New pad - Homogeneous modulus, eigenfrequencies analysis - without coupling & innerpad profile versus with coupling & innerpad profile

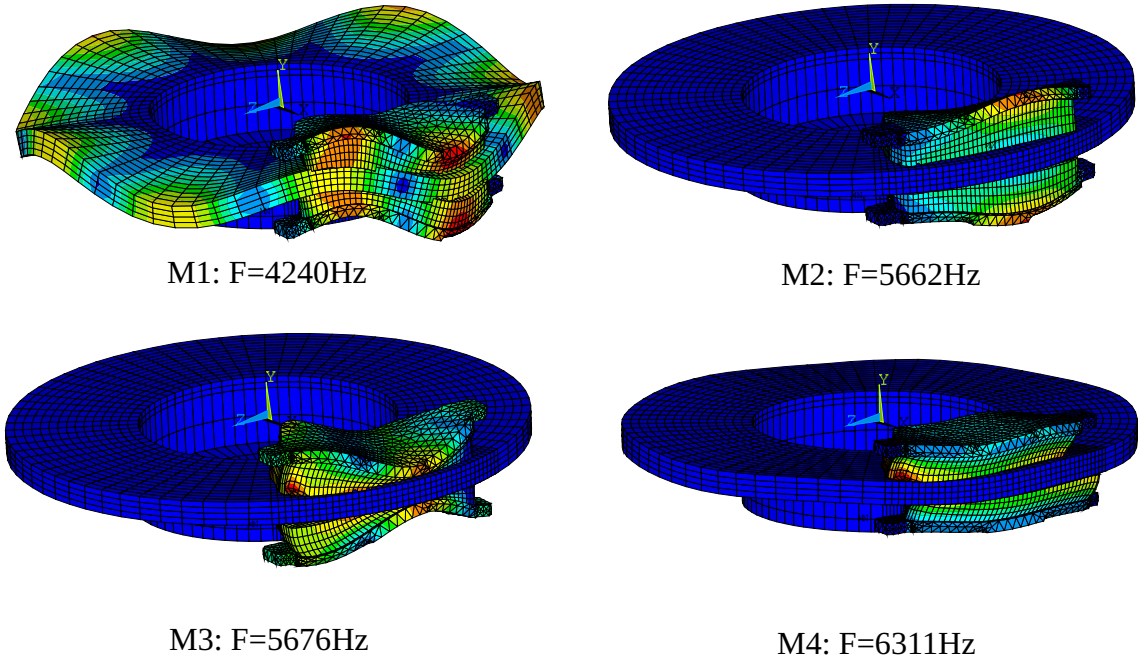

Figure 5.34: New pad - Analysis with coupling BCs at backplate interface (with profile) - Deformed shapes for unstable modes

5.4 Chapter synthesis

The goal of this chapter was to model friction material non-linear behaviour under localized loading. An effort has been made by localised indentation tests to separate surface behaviour to friction material volumic response, on four pad stopped at different friction states:

- surface: a linear contact stiffness coupled with a penetration tolerance
- volume: a non-linear isotropic elastic law

For each pad, the identification has been done with 140 imprints that have been introduced in the numerical model on 140 patches. Identification of material behaviour model shows that the non-linearity is relatively limited, especially at low level (normal stress above 10 MPa) but that the heterogeneity is very strong. Same comment can be done on the identified contact stiffness distribution exhibiting a high heterogeneity. Numerical contact and eigenvalue analysis shows that these two parameters, i.e. contact stiffness and material behavior, and their heterogeneities, have a strong influence on the results (contact pressure distribution and unstable frequencies). Results for test 2 give any unstable modes, which is consistent with the experimental results even if many reserves have to be expressed due to the modelling simplifications. Identified parameters for this test exhibit a higher stiffness distribution and also compressive modulus compared to the values of the other tests.

In this frame of work, the finite element model is different from the real application. This study has emphasized the fact boundary conditions, and so other components are also direct consequences in the system equilibrium. However, the goal here was to determine which relevant parameter would influence mode lock-in.

Regarding noise tests versus finite elements results in terms of system instability, the direct correlation is too strong but there. This suggests the indentation test methodology designed is a correct approach to identified localised contact and volumic parameters. Material and surface heterogeneities have a high impact on mode lock-in. A homogeneous mapping is more unstable than a heterogeneous one.

Though, it is still hard to extract important parameters, or even sort a relevance order. The structure, heterogeneities, contact stiffness and non-linearities appear to be linked. Hence, there are numerous ways to investigate in order to increase the method accuracy and understand the parameters influence deeper:

- The contact stiffness is considered as linear, but numerous works have shown the non-linear behaviour of the interface, even this study which only gives a "placebo" with the couple K_n and $TOLN$.
- The C coefficient is a compensation of defomation mechanisms with loading during indentation (porosity compression, non-symetric profile, sink-in, etc.). It has been seen measured contact depth is too high compared to the real depth. This coefficient could be replaced/corrected by more iterative methods to correlate with experiment, e.g. Finite Element Model Updating (FEMU).
- The material is considered as isotropic. The present work has described transverse isotropic behaviour with compression test but alos by the pad formulation and raw components themselves. Works as [Ciavarella et al., 2001] have developped Hertz theory in transverse isotropic and even anisotropic situation. The contact is known as complex in term of geometry and material properties and linking both approaches (anisotropy + load dependancy) might improve the model
- other indentation tests should be made with different sizes and shapes of indenter in order to take into account profile. Furthermore, the incidence on the affected volume should be investigated.
- the study has shown different types of wear shape and it might be interesting to see the impact of theses profiles on the CEA model.
- a complete model considering the floating caliper and vented disc as in real test application, coupled with datas acquired with indentation & profile measurement is the next step to complete the CEA study and be able to compare with experimental results. Also, to determine unstability propensity and which components

is leading to it, an energy-based approach as in [Papinniemi and Lai, 2004] is a good start. It would permit to select which mode shapes are responsible of unstable frequencies, and if the contact is critical or if it is due to other components, unstable modes of a brake model being numerous.

Conclusions & Prospects

The present work deals with an industrial problematic encountered by the automotive industry and its customers. It represents an important rate of after-sales service recall. The number of cars increasing, with the high solicitation applied on organic brake pads, and the acoustic pollution and wear particles spreading place the disc brake squeal noise as a first order problem in terms of environmental and competitive challenge for the industry.

It is well assumed disc brake squeal noise is a multi-scale and multi-physics problem. The last decades have found countless studies around specific points of the phenomena. The main conclusion common to every studies is the problem can't be analysed without taking into account every aspects of the problem. The brake cast-iron structure (caliper assembly, disc) at the macroscopic scale has the same impact as the friction material itself. Also, at a smaller scale, the friction material composition and its mechanical response modifies deeply the vibration behaviour. At last, the contact interface between the pad and the disc is always changing due to thermo-mechanical transformations. In this study, the effort has been made in having a complete consideration of every aspects, coupling scientific and industrial point-of-views. Therefore, the main goal here was to go though an identification of relevant parameters of the friction material volume and surface, influencing squeal occurrence. The difficulty leaves in the evolution of these parameters with test sequence, temperature, braking history, etc.

First of all, simplified friction material formulations with a known process and identified mechanical and thermal properties have been designed. An industrial formulation has been taken as a reference in terms of performances in order to keep realistic comparisons according industry requirements. Experimental tests for material characterisation have emphasized the complex response of these composite materials through temperature. Thermogravimetry as dilatometry have outlined key temperatures for resin and rubber degradation into the material. It has been shown that, according to fabrication process and raw components degradation temperature, the material would react in consequences. For instance, formulations A, B and C are cured at 200°C, if a braking reaches a temperature over this level, the material will start to change significantly from its surface to its volume. There is also a second threshold observed at 400°C where the resin, mainly, is degraded (with other raw materials). These temperatures are reached during braking and impact subsequently the friction material. These thresholds impacts contact interface layer, modify the coupling with the disc (hence might change noise frequencies) and even change volume properties. So, there is a strong impact of temperature on material degradation, hence on disc brake squeal.

Compression tests from two approaches have been done: on cylindrical and cubic samples. It has been shown the transverse isotropy which is a direct consequence of manufacturing process and the fibres orientation. The normal elastic modulus is around a third of the transverse modulus. Also, the dependency on loading has brought to light the macroscopic heterogeneity on each sample, through a pad cutting. Currently, pads are homogeneous, at best transverse isotropic materials. It has been observed a $\pm 15\%$ deviation on every pad. It asks questions on current industrial model of friction material about the importance to implement these parameters in brake systems numerical studies.

Material characterisation done, experimental bench testing has been performed on two systems: a commercial brake through a normalised braking procedure and a more simplified brake system in order to compare formulations with their noise response. The commercial brake seems to have a robust dependency on formulation, even if additional tests might confirm it. Three different simplified formulations have been tested and each one has given different noise/frequency responses, even if their compositions are close: there is a strong formulation effect.

The raw materials impact the final product response, from a formulation to another and for the same test: The formulation B generates low frequencies noises, whereas A is more high frequencies generating. The main difference between both is the removal of steel fibres in B. Also, it has been seen formulation C is more stable in terms of noise behaviour. Even if the formulations are close, a slight modification can change deeply the noise response. In addition, the sequence paramaters, mostly temperature, have an important impact on noise occurrence and vibrational behaviour: for instance, after fading, noise occurrence is reduced and after high peaks of temperature, the frequencies involved are modified, sometimes permanently.

On the simplified brake system, tests have been done on cylindrical samples, on a procedure below 150°C. It has been seen there were less impact of formulation on squeal noise since the system is very simple, generates almost only one frequency noise (3.6kHz) and friction surface is reduced ($phi30mm$). Main result seen in these tests series is the braking history effect: looking at contact surface by observing it at different time of the braking procedure, for the three formulations, the evolution are very different. The temperatures seen by the material alter the material as long as a certain layer of material is removed by friction. It is translated as a kind of "recovery" with time. The same statement has been found on commercial brake tests, even by repeating the same sequences on other samples from the same formulations.

Parallel to the dependendcy of squeal occurrence with the test sequence, a strong modification of contact surface is observed. Therefore, the braking sequence on the commercial brake has been done 4 times and stopped at different steps of the procedure. The surfaces are differents from a virgin state to a used one, and even more for different temperature levels. It has been chosen to decompose the surface profile into 3 scales: shape, waviness and roughness. With friction, pad geometric analysis has shown a slope from leading to trailing edge. Moreover, with fading, a concave shape at pad leading edge has been notice which can be explained by the dilatation of the material at high temperature loading. Surface geometry analysis has displayed the waviness and roughness profiles are lowered with friction, and even more with fading. Materials characterizations are currently performed at a macroscopic level and without degradation. Complementary to surface analysis, the evolution of material compressive behaviour, with test sequence, has also been investigated, as far as its variability with localisation.

Using the Brinell indentation test, with the use of Hertz contact theory, an elastic modulus load-dependant is identified on several points of the contact pad surface. The goal is to build a numerical material law, with contact parameters associated, which simulates the same response into an indentation finite element static analysis. The post-processing is separating the "surface effect" from the "volumic properties". It identifies a contact stiffness and penetration tolerance to compensate second order profile, then a non-linear uniaxial $\sigma = f(\varepsilon)$ material law which takes into account material stiffening through load in its volume. The majority of numerical material and contact properties identified are accurate regarding experimental points. Therefore, a non-linear material law with an associated contact stiffness mapping is set up for simulation, for different states of friction. From a new pad to friction state, the material is stiffer and the surface and volume properties are more heterogeneous.

These numerical datas are implemented into a Complex Eigenvalue Analysis of a pad-disc simplified model. Compared to homogeneous linear material behaviour, it is shown a strong influence of contact and non-linear volumic properties as heterogeneity. As a first trial on the impact of such parameters, the influence of heterogeneous material properties and surface stiffness is non-questionable. It must be noted the set of parameters representing the fading case has given no unstable modes. Comparing with noise results, the stops are less noisy after fading, which is in the same way for numerical results even if the model is a simplified version of the bench.

The main research perspectives that appear at the end of this thesis can be separated into three steps. First of all, the direct reuse of this work is the completion of the bench testing. More tests should be done in order to confirm the reproducibility of the results previously seen. Moreover, only four friction situations have been studied (compared to virgin state) and it misses less critical tests (e.g. low temperature) but also longer tests to see a more complete history of the material.

The indentation methodology leaves on several hypothesis and the relative sturdiness is questionable. A way of improving the post-processing would be to take into the evolution of the material in its volume, with the anisotropy

implied by th heterogeneities. The surface properties are considered as linear even if the profile is complex. Deeper analysis on the microstructure, regarding both surface and volume, would help to explain the evolution the parameters extracted from the post-processing. These parameters have been implemented into a complex eigenvalues analysis. A numerical study has shown their impact on unstable frequencies but on a simplified model. Therefore, a complete model closer to the experimental test bench would allow to confront with noise results. However, this implies to determine each parameter sensibility and if they are sufficient (and relevant) into the simulation.

A second step is to work on the material characterisation under controlled sollicitations as functions of known thermal transformation thresholds and compression response. Without bench testing, the goal would be to build a predictive tool, for example via a thermo-mechanical simulation, reproducing the material transformation, and furthermore giving an insight on the heterogeneities distribution enhanced by loading.

This would lead to determine the link between friction material formulation and physico-chemical transformations during braking, with squeal occurrence. Focusing on friction material, this work suggests a correlation with threshold temperatures and surface/microstructure modification. Knowing the interactions between pad raw materials under loading and the noise response according material mechanical properties ditribution & evolution with temperature will subsequently help to understand the generation of instability, hence squeal noise.

This work has emphasized the friction material formulation, temperature, and history effects on disc brake squeal. It has been shown that noise occurrence depend on friction material, the history of sequence and that temperature is a key parameter. Thresholds of material degradation have been separately identified highlighting this dependency.

Evolution of the friction material has been characterized regarding surface and volume mechanical properties showing a high heterogenity at these two scales and significant evolution with the test sequence. Implementation in a numerical model of modal coupling with contact conditions, shows the proposed parameters have a significant influence on dynamic instabilities and a consistency with the experimental cases of squeal occurrence.

Appendix A

Appendix - A

Heat capacity - Conductivity

Thermal transport properties of materials are needed: the temperature transfered into the material while braking vary function as materiel ability to conduct heat, hence condition the temperature seen by the pad and the level of transformations achieved.

Material properties are gained from the measurement on device called Hot Disk Thermal Analyser using Transient Plane Source TPS method [He, 2005] which gives information on thermal conductivity, thermal diffusivity as well as specific heat per unit volume of the material under study.

Parameters identified from the thermal flux ϕ into the pad are labeled as:

- λ, the thermal conductivity (W/mK)
- ρ, the density (kg/m^3)
- α, the thermal diffusivity (mm^2/s)
- C, the specific heat $(J/kg.K)$

The Hot Disk sensor described in figure A.1 consists of an electrically conducting pattern in the shape of a double spiral, which has been etched out of a thin metal (Nickel) foil. This spiral is set-up between two thin sheets of an insulating material (Kapton, Mica, etc.) When performing a thermal transport measurement the plane Hot Disk sensor is fitted between two pieces of the sample each one with a plane surface facing the sensor. By passing an electrical current, high enough to increase the temperature of the sensor between a fraction of a degree up to several degrees while record the resistance (temperature) increase as a function of time the Hot Disk sensor is used both as a heat source and as dynamic temperature sensor.

The solution of thermal conductivity equation is based on the assumption that the Hot Disk sensor is located in an infinite medium. Typical sizes are between 1 and $10cm^3$ but can be reduced in special situations to $0.01cm^3$. One can notice the size of the flat sample surfaces should be appreciably larger than the diameter of the Hot Disk sensor in order to allow a longer transient recording.

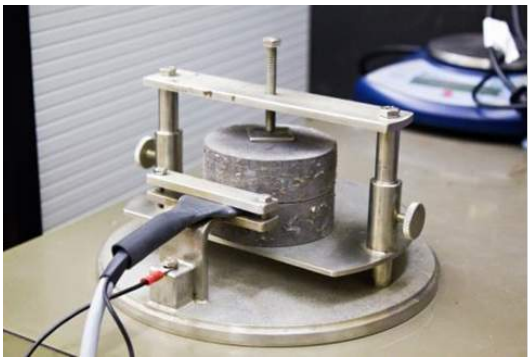

Figure A.1: Hot Disc Sensor being placed between two samples of same nature

Results are shown in table A.1 and A.2 for formulation A and B. Samples were tested at temperature [25:25:150]°C.

For the non-heated teIt can be notice the materials are more "insulators" than "heat dissipators". Also A seems more conductive than B. It might be due to the steel fibres contained into formulation A. Anyway, temperature surface during braking must be higher than expected.

Moreover, since curing is stopped at a final temperature of 200°C, some samples were heated up to 300°C and 400°C in an oven (referenced as HT300 and HT400), then remeasured at 25°C in parameters. It is also shown the heat treatment has an effect on thermal material properties. This change is caused by transformations in materials and their chemical compositions. For material A, a decrease in thermal conductivity is observable. On the other hand the thermal diffusivity has increased. Important material property, the specific heat capacity, is decreased with the heat treatment.

Temperature [°C]	**Formulation A**			**Formulation B**		
	λ [W/mK]	*α[mm²/s]*	*C [J/kg.K]*	*λ [W/mK]*	*α[mm²/s]*	*C [J/kg.K]*
25	1.1142	0.9017	1.2429	0.7587	0.5556	1.3657
50	1.2157	0.7568	1.5873	0.8157	0.5256	1.554
75	1.271	0.7432	1.7102	0.8365	0.4877	1.7258
100	1.316	0.7211	1.8255	0.9257	0.4813	1.9252
125	1.3628	0.6899	1.9761	0.9542	0.4544	2.101
150	1.3967	0.6619	2.1097	0.9822	0.4282	2.2941
HT300/25	0.9171	0.9196	0.9976	0.77	0.5825	1.338
HT400/25	0.7689	1.072	0.7181	0.6606	0.7392	0.9354

Table A.1: Thermal conductivity, thermal diffusivity and heat capacity of two simplified formulations

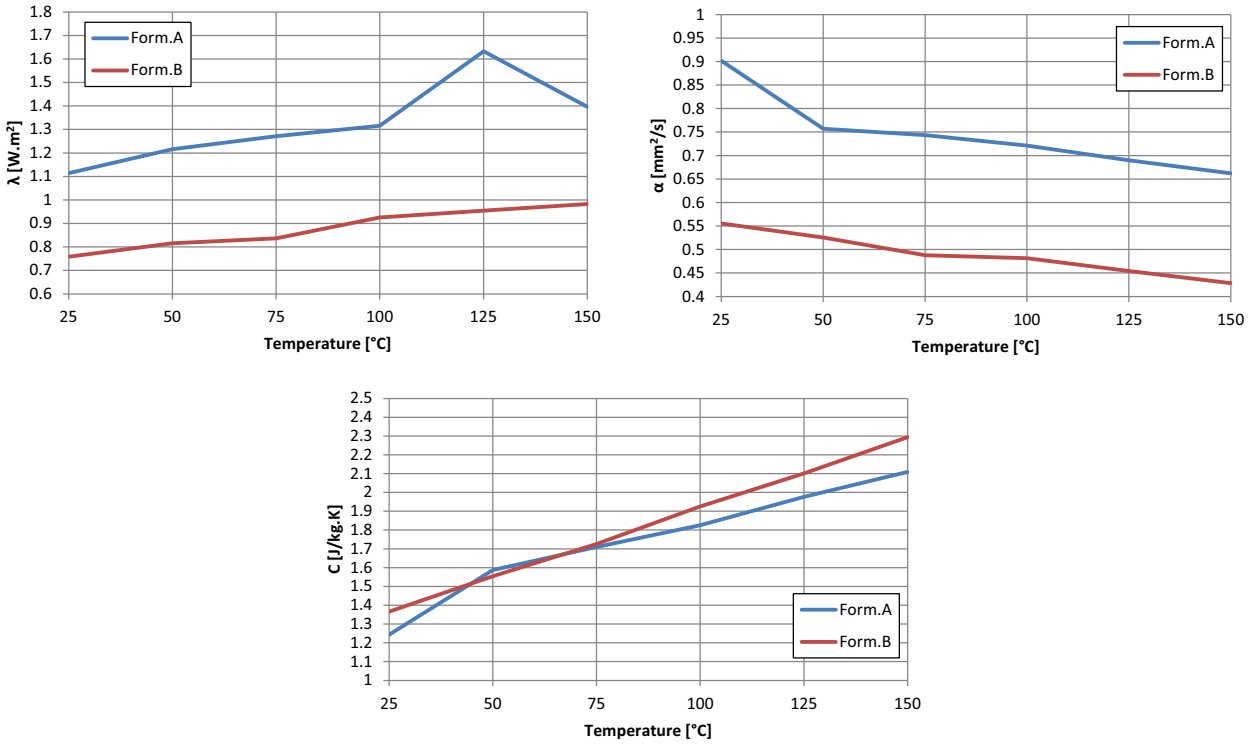

Figure A.2: Thermal conductivity, thermal diffusivity and heat capacity of two simplified formulations - Plot

Appendix B

Appendix - B

In this appendix, complementary SEM analysis of cylinder pad surfaces are shown at differents states of friction. trailing edge is missing.

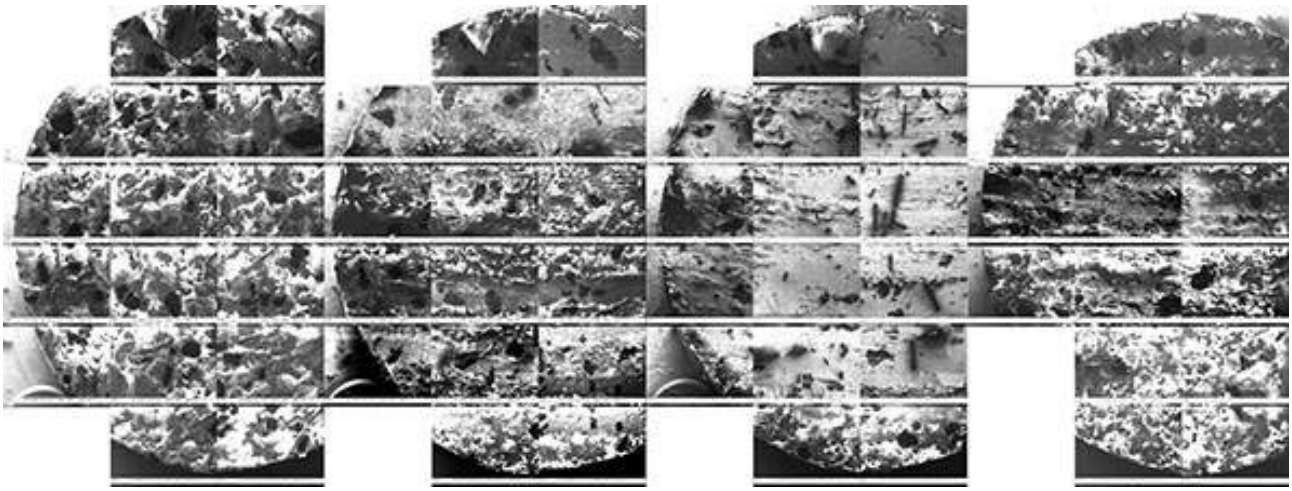

Figure B.1: SEM observation of pad surface at different friction state: new pad, after bedding, after first AK21 & after second AK21 - Formulation A

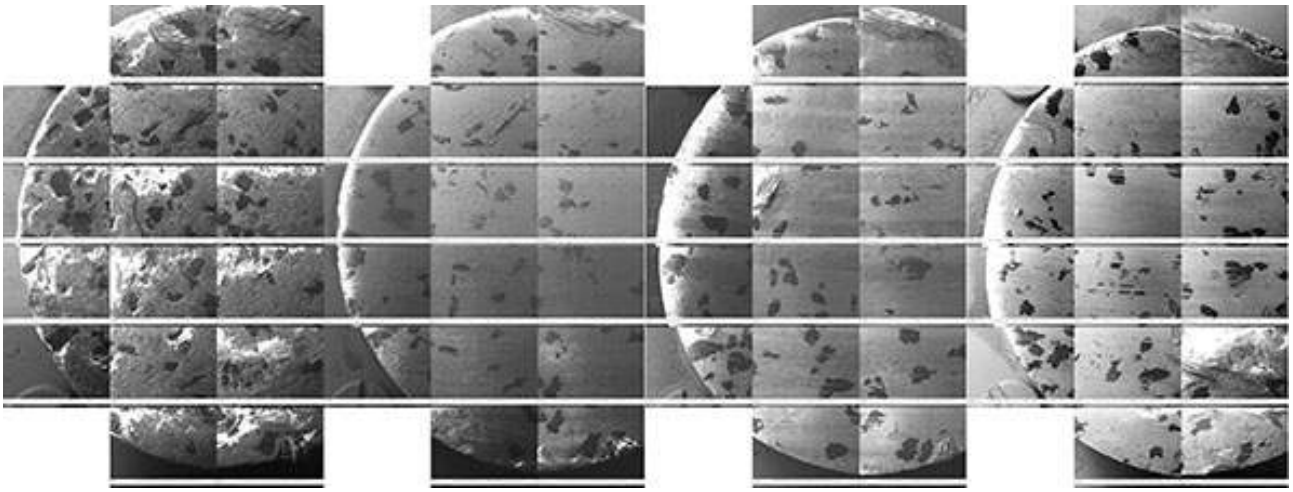

Figure B.2: SEM observation of pad surface at different friction state: new pad, after bedding, after first AK21 & after second AK21 - Formulation B

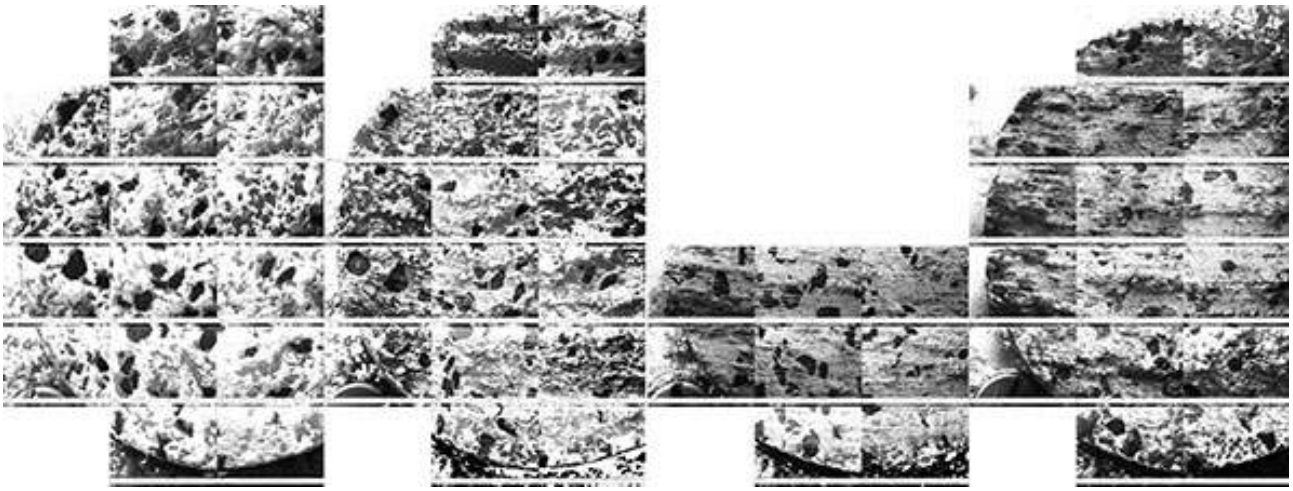

Figure B.3: SEM observation of pad surface at different friction state: new pad, after bedding, after first AK21 & after second AK21 - Formulation C

Appendix C

Appendix - C

To verify that the transverse material assumption were ruled out, two calculations were performed in ANSYS:

- The first takes into account the transverse isotropic material components.
- The second is a simplify model which supposed an isotropic material.

The comparison criteria, throughout this study, is based on the error between the different curve $p = f(h)$. Figure C.1 represents the response of the two models.

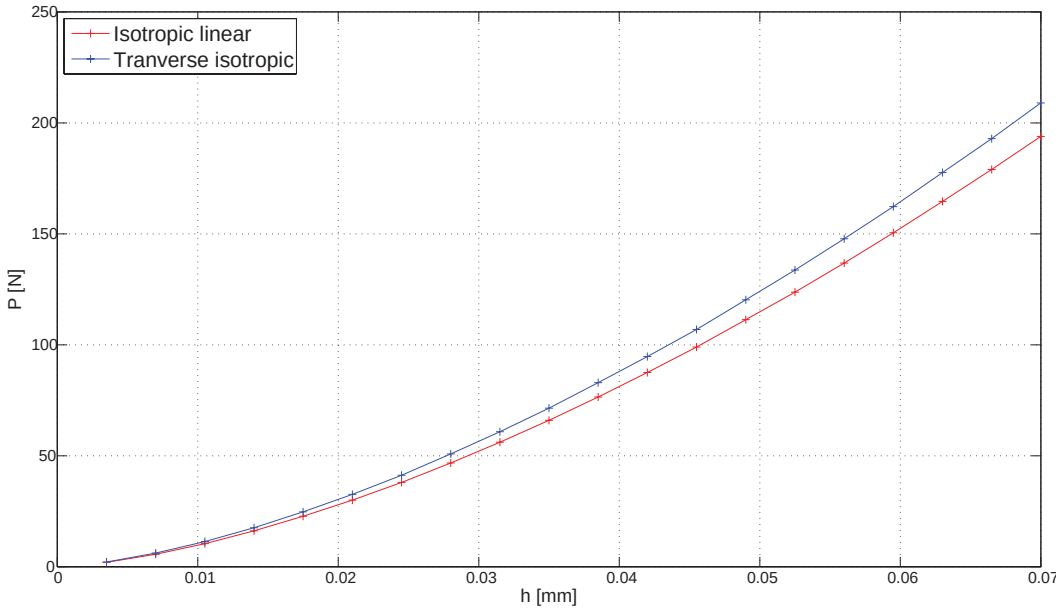

Figure C.1: Comparison between transverse isotropic and isotropic modelling

An error has actually achieved if the material is modelled by an isotropic behaviour. It can be estimated at $4\mu m$ for a load of $150N$. In this study, the error can be assessed, so to simplify the modelling, an isotropic model will be used.

Appendix D

Appendix - D

In this appendix, all comparisons between experimental result (blue curve) and numerical approach (red curve) are represented. This results overview is given for formulation C. Test1.

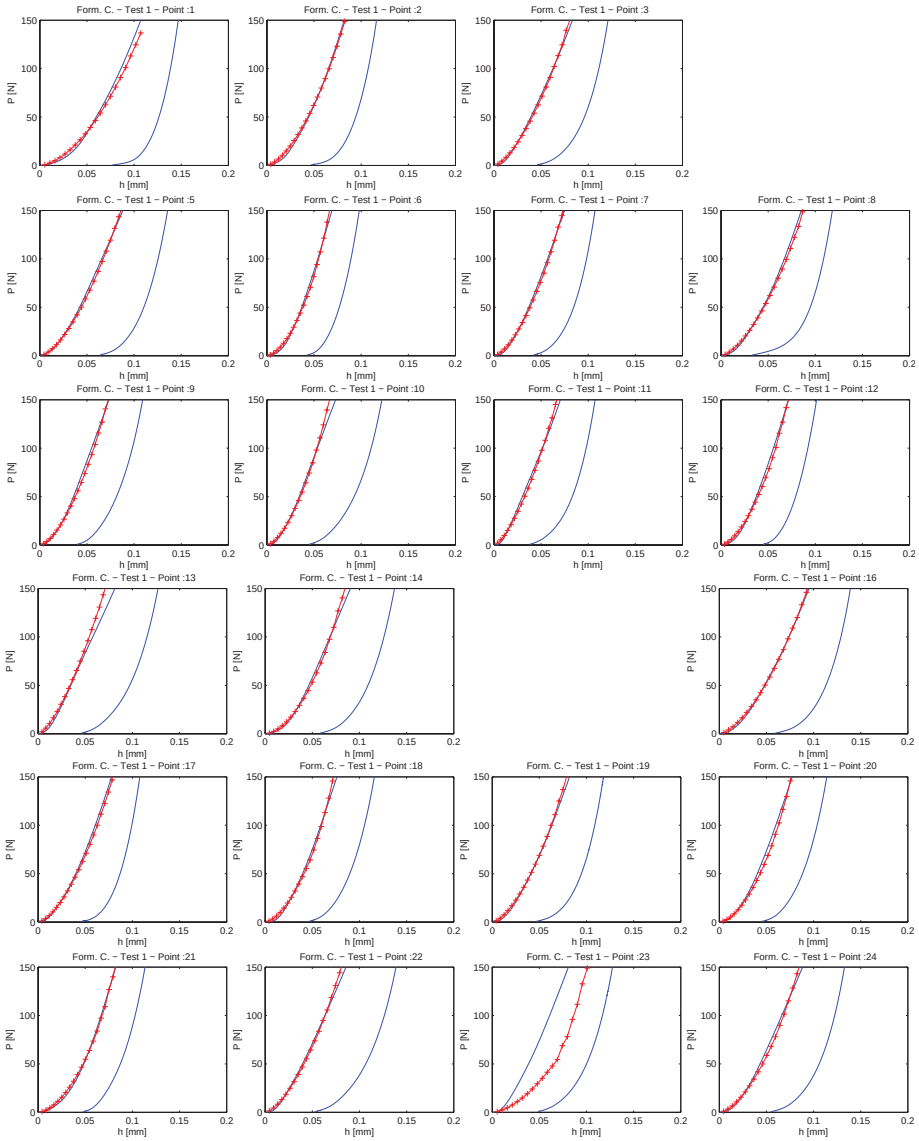

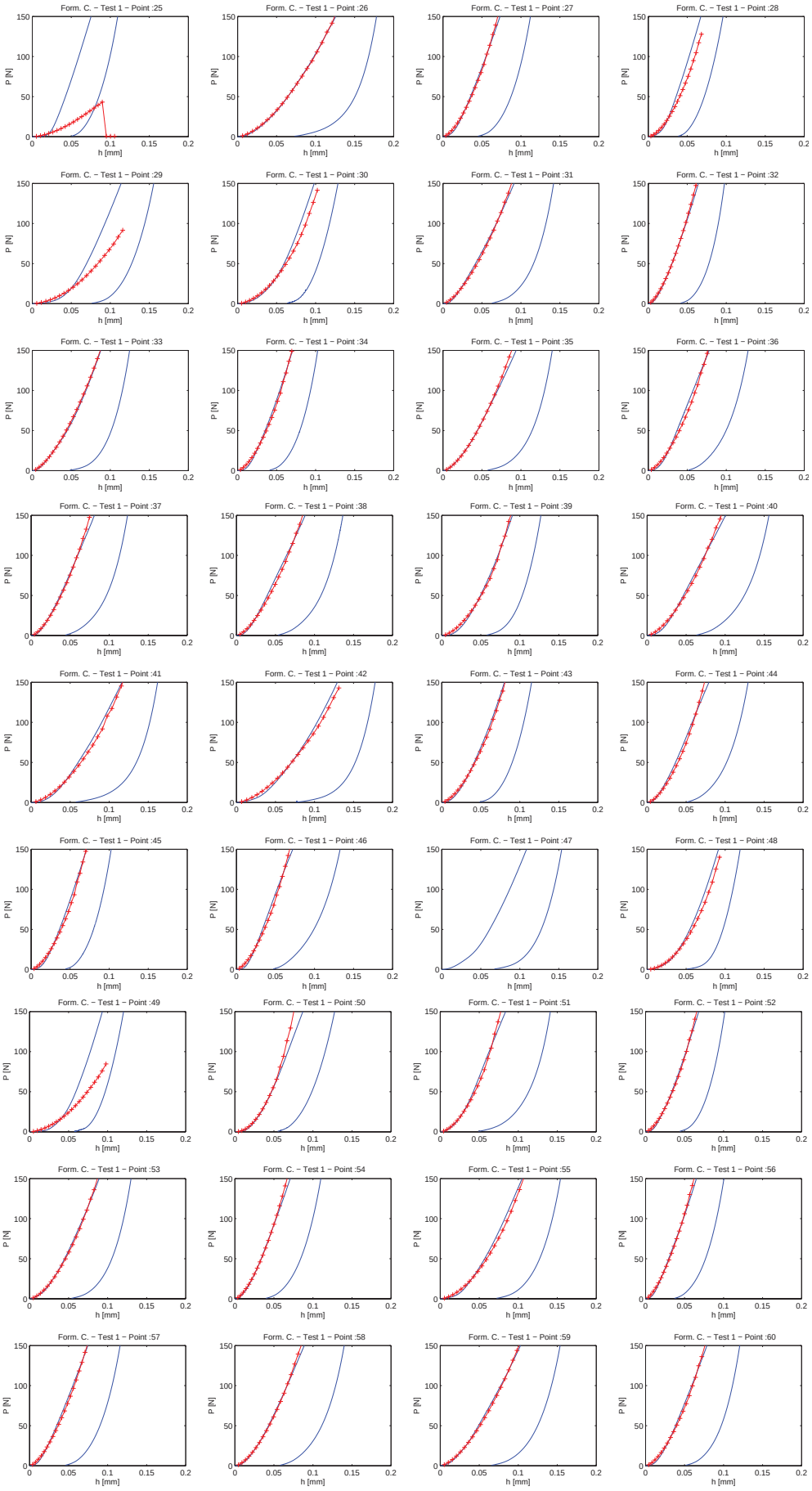

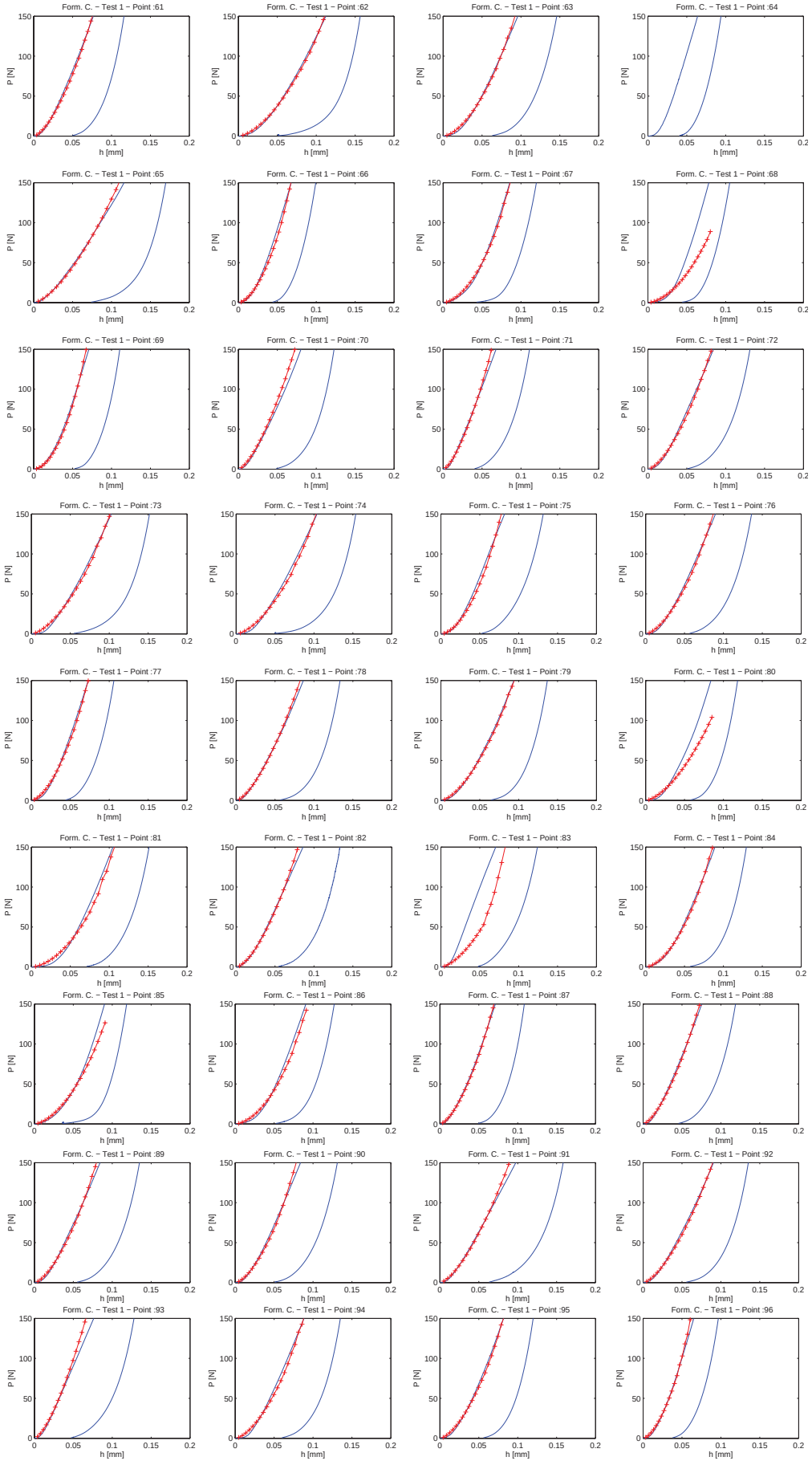

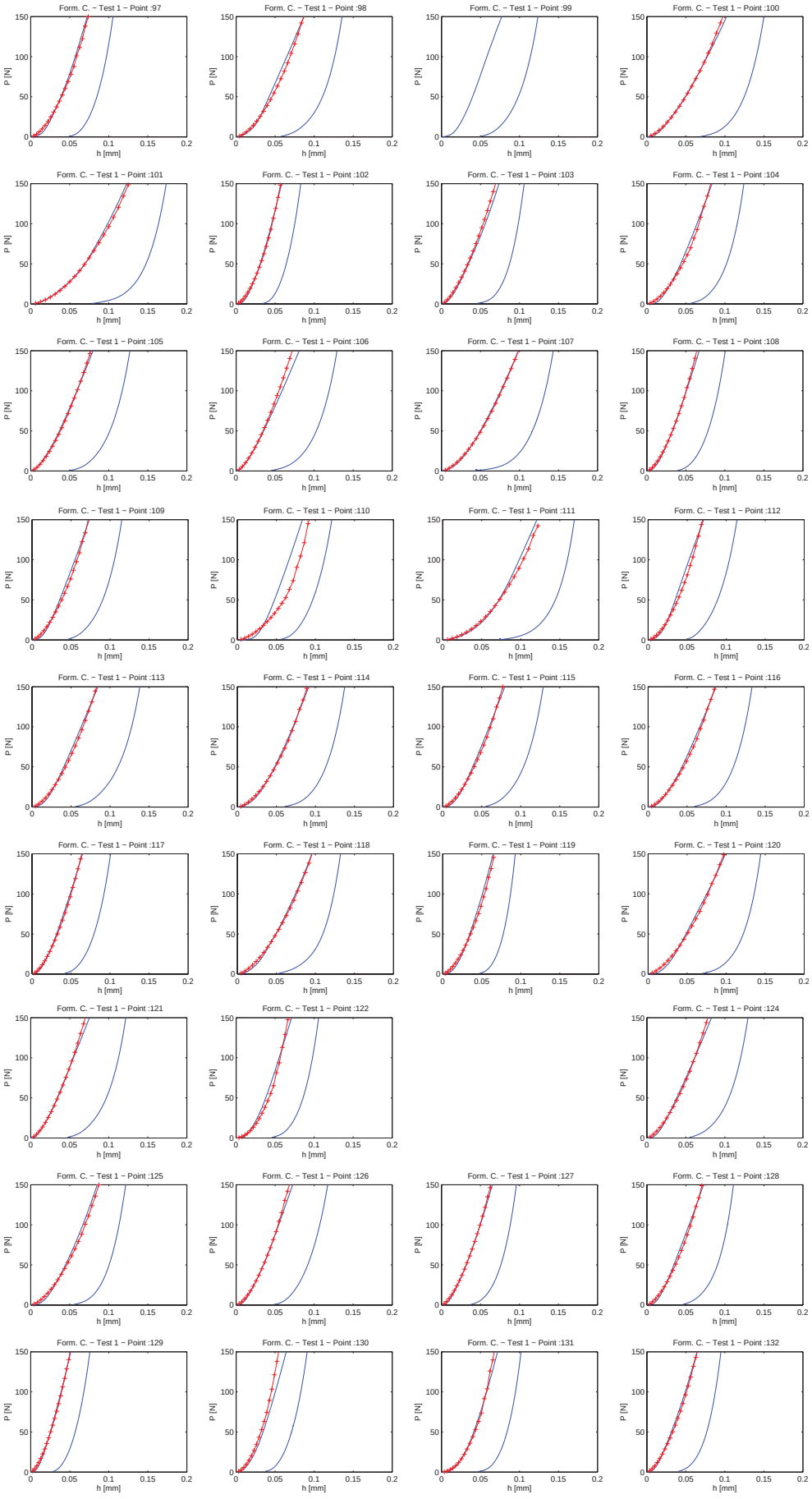

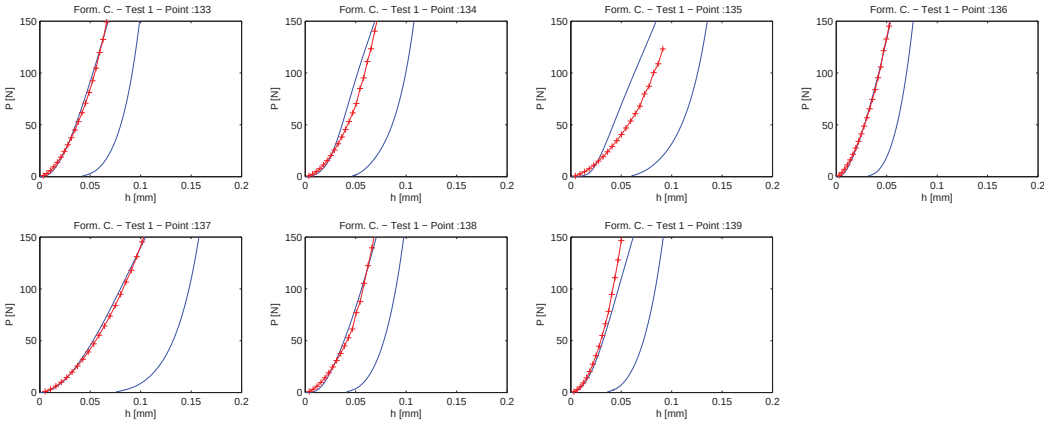

Bibliography

[Abendroth and Wernitz, 2000] Abendroth, H. and Wernitz, B. (2000). The integrated test concept dyno-vehicle: performance and noise. *S.A.E Technical Paper*, 01(2774).

[Abubakar and Ouyang, 2006] Abubakar, A. and Ouyang, H. (2006). Complex eigenvalue analysis and dynamic transient analysis in predicting disc brake squeal. *International Journal of Vehicle Noise and Vibration*, 2(2):143–155.

[AbuBakar and Ouyang, 2008] AbuBakar, A. R. and Ouyang, H. (2008). Wear prediction of friction material and brake squeal using the finite element method. *Wear*, 264:1069–1076.

[Adams, 1995] Adams, G. (1995). Self-excited oscillations of two elastic half-spaces sliding with a constant coefficient of friction. *Journal of applied mechanics*, 62(4):867–872.

[Akay, 2002] Akay, A. (2002). Acoustics of friction. *J. Acoust. Soc. Am.*, pages 1525–1548.

[Allemang, 2003] Allemang, R. J. (2003). The modal assurance criterion. 1(August):14–21.

[Baba H. and Takagi, 2001] Baba H., W. T. and Takagi, T. (2001). Study on reduction of brake squeal caused by in-plane vibration of rotor. In *SAE Paper 2001-01-3158*.

[Bae and Wickert, 2000] Bae, J. C. and Wickert, J. A. (2000). Free vibration of coupled disk–hat structures. *Journal of Sound and Vibration*, 235(1):117–132.

[Baklouti et al., 2013] Baklouti, M., Elleuch, R., Cristol, A.-L., Najjar, D., and Desplanques, Y. (2013). Relationships between the heterogeneous microstructure, the mechanical properties and the braking behaviour of an organic brake lining material. *Proceedings of the Institution of Mechanical Engineers, Part D: Journal of Automobile Engineering*, 227(4):549–560.

[Bartier et al., 2010] Bartier, O., Hernot, X., and Mauvoisin, G. (2010). Theoretical and experimental analysis of contact radius for spherical indentation. *Mechanics of Materials*, 42(6):640–656.

[Bergmann et al., 2000] Bergmann, F., Eriksson, M., and Jacobson, S. (2000). The effect of reduced contact area on the occurence of disc brake squeals for automotive brake pad. *Proceeding of the Institution of Mechanical Egineers*, D 214 (D5):561–568.

[Berthier, 1995] Berthier, Y. (1995). Maurice godet's third body. In *22nd Leeds-Lyon Symposium on Tribology*, pages 2209–2244.

[Bonnay, 2013] Bonnay, K. (2013). *Instabilités vibratoires dans un contact frottant en présence d'hétérogénéités de matériau et de surface*. PhD thesis, Université de Lille 1.

[Brecht et al., 2003] Brecht, J., Elvenkemper, A., Betten, J., Navrath, U., and Multhoff, J. (2003). Elastic properties of friction materials. *SAE transactions*, 112(6):2393–2400.

[Brommundt, 1995] Brommundt, E. (1995). Ein reibschwinger mit selbsterregung ohne fallende reibkennlinie. *ZAMM - Journal of Applied Mathematics and Mechanics / Zeitschrift für Angewandte Mathematik und Mechanik*, 75(12):811–820.

[Chicot and Mercier, 2008] Chicot, D. and Mercier, D. (2008). Improvement in depth-sensing indentation to calculate the universal hardness on the entire loading curve. *Mechanics of Materials*, 40(4):171–182.

[Ciavarella et al., 2001] Ciavarella, M., Demelio, G., Schino, M., and Vlassak, J. J. (2001). The general 3d hertzian contact problem for anisotropic materials. *Key Engineering Materials*, 221:281–292.

[Collignon, 2013] Collignon, M. (2013). *Compréhension des mécanismes de dégradation de disques de frein pour véhicule «poids lourd» et définition de nouvelles solutions matériaux*. PhD thesis, Ecole Centrale de Lille.

[Des Roches, 2011] Des Roches, G. V. (2011). *Frequency and time simulation of squeal instabilities. Application to the design of industrial automotive brakes*. PhD thesis, Ecole Centrale Paris.

[Desplanques and Degallaix, 2009] Desplanques, Y. and Degallaix, G. (2009). Interactions between third-body flows and localisation phenomena during railway high-energy stop braking. *SAE International Journal of Passenger Cars-Mechanical Systems*, 1(1):1267–1275.

[Duboc, 2013] Duboc, M. (2013). *Etude multi-échelle du crissement: dispositif expérimental et éléments de compréhension*. PhD thesis, Université de Lille 1.

[Duboc et al., 2010] Duboc, M., Brunel, J. F., and Dufrénoy, P. (2010). Influence des conditions de contact et de la géométrie sur les occurences de crissement. In *XVII Symposium Vibration, Choc et Bruit*.

[Earles and Badi, 1984] Earles, S. W. E. and Badi, M. (1984). Oscillatory instabilities generated in a double-pin and disc undamped system : a mechanism of disc-brake squeal. *Proceeding of the Institution of Mechanical Egineers*, C198:43–49.

[Earles and Soar, 1971] Earles, S. W. E. and Soar, G. B. (1971). Squeal noise in disc brakes. *IMechE*, C101/71:61–69.

[Eriksson, 2000] Eriksson, M. (2000). Friction and contact phenomena of disc brakes related to squeal. Master's thesis, Uppsala University.

[Eriksson et al., 2002] Eriksson, M., Bergmann, F., and Jacobson, S. (2002). On the nature of tribological contact in automotive brakes. *Wear*, 252:26–36.

[Eriksson and Jacobson, 2000] Eriksson, M. and Jacobson, S. (2000). Tribological surfaces of organic brake pads. *Tribologiy international*, 33:817–827.

[Eriksson et al., 2001] Eriksson, M., Lundqvist, A., and Jacobson, S. (2001). A study of the influence of humidity on the friction and squeal generation of automotive brake pads. *Proceedings of the Institution of Mechanical Engineers, Part D: Journal of Automobile Engineering*, 215(3):329–342.

[Fieldhouse and Newcomb., 1993] Fieldhouse, J. and Newcomb., T. (1993). The application of holographic interferometry to the study of disc brake noise. *SAE Paper*, 930805.

[Fosberry and Holubecki, 1955] Fosberry, R. A. C. and Holubecki, Z. (1955). An investigation of the cause and nature of brake squeal. *M.I.R.A. Technical Report*, No. 1955/2.

[Fosberry and Holubecki, 1961] Fosberry, R. A. C. and Holubecki, Z. (1961). Disc brake squeal: Its mechanism and suppression. *M.I.R.A. Technical Report, No. 1961/2*.

[Godet, 1984] Godet, M. (1984). The third-body approach: a mechanical view of wear. *Wear*, 100:437–452.

[Graf and Ostermeyer, 2011] Graf, M. and Ostermeyer, G.-P. (2011). Instabilities in the sliding of continua with surface inertias : An initiation mechanism for brake noise. *Journal of Sound and Vibration*, 330:5269–5279.

[Guan and Jiang, 1998] Guan, D. and Jiang, D. (1998). A study on disc brake squeal using finite element methods. In *SAE Paper 980597*.

[He, 2005] He, Y. (2005). Rapid thermal conductivity measurement with a hot disk sensor. *Thermochimica Acta*, 436(1-2):122–129.

[Hertz, 1882] Hertz, H. (1882). {Über} die {B} erührung fester elastischer {K} örper. *J. für die reine u. angew. Math.*, 92.

[Hetzler and Willner, 2012] Hetzler, H. and Willner, K. (2012). On the influence of contact tribology on brake squeal. *Tribology International*, 46(1):237–246.

[Heussaff et al., 2012] Heussaff, a., Dubar, L., Tison, T., Watremez, M., and Nunes, R. (2012). A methodology for the modelling of the variability of brake lining surfaces. *Wear*, 289:145–159.

[Hoffmann et al., 2002] Hoffmann, N., Fischer, M., Allgaier, R., and Gaul, L. (2002). A minimal model for studying properties of the mode-coupling type instability in friction induced oscillations. *Mechanics Reasearch Communications*, 29:197–205.

[Hornig and Von Wagner, 2013] Hornig, S. A. and Von Wagner, U. (2013). Experimental identification of brake lining material properties subjected to combined static and high frequency loading-a step towards a better prediction of disc brake squeal? *Training*, pages 02–20.

[Hu and Nagy, 1997] Hu, Y. and Nagy, L. I. (1997). Brake squeal analysis using nonlinear transient finite element method. In *SAE Paper 971510*.

[ISO6310:2009, 2009] ISO6310:2009 (2009). Road vehicles – brake linings – compressive strain test methods. Number ISO 6310:2009. ISO, Geneva, Switzerland.

[Johnson et al., 1971] Johnson, K., Kendall, K., and Roberts, A. (1971). Surface energy and the contact of elastic solids. *Proceedings of the Royal Society of London. A. Mathematical and Physical Sciences*, 324(1558):301–313.

[Johnson, 1987] Johnson, K. L. (1987). *Contact mechanics*. Cambridge university press.

[Kinkaid et al., 2003] Kinkaid, N. M., O'Reilly, O. M., and Papadopoulos, P. (2003). Automotive disc brake squeal. *Journal of Sound and Vibration*, 267(1):105–166.

[Lee and Barber, 1994] Lee, K. and Barber, J. (1994). An experimental investigation of frictionally-excited thermoelastic instability in automotive disk brakes under a drag brake application. *TRANSACTIONS-AMERICAN SOCIETY OF MECHANICAL ENGINEERS JOURNAL OF TRIBOLOGY*, 116:409–409.

[Liles, 1989] Liles, G.-D. (1989). Analysis of disc brake squeal using finite element methods. In *SAE Paper 891150*, page 8.

[Liu et al., 2007] Liu, P., Zheng, H., Cai, C., Wang, Y. Y., Lu, C., Ang, K. H., and Liu, G. R. (2007). Analysis af disc brake squeal using the complex eigenvalue method. *Applied Acoustics*, 68:603–615.

[Liu and Pfeifer, 2000] Liu, W. and Pfeifer, J. (2000). Reducing high-frequency disc brake squeal by pad shape optimization. *SAE transactions*, 109(6):572–576.

[Lorenz et al., 2003] Lorenz, D., Zeckzer, A., Hilpert, U., Grau, P., Johansen, H., and Leipner, H. (2003). Pop-in effect as homogeneous nucleation of dislocations during nanoindentation. *Physical Review B*, 67(17):172101.

[Loyer et al., 2012] Loyer, A., Sinou, J.-J., Chiello, O., and Lorang, X. (2012). Study of nonlinear behaviors and modal reductions for friction destabilized systems. application to an elastic layer. *Journal of Sound and Vibration*, 331(5):1011–1041.

[Massi et al., 2006] Massi, F., Giannini, O., and Baillet, L. (2006). Brake squeal as dynamic instability: an experimental investigation. *Journal of the Acoustical Society of America*, 120:1388–1399.

[Matozo et al., 2006] Matozo, L., Menetrier, A., and Tamagna, A. (2006). Analysis of high damping underlayer materials for brake pads and its effects on nvh performance. *SAE Technical Paper*, pages 01–3223.

[Mendoza Delgado, 2009] Mendoza Delgado, J. A. (2009). *Détermination des propriétés mécaniques et des lois de comportement en fluage par indentation instrumentée*. PhD thesis, Lille 1.

[Millner, 1978] Millner, N. (1978). An analysis of disc brake squeal. *SAE Technical Paper*, (780332).

[Mills, 1938] Mills, H. R. (1938). Brake squeak. Technical report.

[Mody et al., 2002] Mody, P., Rumold, W., Attia, F., and Ansmann, S. (2002). Mojacar and los angeles city traffic vehicle testing: A comparison & analysis of subjective ratings and objective measurements. *Society of Automotive Engineers*.

[Murakami et al., 1984] Murakami, H., Tsunada, N., and Kitamura, T. (1984). A study concerned with a mechanism of disc brake squeal. *S.A.E. Technical Paper*, (841233).

[Nagy et al., 1994] Nagy, L., Cheng, J., and Hu, Y. (1994). A new method development to predict squeal occurrence. In *SAE Paper 942258*.

[Nicholson, 1995] Nicholson, G. (1995). Facts about friction. *Gedoran America, Winchester*.

[Nix and Gao, 1998] Nix, W. D. and Gao, H. (1998). Indentation size effects in crystalline materials: a law for strain gradient plasticity. *Journal of the Mechanics and Physics of Solids*, 46(3):411–425.

[North, 1976] North, M. R. (1976). Disc brake squeal - a theorical model. *Institute of mechanical engineers*, C38/76:169–176.

[Oberst and Lai, 2011] Oberst, S. . A. and Lai, J. C. S. (2011). Statistical analysis of brake squeal noise. *Journal of Sound and Vibration*, 330(12):2978–2994.

[Oden and Martins, 1985] Oden, J. T. and Martins, J. A. C. (1985). Models and computational methods for dynamic friction phenomena. *Computer Methods in Applied mechanics and Engineering*, 52:527–634.

[Oliver and Pharr, 1992] Oliver, W. C. and Pharr, G. M. (1992). An improved technique for determining hardness and elastic modulus using load and displacement sensing indentation experiments. *Journal of Materials Research*, 7:1564–1583.

[Ouyang et al., 2005] Ouyang, H., Nack, W., Yuan, Y., and Chen, F. (2005). Numerical analysis of automotive disc brake squeal: a review. *International Journal of Vehicle Noise and Vibration*, 1:1471–1479.

[Panier et al., 2004] Panier, S., Dufrenoy, P., and Weichert, D. (2004). An experimental investigation of hot spots in railway disc brakes. *Wear*, 256:764–773.

[Papinniemi et al., 2002] Papinniemi, A., Lai, J. C. S., Zhao, J., and Loader, L. (2002). Brake squeal : a literature review. *Applied Acoustics*, 63:391–400.

[Papinniemi and Lai, 2004] Papinniemi, A. T. and Lai, J. C. (2004). Comparison of energy based methods for assessing brake squeal propensity. In *18th International Congress on Acoustics*.

[Popp et al., 2002] Popp, K., Rudolph, M., Kroeger, M., and Lindner, M. (2002). Mechanisms to generate and to avoid friction induced vibrations. *VDI-Bericht 1736*.

[Renaud et al., 2012] Renaud, F., Chevallier, G., Dion, J.-L., and Taudière, G. (2012). Motion capture of a pad measured with accelerometers during squeal noise in a real brake system. *Mechanical Systems and Signal Processing*, 33(0):155 – 166.

[Rhee et al., 1991] Rhee, R. K., Jacko, M. G., and Tsang, P. H. S. (1991). Role of friction film in friction wear and noise of automotive brakes. *Wear*, 146(1):89–97.

[Roussette, 2005] Roussette, O. (2005). *Etude tribologique de couples de matériaux sous sollicitations de freinage tres sévères : application à un frein ferroviaire à performances ameliorées*. PhD thesis, Université de Lille 1.

[Sallit et al., 1998] Sallit, I., Richard, C., Adam, R., and Robbe-Valloire, F. (1998). Characterization methodology of a tribological couple: metal matrix composite/brake pads. *Materials characterization*, 40(3):169–188.

[Sanders et al., 2008] Sanders, P. G., Dalka, T., and Hartsock, D. (2008). Friction material compressibility as a function of pressure, temperature, and frequency. *Training*, 2013:11–18.

[Shi T.S. and Warzecha, 2001] Shi T.S., C. W. K. D. O. J. A. M. and Warzecha, T. (2001). Advances in complex eigenvalue analysis for brake noise. In *SAE Paper 2001-01-1603*.

[Shin et al., 2002] Shin, K., Brennan, M. J., Oh, J.-E., and Harris, C. J. (2002). Analysis of disc brake noise using a two-degree-of-freedom model. *Journal of Sound and Vibration*, 254(5):837–848.

[Sinclair, 1955] Sinclair, D. (1955). Frictional vibrations. *Journal of Applied Mechanics*, pages 207–214.

[Spurr, 1961] Spurr, R. T. (1961). A theory of brake squeal. *Proc. Inst. Mech. Eng. 1*, pages 33–52.

[Spurr, 1971] Spurr, R. T. (1971). Brake squeal. *IMechE*, C95/71:13–16.

[Triches-Jr et al., 2008] Triches-Jr, M., Gerges, S. N. Y., and Jordan, R. (2008). Analysis of brake squeal noise using the finite element method: A parametric study. *Applied Acoustics*, 69(2):147–162.

[von Wagner et al., 2007] von Wagner, U., Hochlenert, D., and Hagedorn, P. (2007). Minimal models for disk brake squeal. *Journal of Sound and Vibration*, 302:527–539.

[Wegmann and Stenkamp, 2012] Wegmann, E. and Stenkamp, A. (2012). Model approach for a load and frequency dependent stiffness in friction materials. *SAE International Journal of Materials & Manufacturing*, 5(1):1–8.

[Yang and Afeneh, 2004] Yang, M. and Afeneh, A.-H. (2004). Investigation of mounted disc brake in-plane and out-of-plane modes in brake squeal study. In for Experimental Mechanics, S., editor, *Proceedings of the 22nd Int. Modal Analysis Conference (CD-ROM)*.

[Yuhas et al., 2006] Yuhas, D. E., Ding, J., and Vekatesan, S. (2006). Non-linear aspects of friction material elastic constants. *SEA Technical Papers*, pages 01–3193.